AIRCRAFT STALLING AND BUFFETING

Advisory Group for Aerospace Research and Development
Paris, France

February 1975

THE MISSION OF AGARD

The mission of AGARD is to bring together the leading personalities of the NATO nations in the fields of science and technology relating to aerospace for the following purposes:

Exchanging of scientific and technical information;

Continuously stimulating advances in the aerospace sciences relevant to strengthening the common defence posture;

Improving the co-operation among member nations in aerospace research and development;

Providing scientific and technical advice and assistance to the North Atlantic Military Committee in the field of aerospace research and development;

Rendering scientific and technical assistance, as requested, to other NATO bodies and to member nations in connection with research and development problems in the aerospace field;

Providing assistance to member nations for the purpose of increasing their scientific and technical potential;

Recommending effective ways for the member nations to use their research and development capabilities for the common benefit of the NATO community.

The highest authority within AGARD is the National Delegates Board consisting of officially appointed senior representatives from each member nation. The mission of AGARD is carried out through the Panels which are composed of experts appointed by the National Delegates, the Consultant and Exchange Program and the Aerospace Applications Studies Program. The results of AGARD work are reported to the member nations and the NATO Authorities through the AGARD series of publications of which this is one.

Participation in AGARD activities is by invitation only and is normally limited to citizens of the NATO nations.

Published February 1975

533.6.013.66:533.6.013.43

Printed by Technical Editing and Reproduction Ltd
Harford House, 7–9 Charlotte St, London, W1P 1HD

PREFACE

This publication contains the papers presented at the von Kármán Institute, Brussels and at Ames Research Center (CA) in March 1975 for AGARD Lecture Series No.74 titled "Aircraft Stalling and Buffeting".

This Lecture Series was recommended by the Fluid Dynamics Panel and the von Kármán Institute for Fluid Dynamics, and has been implemented by the Consultant and Exchange Programme. Aircraft Stalling and Bufteting are related phenomena which limit the useable lift of an aircraft and hence determine its minimum flying speeds, its maximum cruising altitude and its manoeuvrability. The basic physical mechanisms are aerodynamic, involving separations of the airflow over the wings, but the limitations on the performance of the aircraft depend on its aeroelastic and dynamic response. The Lecture Series aims to give an account of recent developments in the understanding of the fluid dynamics of stalling and buffeting, of the dynamic response of the aircraft and of techniques for buffet prediction, with consideration of the implications for aircraft design. This publication should be of interest to aircraft aerodynamicists and research workers in fluid dynamics and flight mechanics.

Cyril R.TAYLOR
Lecture Series Director

LIST OF SPEAKERS

Lecture Series Director

Mr Cyril R.Taylor
Head, High-Speed Aerodynamics Division
Royal Aircraft Establishment
Clapham
Bedford MK41 6AE
UK

Dr H.John
Section Leader in Project Aerodynamics
Messerschmitt-Bölkow-Blohm GmbH
8000 München 80
Postfach 801160
Germany

Mr J.G.Jones
Principal Scientific Officer
Flight Dynamics Division
Royal Aircraft Establishment
Clapham
Bedford MK41 6AE
UK

Mr William McIntosh
Senior Group Engineer
High Lift Research Aerodynamics,
Boeing Commercial Airplane Company
Seattle
Washington 98124
USA

Mr B.Monnerie
Chef de Division Adjoint
Division Aérodynamique Appliquée
Office National d'Etudes et de Recherches
Aérospatiales
29, Avenue de la Division Leclerc
92320 Châtillon-sous-Bagneux
France

Mr D.E.Shaw
Principal Aerodynamicist
Aerodynamics Department
British Aircraft Corporation (M.A.D.)
Warton Aerodrome
Preston PR1 8UD
Lancs
UK

Mr A.M.O.Smith
Chief Aerodynamics Engineer, Research
Douglas Aircraft Company, Long Beach
3855 Lakewood Boulevard
California 90846
USA

CONTENTS

AIRCRAFT STALLING AND BUFFETING
INTRODUCTION AND OVERVIEW

by

C. R. Taylor
Royal Aircraft Establishment
Bedford, England

SUMMARY

Stalling and buffeting are related phenomena which limit the maximum useable lift of an aircraft and hence its minimum safe flying speed, its cruising altitude and its manoeuverability. The basic physical mechanisms are fluid mechanic, involving separations of the airflow over the wings, but the limitations on the performance of the aircraft depend on its aeroelastic and dynamic response.

1. PREAMBLE

Stalling and buffeting mean different things to different people. For the unfortunate passenger in an aircraft which inadvertently stalls or penetrates the buffet regime each could represent an unforgettable and terrifying experience. Whereas, a mathematician, who has never had the misfortune to experience the real thing, might regard them merely as convenient words to associate with a particular behaviour of the solution of his equations. It hardly needs to be said that the lecturers for this Series are both less emotional and more practical than the two extreme cases I have just quoted. The material of their lectures deals with some of the vastly complex engineering and physical aspects of the subject. Nevertheless the lectures will show that the passenger is never forgotten and that mathematical theory is readily absorbed.

Because the lecturers are specialists and they will deal with specialised aspects of this subject, my task in presenting an "introduction and overview" is to provide a lead-up to each of the topics covered (introducing some of the basic ideas and the essential nomenclature). I will also draw your attention to some of the aspects of the subject which are not covered by the specialist lectures. To do this I will continue the theme which I introduced at the beginning, i.e. "stalling and buffeting mean different things to different people" taking as particular cases the pilot, the aircraft designer, the aircraft aerodynamicist, the aircraft development engineer. I have not forgotten research aerodynamicists - I am sure that they will find much to interest them in the specialist lectures.

2. THE VIEWPOINTS OF THE PILOT AND OF THE AIRCRAFT DESIGNER

For a pilot, stalling and buffeting are words which describe the behaviour of his aircraft. He recognises the stall as the point at which his aircraft begins an uncontrollable nose-down pitching motion and ceases to maintain altitude, or normal acceleration, because the growth of flow separation on the wings prevents further increases in lift coefficient with reduction of speed. The flow separations may give him warning of the approach of the stall by exciting vibrations of the aircraft and its structure or by changing the "feel" of the controls. The experienced pilot is able to make a clear distinction between stalling and loss of normal acceleration due to lack of engine thrust. However, for some types of aircraft, he is less able to differentiate between the various forms of aircraft vibration and instabilities which make it difficult for him to increase his rate of turn in manoeuvres at high speeds. Buffeting, which we define as "the aeroelastic response of the aircraft structure to aerodynamic excitation arising from flow separations" is almost always encountered when approaching limiting lift at high speeds and, although this may not be the factor which restricts the manoeuverability, the word buffet is often used, rather loosely, to describe any unsteady phenomena which may induce the pilot to restrict the manoeuvre. It is in this broad sense that buffeting is coupled with stalling as the subject matter of this lecture series.

For an aircraft designer, stalling and buffeting are phenomena which limit the amount of lift on an aircraft and, for any aircraft specification, maximum useable lift has an influence on the aerodynamic design which is rivalled only by drag. For civil aircraft, airworthiness regulations (such as FAR and BCAR) place very definite limits on the extent to which an aircraft may approach limiting-lift conditions under normal operation. These rules (see Table 1) govern airspeeds on the approach to landing and on take-off and climb-out, by specifying speed margins, relative to stalling speed. The regulations also define two levels of buffet and lay down associated increments of normal acceleration, relative to 1-g level flight, which must be available with en-route configurations, at speeds at and near the upper end of the flight envelope.

Flight conditions	Speed margin	Manoeuvre margin	Limiting factor
Approach to landing	0.3 V_{ms} ($V_{ms} \geq 0.96\ V_{sig}$)	0.5g at VAT	Stall
Take off (2nd segment climb)	0.2 V_{ms1}	0.3g at 1.2 V_{ms1}	Stall
En-route $V < V_{mo}$	-	0.8g at V_{RA} 0.6g at V_{mo}	Buffet (maximum demonstrated)
Climb and descent h < 20,000 ft)		1.0g	Buffet (maximum demonstrated)

Table 1. Some airworthiness requirements for Civil Aircraft related to stalling and buffeting.

Taken together with the performance requirements (eg Mach number, altitude and lift/drag ratio at cruise, approach speed for landing, field length and noise characteristics for take-off) these regulations provide the basic ground-rules within which the aircraft designer optimises the size and configuration of the wing and defines the maximum useable lift coefficients he must achieve for both low-speed and high-speed flight. The designer is also required to ensure that, should the aircraft enter a stall, it shall be possible, using normal piloting skill, to make a prompt recovery and regain control of the aircraft.

Combat aircraft are designed to somewhat different rules but in many cases the requirements for low approach speeds and short take-off have a powerful influence on the choice of configuration and on the design of the wing for high lift at low speeds. Manoeuverability at high speeds is vitally important. So much so, that the pursuit of higher useable lift at high subsonic speeds has led the designers of current operational aircraft to employ a wide range of devices which help either to optimise the wing planform for the manoeuvre (e.g. variable wing sweep) or to inhibit the occurrence and growth of flow separation (e.g. LE droop, manoeuvre slats, vortex generators). Several papers at the 1972 AGARD specialists meeting on the Fluid Dynamics of Aircraft Stalling[1] gave qualitative evidence of the gains in useable lift to be had from the use of some of these devices, but their efficacy must be evident to any intelligent observer of aircraft design trends. More recently experimental fighter aircraft have been designed with improved power/weight ratio, higher structural load factors and means of increasing pilot tolerance to steady normal acceleration - all of which improve the potential manoeuverability and increase the emphasis for more useable lift.

3. MAXIMUM USEABLE LIFT

In what I have said so far, I have repeatedly stressed the importance of maximum useable lift and its connection with stalling and buffeting. It is time that I began to explain that connection - in doing so I shall be talking the language of the aircraft aerodynamicist and the aircraft development engineer and I shall be coming quite close to the subject matter of some of the main lectures. For the time being, I shall consider a particular class of aircraft which (following Küchemann[2]) I call "classical swept-winged aircraft". As you can see from the sketches in Fig. 1 this covers most of the aircraft flying today. However I shall later go on to talk, very briefly, about two other classes of aircraft.

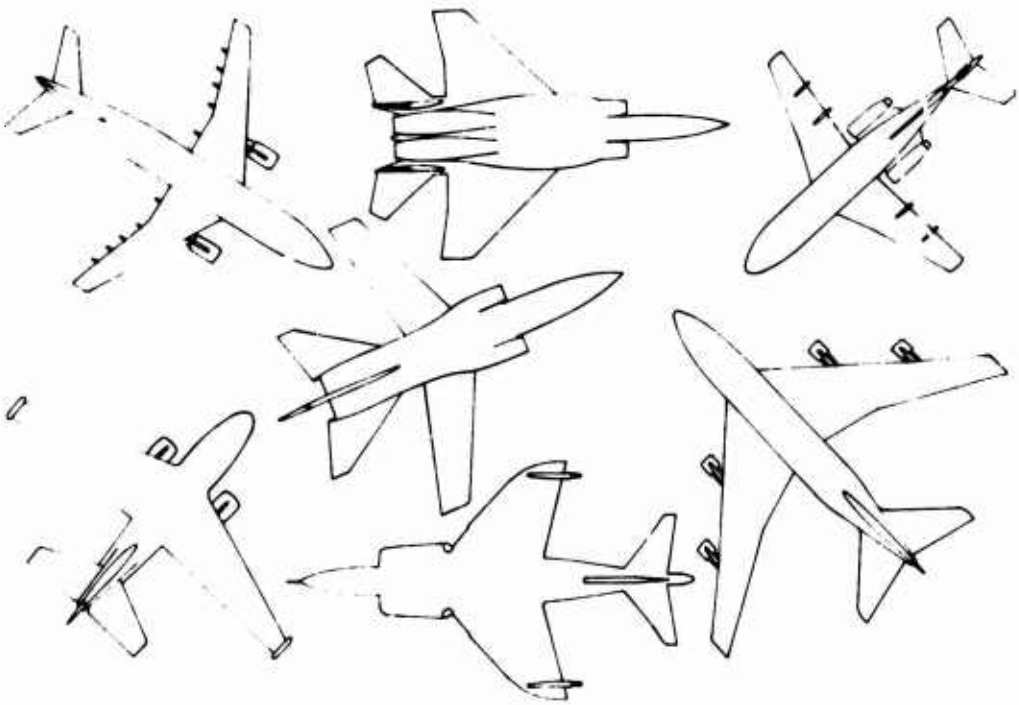

FIG 1 CLASSICAL SWEPT-WINGED AIRCRAFT

A basic difference between the low-speed characteristics of aircraft wings near limiting-lift conditions and those at high speed is shown by the plots in Fig. 2. These are curves of lift coefficient versus incidence over a range of Mach numbers and they are fairly typical of wind-tunnel measurements for wings of moderate aspect ratio and low sweep. They indicate quite clearly that for low Mach numbers the lift-coefficient has a definite maximum value which must present an upper limit to the amount of useable lift available. By contrast, at high free-stream Mach numbers no such overall limit is apparent (for the range of incidence covered by the tests). However the kinks and wiggles in the C_L vs α curves show that rather dramatic changes are occurring in the patterns of flow over the wing and we should anticipate that not all the lift measured on the model will be useable in flight. Similar plots for a wing which has nearly the optimum sweep for manoeuvres at high subsonic speeds (Fig. 3) again show that there is no clearly defined upper limit for the lift coefficient and that the maximum useable lift will be determined

by buffet or related unsteady phenomena.

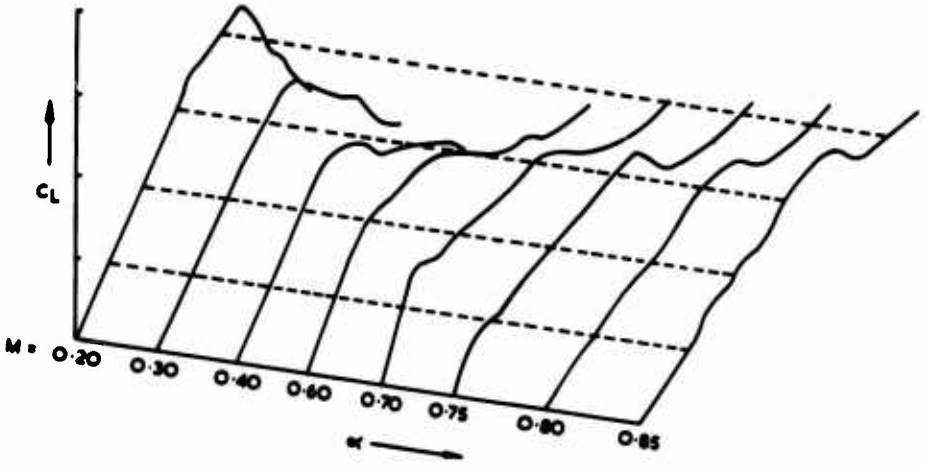

FIG. 2 VARIATIONS OF LIFT COEFFICIENT WITH INCIDENCE AND MACH NUMBER ($\phi = 25°$)

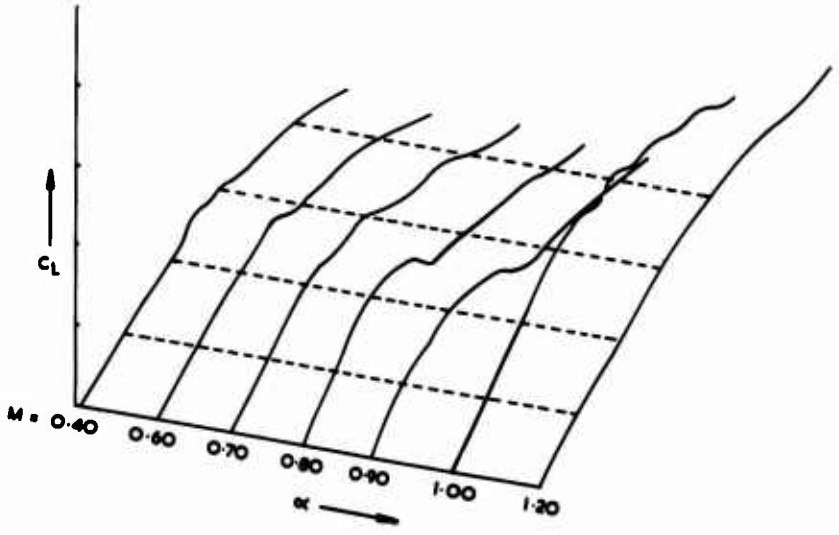

FIG. 3 VARIATIONS OF LIFT COEFFICIENT WITH INCIDENCE AND MACH NUMBER ($\phi = 45°$)

Even at low speeds, not all the lift available may be useable. One effect of wing taper and sweepback is to increase the lift coefficients near the wing tips, relative to values near the body, when the wing is at high incidence (Fig. 4). Of course this can be offset by spanwise variations of camber and twist but for many wing planforms these variations (Fig. 5) would create severe manufacturing problems and the resulting shape would be far from ideal at other incidences and Mach numbers. The compromise struck by the aircraft aerodynamicist invariably results in a wing on which (unless prevented) separations which lead to the stall originate on the outer wing - where the lift coefficient is highest and the effects of spanwise flow tend to thicken-up the boundary layer. These separations will cause a forward movement of the wing centre of pressure, which results in a tendency for the aircraft to pitch-up and hence move further into the stall. They may also give rise to unwelcome rolling motions and loss of lateral control. For these reasons it is usually necessary for the designer to use some means of triggering off the stall in a way which gives a rearward movement of the centre of pressure. The stall-trigger usually generates a separation on the inner wing and, if carefully designed, the aircraft will be able to complete the stalling manoeuvre without the separation spreading to outer parts of the wings. The ailerons will thus retain much of their effectiveness and roll control will not be lost. Various forms of stall

trigger have been used but for aircraft with rear engines, overwing fences or under-wing "vortilons" are the most common (see Refs. 2 and 3).

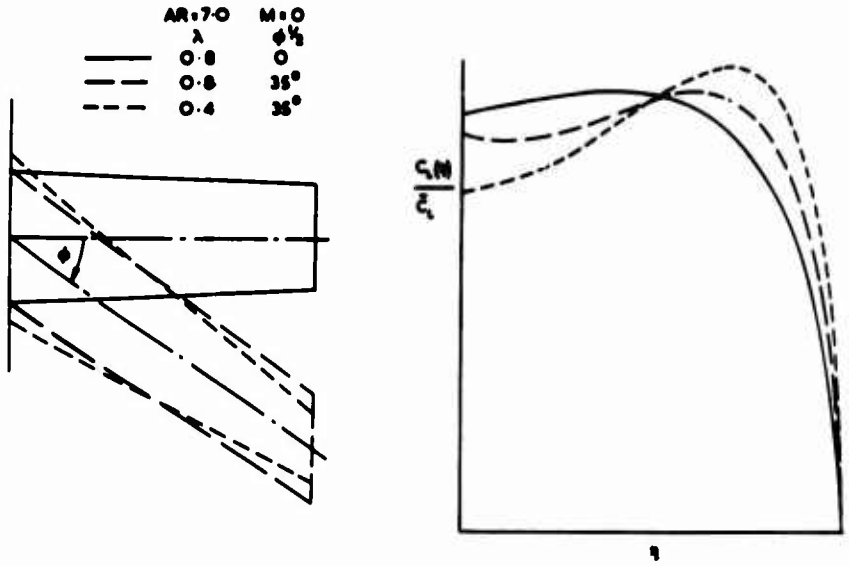

FIG. 4 VARIATION OF SPAN LOADING WITH SWEEPBACK & TAPER

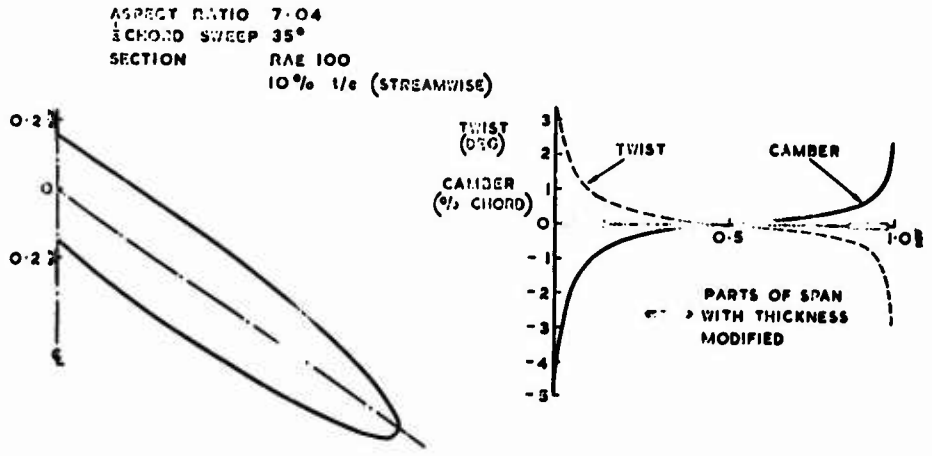

FIG. 5 WING DESIGNED FOR UNIFORM PRESSURE DISTRIBUTION AT $C_L = 0·8$

Fig. 6 shows the effect of a fence on the progression of flow separation on a model of the Fokker F.28[2]. The stall progression for a more highly swept wing, employing both stall strips and a wing fence[4], is shown in Fig. 7.

The pylons of underwing engines can trigger the stall of the clean wing but it is usually necessary to "degrade" the high-lift device on the inner wing, in one of a number of ways, to get the desired pitching moment characteristics for the take-off and landing configurations.

Of course, the need to provide acceptable handling and control at the stall results in the maximum usable lift being somewhat less than the maximum lift available from a wing without stall triggers. Some idea of the penalties involved may be deduced from Fig. 8.

The problems in obtaining an adequate nose-down pitching moment at the stall are compounded for large aircraft by the high angular momentum in pitch which these aircraft acquire during the decelerating approach to the stall and, for aircraft with T-tails, by the need to avoid the "deep-stall"[5,6].

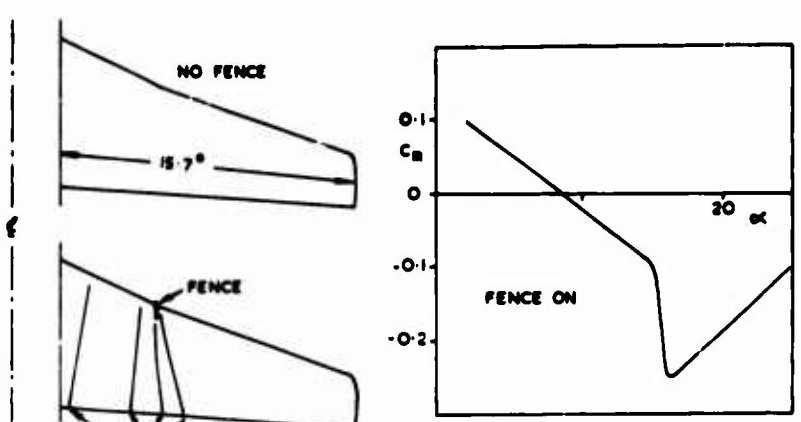

FIG 6 THE EFFECT OF A FENCE ON THE PROGRESSION OF SEPARATION ON F28

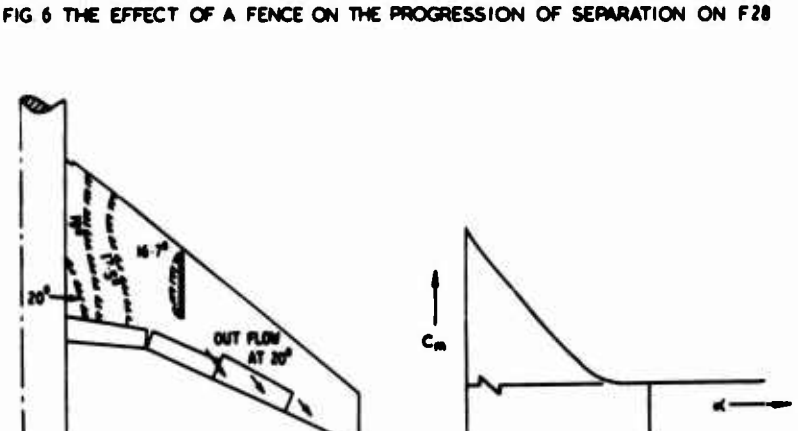

FIG 7 THE PROGRESSION OF FLOW SEPARATION ON A MODEL OF THE TRIDENT IC

Some insight to the problem can be derived from the simple exercise of equating the angular momentum in pitch ($mk^2\dot{\theta}$) to the rotational impulse produced by a sudden change in pitching moment ($-\Delta C_m$). Fig. 2 shows the problem. The aim is to bring the pitch rate to zero, from its initial value for level flight ($\dot{\theta}_o$), by the time the aircraft reaches a specified incidence α_s. The sudden change in pitching moment has to be applied, to the trimmed aircraft, at incidence $\alpha_o = \alpha_s - \Delta\alpha$. Assuming that the aircraft continues in level flight (i.e. $\dot{\theta} = \dot{\theta}_o$) and that $\Delta\alpha$ is small, the moment impulse is

$$(-\Delta C_m)\, \rho\, U^2 Sc\, \Delta\alpha/\dot{\alpha}_o \quad \text{and hence}$$

$$\Delta\alpha = mk^2(\dot{\theta}_o)^2/(-\Delta C_m)\, \rho U^2 Sc$$

$$= \frac{C_L}{(-\Delta C_m)} \frac{k^2}{2c} \frac{(\dot{\theta}_o)^2}{\dot{C}} \qquad (1)$$

Here m is the mass of the aircraft

k the radius of gyration in pitch

g the gravitational constant

and ρ, U, S, c have their usual meanings. If a_1 denotes the slope of the lift curve between α_o and α_s, the associated difference in lift coefficient is $\Delta C_L = \Delta\alpha/a_1$, which, after manipulation, reduces to:-

$$\Delta C_L = \frac{C_L}{a_1} \frac{1}{(-C_m)} \left(\frac{1}{\dot{C}} \frac{dU}{dt}\right)^2 \left(\frac{k}{c}\right)^2 \left(\frac{\rho Sc}{m}\right) \qquad (2)$$

where $\frac{\Delta n}{dt}$ is the deceleration at $\alpha = \alpha_0$. Airworthiness regulations require that the stall shall be demonstrated at a deceleration of 1 kn sec^{-1}. Two conclusions can be drawn immediately - the change of trim ($-\Delta C_m$) needed to bring the pitch rate to zero increases dramatically with lift coefficient and, since wing loading (W/S) does not vary very much with aircraft size, larger aircraft need larger changes in trim. Although this simple analysis cannot be applied to the incidence range covered in the stalling manoeuvre the two conclusions quoted are believed to remain valid.

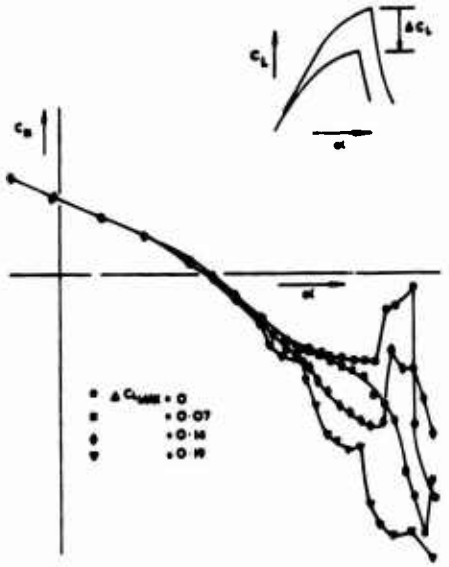

FIG 8 EFFECTS OF STALL FIXES ON MAXIMUM LIFT

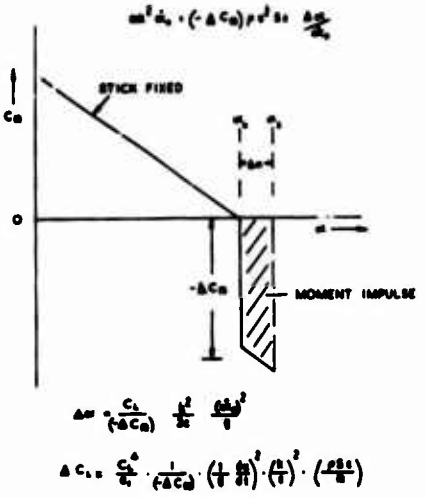

FIG 9 IMPULSE NEEDED TO COUNTER ANGULAR MOMENTUM IN PITCH

The deep-stall, or superstall, problem for aircraft with high-set tailplanes is due to the loss of stability and tailplane effectiveness at high incidence, resulting from the tail remaining in the low-kinetic-pressure wakes from the wing and aft nacelles (Fig. 10). This can result in the incidence increasing (due to rotation and rate of sink following the stall) until the aircraft stabilises at a high incidence (i.e. becomes lock-in a deep stall) when the tail emerges from the wake.

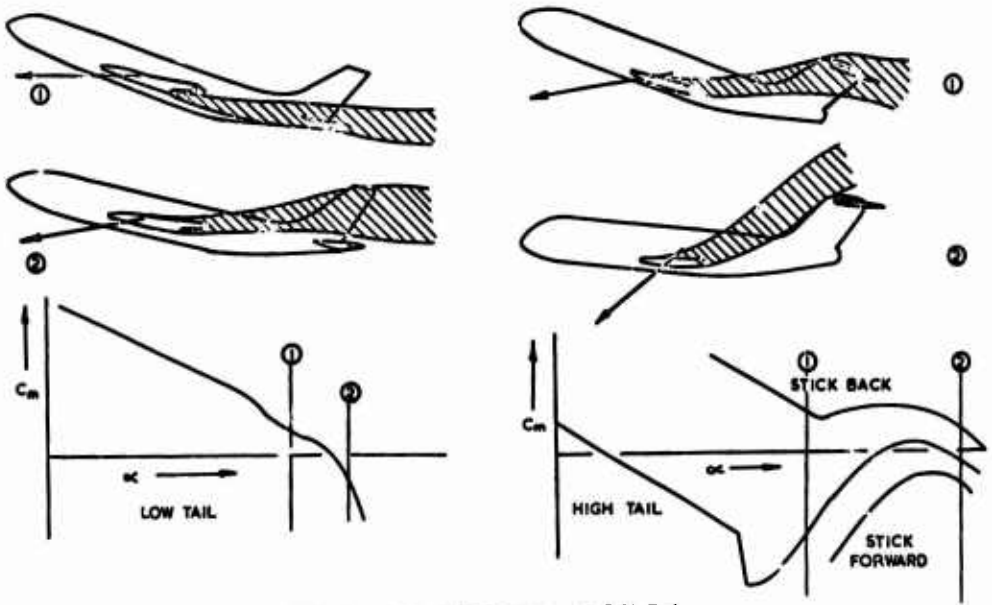

FIG. 10 THE SUPERSTALL PROBLEM

The flight dynamics of the post-stall motion are quite complex[5,6] but, by analogy with the simple level-flight pre-stall analysis leading to equation 2, it can be seen that the designer must provide a means of obtaining sufficient nose-down pitch impulse to prevent the aircraft entering a deep stall. With some

aircraft part of this nose-down impulse is applied by the automatic application of a stick-pusher.

The specialist lecture by Mr W McIntosh deals with an aircraft with a low tail but will cover the flight-dynamic problems I have mentioned and their impact on aircraft design.

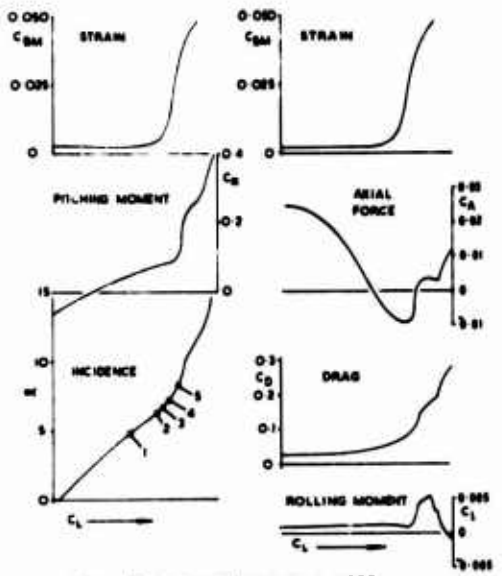

FIG.11 VARIATIONS OF FORCES ON A MODEL NEAR LIMITING LIFT (M=0·8)

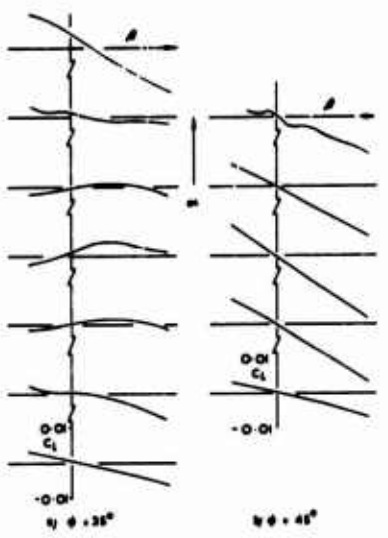

FIG.12 VARIATIONS OF ROLLING MOMENT WITH ANGLE OF SIDESLIP OVER A RANGE OF INCIDENCE (M=0·8)

In contrast to the situation at low speeds, the phenomena which limit useable lift at high subsonic speeds are both more varied and more complex. As already mentioned, the lift coefficient may not reach a maximum value but the separation of the airflow over the wings leads to irregular variations of overall forces with incidence and to unsteady excitations. Some of these effects are shown in Fig. 11 which gives plots of results from wind-tunnel tests of a conventional force model of a wing-body combination with a wing of 40° sweep. The graphs at the top of the figure show the variation of the narrow band-width root-mean-square dynamic strain at the wing root, plotted against lift coefficient. The plots lower down show the variations of pitching moment, incidence, axial force, drag and rolling moment at zero sideslip. The various stages of flow breakdown corresponding to points 1 to 5 on the incidence plot are shown in Fig.13.

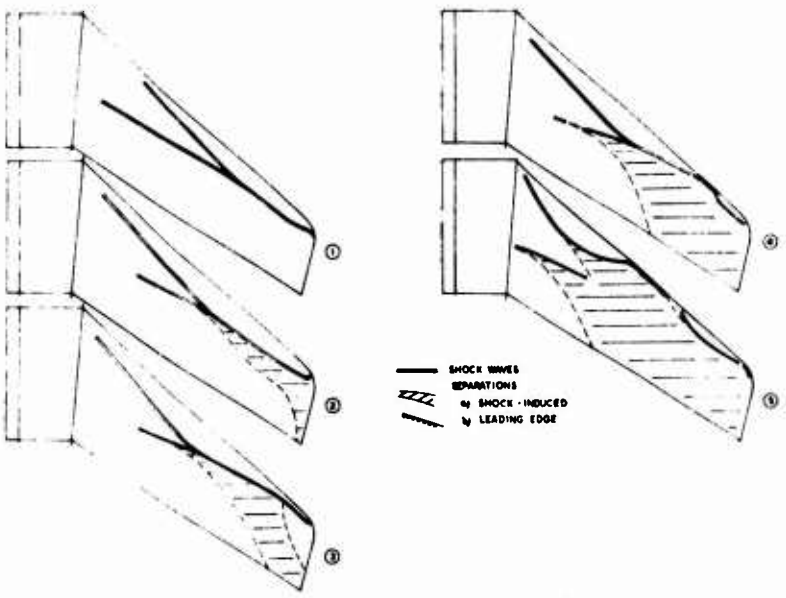

FIG 13 WING FLOW PATTERNS NEAR LIMITING LIFT (M=0·80, Φ=40°)

It can be seen that the collapse of the flow over the outer wing has resulted in a marked pitch up and a dramatic increase in drag but a combat aircraft with this type of wing would have sufficient tailplane power and engine thrust to prevent these factors limiting the manoeuverability and we must look for another possible cause. Buffet, is of course, a possibility and the RMS wing-root strain which is a measure of the response of the model to buffet excitation[7], clearly shows a significant rise in excitation. The rolling moment excursion shows a tendency to flow asymetrically but it is none too obvious how significant this might be. Moreover, measurements of rolling moment over a range of angles of sideslip (Fig. 13) show that there may be dramatic changes in the value of C_{l_β} (lv) well before the moment at zero sideslip is affected. The other lateral derivatives change in a similar manner and at very high incidence there may be significant hysteresis during a (quasi-steady) sideslip excursion.

These wind-tunnel data, which are thought to be fairly typical for wings of this thickness ($.09 \leq t/c \leq .11$) and sweep $35^\circ \leq \beta \leq 45^\circ$), indicate that, for the aircraft, the onset of wing buffeting will give an indication of the approach to limiting lift conditions but either buffet or some form of stability and handling problem will determine the maximum useable lift.

C Hwang and W S Pi have recently published the results of their measurements of the dynamic and aeroelastic response of a F5A aircraft in high-g wind-up turns[8]. These show that, for this aircraft, which has a wing sweep of 25°, buffet onset gave the pilot warning of flow separations near the wing tip and that, as the incidence increased there was a rapid build up of rigid-body oscillations (described as "wing rock") and structural vibration (buffet). The pilot terminated the turn and returned to level flight when the vibrations and oscillations prevented him controlling the manoeuvre. In their report of similar measurements with a F111A aircraft at 26° sweep, Benepe, Cunningham and Dunmyer[9] do not say what factor limited the manoeuvres but they draw specific attention to the asymmetry of the buffet response.

The sum of our present knowledge indicates that the manoeuvering capability of swept-wing combat aircraft will be limited by buffet and/or by a buffet-related loss of lateral stability. The lateral stability phenomena are usually described by pilots as wing rock, wing drop or nose slice.

Buffeting is a structural vibration which is often defined as the structural response of the aircraft to the aerodynamic excitation produced by separated flows[7]. The dynamics of the response will be discussed by Mr J G Jones in his specialist lecture, but I should like to draw your attention to the block diagram (Fig. 14), illustrating the interaction between response and excitation, which he presented at the AGARD Specialists' meeting at Lisbon in 1972[10]. The main thing to notice is that the motion is influenced by structural inertia, stiffness and damping as well as by the aerodynamic forcing and damping. However the essential feature of buffeting is that it arises from an increase in the level of the aerodynamic forcing. This is in contrast to the phenomenon known as stall-flutter[11], which gives structural vibrations under much the same conditions as buffeting but these are due to a reduction in aerodynamic damping to negative values.

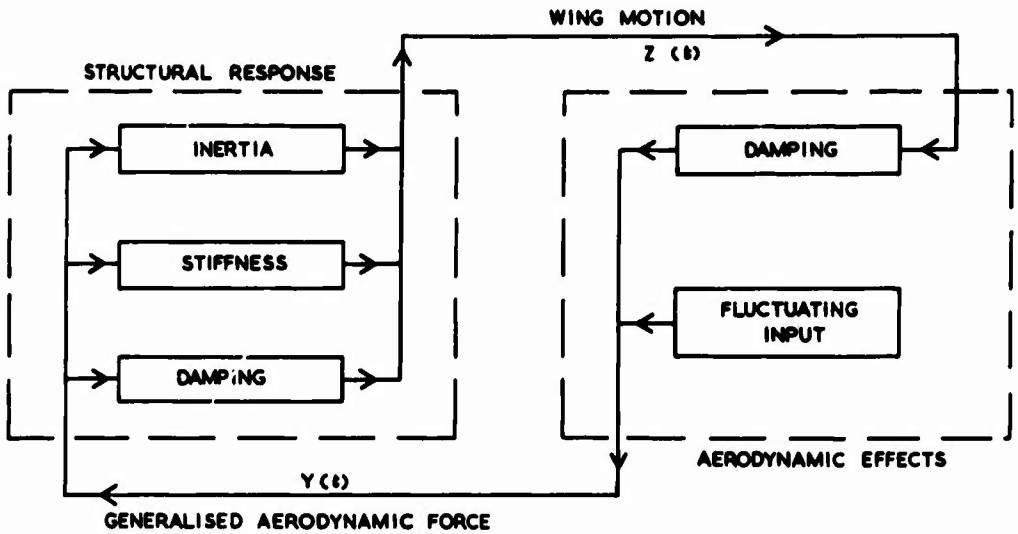

FIG. 14 BLOCK DIAGRAM FOR STRUCTURAL BUFFETING

Wing rock, wing drop and nose slice describe rigid-body motions of the aircraft. The general block diagram for these dynamics (Fig. 15) contains aerodynamic stiffness and damping and possibly an aerodynamic forcing term but only the one non-aerodynamic term - inertia. Mr D E Shaw will give a detailed discussion of these motions and their probable causes in his lecture but I do not think I will be detracting much from his contribution if I make a few general points. The motion described as wing rock could be the rigid-body equivalent of buffeting (i.e. a response to aerodynamic forcing) or it could result from a sudden loss in damping. Wing dropping is presumably initiated by the sudden loss of lift on one wing but the divergence in roll following this lift loss must be due to a low stiffness in roll, which would result from the stalling of the outer portions of the wing. Nose slice is again a divergent motion and must have as its root cause a loss of stiffness. Of course all these phenomena

relate to lateral/directional stability whereas at low speed it is the longitudinal motion which governs the useable lift.

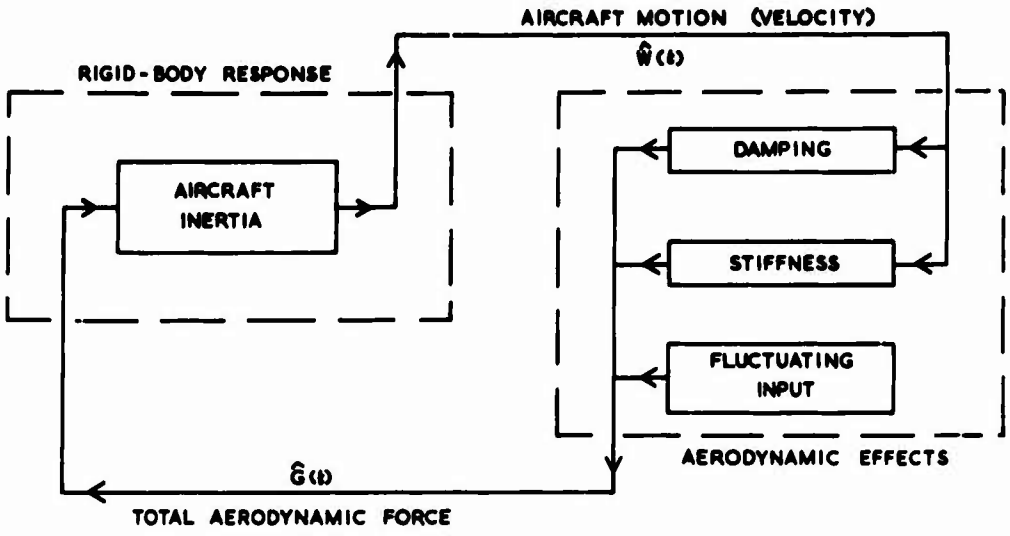

FIG. 15 BLOCK DIAGRAM FOR RIGID-BODY DYNAMICS

The unifying aspects of all the factors which limit the useable lift at high speeds are that they are all responses in the dynamic sense (i.e. motions) and that it is the pilot's reaction to these motions which determines the limit of the manoeuvre. The extent to which the pilot can cope with the vibrations, oscillations and divergence depends on training and the nature of the task he is faced with. It follows that, in contrast to the situation at low speed, the limits on useable lift at high speed may be rather variable, with the pilot being willing and able to achieve higher limits in evasive manoeuvres than in attack, for he has a high work load and needs to perform a precise tracking task (Fig. 16). However, since buffeting is a structural response, the level of vibration felt by the pilot depends on his position relative to the nodal lines of the modes and he may not get any real appreciation of either the punishment being dished out to the structure or the vibration levels to which various pieces of essential instrumentation are being subjected. This latter aspect has been considered by Dr H John in a recent AGARD report[12] and he will refer to it in his lecture.

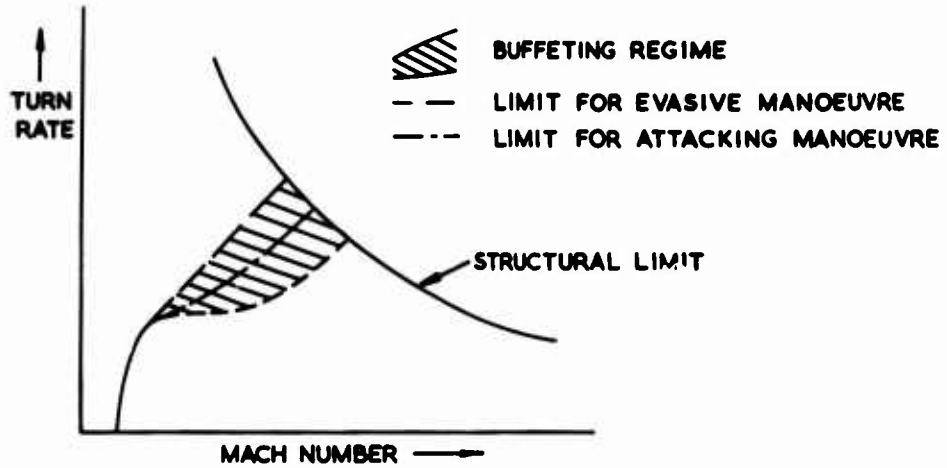

FIG. 16 MANOEUVRABILITY LIMITS FOR COMBAT AIRCRAFT

As a further contribution to the general discussion of buffeting and related phenomena I should point out that it has been widely observed that the rate of build-up of the buffeting response with incidence decreases with increasing sweep-back of the wing. Although this implies that the amount of buffet penetration (i.e. the difference between maximum useable lift and lift at buffet onset) must be less for the lower sweeps (in general), it is by no means universally the case that buffeting is a limiting factor for wings of low sweep - as was shown by the flight tests of the F-5A[8].

Because of their low structural load factors, civil transport aircraft present difficult vehicles for detailed flight experiments on lift limitations at high speeds and I know of no published data on the relative importance of the structural and rigid-body responses for this type of aircraft. The airworthiness regulations define two levels of buffet response (see Table 2) but make no specific reference to rigid-body phenomena at high speeds and high lift. However, it seems plausible that strength limitations and the structural and inertial characteristics of these aircraft (particularly the larger ones) would swing the balance in favour of buffeting as the limiting factor.

FAR	Significant Buffet	Buffet of intensity such that the pilot would be considered likely to modify the manoeuvre which causes the buffet
FAR	Maximum Demonstrated Buffet	Maximum buffet intensity which has been demonstrated to cause neither loss of control nor structural damage
BCAR	Buffet onset	The lowest level of buffet intensity consistently detectable during normal acceleration demonstrations in smooth air conditions
BCAR	Maximum Demonstrated Buffet	The maximum level of buffet intensity at which it has been shown in flight tests that controllability and structural integrity are unimpaired

Table 2. Definitions of buffeting intensity for civil aircraft

4. SOME FLUID-MECHANIC AND AIRCRAFT-DESIGN ASPECTS

From what I have said already about the low-speed stalling of swept-winged aircraft you will have deduced that the upper limit to the maximum useable lift is set by the stalling of the outer wing. The importance of the low-speed stalling performance is so great that the outer wing is usually designed very carefully to have quasi two-dimensional flow and to achieve the full maximum-lift potential of the wing section and its high-lift devices. Hence the fluid mechanics we are concerned with are essentially two-dimensional and the classical exposition of McCullough and Gault[13] provides the basic starting point. Fig. 17 (after Foster[14]) shows some features of the three types of stall they identified. The short bubble type (3) and the long bubble stall (2) are due to separation of a laminar boundary layer under the steep adverse pressure gradient which follows the sharp suction peak near the leading edge of uncambered aerofoils of low thickness chord ratio. The long bubble only occurs on very thin aerofoils and the short bubble stall is unlikely to be found at high Reynolds numbers. Wing sections designed to avoid very high section peaks near the leading edge will, in general, experience stalls which develop from separation of the turbulent boundary layer near the trailing edge. These sections will have higher maximum lifts than those stalling at the leading edge and hence a trailing edge stall (type 1) should be the design aim. The question what is the optimum upper surface pressure distribution (i.e. what shape of pressure distribution gives the greatest lift with attached flow) appears to have been answered first by Liebeck[15] who utilised Stratford's work on the separation of turbulent boundary layers[16]. The optimum pressure distribution has a suction plateau extending from the leading edge over a significant proportion of the chord, with the recompression to near freestream conditions following a relaxing pressure gradient, of the type devised by Stratford to continuously just avoid separation. The optimum length of the plateau depends on Reynolds number and transition position. Mr A M O Smith will discuss these flows in detail in his lecture but, as an appetiser, I will show you a result obtained by D J Weeks at the RAE just before Liebeck's paper was published. Here (Fig. 18) you can see the shape of an optimum pressure distribution and also how that shape can be obtained, fairly closely, by application of nose camber. Of course this camber would be most unsuitable for other conditions of flight but since it is confined to the first 20% of wing chord, it could be obtained by application of a variable-camber mechanism such as RAEVAM[17].

At low speeds however nose camber is less effective than a well designed slat but all leading-edge devices suffer from the disadvantage that, on their own, they simply delay the stall to higher incidences. There are very practical reasons why aircraft incidence is limited and for this reason it is usual, for landing and take off, to use slats in conjunction with trailing edge flaps (which increase the lift at constant aircraft incidence). The most efficient arrangement of slats and flaps uses slots connecting the upper and lower surfaces at the slat-wing, wing-flap and flap-flap junctions.

The precise fluid mechanics of these slots has only recently been explained. Foster et al[18] have shown that, for a wing section with a slotted flap, the lift at constant incidence decreases with increasing slot gap according to calculations for inviscid flow. In real flow the lift increased with gap until a well defined maximum is reached, thereafter it decreases (Fig. 19). The maximum lift is obtained when the mixing of the wake from the main portion of the wing with the boundary layer on the flaps is delayed to near the trailing-edge of the flap. The action of slots, therefore, is to break up the long region of adverse pressure gradient, which extends from near the nose of the aerofoil to the trailing edge, into a number of short lengths each having its own boundary layer growing, more or less, uncontaminated by the other boundary layers and their wakes (Fig. 20). The proper use of slots allows very high peak sections to be obtained without separation, as is shown in Fig. 21. This is a case where the slat carries 35% of the total lift. Both the slat flow and the flow at the rear of the main wing are close to separation. Slat stall could be avoided by increasing the slat angle. The lift at constant incidence could be increased by increasing the angles of the flap and tab but this risks stalling them.

In applying slotted high-lift devices to practical wings great care has to be taken in the design of the supporting brackets, as the wakes from the brackets can provoke premature separation.

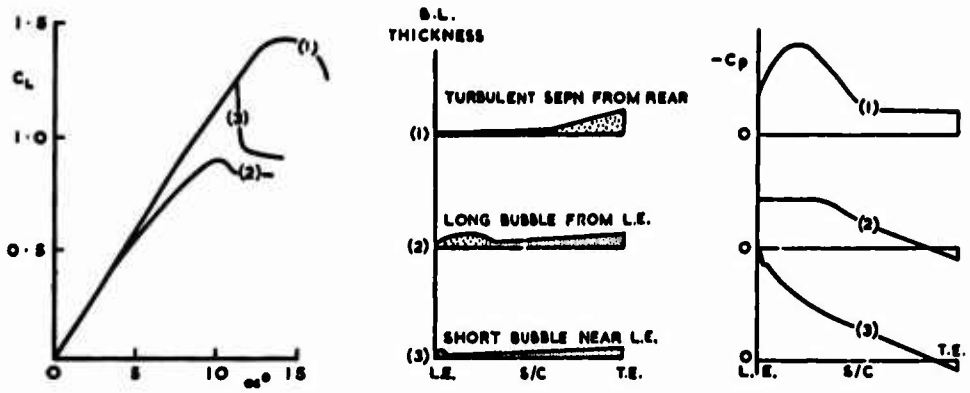

FIG.17 STALLING CHARACTERISTICS OF SINGLE AEROFOILS (DIAGRAMMATIC ONLY)

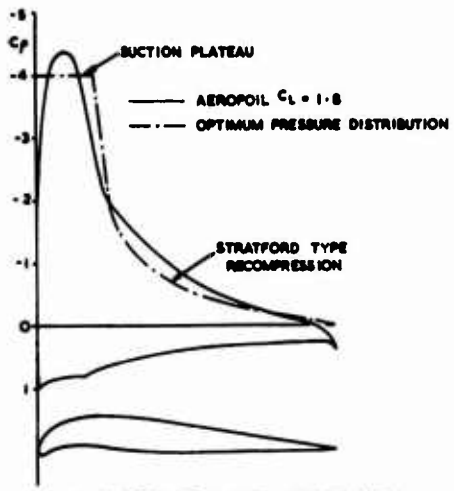

FIG. 18 AEROFOIL WITH NOSE CAMBER FOR OPTIMUM PRESSURE DISTRIBUTION

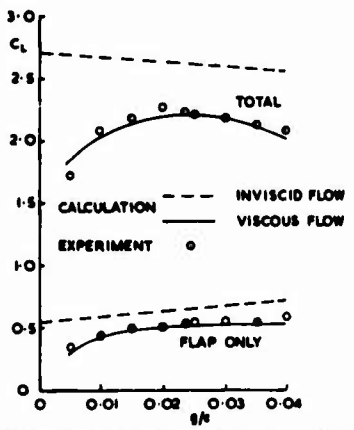

FIG.19 LIFT ON AN AEROFOIL WITH SLOTTED FLAP AS A FUNCTION OF FLAP GAP

As might be expected the flows over finite wings near limiting lift at high speeds are appreciably more complicated. Fig. 13 shows some examples. Wings of lower sweep would have regions of quasi-two-dimensional flow near mid-span, with forward movements of the shock wave near the root and tip, while for higher sweeps the flow might be dominated by part-span vortices. However, since the aim of the aircraft aerodynamicist is to achieve most of the potential performance of the equivalent two-dimensional section in the design of his finite wing, I think I should begin my introduction to the fluid-mechanics of flows at high speed by saying something about the flows over aerofoils at incidences near that for the first appearance of separation. The equivalent two-dimensional section and equivalent free-stream Mach number for a swept-back wing are defined in Fig. 22. Figure 23 shows typical envelopes for separation onset on aerofoils of medium thickness.

I have already mentioned that at low speeds and high incidence the single aerofoil develops a very sharp suction peak close to the leading edge. With increasing Mach number the flow near the nose becomes supersonic ($C_{p^*} \Phi$ - 10 for M_∞ = 0.25) and the general tendency is for the peak to broaden and flatten. Part of the initial recompression develops into a shock wave which moves further back on the chord with increasing incidence. With the older type of aerofoils the pressure distribution behind the

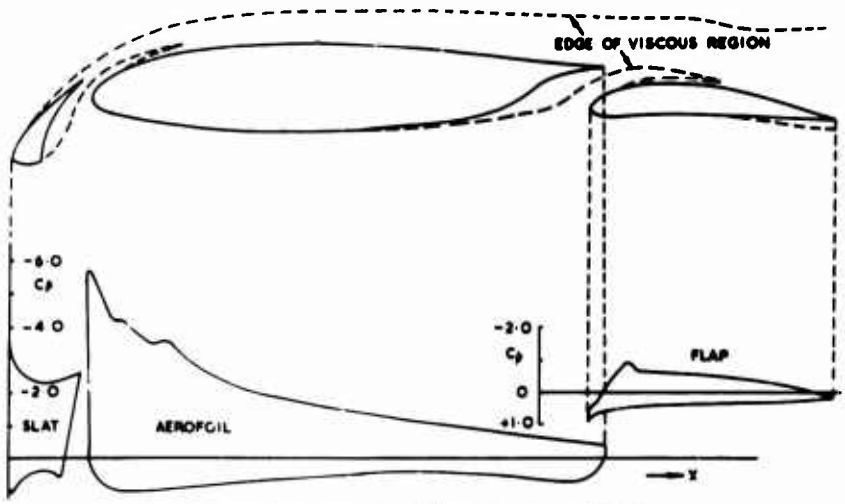

FIG 20 FLOW AROUND AEROFOIL WITH SLAT & FLAPS

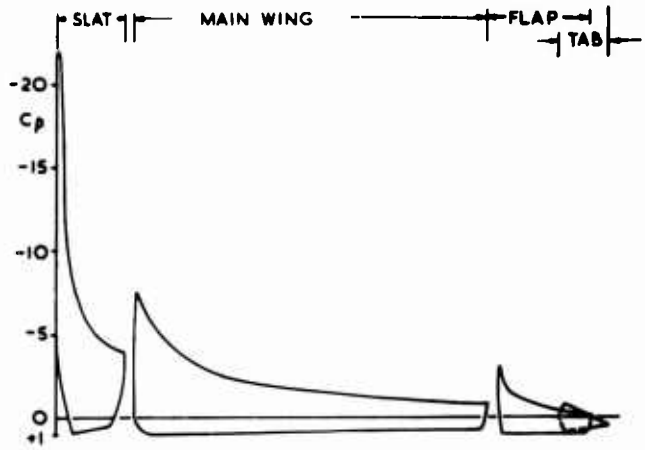

FIG 21 PRESSURE DISTRIBUTION ON WING WITH SLAT AND FLAP, NEAR THE STALL

shock wave by the relaxing pressure gradient (Fig. 24) and the initial separation forms as a bubble at the foot of the shock. With increasing incidence this bubble grows rapidly in extent until it approaches the trailing edge. It then provokes a rapid divergence of the trailing edge pressure and a collapse of the flow. The region of separated flow is, of course, a source of buffet excitation. This type of flow development was termed "flow model A" in a classic paper on scale effects by Pearcey, Osborne and Haines[18]. Again, for the older types of wing sections, this type of separation is typical of flows for both limbs of the C_L vs M envelope for separation onset, although typical pressure distributions change from having modest amounts of isentropic recompression upstream of the shock to monotonically expanding flows up to the shock (Fig. 24). Since for these sections the initial separation is directly due to the shock, the high-lift performance can be improved by reducing the strength of the shock wave, for a given lift coefficient. This can be achieved by designing the upper surface to have a measure of isentropic compression upstream of the shock with a further aft shock location. This is more effective at Mach numbers at the upper end of high-lift range (i.e. $M_1 \geq M_2$ in Fig. 24), and usually requires an increase in leading-edge radius with a marked reduction in upper surface curvature farther back[20]. At lower speeds a reduction in the peak suction level near the leading edge (by nose camber) is beneficial. To a certain extent these modifications are conflicting and a careful balance has to be struck.

The latest type of wing sections are designed with the aid of powerful theoretical methods[21,22] and combine extensive regions of supersonic flow upstream of the shock with large amounts of rear loading (Fig. 25). This type of design is heavily biased to improving the high-speed end of the separation envelope (Fig. 23). As shown in Fig. 25, high suction levels develop at the lower Mach numbers and separation might be expected to start at the trailing-edge, due to the severe adverse pressure gradient there. However, in these cases it seems that the trailing-edge separation is partly provoked by the bubble under the shock. This is an example of Pearcey's model B1 flow [19].

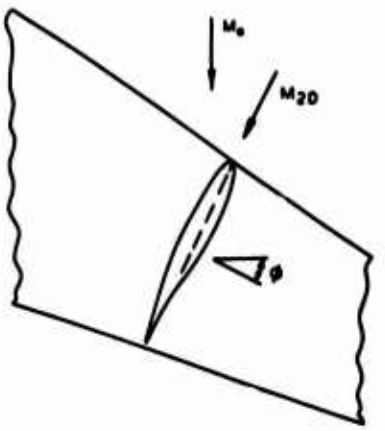

$M_{2D} = M_\infty \cos\phi$

$\left(t/c\right)_{2D} = \left(t/c\right)\sec\phi$

$\left(C_L\right)_{2D} = C_L \sec^2\phi$

FIG.22 EQUIVALENT TWO-DIMENSIONAL SECTION FOR SWEPT WING

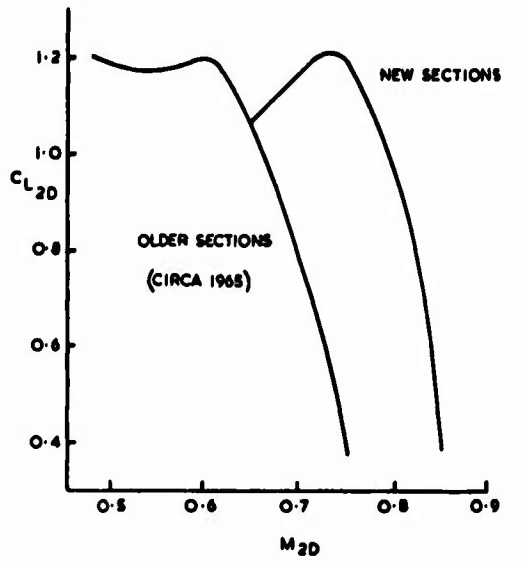

FIG. 23 C_L vs M FOR SIGNIFICANT SEPARATION ON SECTIONS WITH MODERATE THICKNESS

At Mach numbers close to M_2 in Fig. 25 an increase in incidence increases the suction levels for the plateau upstream of the shock and causes the shock to move back on the aerofoil. The re-expansion following the shock appears to be modified by the separation bubble and the flow separates at the trailing edge when the shock reaches the crest of the re-expansion.

Wing sections in current use fall half-way between the two types I have mentioned, having less rear loading and less supercritical lift at separation-onset than the modern section in Fig. 25. They represent a class of aerofoil for which, except possibly at high Reynolds numbers, rear separation will occur before the bubble separation reaches the trailing edge. They therefore provide examples of Pearcey's Model B flow[19].

Well designed wings of moderate to high aspect ratio (i.e. greater than 5) and lowish sweep ($\phi < 30^\circ$) still exhibit flow separations typical of their equivalent two-dimensional sections. The initial separation, leading to buffeting, is likely to occur either on the outer wing, where the local lift coefficient reaches its maximum value, or where the main shock wave loses sweep, due to the effects of planform kinks or the influence of the body. When the shock is swept more than about 30° the spanwise flow component causes the bubble separation to roll up into a vortex which at high incidence breaks away from the line of the shock and sweeps obliquely across the wing. Sweepback of the trailing edge leads to a thickening of the boundary layer there, due to crossflows and the lengthening of the path swept out by the surface streamlines. This results in loss of rear loading and an increased tendency to separation. Both vortices and boundary-layer thickening are evident in the flow diagrams in Fig. 13. The diagrams also show that pockets of supersonic flow develop outboard of the first part-span vortex, new vortices form under the shocks there and, with increasing incidence, the flow pattern moves progressively inboard. At lower Mach numbers and/or higher sweeps this tendency to multiple vortices increases. Moreover, it should be noted that this type of flow development results in severe increases in drag. The bubble vortex appears to generate more lift on a spanwise section than its equivalent bubble in two-dimensional flow and it also inhibits the spanwise drift of the boundary layer, inboard of where it crosses the wing trailing edge.

Although several investigations of buffeting excitation have been made, there is little published data on the fluid-mechanics of the aerodynamic excitation. Some results of measurements of fluctuating pressures, however, have been presented by Lemley and Mullans[23], Hwang and Pi[8], Monnerie and Charpin[24], John[12] and by Mabey[7] (who summarised the work of Koss and Mundell). The indications are that rear separation does not contribute significantly to buffeting - the major excitations occur under the shock waves, vortices and extensive regions of separation. There is a possibility that significant fluctuations in local normal force could be generated, in Pearcey's model B flows[19], by the time-lag between increasing shock strength and trailing-edge separation. The potential magnitude of such fluctuations would be proportional to the divergence of the local normal-force curve from the extrapolation of its shape prior to separation onset (Fig. 26). This type of excitation could only be detected by a specific analysis of one or more chordwise distributions of pressure fluctuations and no such investigation has yet been reported. However the proportionality of buffeting force to the divergence of overall lift has been reported by Bore[25].

The magnitude of buffeting excitation (the fluctuating input in Fig.14) is the product of the narrow-bandwidth RMS pressure fluctuations and the normalised wing deformation in the mode under consideration. Hence we should expect that, for a given level of pressure fluctuation, the response of the wing in its first bending mode would be greater at lower wing sweeps (when the locus of the shock and its bubble separation lies normal to the nodal line) than at high sweeps (when the vortices cross the wing

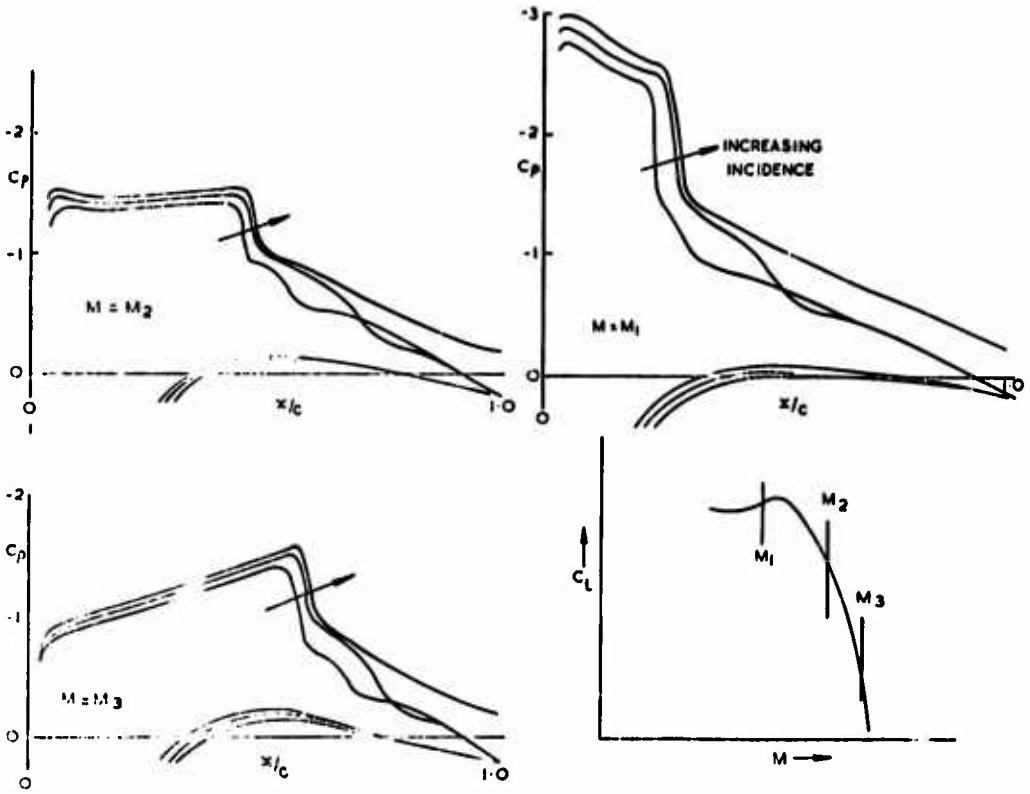

FIG 24 SEPARATION ONSET FOR THE OLDER TYPE OF WING SECTION

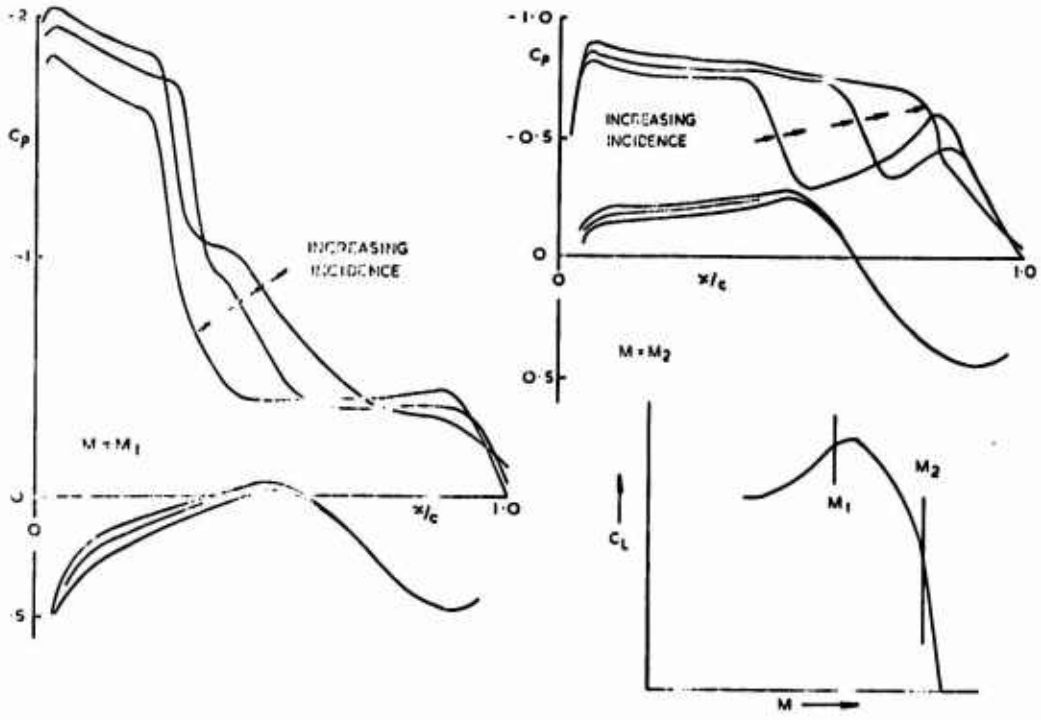

FIG 25 SEPARATION ONSET FOR A NEW WING SECTION

obliquely. This is probably why wind-tunnel measurements of R'S wing-root-strain show more rapid increases of model response with lift coefficient for wings of lower sweep. We should also expect that the relative importance of the higher modes of wing deformation will increase with increasing sweep.

Monsieur Ponnerie will be telling you more about these very complicated and varied flows in his specialised lecture. However before finishing this part of my talk I would like to make a brief reference to the fluid-mechanics of slats and variable camber at high speeds. The efficacy of leading-edge devices in improving useable lift at high speeds is well recorded in the literature[26,27,28] and a discussion of their fluid mechanics when applied to wings of moderate thickness has been given by Foss, Haines and Jordan[17].

At low speeds a well-designed slat is superior to nose camber because it effectively isolates the boundary layer on the upper surface of the main part of the wing from that on the slat upper surface and, in consequence, allows higher suction peaks to develop on the slat; whereas nose camber suppresses the suction peaks at the nose to avoid separation. The ability of the slat to carry high suctions is diminished with increasing Mach number by shock-induced separation. The main benefit derived from the deployment of the slat is the reduction in suction levels, compared with these for the plain wing, and hence its effectiveness in delaying separation onset may owe little to the flow through the slot as is shown in ref. 17. However it was found that slats (with open slot) are effective in halting the forward movement of the shockwave at a position 10% to 15% behind the slat trailing edge, until the flow separates on the slat. This maintains shock sweep and helps the growth of lift beyond separation onset. It seems likely that slats on wings of medium thickness should have a very beneficial effect on lateral stability at high lift as they have on thin wings[26].

5. SLENDER-WING AIRCRAFT

In my introductory remarks on maximum useable lift I promised to say something about aircraft other than the classical swept-winged variety shown in Fig. 1. The first type I will deal with is slender aircraft[29]. Some examples are shown in Fig. 28. The distinction between slender aircraft and swept-winged aircraft with very high angles of sweep is that the former are designed to have flow separation from the leading-edges of the wings over their entire operating range. Ideally the leading-edge separations should develop regularly with change of incidence and only one primary vortex should form above each wing leading edge[30]. In practical applications of the slender-wing concept however it is usual to have part of the fuselage extending forward of the wing leading-edge apex and unless chines (Fig. 28c) or moustaches (Fig. 28a) are fitted, irregular body vortices may develop on the leeward side of the aircraft nose at high incidences.

Distinctive features of this type of aircraft are its low lift-curve slope and the absence of a lift maximum in the range of incidences likely to be reached by the aircraft. The low aspect ratio and low thrust force on the wings lead to very high drag at high incidence. Consequently there is a flight speed at which the aircraft can only just maintain altitude due to thrust limitations. This speed, which is known as "zero rate of climb speed"[31] can provide the same datum for speed margins on approach and take-off as the "minimum speed in the stall" provides for swept-winged aircraft. Other limitations on maximum useable lift may come from stability and control considerations i.e. that control of the aircraft shall not require undue piloting effort nor unusual piloting skill. The tendency for slender wings of quasi-delta planform to exhibit a gradual nose-up change of trim can be counteracted by the use of an artificial pitch stabiliser and then the main problem is lateral stability. This is associated with the high angle of incidence of the aircraft and the shedding of vortices from the forward fuselage. The chines and moustaches referred to earlier help to stabilise the separation locii for the body vortices and increase the useable incidence.

The rapid changes in pitching moment in Fig. 17 are associated with the forward movement of vortex breakdown to the trailing edge of the wing. The breakdown, or bursting, of the vortices from the wing leading edges has been explained by Lambourne and Bryer[32]. It clearly imposes a limit to the useable lift of the aircraft. Experiments have shown that the incidence for vortex breakdown can decrease quite markedly with increasing angle of sideslip.

The leading-edge vortices are also a source of buffet excitation on slender wings. The phenomenon was investigated quite intensively in the mid-to-late sixties[7], during the early development of Concorde. A variety of measurements were made on wind-tunnel models including unsteady wing strain on both solid and aeroelastic models[33] and unsteady pressure measurements[34,35]. Dr John in his specialist lecture will talk about the use of these techniques for swept-winged aircraft. Both tunnel and subsequent flight measurements have shown that, at incidences below incidence bursting, the buffeting is very mild and imposes no limit on useable lift. Since the strength of the vortices decreases with increasing Mach number high speeds present no additional problem.

6. HYBRID CONFIGURATIONS

The other type of aircraft I ought to refer to combines leading-edge vortex flows with the advantages of lifting capability of swept-wings, Figs. 29 and 30. There is little published information on the aerodynamics of these configurations but it seems likely that the chines, or strakes, which extend forward from the wing leading edges to near the nose of the aircraft could improve the manoeuvre performance in a number of ways. Firstly they will stabilise the vortices shed from the body at high incidence - improving lateral stability. They could also increase the lift on the forebody and, although this would tend to give a progressive forward shift in the centre of lift with increasing incidence, the trimming action of the tailplane would be more favourable (i.e. less negative lift) than for conventional configurations. At high subsonic speeds the chines and their vortices could improve the wing design problem both by increasing the effective twist of the wing (i.e. increasing the induced upwash near the wing/chine intersection) and by softening the body effects which give rise to the traditional two-shock system near the fuselage of a conventional design[36]. It also seems that the vortices from the chines tend to suppress separation on the outer wing panels by reducing the outflow[27]. This suggests that they may be best used in conjunction with wings of lowish aspect ratio and low trailing-edge sweep. An increase in the sweep of the chine to 90° before it meets the wing leading edge seems to be an essential feature.

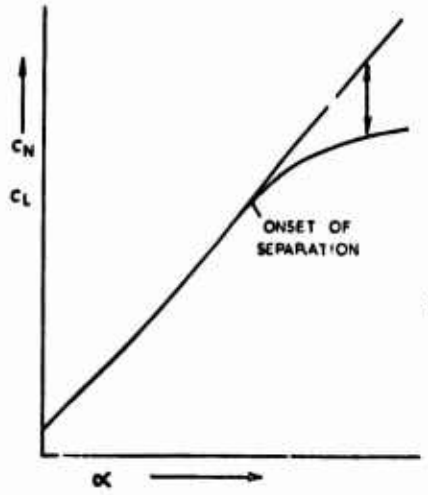

FIG. 26 NORMAL FORCE/LIFT DIVERGENCE BEYOND SEPARATION ONSET

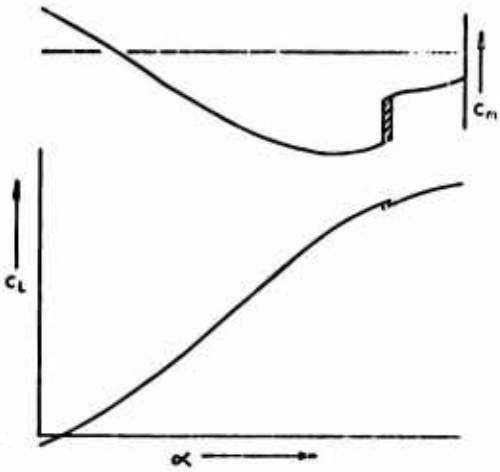

FIG. 27 C_L vs α, C_m vs α FOR A SLENDER-WING-BODY

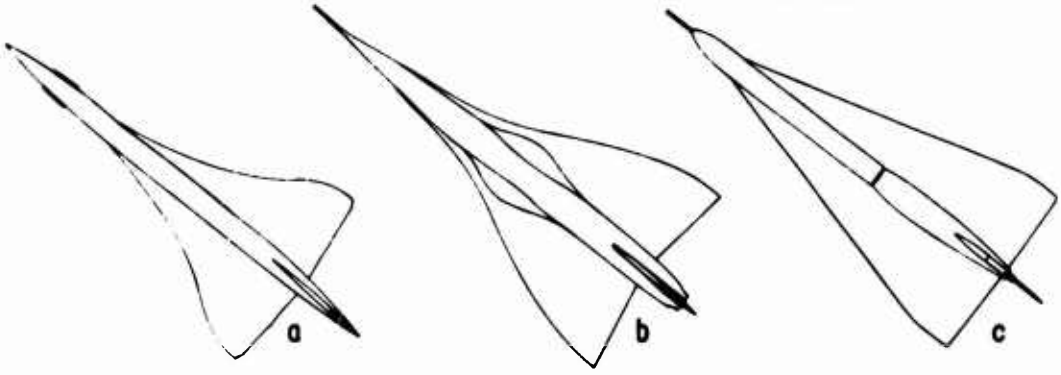

FIG. 28 SLENDER AIRCRAFT

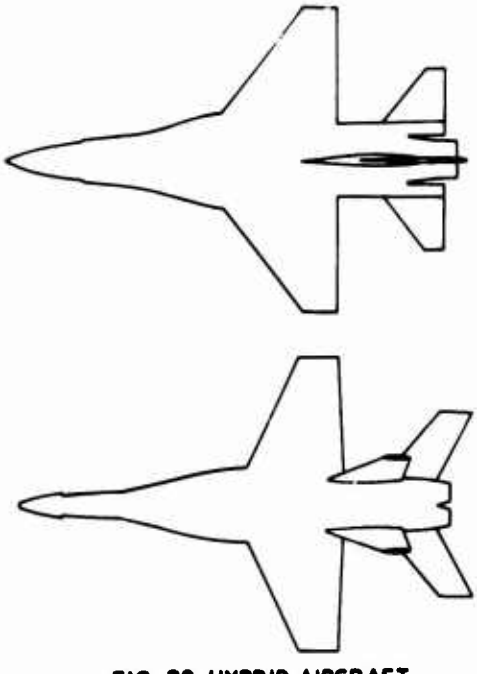

FIG. 29 HYBRID AIRCRAFT

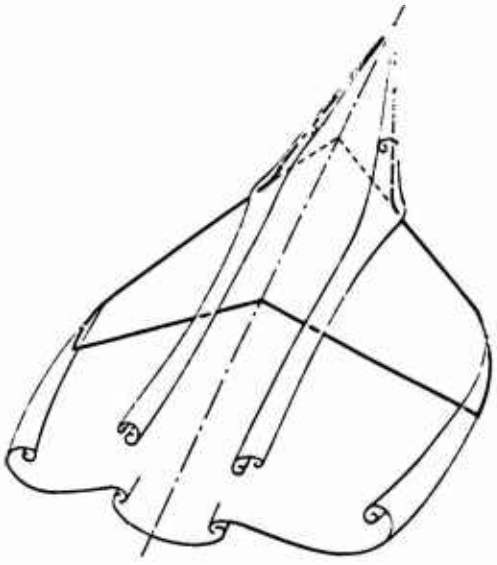

FIG. 30 VORTEX SHEETS FOR A HYBRID CONFIGURATION

7. ACKNOWLEDGEMENT

In writing this introduction and overview I have drawn freely on the material and experience of the lecturers for this series and of my colleagues in the United Kingdom - to them my appreciation and thanks.

8. REFERENCES

1		Third Dynamics of Aircraft Stalling. AGARD Conference Proceedings CP102 April 1972
2	J.J. Schurenga	Aerodynamics of wing stall of the Fokker F28 AGARD-CP-102 (paper 20), November 1972
3	R. J. Shevell R. D. Schaufele	Aerodynamic design features of the DC9 Journal of Aircraft, Vol. 3, No. 6, Nov-Dec 1966
4	D. Isaacs	Wind tunnel measurements of the low speed stalling characteristics of a model of the Hawker-Sidieley Trident 1C RAE Report 6810 (1961) ARC R&M
5	R. L. Montgomery M. T. Noul	Analysis of deep-stall characteristics of T-tailed aircraft configurations and some recovery procedures Journal of Aircraft, Vol. 3, No. 6, Nov-Dec 1966
6	H. H. M. M. Thomas John Sullingbourne	Longitudinal motions of aircraft involving high angles of attack RAE Technical Report 73011 (1973)
7	D. T. Mabey	Beyond the buffet boundary Aeronautical Journal (Supplementary Paper), April 1973
8	C. Hwang A. S. Pi	Transonic buffet behaviour of Northrop F-5A aircraft AIAA Report No. 624, September 1974
9	D. B. Benepe A. M. Cunningham Jr. W. D. Dunmyer	A detailed investigation of flight buffeting response at subsonic and transonic speeds AIAA Paper No. 74-358 (1974)
10	J. P. Jones	The dynamic analysis of buffeting and related phenomena AGARD-CP-102 (paper 23), 1972
11	L. L. Erickson	Transonic single-mode flutter and buffet of a low aspect ratio wing having a subsonic airfoil shape NASA Technical Note D-7546 (1974)
12	H. John	Critical review of methods to predict the buffet capability of aircraft AGARD Report No. 625, September 1974
13	S. B. McCullough D. E. Gault	Examples of three representative types of airfoil-section stall at low speed NACA Technical Note 2502 (1951)
14	D. W. Foster	The low-speed stalling of wings with high-lift devices AGARD-CP-102 (paper 11), 1972
15	R. H. Liebeck M. I. Ormsbee	Optimisation of airfoils for maximum lift AIAA Paper No. 69-739, July 1969
16	B. S. Stratford	An experimental flow with zero skin friction throughout its region of pressure rise J. Fluid Mech., Vol. 5, 1959
17	J. F. Moss A. B. Haines R. Jordan	The effect of leading-edge geometry on high-speed stalling AGARD Conference Proceedings, CP-102 (paper 15), April 1972
18	D. W. Foster F. R. Ashill M. R. Williams	The nature, development and effect of the viscous flow around an aerofoil with high-lift devices RAE Technical Report 72227, January 1973
19	H. H. Pearcey J. Osborne A. B. Haines	The interaction between local effects at the shock and rear separation - a source of significant scale effects in wind-tunnel tests on aerofoils and wings AGARD Conference Proceedings CP-35 (paper 11), September 1968
20	H. H. Pearcey	The aerodynamic design of section shapes for swept wings ICAS, Zurich, September 1960, published in Advances in Aeronautical Sciences, Vol. 3, Pergamon Press Ltd., 1960
21	F. Bauer P. R. Garabedian D. C. Korn	Supercritical wing sections (Lecture notes in economics and mathematical systems, No. 66) Springer-Verlag, Berlin, 1972

22	T. D. Taylor	Numerical methods for predicting subsonic, transonic and supersonic flow AGARDograph No. 187, 1974
23	C. E. Lemley R. E. Mullans	Transonic wind-tunnel and flight buffet pressures on a swept wing Journal of Aircraft, Vol. 11, No. 5, March 1974
24	B. Monnerie F. Charpin	Essais de buffeting d'une aile en fleche en transsonique 10eme Colloque d'Aerodynamique Appliquee de la AAAF, November 1973 (To be published in "Aeronautique et Astronautique")
25	C. L. Bore	Post-stall aerodynamics of the "Harrier" GR1 AGARD Conference Proceedings CP-102 (paper 19), April 1972
26	N. R. Burris D. E. Hutchins	Effect of wing leading-edge geometry on manoeuvering boundaries and stall departure AIAA Paper No. 70-904, 1970
27	E. J. Ray L. W. McKinney J. G. Carmichael	Maneuver and buffet characteristics of fighter aircraft AGARD Conference Proceedings CP-102 (paper 24), April 1972
28	P. J. Butkewicz	On airflow separation and buffet onset during fighter aircraft maneuvering AGARD Conference Proceedings CP-102 (paper 22), April 1972
29	D. Küchemann	Aircraft shapes and their aerodynamics for flight at supersonic speeds Aivances in Aeronautical Sciences, Vol. 3, Pergamon Press, 1962
30	E. C. Maskell J. Weber	On the aerodynamic design of slender wings J. Royal Aero Soc., Vol. 63, p.709, December 1959
31	W. J. G. Pinsker	Zero rate of climb speed as a low speed limitation for the stall-free aircraft RAE Technical Report No. 66144, May 1966
32	N. C. Lambourne D. W. Bryer	The bursting of leading-edge vortices - some observations and discussion of the phenomenon ARC R&M 3282, April 1961
33	D. G. Mabey	Measurements of buffeting on slender wing models ARC Current Paper 954 RAE Technical Report 66086, May 1966
34	C. G. B. Mitchell	Calculations of buffeting of slender wing aircraft at low speed RAE Technical Report 68165, 1968
35	D. A. Lowell T. B. Owen	Low-speed wind-tunnel measurements of surface pressure fluctuations on two slender-wing models RAE Technical Report 70168, September 1970
36	W. A. E. Rogers I. M. Hall	An introduction to the flow about plane swept-back wings at transonic speeds J. Royal Aero Soc., August 1960

REMARKS ON FLUID MECHANICS OF THE STALL

by

A.M.O. Smith
Chief Aerodynamics Engineer, Research
Douglas Aircraft Company
3855 Lakewood Boulevard
Long Beach, California 90846

LECTURE 1 BASIC THEORY

SUMMARY

The lecture is in two parts. The first describes much of the basic fluid mechanics phenomena that occurs with stall and separation. Some flow photographs of separation are presented together with general comments on the phenomenon. Limits to pressure rise for both laminar and turbulent flows are given as well as their general theory. Then comments are made about Reynolds number, Mach number, and airfoil shape effects upon separation. The second part of the lecture considers the more complete aerodynamic problem and especially shows diagrams that point out all the possible phenomena entering into a full aircraft stall and buffeting process. Some discussion is given of the problem of calculating flows with separation. The lecture is not particularly a review of existing information but important references are identified.

PRINCIPAL NOTATION

c	chord
c_f	local skin friction coefficient $\tau_w / \frac{1}{2} \rho u_e^2$
c_l	section lift coefficient
C_L	lift coefficient
C_p	conventional pressure coefficient, $(p - p_\infty)/\frac{1}{2} \rho u_\infty^2$
C_p^*	C_p for sonic flow
$\bar{C}_p$	canonical pressure coefficient, $(p - p_0)/\frac{1}{2} \rho u_0^2$
m	exponent in $\bar{C}_p = x^m$ flows
M	Mach number
p	pressure
q	dynamic pressures
R	Reynolds number ($= u_0 x/\nu$ in Stratford flows)
R_x	x-Reynolds number $u_e x/\nu$
R_θ	Reynolds number based on momentum thickness, $u_e \theta/\nu$
S	Stratford's separation constant (6.2), also wing area
u	velocity in x-direction
u_0	velocity at start of deceleration in Stratford and canonical flows
v	velocity in y direction
V	a general velocity
x	length in flow direction, or around surface of body measured from stagnation point, if used in connection with boundary-layer flow
	GREEK
α	angle of attack
δ	flap deflection, also boundary layer thickness
δ^*	boundary-layer displacement thickness
θ	boundary layer momentum thickness
ν	kinematic viscosity
ρ	mass density

SUBSCRIPTS

c chord

e edge conditions

o reference condition, as in Stratford flows

∞ reference condition at infinity

sep at separation

1. INTRODUCTION

In a "hard" science one could treat the problem by giving a few equations that covered a certain class of phenomena. They would predict known results. Furthermore, if one wanted to know answers for other conditions he would only have to enter new constants and boundary conditions into the descriptive equations and crank out the new answers. Consider Keplar's laws for instance. There are other sciences which are mainly descriptive, botany for instance. Unfortunately, the special science of stall and buffeting lies mostly in this later class, meaning that there are only a few facts that can be covered with any semblance of a law.

There is no dearth of work on the general subject, in fact, the literature is very large. The problem is that most experiments and observations tend to be isolated and do not fall under some kind of blanket analysis method. Contrast that situation with laminar boundary-layer theory. We know that the equations are nearly exact, so that if the boundary layer is thin, whatever the equations predict, must be right. That is, in order to predict, one need only know how to solve the governing equations. Because of lack of such unifying principles, stall and separation technology tends to be a collection of isolated experiences instead of a unified science. This disconnected collection makes it difficult to organize a talk and makes it difficult for engineers to make predictions, even though there is a large body of data.

The situation is epitomized by Chang's book on flow separation [1]. While it contains a great deal of information; like the science itself, it is really a disconnected series of articles rather than a unified treatise. This is not to be taken as a criticism of the book, because it is a very useful one. It is rather a criticism of the science. There are so many papers on the broad subject that it is impractical to do any more than mention some that the author thinks important. Because he has not really been a student of this subject, there are probably important oversights. Stalling was known by the Wright Brothers and flow separation even earlier; the earliest work we choose to mention here is that by B. M. Jones [2]. In 1972 AGARD sponsored a special conference on the Fluid Dynamics of Aircraft Stalling [3] that contained a wide variety of subject matter. This conference in fact is the antecedent of the present lecture series. An earlier one that also contains important subject matter related to the present lecture series is one on Separated Flows [4]. In addition, there are numerous expositions of the details of the separation process including state-of-the-art empirical correlations. One such paper is that by Chappell [5]. A broad picture of the state-of-the-art of predicting aerodynamic properties including stalling has been presented by Callaghan [6] in an earlier AGARD lecture series. In this connection we cite one of his figures to illustrate the present state of analytical capability, figure 1.

ANALYTICAL STATUS	TYPE OF METHOD	APPLICATION
FIRM ANALYTICAL FOUNDATION IN THREE DIMENSIONS	• 3 D LIFTING POTENTIAL FLOW SOLUTION • LIFTING SURFACE THEORIES	LIFT AND PITCHING MOMENT CHARACTERISTICS WHERE VISCOUS EFFECTS ARE NEGLIGIBLE
FIRM ANALYTICAL FOUNDATION IN TWO DIMENSIONS INCLUDING VISCOUS EFFECTS REQUIRES EMPIRICISM TO ADJUST TO THREE DIMENSIONS	• MULTI-ELEMENT AIRFOIL ANALYSIS METHODS • FINITE DIFFERENCE BOUNDARY LAYER SOLUTIONS	• LIFT AND PITCHING MOMENT CHARACTERISTICS WITH VISCOUS EFFECTS PRIOR TO FLOW SEPARATION • CLEAN CONFIGURATION SKIN FRICTION
EMPIRICAL TECHNIQUES COMBINING ANALYTICAL TOOLS AND EXPERIMENTAL DATA	• $C_{L_{MAX}}$ OF CLEAN CONFIGURATION • $C_{L_{MAX}}$ INCREMENT OF HIGH LIFT DEVICES • DRAG OF HIGH LIFT DEVICES	
FULL RELIANCE ON EXPERIMENTAL DATA	• INTERFERENCE EFFECTS • REYNOLDS NUMBER EFFECTS • MACH NUMBER EFFECTS • CHARACTERISTICS OF HIGH LIFT SYSTEMS DEPARTING FROM EMPIRICAL DATA BASE	

Figure 1. The analytical status of methods for estimating high-lift characteristics, according to Callaghan [6].

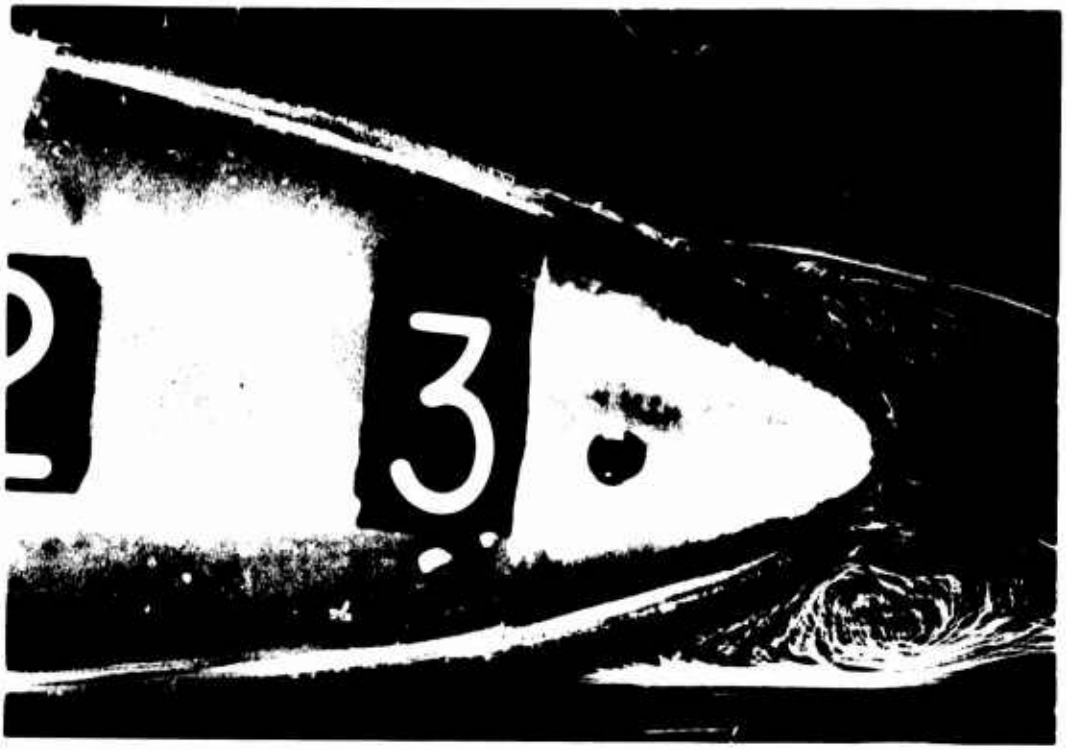

Figure 2. Turbulent separation on a body of revolution. Body length Reynolds number = 130,000; α = 7°, V_∞ = 1/2 ft/sec.

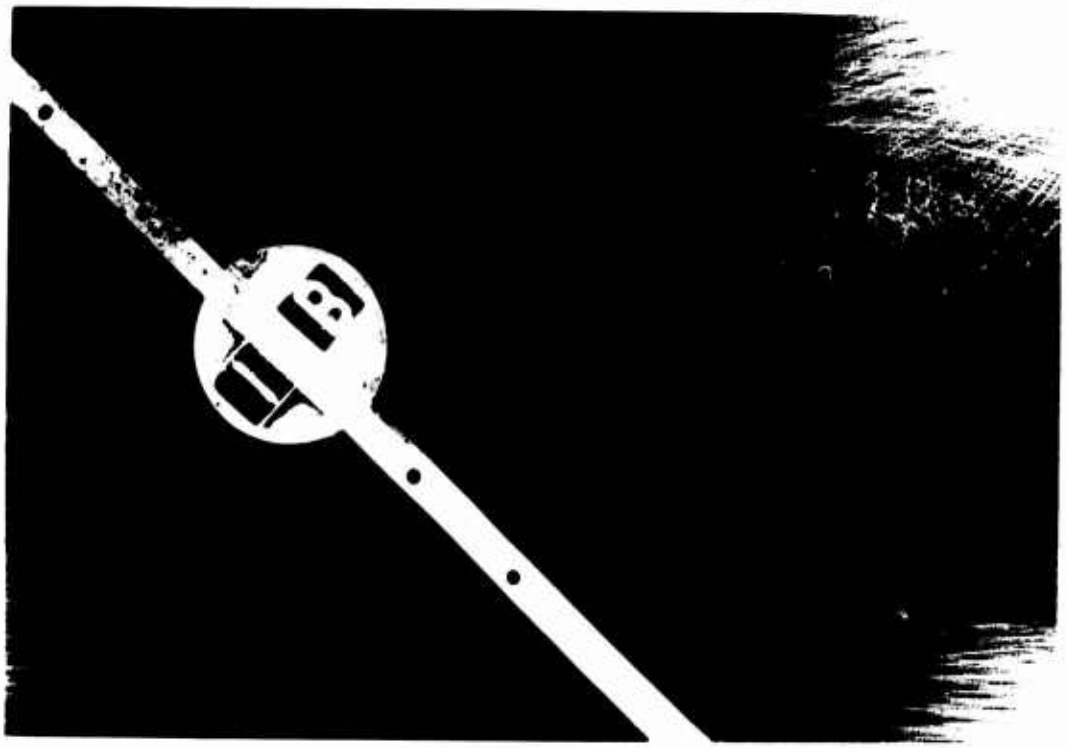

Figure 3. Separation and wake behind a circular cylinder. (a) Long exposure time, showing the large migratory motion of the marked particles.

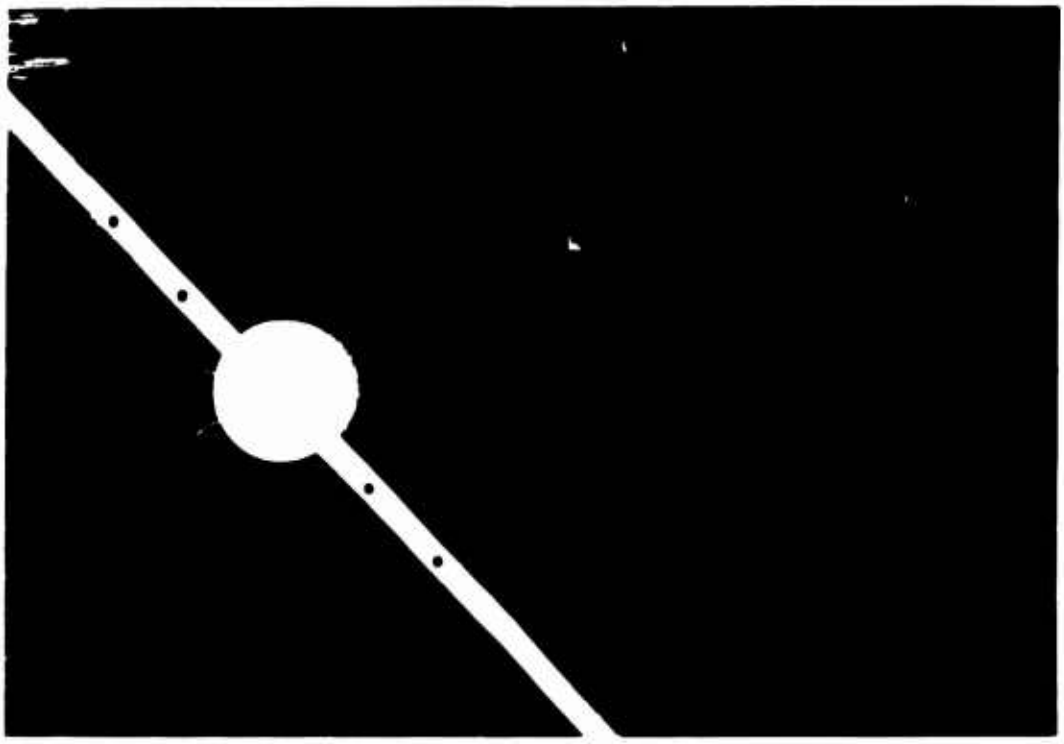

Figure 3. (b) Shorter exposure showing elements of regularity in the motion.

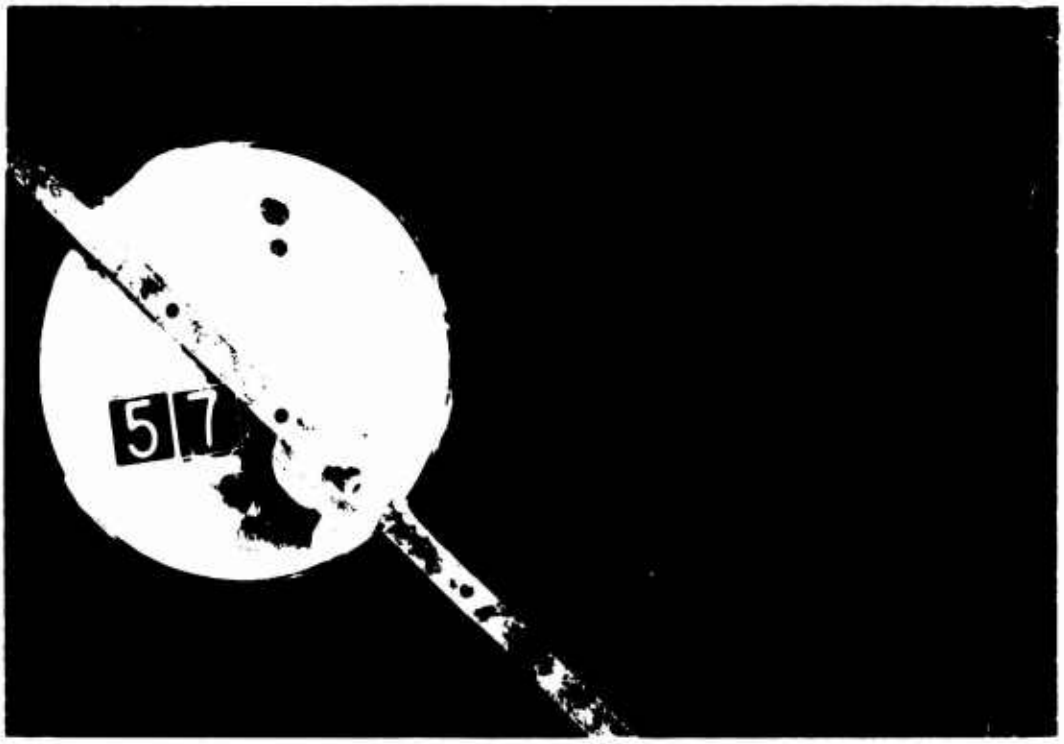

Figure 4. Close up of flow past a circular cylinder, showing clearly the separation point and the great undulating character of motion in the separated region.

In view of this background where analysis depends so strongly on experiment and empiricism it was felt that it would be a useful contribution first to review what is on a relatively solid foundation and then proceed to certain of the more important or interesting aspects of the complete problem.

2. THE SEPARATION PHENOMENON

It seems in order to define and discuss the basic subject of the lecture series, separation. Hancock in [3] gave a useful general lecture on the whole subject of aircraft stall. He distinguishes three steps on the way to the stall. They are: (1) flow separation, (2) flow breakdown, and (3) the stall. There may be a certain amount of flow separation with only mild consequences. Bubbles and small amounts of trailing-edge separation are examples. If the separation grows in extent to the point where the gross character of the flow changes, it is flow breakdown. Finally there is the stall which is more of a property of a complete airplane in flight than a fluid mechanic phenomenon. Hancock defines it thus: "Aircraft stall is a limiting condition of normal flight when the pilot experiences a noticeable change in the orthodox handling characteristics of the aircraft." Hence stall and separation are not the same, but separation leads to and precedes stall.

Figures 2, 3 and 4 are some photographs of flows with separation taken in a water tow tank. The flow is made visible by means of aluminum powder on the surface. Figure 2 shows a body of revolution at angle of attack. The boundary layer was tripped to make it turbulent. Forward of the separation point the flow is very regular right to the surface and seems attached to the body. Then it suddenly takes off, leaving the body. According to Figure 2 as well as 3 and 4, the word separation is a very apt name. Figure 3 shows separation behind a 2-1/2 inch diameter circular cylinder. This is a long duration photo and the edges of the wake appear fairly regular. But the pathlines are highly irregular. Figure 3b is a shorter duration photo that catches an organized irregularity, a vortex. In Figure 3a this has been averaged out. Figure 4 is effectively a closeup that has been made on a 6-inch diameter cylinder. The Reynolds number is about 23,000. Again separation is vividly shown and the large random motion of the marked particles is clearly indicated. A careful examination of the edges of the main flow shows that the edge of the separation region is by no means fixed, for several path lines go far out into what appears to be the unseparated main flow.

Any separation of a flow that may occur along any slowly curving surface is caused by the boundary layer. (Probably separation at the rear of a sharp curved, flat base can also be attributed to the boundary layer, but that question is beyond the scope of this lecture.) Figure 5, taken from [7] shows a set of turbulent boundary-layer profiles as they approach separation. The flow is one studied by Moses. Early, as at Station 11, the velocity profile is full near the wall and the velocity gradient at the wall

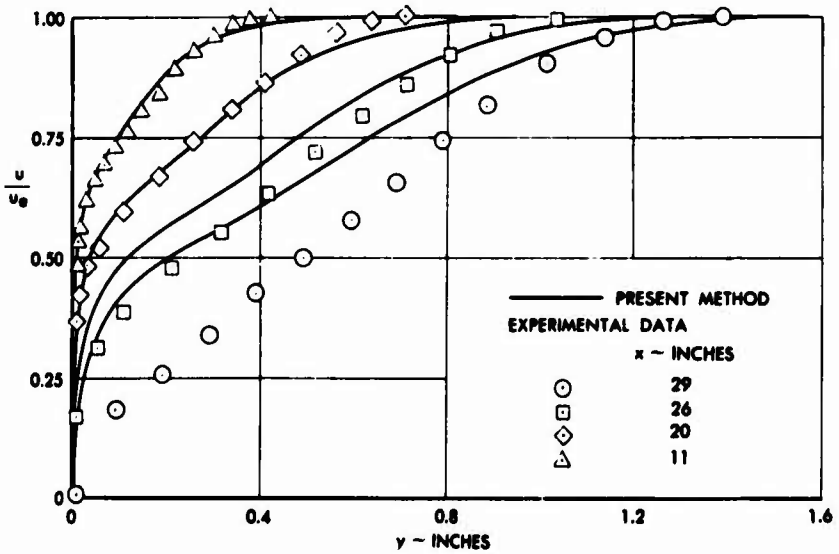

Figure 5. Typical sequence of turbulent boundary-layer profiles in their evolution toward separation. (Moses Pressure Distribution 2, measured separation is at $x = 29$ inches) [7].

is large. Then as the flow proceeds into the higher pressure region the boundary layer thickens. Much of the thickening is just due to continuity because the fluid in the boundary layer is now moving at a lower velocity. However, the slower parts near the wall are slowed up relatively more than the outer. One important reason is that the fluid elements are giving up their kinetic energy in order to enter the higher pressure region. Near separation, as for the experimental profile at Station 29, the inner portion has very little velocity left. If the profiles were squared to indicate their kinetic energy, the bottom part of the profile at Station 29 would have virtually none. Slightly later the adverse pressure gradient or the higher pressure is too much for the remaining kinetic energy of the boundary layer, assisted by shear forces. The bottom portions of the boundary layer can go no further in this uphill climb into

a high pressure region. They stop. Then the following fluid detours around them and away from the body and the phenomenon of separation has developed. Figures 2 and 4 clearly show the flow lines near this point. Much more could be said about the process but the important thing here is that the elemental process is the inability of "tired" fluid near the wall to flow any farther downstream into a high pressure region. These stagnant particles then divert the following flow away from the wall. On straight and slowly curving walls there is no other process that will cause separation. Even cavitation bubbles in water which we think of as an inviscid phenomenon are due to local separation. If there were no local separation there could be no vapor cavity. Once separated, the flow becomes highly irregular as seen in Figures 2, 3 and 4, but velocities are low. Some qualitative indication of that fact may be seen in Figures 2 and 3. The length of the marked particle streaks is proportional to the velocity. Many short lines can be seen in the wake, but in the outer flow the few streaks that can be identified are several times longer.

So far we have been talking about two-dimensional separation. Three-dimensional can be far more complicated. For instance, on an infinite swept wing the chordwise component might come to rest. But there is a spanwise component that suffers no adverse gradient and so it flows with uniform velocity. Hence in this case the separated flow moves spanwise. The basic concepts are treated in a number of references, one being [1]. Lighthill in [8] has a fundamental discussion of the problem treated as a problem in topography.

Callaghan in [6] observes from a number of wind-tunnel tests on airfoils that maximum lift seems to occur when nose pressures just become sonic, which we indicate by the coefficient C_{p^*}. Figure 6 is a summary of his data and Figure 7 shows one of the tests that supplied the data. The tests all showed

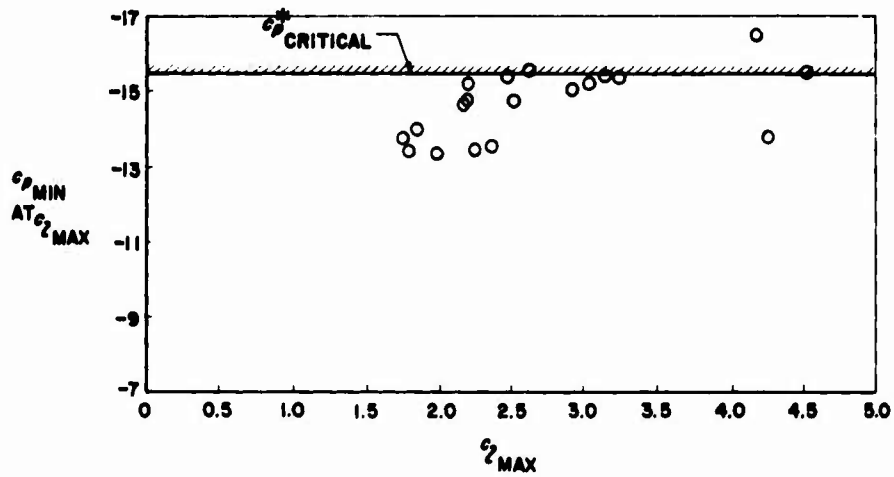

Figure 6. Experimentally measured leading-edge minimum pressure coefficient at $c_{\ell_{max}}$ for a variety of two-dimensional high-lift configurations. Test Mach number = 0.20.

that when C_p of approximately -16 was reached the lift collapsed as shown by the two halves of Figure 7. Whether C_p^* corresponding to the sonic value would be developed at a different Mach number (e.g., M = 0.15) is not known. The observation offers a lead for estimating $c_{\ell_{max}}$ of a section. Just use an inviscid transonic airfoil calculation method and find where the nose velocities first become sonic. The c_ℓ at this condition is then $c_{\ell_{max}}$, and the entire problem is solved by inviscid calculations. Garabedian's method can handle well the inviscid problem for the single airfoil.

3. LIMITS OF LIFT

Callaghan's observations lead us into a more general examination of the problem of lift limits. It is believed that his observations tie into the discussion to follow, but exactly how has not been established. The following discussion is based on material contained in [9].

High values of C_L cannot be maintained indefinitely as speed is increased, for soon surface pressures less than absolute zero would be indicated. Let us look into the problem briefly, and search especially for the limits of lift rather than of lift coefficient. The equation for lift is

$$L = \frac{1}{2} \rho_\infty V_\infty^2 C_L S \tag{3.1}$$

An alternate form, one that uses a different expression for dynamic pressure is

$$L = \frac{1}{2} \gamma p_\infty M_\infty^2 C_L S \tag{3.2}$$

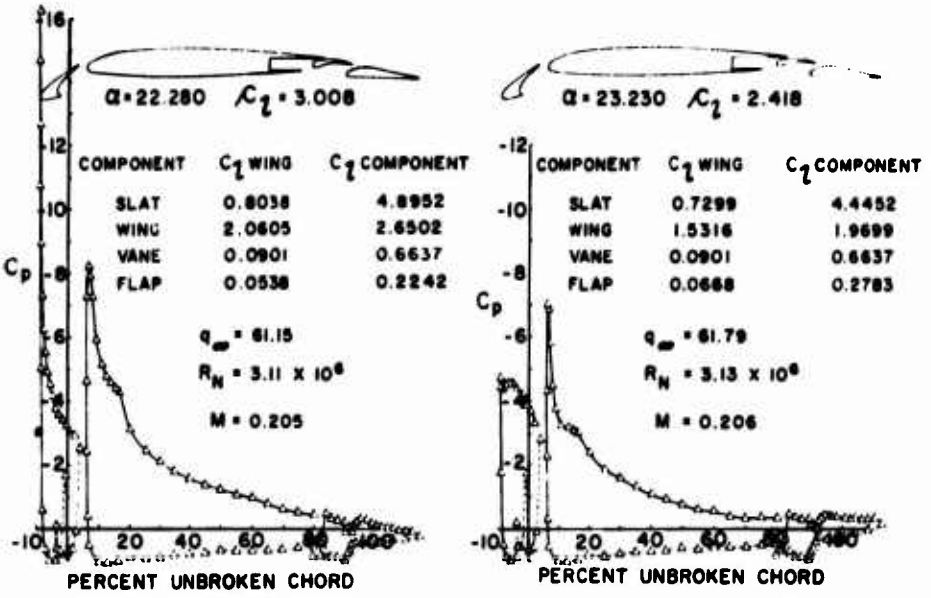

Figure 7. Experimental pressure distribution on two-dimensional wind-tunnel model with leading-edge slat and trailing-edge flap.

With . = 1.4, we can rewrite it as

$$L/p_\infty = 0.7(M_\infty^2 C_L)S \tag{3.3}$$

Since C_L is known to be a function of M_∞, the product $M_\infty^2 C_L$ is the quantity that is of real significance, and so we seek to make statements about its value. Observe that for a given value of $M_\infty^2 C_L$ the lift is now proportional to the atmospheric pressure.

A gas cannot be in tension. Hence the limiting suction pressure is a perfect vacuum over the entire upper surface. The limiting pressure on the lower surface is stagnation pressure.

By definition, with γ = 1.4,

$$C_p = \frac{p - p_\infty}{1/2\rho_\infty V_\infty^2} = \frac{p - p_\infty}{0.7p_\infty M_\infty^2} \tag{3.4}$$

If the flow is assumed to be isentropic, C_p can be written in the form

$$C_p = \frac{1}{0.7M_\infty^2}\left[\left(\frac{1 + 0.2M_\infty^2}{1 + 0.2M^2}\right)^{3.5} - 1\right] \tag{3.5}$$

Before proceeding to the determination of lift limits, it is interesting to pause and consider the limits of C_p-values. As already noted, in high-lift testing, maximum lift is often found to occur about when the highest local velocities reach a Mach number of 1.0. If a perfect vacuum were reached, we would obtain, according to (3.4), a value of $M_\infty^2 C_p$ equal to -1.43. Mayer [10] looked for the highest possible negative C_p-values in experiment by examing hundreds of NACA test data points from all sorts of tests. He found the remarkable empirical result that the highest experimentally measured values corresponded with reasonable accuracy to $M_\infty^2 C_p$ = -1. The value corresponds to 0.7 of a vacuum (see (3.4)). Figure 8 shows the test data he used to support the finding. Note that 0.7 of a vacuum does not correspond to a constant local Mach number.

Since much of our interest is in high-lift testing, which is done at low Mach numbers, we convert some of the results from Figure 8 into C_p-form and present them below.

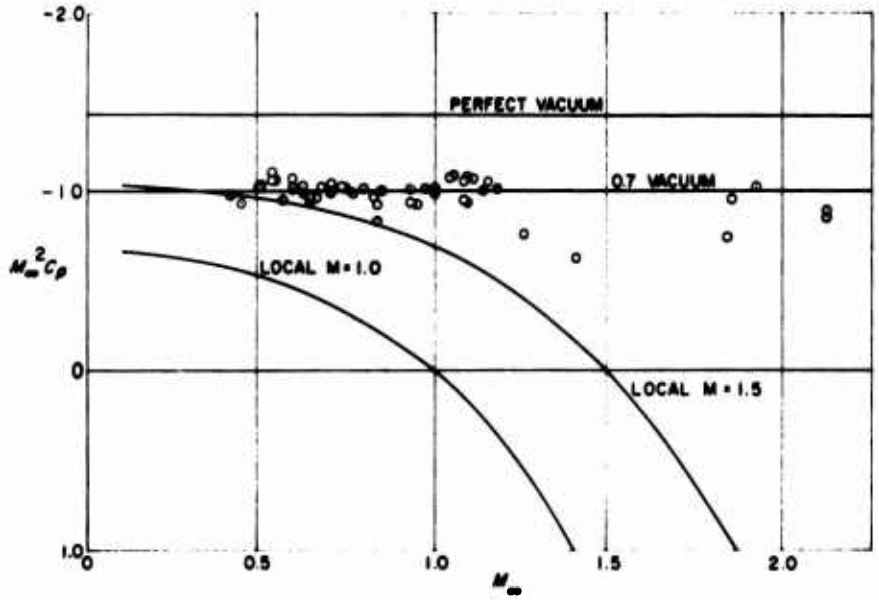

Figure 8. $M_\infty^2 C_p$ values as a function of Mach number for four conditions. 0.7 vacuum corresponds to $M_\infty^2 C_p = -1$.

Table I Limiting values of C_p at low Mach Numbers

M_∞	0.10	0.15	0.20	0.30	0.40	0.50
C_p^* (M = 1)	-67	-29.3	-16.3	-7	-3.7	-2.1
C_p (perfect vacuum)	-143	-63.6	-35.8	-15.9	-8.9	-5.7
C_p (0.7 vacuum)	-100	-44.5	-25	-11.1	-6.3	-4.0

At low Mach numbers, quite high values of C_p are obtainable before compressibility becomes very important, but at higher Mach numbers the limiting C_p-values are not very high. Note, however, that Mayer's data in Figure 8 do not cover the lowest Mach numbers; hence its validity there is not truly established.

The author knows of no theoretical explanation for Mayer's 0.7-vacuum correlation. It does not correspond to a constant local Mach number. By the use of (3.5), it is easily deduced that $M_\infty^2 C_p = -1$ corresponds to $M_{local} = 1.43$ at $M_\infty = 0$ and 1.55 at $M_\infty = 0.5$.

Now consider the airfoil problem. If we hold M constant at one value on the upper surface and constant at another value on the lower surface, C_p represents the C_L for each surface. The total C_L is the difference. Hence from (3.5)

$$M_\infty^2 C_L = \frac{1}{0.7}\left[\left(\frac{1 + 0.2M_\infty^2}{1 + 0.2M_\ell^2}\right)^{3.5} - \left(\frac{1 + 0.2M_\infty^2}{1 + 0.2M_u^2}\right)^{3.5}\right] \tag{3.6}$$

where ℓ and u denote lower and upper surfaces. A perfect vacuum on the upper surface corresponds to $p_u = 0$ or $M_u = \infty$. In that case, the second term in (3.6) is zero. With respect to atmospheric pressure, the load carried by the upper surface when there is a perfect vacuum is (see (3.4))

$$M_\infty^2 C_L = \frac{1}{0.7} = 1.43, \text{ a constant} \tag{3.7}$$

If the entire flow on the lower surface is a stagnation flow, $M_\ell = 0$, and hence with a vacuum on the upper surface we have

$$M_\infty^2 C_L = \frac{\left(1 + 0.2M_\infty^2\right)^{3.5}}{0.7} \tag{3.8}$$

Equation (3.8) represents the absolute lifting limit. The quantity increases with Mach number because lower-surface pressures can increase with Mach number. Equation (3.8) is optimistic, because isentropic compression is assumed, whereas in reality there surely will be a shock when $M \cdots 1$. Table II shows

values of M^2C_L for several flow conditions, including Mayer's $M^2C_L = 1$ limit. The maximum value possible in subsonic flight is 2.71, and the contribution from each surface is about equal. If Mayer's $M^2C_p = -1$ value is accepted, the limit decreases to 2.28. At $M_\infty = 0.5$, the absolute maximum value is only 1.70 and Mayer's value is 1.27. Those are the limiting values, regardless of the kind of high-lift devices that are used. At $M_\infty = 1.0$ and below, the assumption of isentropic recompression on the lower surface is very good, as is well known. As Mach numbers become large, pressures on the lower side become great, and large values of M^2C_L develop, values that exceed 11 at $M_\infty = 2.0$. Mayer considers the case where under-surface pressures in supersonic flight correspond to a normal shock. He gives considerable information on maximum-lift values in supersonic flight, including correlations of theory and experiment. But since our interest is principally in subsonic flight, we shall not discuss his work further.

3.1 Demonstrated Lifting Limits

It is interesting that the question of aerodynamic lifting limits in subsonic flight was posed to the author in 1946 by E. H. Heinemann. The problem was fighter maneuvering – what lift could a wing really develop?

Table II Maximum-lift limits assuming isentropic compression, and uniform chordwise loading.

M_∞	M_{upper}	$M^2C_{L_{upper}}$	M_{lower}	$M^2C_{L_{lower}}$	$M^2C_{L_{total}}$
0.5	·	1.43	0	0.27	1.70
0.5	1.55	1.00	0	0.27	1.27
0.5	1.5	0.97	0	0.27	1.24
1.0	·	1.43	0	1.28	2.71
1.0	1.86	1.00	0	1.28	2.28
1.0	1.5	0.69	0	1.28	1.97
2.0	·	1.43	0	9.75	11.18
2.0	4.97	1.00	0	9.75	10.75

All the available flight and wind tunnel data were examined. The examination included the large supply of German World War II data, which covered tests of a great variety of airplane and missile-type wings. The results were reported in [11]. The study, which was strictly one of observation, concluded that the maximum possible lift was about 1/2 atmosphere. That number corresponds to a value for M^2C_L of about 0.7.

Since that time, the design of swept wings has advanced considerably. Now, the highest value of M^2C_L seen by the author is 1.20 on a swept wing using an aft-loaded airfoil section with no auxiliary lift devices. The value corresponds to $C_L = 1.26$ at $M_\infty = 0.975$. It was not really a maximum-lift value but, rather, a stopping point in a wind-tunnel test that was determined by strength of the sting support. Hence the value can surely be exceeded. It should be pointed out that this is not a buffet limit, which is usually considerably lower. Furthermore, the wing was not in any high-lift configuration. If one went all out to maximize M^2C_L, without regard to low-lift performance, much better could surely be done. Leading-edge and trailing-edge devices undoubtedly would raise the limit. Variable-camber wings are currently receiving attention as another possible means of raising the limit.

4. CANONICAL PRESSURE DISTRIBUTIONS

In almost all design work, pressure distributions are presented in terms of $C_p = (p - p_\infty)/(1/2\,\rho u_\infty^2)$. In that kind of presentation, high negative values of C_p invariably look bad, and one is unable to tell by inspection much about the margin of safety of the boundary layer against separation. Yet we know from basic scaling considerations that if two pressure distributions can be made congruent by proper scaling in the x- and c_p-directions, then the two flows are identical except for the Reynolds number effect, which is weak. Then if separation occurs, it will be the same scaled point for both flows. A particular 2-inch airfoil model at 100 mph will have very high values of velocity gradients, but a similar 200-inch model at 1 mph will have extremely low values. Yet the flows are exactly similar because their Reynolds numbers are the same. It is the dimensionless shape that counts. Hence it is particularly useful to scale out the magnitude of the velocity and also to scale out the chord. Where separation is important, the best scaling factor is the velocity just before deceleration begins. Because all pressure distributions are put in a standard form, it is natural to call them canonical pressure distributions and use a new variable - $\bar{C}_p$. A typical one is illustrated in Figure 9, which shows the idea and basic relations. The exact details of the normalization may well depend on the problem and the nature of the pressure distribution. The canonical pressure distribution, together with a Reynolds number, completely describes the flow. A convenient Reynolds number is R_{θ_1} at the beginning of pressure rise. The left-hand part in Figure 9 might represent the nose of an airfoil. Distance x is measured along the surface, the origin of x is a matter of convenience. Often it is convenient to locate it at the beginning of pressure rise, as in the figure. Separation may occur at some point as noted.

In the canonical system, $\bar{C}_p = 0$ represents the start of pressure rise and $C_p = +1$ the maximum possible, that is, $u_e = 0$. There are no negative values of $\bar{C}_p$. Furthermore, if two pressure distributions can be made congruent by proper scaling, a flow having a deceleration of $(u_e/u_\infty)^2$ from 20 to 10 is no more and no less likely to separate than one decelerating from 1.5 to 0.75 or even from 0.10 to 0.05. The canonical plot is the one that is meaningful in separation analysis. With magnitude effects scaled out, much more can be told by a simple inspection than by a conventional plot. We dwell on the canonical pressure distribution at some length, because most working aerodynamicists do not realize its value. Figures 10 and 11 show conventional and canonical pressure plots for a typical high-lift airfoil. The

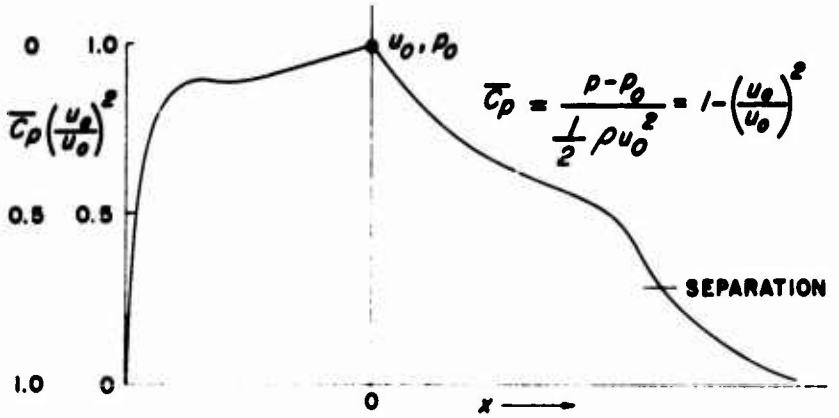

Figure 9. A canonical pressure distribution $\bar{C}_p(x)$. The left-hand part might represent the nose of an airfoil.

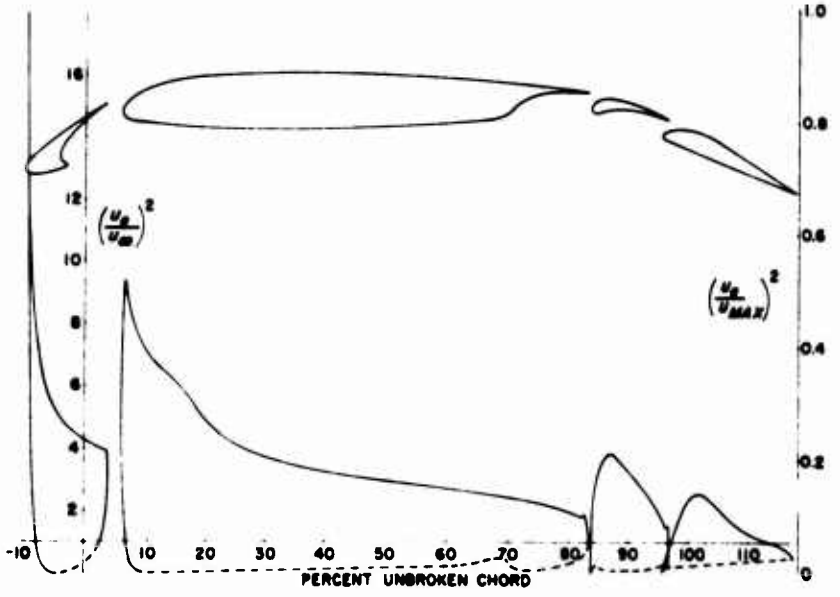

Figure 10. A conventional theoretical C_p plot of a four-element airfoil. The R.H. scale is the canonical form, referred to peak velocity at the nose of the flap. $\delta_s = 15°$, $\delta_f = 25°$, $\delta_S = -25°$, $c_\ell = 4.08$.

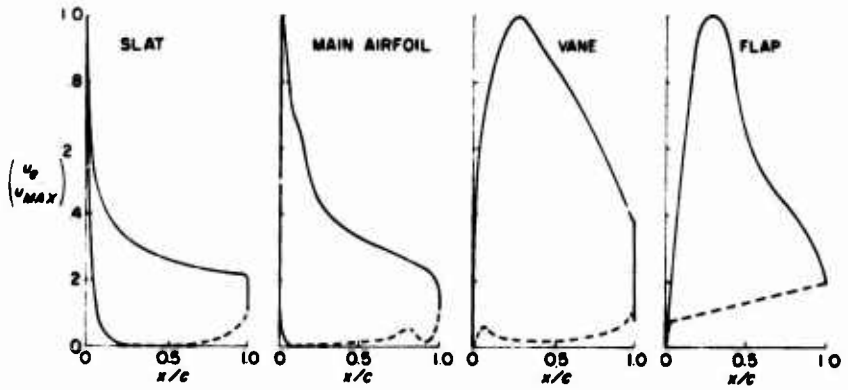

Figure 11. The airfoil C_p of Figure 10 plotted in canonical form.

basic character of the four pressure distributions is much more apparent in Figure 11. Figure 10 includes a canonical scale at the right, for the complete ensemble.

The relations between canonical and conventional pressure distributions are very simple, but because there has been confusion on the subject, it will be discussed somewhat here. The canonical pressure distribution is easily related to the conventional form, where the reference velocity and pressure are u_∞ and p_∞. Because the square of the velocity is never negative, it is simpler to deal with velocity than with pressure coefficient. The fundamental relation is quite simple. It is

$$\left(\frac{u_e}{u_\infty}\right)^2(x) = \left(\frac{u_e}{u_0}\right)^2(x) \cdot \left(\frac{u_0}{u_\infty}\right)^2 \tag{4.1}$$

With the two definitions for pressure coefficient in incompressible flow

$$C_p = 1 - \frac{u_e^2}{u_\infty^2}, \quad \bar{C}_p = 1 - \frac{u_e^2}{u_0^2}$$

we can write (4.1) in terms of C_p, $\bar{C}_p$.

$$1 - C_p(x) = [1 - \bar{C}_p(x)][1 - C_{p_0}] \tag{4.2}$$

The notion of canonical pressure distribution is emphasized, because frequently by its use one can collapse data or make intelligent estimates without resorting to lengthy boundary-layer calculations. As an example, we cite Figure 12 which was given as Figure 9 in [12]. The front of the hatched region is the front of the separation bubble, or in other words the beginning of separation. As the data stands there is a regularity to it but no particular law is evident. The author looked at the data and observed that all the nose pressure distributions had roughly the same shape. If that is so, then the ratio of velocity at separation to peak velocity should be a constant for the set. Since the front of the bubble must be essentially the laminar separation point, he worked out the ratio u^2_{sep}/u^2_{max} for each C_L and found a single value within the accuracy of the data, namely $(u_{sep}/u_{max})^2 = 0.89 \pm 0.01$. All the variation has been scaled out by means of the canonical approach. Furthermore, a constant such as the above varies only over a narrow range for a wide variety of flows. For example, Howarth's flow $u_e = 1 - x$, which begins deceleration immediately and so should sustain a greater deceleration ratio has a ratio $(u_{sep}/u_{max})^2 = 0.77$. In Figure 8 of [13] are shown a variety of laminar flows with four kinds of forward flow and two kinds of decelerating flow. Unlike Howarth's flow the momentum thickness was finite at the beginning of deceleration. For the entire set $(u_{sep}/u_{max})^2$ varied only from 0.91 to 0.82. This rough constancy as indicated by the $\bar{C}_p$ approach is often useful in understanding boundary layers and the onset of separation.

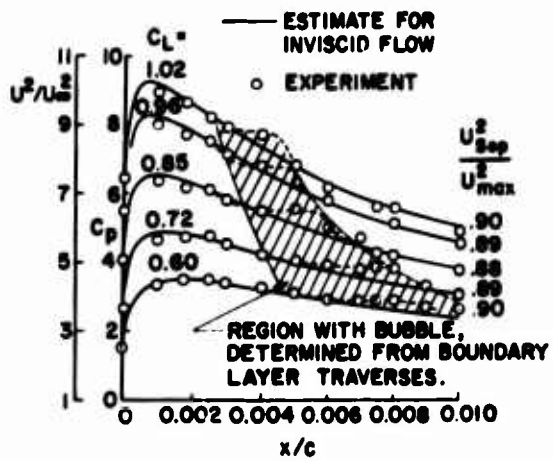

Figure 12. Pressure distribution near the leading edge of an NACA 63009 section, showing the region in which a bubble exists.

5. LAMINAR SEPARATION

After the first few lengths of boundary-layer flow, measured from the front stagnation point in terms of boundary-layer thickness, the laminar boundary-layer equations apply. They are highly accurate – because the terms dropped in deriving these equations are quite negligible. At airfoil chord Reynolds numbers of a million or more these equations are potentially precise enough to give four figure accuracy or more. If the conventional dimensioned form of the equations is made dimensionless by proper combinations of terms we obtain an equation that directly brings in $R_c = u_\infty c/\nu$ and this one universal equation gives solutions in terms of the following quantities u/u_∞, $(y/c)\cdot\sqrt{R_c}$, $(v/u_\infty)\cdot\sqrt{R_c}$, and $c_f\cdot\sqrt{R_c}$ all for a given relation between C_p and x/c, where x is distance along the surface measured from the forward stagnation point. No approximations have been made in these scaling studies. Then the above parameters tell us that the boundary height changes as $R_c^{1/2}$. However, a laminar layer is always so thin that it virtually does not change the effective shape of the airfoil.

Of more importance to us is the $c_f\cdot\sqrt{R_c}$ relation, where c_f is the local skin friction coefficient. If for a given C_p, x/c pressure distribution relation we find $c_f = 0$ at one Reynolds number it will be zero at any Reynolds number so long as the flow stays laminar. We have the important fact that <u>for a given dimensionless pressure distribution the laminar separation point is unaffected by Reynolds number</u>. Hence if a laminar separation bubble exists, its front should not change with Reynolds number. The only reason there might be some change is that the flow within the bubble does change with Reynolds number and then it has a very weak upstream influence.

As mentioned at the end of Section 4 the pressure rise that a laminar boundary layer can tolerate is very small. A useful formula that often can replace solution of the full partial differential equations is Stratford's separation formula for laminar flows, that can be found in [8]. The relation is

$$\left[x^2 \bar{C}_p \left(\frac{d\bar{C}_p}{dx}\right)^2\right]_{sep} = 0.0104 \tag{5.1}$$

In Stratford's analysis he assumes a flat plate laminar boundary layer from the flow origin $x = 0$ to a point x_0 where the pressure starts to rise. When the L.H. side of (5.1) rises to the value 0.0104 separation is said to occur. $\bar{C}_p$ is the canonical pressure coefficient as discussed earlier. Note that this formula for locating separation is in agreement with our earlier and more fundamental statements about the invariance of a laminar separation with Reynolds number. (5.1) does not have a Reynolds number in the expression. Later we will give a similar formula for turbulent separation. That kind of flow shows a weak Reynolds number effect. There Reynolds number enters as $R^{1/10}$.

Reference 9 presents charts for turbulent flow showing the location of separation for retarded flows whose equations are:

$$\begin{aligned} \bar{C}_p &= 0 \qquad\qquad x \le x_0 \\ \bar{C}_p &= (x - x_0)^m, \quad x \ge x_0 \end{aligned} \tag{5.2}$$

where m is an exponent, usually in the range 1/4 to 4. More will be said about them in Section 6. Similar charts should be worked out for laminar flows, for the charts for turbulent flows have been found very useful. The laminar case is of interest when leading-edge bubbles and separation are likely to occur. Because of the analytic nature of (5.2) it is very easy to introduce it into (5.1). With x_0 as the start of pressure rise, one useful form of the equation is to present the relation in terms of $\bar{C}_p$ at separation. The alternate form of course is one in terms of x at separation. By some simple algebra we obtain

$$\left[\left(\frac{\bar{C}_p^{1/m} + x_0}{\bar{C}_p^{1/m}}\right)^2 m^2 \bar{C}_p^3\right]_{sep} = 0.0104 \tag{5.3}$$

For assigned values of x_0 and m it is not difficult to find $\bar{C}_{psep}$. A limiting case is when there is no forward flat plate run, i.e., $x_0 = 0$. With $m = 1.0$ we somewhat approximate Howarth's flow. According to (5.3) for this case $(u_{sep}/u_{max})^2 = 0.78$. In Section 4, the value for Howarth's flow was given as 0.77. Of course the two flows are not really the same. Howarth's is $u/u_0 = 1 - x$ or $(u_e/u_0)^2 = 1 - 2x + x^2$, while the present is $(u_e/u_0)^2 = 1 - x$. By way of comparison, if the flow were turbulent, $(u_{sep}/u_{max})^2$ would be about 0.3, see Figure 19. This comparison again emphasizes the well-known fact that laminar boundary layers can endure only weak pressure rises compared with the turbulent.

6. TURBULENT SEPARATION

The subject of this section is the features, possibilities and limitations of turbulent flow up to separation. Justice can be done to this problem, but turbulent flows beyond are a different matter. We begin by reviewing the accuracy with which separation points in a purely rear separation type flow can be predicted.

6.1 Accuracy of Predicting Separation Points

Because this question is so vital to many aerodynamic design problems, the accuracy of four leading methods was studied recently in [14] for the case of turbulent flows, which is the one of interest. All the flows considered involved simple rear separation. Laminar bubble or laminar leading-edge separations were not considered. Four leading methods were examined: those of (1) Goldschmied, (2) Stratford, (3) Head, and (4) Cebeci-Smith. Four cases representative of the fairly large number examined in [14] are shown in Figures 13, 14, 15, and 16. Separation points (solid black symbols) were carefully measured. The predicted separation points are marked on the pressure-distribution curves, which were supplied by the experiments. For the flow of Figure 13, Goldschmied's method failed to predict separation. The fourth case, which is shown in Figure 16, consists of measurements and predictions on one airfoil at five different angles of attack. Separation points were not measured in that case, but inspection of the pressure-distribution curves clearly shows that separation existed in all cases. Goldschmied's method was erratic. The other three were in reasonable agreement, both in what is shown here and in the complete study [14]. Stratford's method tended to predict separation slightly early. The Cebeci-Smith method appeared best, with the Head method a strong second.

Hence, the Cebeci-Smith method has been chosen as the basic method, although much use is made of Stratford's method and ideas in this paper, mainly because of their great convenience. Figure 17 summarizes the prediction accuracy of the Cebeci-Smith method. The data consist of the results from [14] together with other, unpublished studies. One should not conclude from Figure 17 that the general accuracy of turbulent-boundary-layer calculation is as good as it appears to be. Near separation, the accuracy of many of the boundary-layer quantities, such as the momentum thickness θ and the velocity profile, becomes poor. Nevertheless, accuracy of predicting the location of separation remains good. The Cebeci-Smith method predicts separation to be at the point where c_f, the local skin-friction coefficient equals zero.

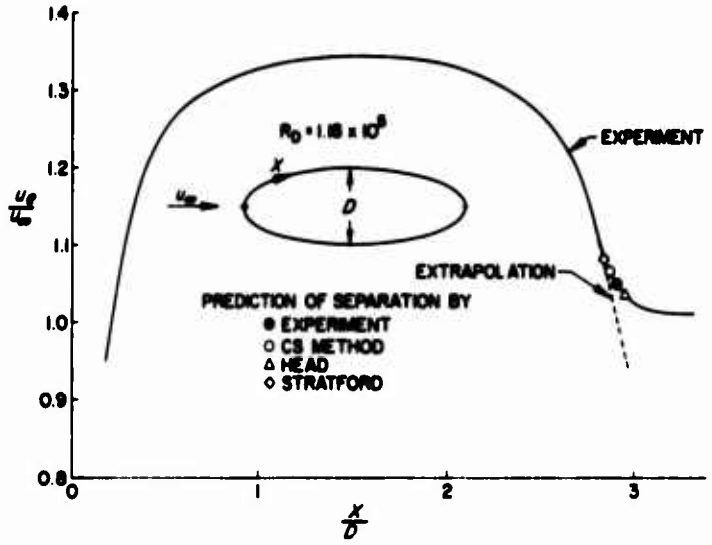

Figure 13. A comparison of predicted and experimental separation points for Schubauer's elliptic cylinder.

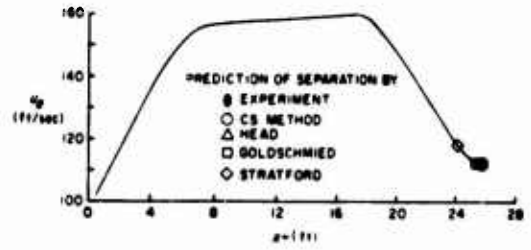

Figure 14. Comparison with experiment of predicted separation points for the airfoil-like body of Schubauer and Klebanoff.

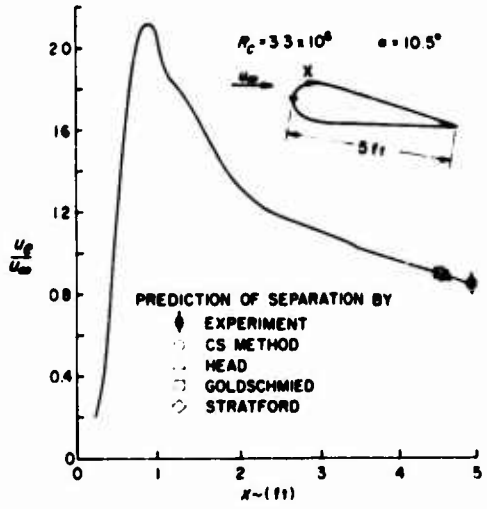

Figure 15. Comparison with experiment of predicted separation points for Neuman's airfoil.

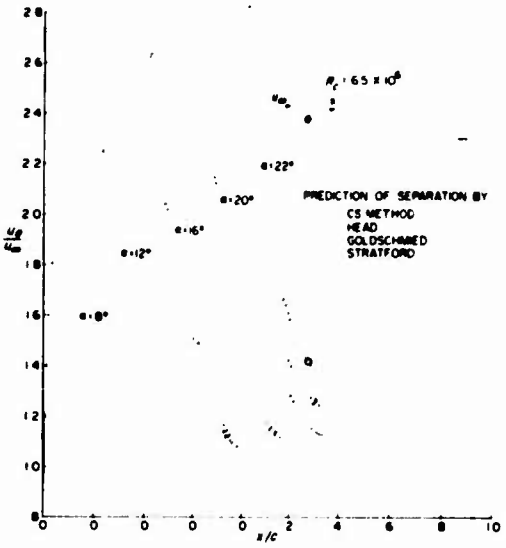

Figure 16. Predicted separation points for the experimental pressure distribution on the NACA 66,2-420 airfoil.

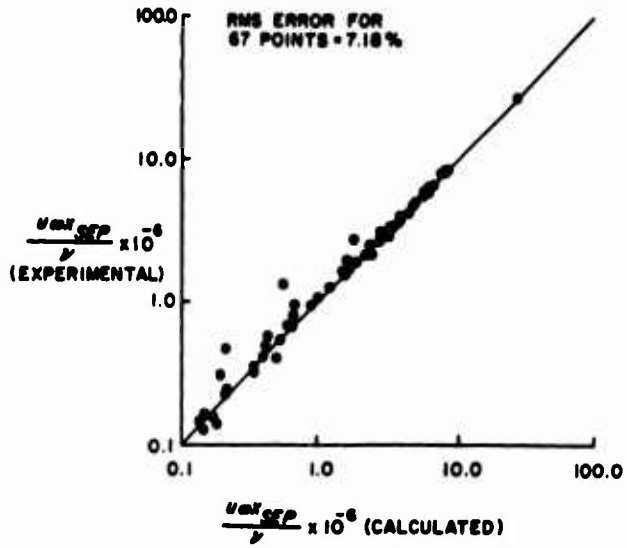

Figure 17. Accuracy of predicting turbulent separation points by the Cebeci-Smith method.

In view of those results, the method of predicting separation appears to be accurate enough, in an engineering sense, to be used in determining relations, limits, and the like. It should be noted that the Cebeci-Smith method can handle with great accuracy the effects of Reynolds number or Mach number up to 5 or more. Also, it is the only one of the four methods that can analyze the case of axisymmetric boundary-layer flow.

6.2 The Pressure Rise that Turbulent Boundary Layers can Stand without Separation

Having just shown you that we can reliably predict turbulent separation, let us put the method to use and explore what pressure rises can be endured by a turbulent boundary layer before it separates. A useful way is to work out charts covering a systematic family of flows. Two such plots are given in Figures 18 and 19. The flows are the same as discussed briefly in Section 5, that is, they consist of a length of constant-velocity flow followed by a pressure rise described by the equation

$$\bar{C}_p = x^m \tag{6.1}$$

The unit Reynolds number is 10^6 per foot in Figure 18 and 10^7 per foot in Figure 19. Pressure rise is set to start at $x = 0$, but forward of that point are various lengths of flat-plate flow. It seemed more convenient to construct the plots in terms of feet and u_∞/ν rather than in terms of Reynolds number, although conversion into Reynolds number is easy. The total region of pressure rise is seen to be 1 foot.

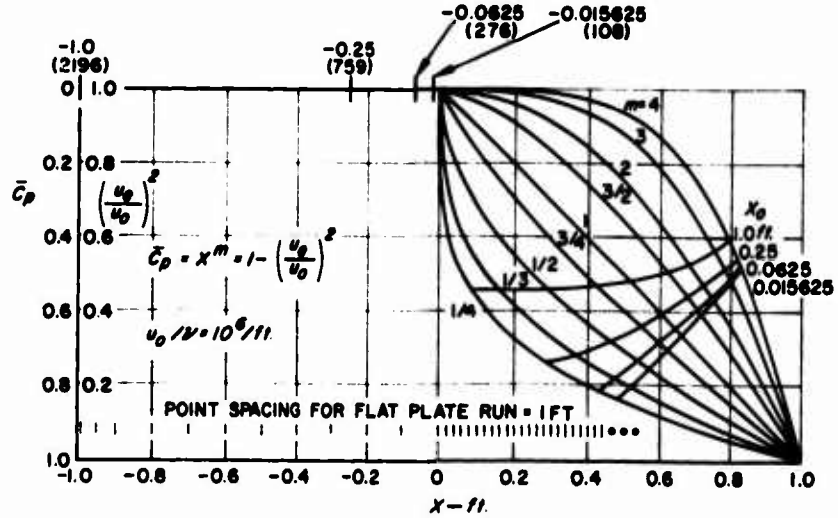

Figure 18. Separation loci for a family of canonical pressure distributions. Point spacing used in the boundary-layer calculations for the one-foot rooftop run is noted. Values in parentheses under origins of flow are values of R_θ at $x = 0$.

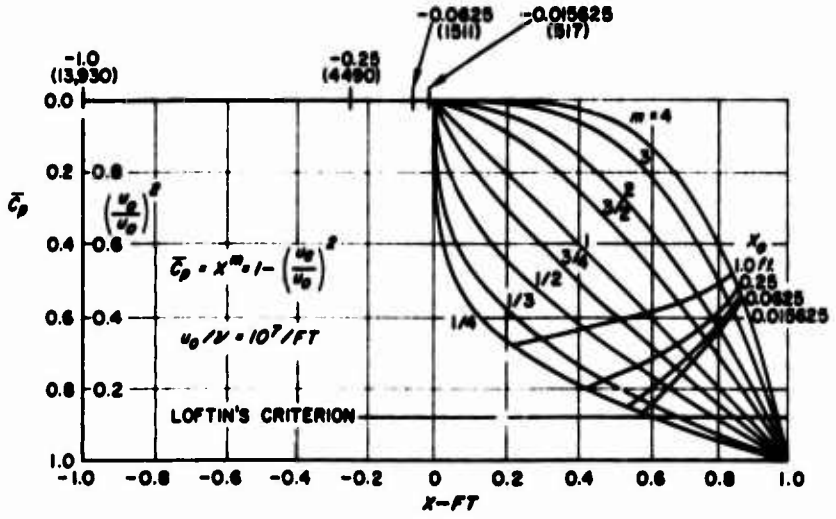

Figure 19. Separation loci for a family of canonical pressure distributions. Loftin's criterion $\bar{C}_p = 0.88$ is noted.

Four lengths of flat-plate run were studied: 1/64 foot, 1/16 foot, 1/4 foot, and 1 foot. The initial flows then developed boundary layers of various thickness at the beginning of pressure rise, as indicated by values of R_θ in the figures. The flat-plate flow is assumed to be entirely turbulent. If it were mixed laminar and turbulent, values of R_θ at $x = 0$ would be less and different.

Calculations of the flat-plate and $\bar{C}_p = x^m$ parts of the flow were then made by the Cebeci-Smith method until separation was reached. Lines cutting across the $\bar{C}_p = x^m$-curves mark separation points for the four lengths of flat-plate runs. The straight-line or concave pressure rises permit the greatest recovery before separation occurs. Also, the curves show that the amount of recovery is sensitive to the length of flat-plate run before the beginning of recovery. The separation loci, while indeed functions of the length of flat-plate run, are more fundamentally functions of the boundary-layer thickness, that is, R_θ, at the beginning of pressure rise. Hence, the separation loci could just as well be identified by the noted values of R_θ at the beginning of pressure rise. Then Figures 18 and 19 become applicable for any combination of rising pressure and transition. For any arbitrary forward flow, one would then calculate R_θ at $x = 0$ and interpolate between the loci as a function of R_θ. In brief, we are saying that any flow that develops one of the set of values of R_θ and that has the same aft flow will have the same separation point as that of a forward flow developed by an equivalent run of flat plate. The equivalence is not rigorous, because a separation point is a function not only of initial R_θ but also of the shape of the profile as described by H. But R_θ is the dominant parameter, and, considering the accuracy of turbulent boundary-layer calculations, it is the only one that need by considered here.

These comments point out the fact that extensive laminar flow in the forward part helps to delay separation considerably, because it reduces R_θ. Furthermore, boundary-layer suction forward of the pressure rise would delay separation. Another fact that is surprising is that if the pressure rise is not too great, it may be extremely steep; in fact, $d\bar{C}_p/dx$ may be nearly infinite. (Owing to the use of finite steps, the slope of $\bar{C}_p$ is never quite infinite in the Cebeci-Smith method. If it were, a constant in the partial differential equation would be infinite and the method would fail.) In the next section, we see that the infinite rate of pressure rise is confirmed by Stratford's equations, which he derived by an analytical approach.

Loftin and von Doenhoff [15] studied a large number of thin airfoils and arrived at a separation criterion that in our terms is $\bar{C}_p = 0.88$. It is plotted in Figure 19. A thin airfoil at angle of attack has an effective forward flow about the same as that of the $x = 1/64$-foot distance, and the pressure-rise region is approximated by the $m = 1/3$ or $m = 1/2$ curve. Hence, we see that Loftin's criterion is rather closely predicted by the charts. But we also see that it is far from universal.

The set of charts provides an "eyeball" method for estimating separation points. We shall illustrate by considering Figure 15. Try to relate that flow to one of the canonical plots. If the pressure distribution of Figure 15 is replotted in u_e^2/u_∞^2, or canonical form, the rear flow is approximately like the $x^{1/3}$ flow and the front flow is effectively quite short. Transition was measured at $x = 1.169$ feet. Hence the logical equivalent flat-plate length is 0.015625 foot. Which chart should be used? Probably Figure 19. To use the figures, convert the chord of the airfoil to 1 foot. Because it is so small, there is no need to be concerned about the 0.015625 forward part. In order to hold Reynolds number at 3.3×10^6 with the reduced chord, we need to increase u_∞/ν to 3.3×10^6/ft. But the charts are in terms of u_0/ν. Now from Figure 15, $u_0/u_\infty = 2.1$. Hence, $u_\infty/\nu = 3.3 \times 10^6$ corresponds to $u_0/\nu = 7 \times 10^6$. Then Figure 19 seems to be the better of the two to use. Of course, interpolation between the two is possible. From Figure 19 for $m = 1/3$, we find that separation occurs at $(u_e/u_0)^2 = 0.17$ or $u_e/u_0 = 0.41$. In Figure 15, $(u_e/u_\infty)_{max} = 2.1$. Hence separation should occur at about $0.41 \times 2.1 = 0.87$, a ratio that is satisfactorily close to the measured separation point. More care in the analysis probably would increase the accuracy. For instance, a careful calculation of R_θ at $x = 0$ by Truckenbrodt's method would be better than a guess. Also, the exponent in the pressure-rise region could be determined more accurately by the use of log graph paper.

The canonical plots contain much useful information. For instance, if load is being carried by an airfoil in cruise, the pressure rise at the trailing edge is not great. If it corresponds to $\bar{C}_p = 0.4$, any m-curve will sustain the pressure rise, and therefore suitable airfoils with all kinds of pressure distributions can be made. But if one is striving for all the lift he can get, the pressure-rise curve for $m = 1/4$ or $1/3$ is the best, because that gives the greatest ratio and the highest mean value of $\bar{C}_p$ along the upper surface.

Reference 16 gives two charts for a different family of pressure distributions; they are arcs of circles. Results are not significantly different from those of the $\bar{C}_p = x^m$ family. In closing this section, we remark that because of the analytical nature of our canonical pressure distributions $\bar{C}_p = x^m$, it is very easy to apply Stratford's criterion. That has been done. If Stratford's predictions had been added to the plots of Figure 18 and 19, the differences in separation loci would appear considerable. Still they are so small that use of the charts and the findings is not negated. Addition of Stratford-type loci would only cause confusion. Therefore, we show only one type of calculation, the Cebeci-Smith, which in general is believed to be the most accurate. Furthermore, it should be noted that Figures 18 and 19 differ from their earlier forms in [16]. The main reason is that here we used the analytic nature of the $\bar{C}_p = x^m$ flows to compute certain necessary derivatives. In the earlier work, finite-difference formulas were used. Disagreements such as those just indicate the state of the art of turbulent-flow calculation.

6.3 Limiting Pressure Recovery Distribution

The $\bar{C}_p = x^m$ families are very useful for almost all practical flow problems, but of course the shapes of the $\bar{C}_p(x)$ curves are arbitrary; the shapes are selected as a matter of analytical convenience. Just as in many other problems, there is one shape that is "best," Stratford's solution. We do not mean to imply that the solution is exact, but as is indicated by Figures 13 through 16, it has acceptable accuracy. Stratford has derived a formula, [17], for predicting the point of separation in an arbitrary decelerating turbulent flow:

$$\frac{\bar{C}_p\sqrt{x(d\bar{C}_p/dx)}}{(10^{-6}R)^{1/10}} = S \tag{6.2}$$

where if $d^2p/dx^2 \geq 0$ $\qquad S = 0.39$

or if $d^2p/dx^2 \leq 0$ $\qquad S = 0.35$

Also $\qquad \bar{C}_p \leq 4/7.$

The flows examined by Stratford consist first of a flat-plate flow, just as with the $\bar{C}_p = x^m$ flows. Hence, x is distance measured from the leading edge of the plate, and $R = u_0x/\nu$. If the flows begin the pressure rise at a point x_0 such that $\bar{C}_p = (x - x_0)^m$, the left-hand side of (6.2) starts from a zero value, provided that $m > 1/3$. The left-hand side then grows. When it reaches the limiting value of S, separation is said to occur. The study of [14] showed the constants to be slightly different, but here, for our purposes, we accept Stratford's values. See [17] for further details.

If S is held at its limiting value of 0.39 for $d^2p/dx^2 \geq 0$, (6.2) amounts to an ordinary differential equation for $\bar{C}_p(x)$. It is evident from (6.2) that the equation describes a flow that is everywhere ready to separate. Stratford presents the following solutions:

$$\bar{C}_p = 0.645\left\{0.435\,R_o^{1/5}\left[\left(\frac{x}{x_o}\right)^{1/5} - 1\right]\right\}^{2/n} \quad \text{for } \bar{C}_p \leq \frac{n-2}{n+1} \tag{6.3a}$$

and

$$\bar{C}_p = 1 - \frac{a}{[(x/x_o) + b]^{1/2}} \quad \text{for } \bar{C}_p \geq \frac{n-2}{n+1} \tag{6.3b}$$

In that two-part solution, x_o is the start of pressure rise, $R_o = u_0x_o/\nu$ and x is the distance measured from the very start of the flow, which begins as flat-plate, turbulent flow. The number n is a constant that Stratford finds to be about 6. The quantities a and b are arbitrary constants used in matching values and slopes in the two equations at the joining point, $\bar{C}_p = (n-2)/(n+1)$. Of course, (6.3a) describes the beginning of the flow, and (6.3b) the final part. The flow is an equilibrium flow that always has the same margin, if any, against separation.

Two families of such flows have been computed; they are shown in Figure 20. They correspond to the same set of conditions that were used in the $\bar{C}_p = x^m$ flows. As has already been mentioned, they represent true limiting flows — the slightest increase in adverse gradient anywhere should cause separation. The curves assume the length of flap-plate runs indicated, but just as for the $\bar{C}_p = x^m$ families, what is of more fundamental significance is the boundary-layer thickness at the beginning of pressure rise. Hence, a table of initial values of R_θ is included. With the aid of those R_θ-values, the curves could be applied to arbitrary forward pressure distributions having mixed laminar/turbulent flow.

Within the accuracy of the theory, which tests have proved to be correct and somewhat conservative, those curves show the fastest possible pressure rise that can be obtained from a natural boundary layer. Also, when compared with Cebeci-Smith predictions, the theory appears conservative. Figure 20, together with (6.3), exhibits the following features:

1. The initial slope $d\bar{C}_p/dx$ is infinite, so that small pressure rises can be made in distances from very short to zero.

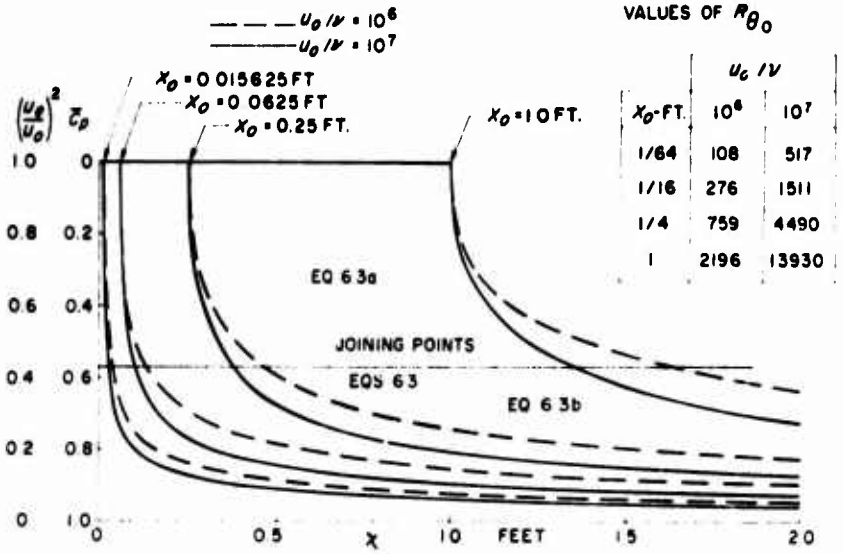

VALUES OF R_{θ_0}

	u_0/ν	
x_0-FT.	10^6	10^7
1/64	108	517
1/16	276	1511
1/4	759	4490
1	2196	13930

Figure 20. Stratford limiting flows at two values of unit Reynolds number.

2. It is easy to show that $C_p \sim x^{1/2}$ in the early stages.

3. The dominant variable is x/x_0 [see (6.3)]. Hence, when x_0 is small (i.e., the boundary layer is thin), pressure recoveries may be very rapid. When the initial run is long and the boundary layer is thick, the allowable average pressure gradient is much less. Or conversely, thick boundary layers are much more likely to separate than thin.

4. The unit Reynolds number effect is rather small (see Figure 20).

5. Theoretically, 100 percent of the dynamic pressure can be recovered, but the distance required is infinite.

6. Aside from error in the theory, the curves of Figure 20 are the shortest possible pressure recoveries – they are the "end of the line." Nothing better can be done except by boundary-layer control.

7. The Stratford pressure distribution is the path of least resistance connecting two pressure points A and B. See [9].

A Stratford flow has a continuous margin of safety over its entire length with respect to separation, whether at the beginning of pressure rise or far, far downstream. The margin of safety can be adjusted by changing the constant S in (6.2). Eq. (6.3b) shows that an infinite distance is required to bring a flow in the boundary layer to complete rest.

7. REYNOLDS NUMBER EFFECTS

In one sense Reynolds number effects are minor. We have already seen that there are no Reynolds number effects on the position of separation within a laminar boundary layer, and this is a fundamental result. For turbulent flows, Figures 18 and 19 show rather small shifts in separation when the Reynolds number is changed by a factor of ten.

In Section 6.3 we presented Stratford's turbulent separation formula, (6.2). Unlike the laminar separation formula (5.1), which does not bring in Reynolds number at all, the turbulent does, but only to R to the one-tenth power. This means that a change in Reynolds numbers by factors of 10 and 100 change $R^{1/10}$ only by factors of 1.26 and 1.58, respectively. Normally, then, when (6.2) is solved to find the separation point there will be only a slight shift of position with Reynolds number.

If the basic boundary layers have low separation sensitivity to Reynolds number why do airfoil characteristics often change considerably with Reynolds number? The answer, basically, is transition. As already seen, turbulent and laminar boundary layers have widely different separation propensities. Perhaps at low Reynolds numbers, as on a wind-tunnel model, laminar separation occurs near the leading edge. But at flight conditions the scale is so great that transition occurs forward of the laminar separation point. Then the adverse pressure gradient is negotiated by a turbulent boundary layer, which may have enough vigor to avoid separation. If so the stall characteristics may be drastically changed.

A convenient method for estimating the location of transition is Michel's transition criterion. Michel plotted available transition data in the form $R_{\theta_{tr}}$ vs $R_{x_{tr}}$. The transition points established a fairly well defined curve. If we plot the evolution of R_θ vs R_x for some particular airfoil, we

find that R_θ starts out below the Michel correlation curve. But later as we proceed downstream in terms of R_x, R_θ crosses the line. The crossover point is said to be the point of transition. According to [18] an interpolation formula defining Michel's curve is

$$R_{\theta_{tr}} = 1.174 \left[1 + \frac{22{,}400}{R_x}\right] R_x^{0.46} \qquad 0.1 \times 10^6 \leq R_x \leq 40 \times 10^6 \tag{7.1}$$

The growth of R_θ needed in (7.1) can conveniently and accurately be calculated by means of Thwaite's formula which can be written in the following form

$$R_{\theta_1}^2 \left(\frac{u_e \theta}{\nu}\right)_1^2 = \frac{0.45 R_c}{(u_e/u_\infty)_1^4} \int_0^{x/c} \left(\frac{u_e}{u_\infty}\right)^5 dx/c \tag{7.2}$$

where $R_c = \dfrac{u_\infty c}{\nu}$

This pair of equations makes it rather easy to test for the likelihood of transition. Of course, a pressure distribution for the nose portions of the airfoil must be available if (7.2) is to be evaluated. Also, it should be noted that (7.1) is applicable only to unswept airfoils; on swept wings a leading-edge instability may develop. Furthermore, if the surface is not hydraulically smooth transition may occur forward of the predicted point.

This leads us into the next comment. Figures 18 and 19 together did not show a strong effect of Reynolds number. But they do show a considerable sensitivity to the length of initial flat plate run. Now the extent of laminar flow determines the effective flat plate run. At $u_0/\nu = 10^7$ as in Figure 19, if the flow for the one-foot run were all laminar the equivalent turbulent flat-plate run would be only about 0.13 ft. Hence, separation is sensitive to Reynolds number in an indirect way because Reyno'ds number affects the proportions of laminar and turbulent flow. Bubble bursting of course is Reynolds number sensitive.

Because most papers are readily available, there is no reason to spend much time reviewing the considerable literature on the subject. Instead we shall stop with occasionally pointing out a useful article in some aspect of our concern One is an article by Thain [19] which bears on the problem of this section. The paper reviews a large amount of data. It includes not only a review of the possible separation processes but especially a large amount of data on the effect of Reynolds number and Mach number on maximum lift at low speeds. His Figure 3 is reproduced here as Figure 21 because of its interest. It is typical of the kinds of correlation attempted in connection with trying to analyze the various flow regimes. The correlation is made on certain geometrical properties of the airfoils. Gault did this a long time ago. Now that we can readily calculate velocities for any geometry, correlations should be made on velocities. The ultimate determinant of the flow behavior is the boundary layer. The boundary layer equations demand u_e, x input data, not geometry. Up to the point of initial separation the left and right hand extremes of Figure 21 can now be handled analytically. The middle portions remain the problem.

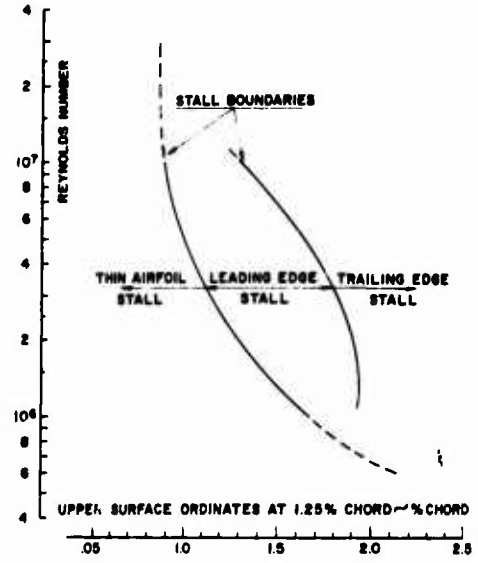

Figure 21. Effect of Reynolds number on the stalling characteristics of clean aerofoil sections as a function of aerofoil geometry, according to Thain and Gault [19].

Wimpress of Boeing [3] states that for $C_{L_{max}}$ estimates on new designs they depend on wind tunnel tests. Then based on a wealth of past experience these values are ratiod up by a factor that mainly depends on wing loading of the airplane.

8. MACH NUMBER EFFECTS

This section presents a few special comments on Mach number effects. Section 2 contained some, of course, in Figure 6 as well as Section 3. But what can be said about boundary layers directly? First, consider laminar flows. One transformed form of the full laminar boundary-layer equation is (3.1.9) of [20]. It is here repeated.

$$\frac{1}{C_\infty}(Cf'')' + P\left(\frac{\rho_e}{\rho} - f'^2\right) + Nff'' = x\left(f' \frac{\partial f'}{\partial x} - f'' \frac{\partial f}{\partial x}\right) \tag{8.1}$$

where

$$C = \frac{\rho\mu}{\rho_e\mu_e} \qquad \rho = \text{mass density}$$

$$P = \frac{x}{u_e}\frac{du_e}{dx} \qquad N = \frac{P+1}{2}$$

f = dimensionless stream function

We consider only two-dimensional flow. This equation is a weak function of Mach number. Its boundary conditions do not change with Mach number. They are $y = 0$, f, $f' = 0$, $y = \infty$, $f' = 1$. Next consider C. Determine ρ by Boyles' law and μ by the common formula $\mu \sim T^{0.76}$. Then

$$\frac{\rho\mu}{\rho_e\mu_e} = \frac{p/PT}{p_e/PT_e}\frac{T^{0.76}}{T_e^{0.76}}$$

But pressure is constant across the boundary layer. Therefore,

$$\frac{\rho\mu}{\rho_e\mu_e} = C = \left(\frac{T_e}{T}\right)^{0.24} \tag{8.2}$$

Furthermore, a guide to temperature variation across the boundary layer, assuming the flow to be adiabatic is

$$\frac{T_{recovery}}{T_e} = 1 + Pr^{[illegible]} \ldots M_e^2 = 1 + 0.146M_e^2 \quad (\gamma = 1.4,\ Pr = 0.73) \tag{8.3}$$

Then if edge Mach number is 1.0 the greatest value that C in 8.2 can obtain is

$$C_{max} = (1.146)^{0.24} = 1.033$$

Hence C is very nearly constant, and it is even more so at lower speeds. The term [illegible] in [illegible] changes somewhat more, but the change is still small. The pressure distribution enters into the problem through the term $P = (x/u_e)(du_e/dx)$. Now, if as we change speed we hold $P(x)$ invariant with some kind of pressure distribution that would produce a laminar separation, what would happen to the separation point? The answer is very little; $P(x)$ does not change, the boundary conditions do not change, and C and [illegible] change very little, as long as we are restricting ourselves to subsonic, adiabatic flow. For compressible flow the energy equation is needed to give information on the temperature but in our approach we were able to establish bounds without using it.

Montuschi [2] reports studies made by a variety of methods on the effect of compressibility on separation in Howarth's retarded flow. [illegible] At Mach zero separation is at [illegible] at Mach [illegible] it moves forward to about [illegible]

In short, the effect of compressibility on a laminar boundary that is subject to a fixed velocity distribution is small. But as commonly observed there is considerable effect. What happens is that compressibility affects the pressure distribution, so that the flow is subject to a different and usually more severe $(x/u_e)(du_e/dx)$ distribution.

Now consider turbulent flow. Some study was made of the problem by the author in [3]. He calculated separation loci for the canonical $C_p = x^m$ flows discussed in Section 6, but at $M_o = 1.0$. The results are shown in Figures [illegible] and 23. When compared with Figures 18 and 19 it is seen that separation is clearly delayed at $M_o = 1.0$. This should not be too surprising in view of the formula for compressible pressure coefficient

$$C_p = \frac{2}{\gamma M_o^2}\left\{\left[1 + \frac{\gamma-1}{2}M_o^2\left(1 - \frac{u_e^2}{u_o^2}\right)\right]^{\gamma/(\gamma-1)} - 1\right\} \tag{8.4}$$

When this is solved for $(u_e/u_o)^2$ the adverse velocity gradients are found to be considerably reduced. In fact, for $\bar{C}_p = 1.0$, $(u_e/u_o)^2$ is 0.18, a considerable distance from stagnation. If the flow is brought to complete rest, C_p reaches a value of 1.28.

The alternate treatment is to set $1 - (u_e/u_o)^2 = x^m$ independent of Mach number. One case has been studied and the result is shown in Figure 24, taken from [3]. Differences between $M_o = 0$ and 1.0 are small. Again as with the laminar case this is to be expected from examination of the governing momentum equation. Like the laminar, Mach number only mildly changes its constants. Figures 22, 23 and 24 were run earlier by a less accurate computational method and results do not agree precisely with those of Figures 18 and 19. Normally Figures 18 and 19 should be used.

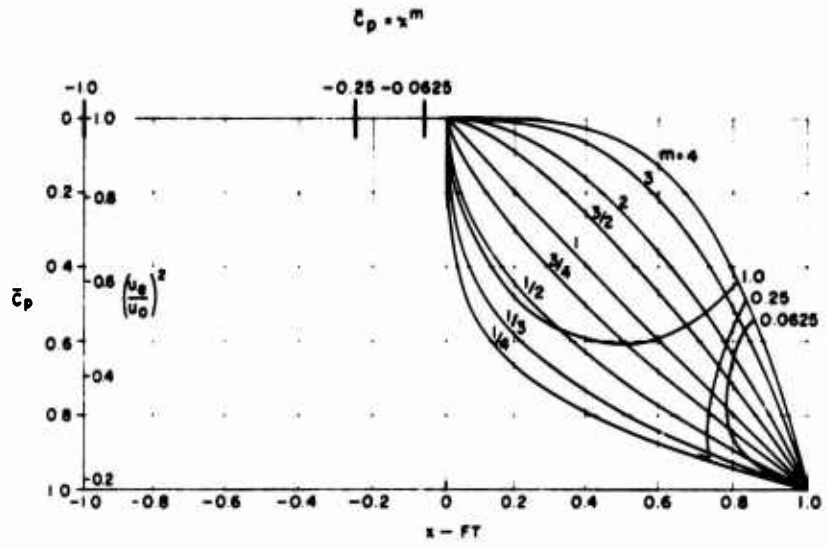

Figure 22. Separation loci for a family of canonical pressure distributions. $u_0/\nu = 10^6$, $M_0 = 1.0$.

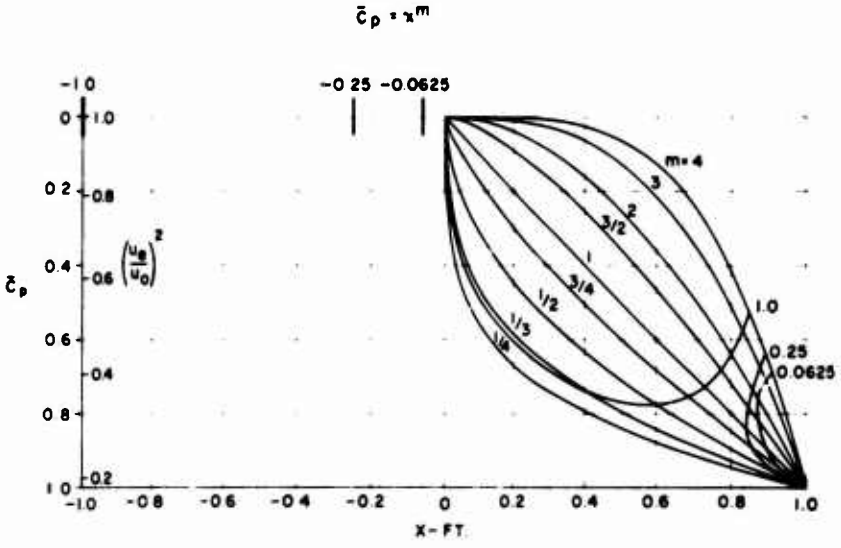

Figure 23. Separation loci for a family of canonical pressure distributions. $u_0/\nu = 10^7$, $M_0 = 1.0$.

Reference 1 contains an extension of Stratford's turbulent separation criterion to compressible flows, made by Gadd. The author has not personally tried to assess its accuracy. But it is worthy of consideration, particularly because of its analytic simplicity. Wooten [22] has a useful paper on the effect of compressibility on maximum lift of airfoils. It is a comprehensive survey of the subject, but entirely of a descriptive nature. It is useful in both showing the state of the art of the maximum lift problem and the complexities of the subject.

9. SHAPE EFFECTS

Because this lecture is not concerned with design particularly, it is assumed that shapes are given. Nevertheless it is felt that this lecture would not be complete without mentioning something about the importance of shape. As far as possible, the nose of the airfoil should cleave cleanly into the flow. That is, for high lift is should have camber or flaps, which amount to the same thing. Figure 25 shows the effectiveness of flaps in reducing pressure peaks and adverse gradients.

$$C_p = x^m = 1 - \left(\frac{u_e}{u_o}\right)^2$$

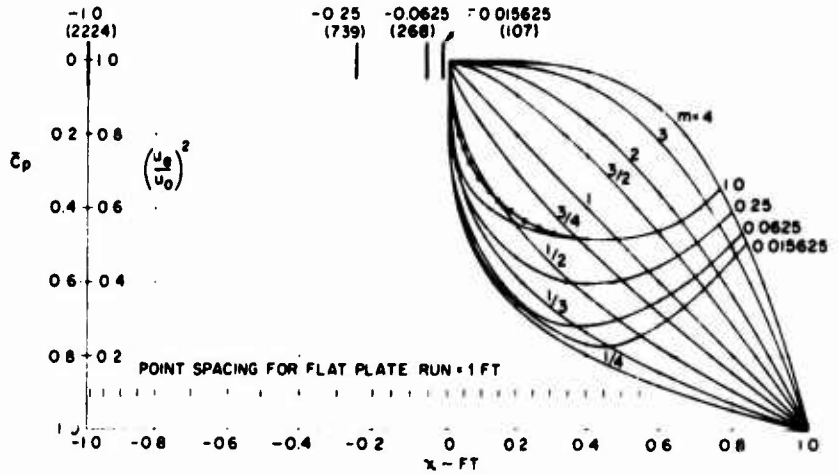

Figure 24. Separation loci for a family of canonical pressure distributions. The dotted curve for the one-foot rooftop run is the separation locus for $1 - u_e^2/u_o^2 = x^m$ when $M = 1.0$. $u_o/\nu = 10^6$/ft, $M_o = 0$ except as noted.

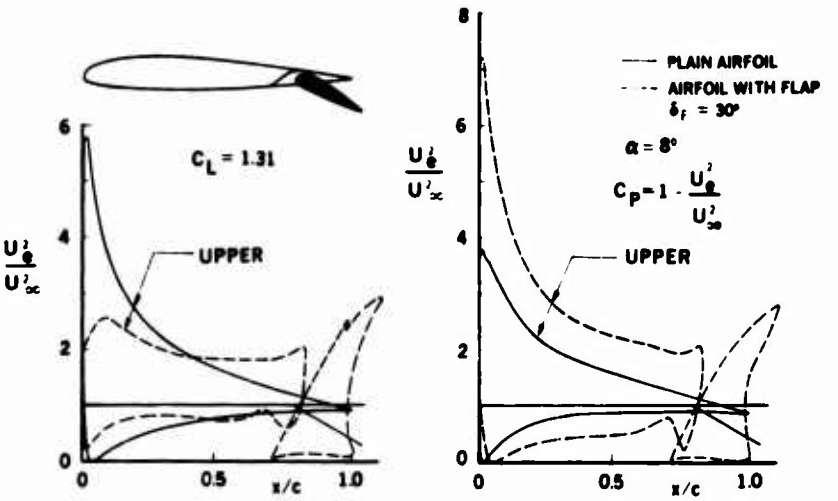

Figure 25. The effectiveness of flaps in reducing pressure peaks.

Thin leading edges are another cause of high pressure peaks. To illustrate we will consider the ellipse family with circulation sufficient to fix the rear stagnation point on the end of the major axis. The values of peak velocity for $\alpha = 10°$ are shown below.

Peak Nose Velocities on Ellipses with Circulation

$\alpha = 10°$

Thickness Percent	2	4	6	9	12	15	18
c	1.113	1.135	1.157	1.189	1.222	1.255	1.287
$(u_e/u_\infty)_{max}$	17.74	9.09	6.22	4.34	3.43	2.90	2.56

The necessary formulas were taken from [23].

Slats are an effective means of reducing nose pressure peaks. Figure 26 shows that a slat reduced nose velocities squared from 10.04 to about 3.3.

Shaping in general is advantageous. Discontinuities can be causes of early separation. Figure 27 shows how two kinds of flap treatment cause undesirable bumps in a pressure distribution. Reference 9 was greatly concerned with the shaping process. For more details consult it.

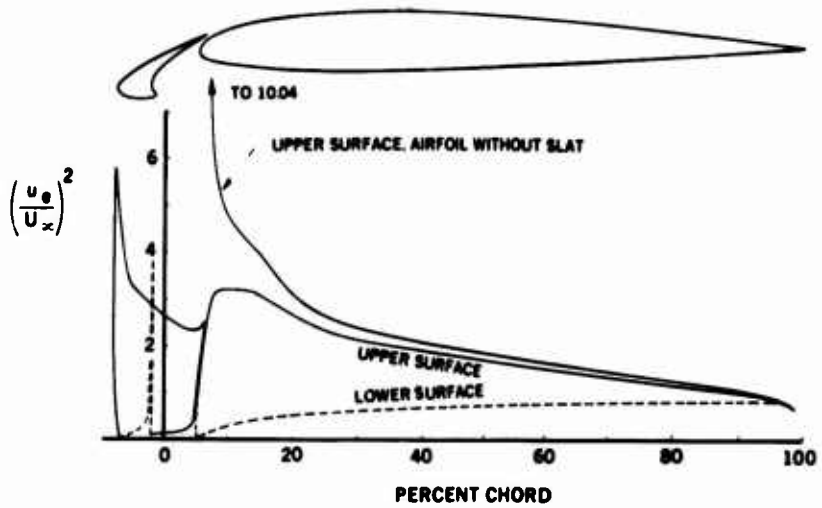

Figure 26. A typical pressure distribution for an airfoil with and without slat. Note drastic change on upper surface pressure distribution caused by slat. α = 13.15° c_ℓ = 1.45 for two-element airfoil.

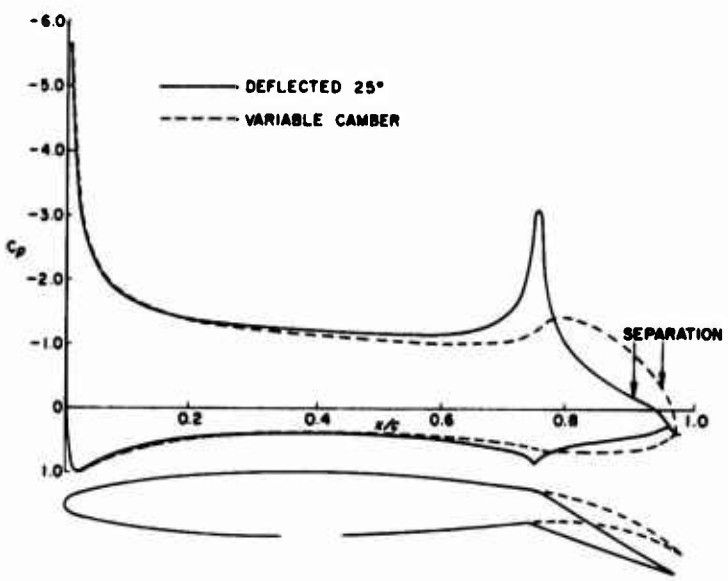

Figure 27. Comparison of two kinds of flaps on a NACA 63A010 airfoil. For the plain flap α = 0° and inviscid c_ℓ = 1.78. The airfoil with variable camber flap was set at α = 1.06° in order to obtain the same c_ℓ. Separation points are marked by arrows. R_c = 10^7. Transition is at suction peak.

LECTURE 2 SEVERAL SPECIAL TOPICS

10. STALL PROCESSES ON AIRFOILS

A few years back Arvel Gentry and Wayne Oliver of my group completed a two year contract for the Office of Naval Research. The subject was transonic maneuvering. Because of the applicability and timeliness of much of the material, we intend to quote from it at some length. The study is the latest broad survey of the problem that the author knows of. The work is in two volumes given here as [24] and [25]. Its general purpose was to assess the state of the art of analysis of this problem and implement methods by computer if they were available but not presently programmed. Reference 24 contains 124 references on the subject.

Before getting into the subject of stall processes on airfoils, it is useful to get the complete picture of the aerodynamics and dynamics of transonic maneuvering and buffeting. Figure 28 summarizes it. This figure should be studied carefully. It graphically brings out the tremendous variety of problems and effects that must be considered in the complete stall and buffet problem. The figure moreover neglects the elastic and inertial aspects of an airplane. Two different size airplanes with different weights and rigidities but with identical force and moment coefficients are likely to have considerably different stalling and buffeting characteristics.

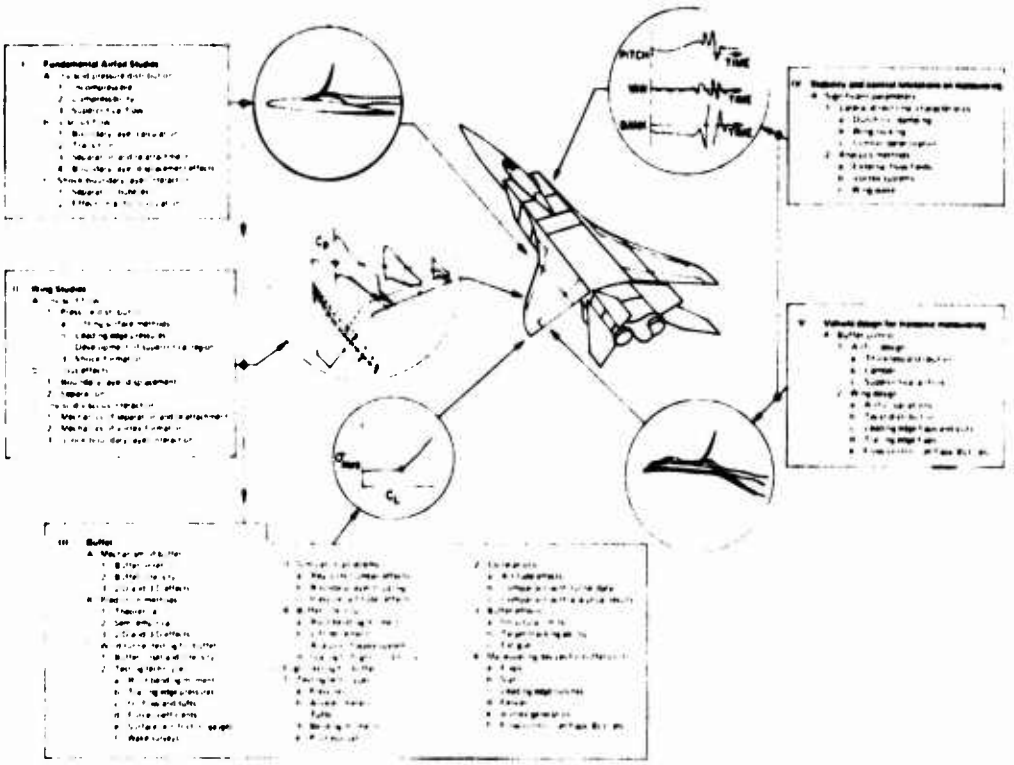

Figure 28. Aspects of transonic maneuvering aerodynamics.

We shall now review some of the general stall and separation characteristics of airfoils. In Lecture I we stopped with predicting the start of separation. Now we consider the problem after separation has started. Figure 29 shows the experimentally observed evolution of the two primary classes of separation at low speed. One class is leading-edge separation due to the flow being laminar at the separation point. In the upper left illustrations, the white portion adjacent to the airfoil is the separated region. The cross hatched portion generally depicts the boundary layer. A typcial evolution for thin airfoils begins with I. There is no separation and a typical pressure distribution is shown by I on the right as well as 0 which represents a flow at still lower α. Then, as angle of attack is increased, a small bubble in II forms near the nose. It turns turbulent at the rear so that the flow reattaches and the bubble ends. It may be only 1%-chord long. The accompanying pressure distribution shows a small flat spot. At higher angles the bubble may lengthen as in III, with an accompanying larger flat spot in the pressure distribution. Finally, the bubble may stretch clear back to the trailing edge as in IV.

Now look at the middle part of the figure, dealing with trailing-edge separation. This type occurs on thicker or more highly cambered airfoils. There is no leading-edge separation and the turbulent boundary-layer separates because it simply cannot make the grade at the rear. In this sequence I is unseparated, as is 0 in the pressure distribution. Number II has a small amount of separation. It is evidenced by the leveling off of the pressure distribution at the rear. Numbers III and IV show increasing amounts of separation and their characteristic pressure distributions.

The bottom of the figure shows characteristic C_L vs α curves. As to be expected from the process, trailing edge separation produces a well-rounded peak. The short bubble that bursts usually leads to a sharp stall. The long bubble brings on a gradual distortion of the effective airfoil shape and introduces early rounding over the lift curve.

Figure 30 is a continuation of the process into high speeds. Figures 30A and B are enlarged illustrations of two states that were shown in Figure 29. They could be at either high or low speed so

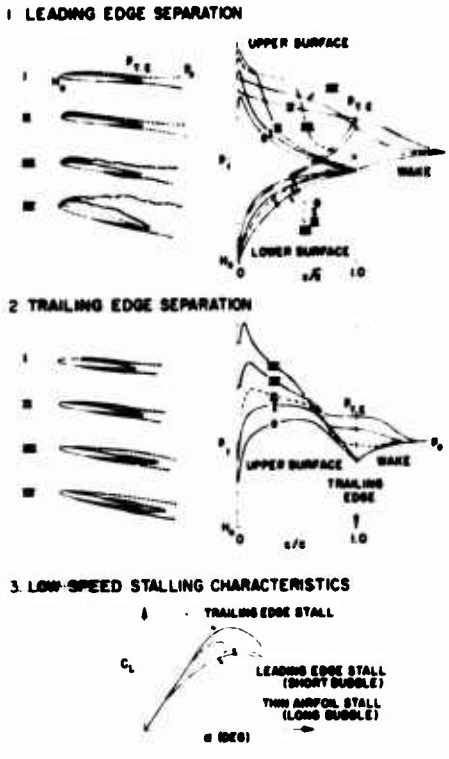

Figure 29. Low speed flow separation characteristics.

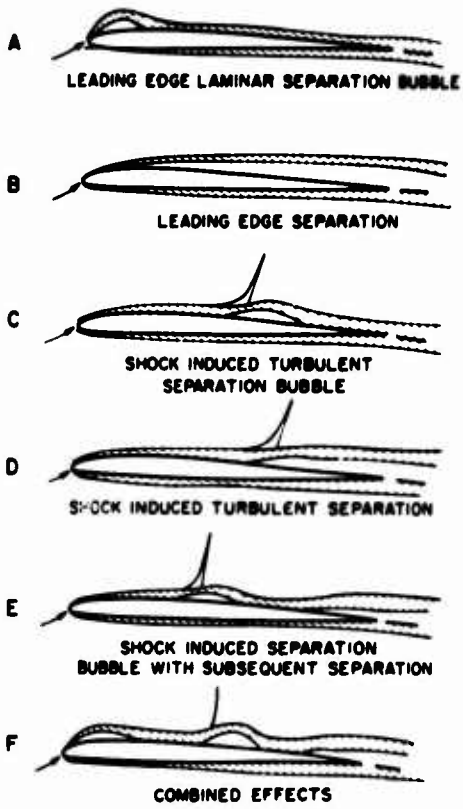

Figure 30. Flow separation characteristics at transonic speeds.

long as shocks had not developed. In 30C a weak shock has developed. It has caused a separation bubble but not complete separation. As the Mach number gets higher the shock moves back and becomes stronger. Also towards the rear the boundary layer is thicker and more ready to separate. Then full separation may set in as shown. Other combinations can occur and two possibilities are illustrated in Figures 30E and 30F.

Figure 31 is an elaboration of the shock growth and rearward movement process illustrated in Figure 30 C and D. The shock gets stronger, it moves back and the induced separation bubble grows until finally the end of it is located past the trailing edge.

Figure 32 shows still more variations on the process, and these are ones that should lead to buffeting.

Figures 33 and 34 give still more information on the processes and possibilities. Figure 33 shows typical angle of attack effects at constant Mach number and Figure 34 typical Mach number effects at constant α.

With regard to the fluid mechanics of laminar bubbles and their bursting Gaster's careful investigations and criteria [26] are probably the best. Horton [27] however, has a very useful semi-empirical method for predicting the length of a bubble and whether it might burst. It is interesting that if a theoretical shock is smeared out slightly (over about 4-) the Cebeci-Smith method can predict separation or the lack of separation.

11. CALCULATION OF FLOWS WITH SEPARATION

In this section we will give a few comments on the problem and the embryonic methods. It is by no means a complete survey. In inviscid flow, the flow is normally assumed to follow the boundary so that calculations with relative ease become possible. A boundary layer is a thin layer in which pressures are impressed by the main flow. But when separation occurs, the flow neither follows the body nor is the separated region thin. Hence, pressures are not just impressed upon the separated region. This region

then becomes an equal partner with the main flow in determining pressures. However, in many cases velocities in a separated region are low, and while viscosity has indeed caused the separation, it may not enter importantly after the event.

Klaus Jacob has probably the most successful method of accounting for separation [28] [29]. He assumes that the separated flow can be simulated by a purely inviscid flow. Figure 35 illustrates his approach. A separation on the flap is assumed to begin at S and the line SW is the edge of the separated region. The separated region is simulated by blowing which starts at S as sketched. The basic conditions that must be satisfied in the solution are:

1. The flow must follow the airfoil surface except downstream of S.
2. Blowing is such as to make velocities at S, W and L equal. Velocities at S and W are made equal because SW is approximately a free streamline. Velocities at W and L are made equal to approximate the Kutta condition.
3. The separation point S is found by boundary-layer calculations.

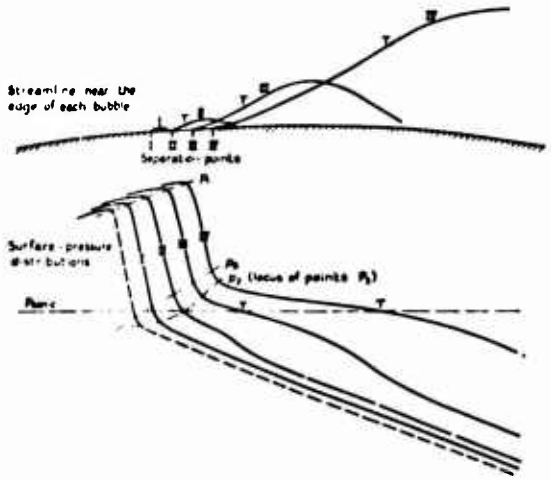

Figure 31. Successive stages in the development of the separation bubble for a prescribed variation of p_1.

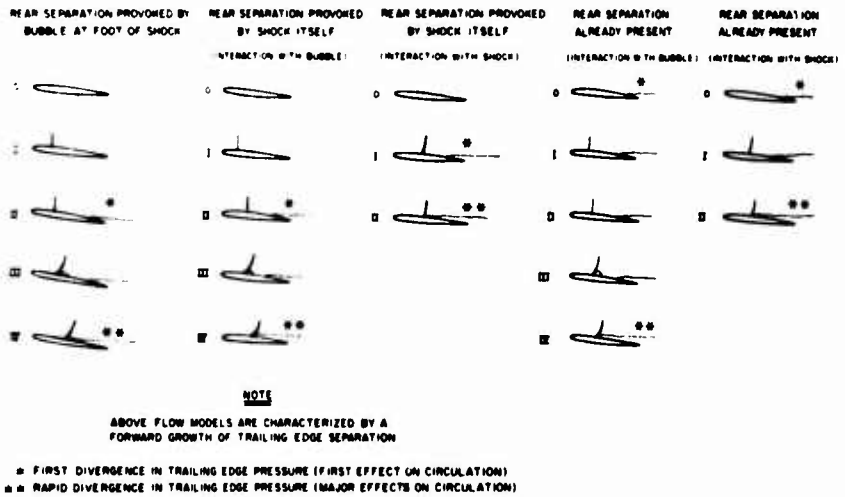

Figure 32. Forms of high-speed flow separation.

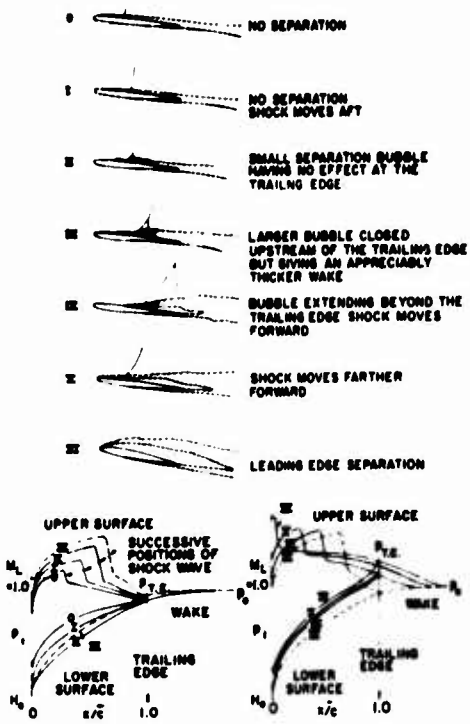

Figure 33. High-speed flow separation with α increasing and Mach number constant. Rearward growth of bubble, followed by leading-edge separation at high α.

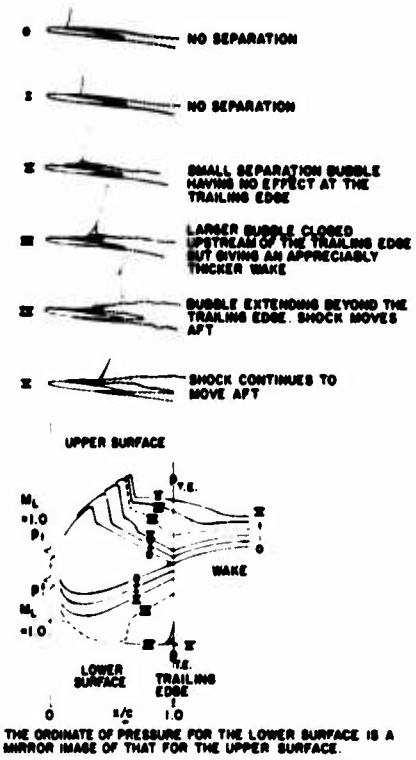

Figure 34. High-speed flow separation with Mach number increasing and α constant. Rearward growth of bubble, with continued aft movement of shock toward trailing edge.

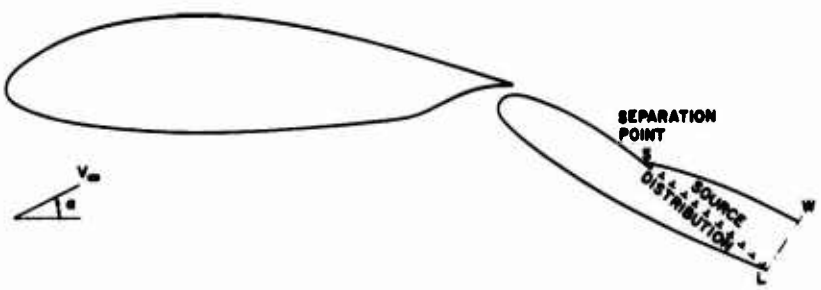

Figure 35. A potential flow model for separated flow on multi-element airfoils.

In essence one starts the calculation with unseparated flow. This gives a pressure distribution from which boundary-layer calculations can first be made to find an initial separation point, S. Then with blowing beginning at this point, a new inviscid calculation is made, and the process iterated. Various potential flow methods can be used, of course.

Figure 36 shows one of Jacob's results. $C_{L_{max}}$ is predicted and there is definitely a peak in its value. At $R_C = 2.7 \times 10^6$ agreement with test is good. Reynolds number effects come in through the boundary-layer calculations. The method now only handles trailing-edge separation. It is being studied at Douglas. Sometimes this excellent success is found, other times not, but success is good enough to justify further effort.

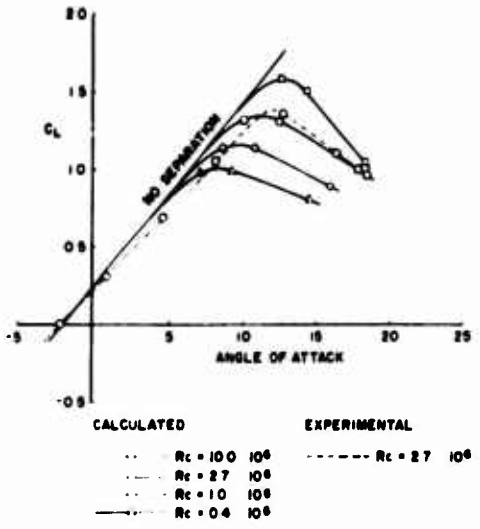

Figure 36. Calculations made by Jacob [28] of C_L vs α for the NACA 2412 airfoil at several Reynolds numbers.

The same basic philosophy can be followed by other approaches. It is theoretically possible to solve the problem of Figure 35 as a mixed boundary value problem, that is given the shape everywhere but along SL; and starting at S given the pressure, find the line SW. That, in fact, has been done for special airfoils by Lang and Fabula [30], [31]. In connection with torpedo guidance they studied the concept of blowing some of the exhaust gas out one side or the other of the stabilizing fins as a means of replacing movable elevators and rudder. The gas bubble formed on the side effectively changed the airfoil shape and hence the lift. A mixed boundary value problem was solved, several water tunnel tests were run and the agreement between test and theory was in general very good. In this problem, of course, the deadwater region is filled with a gas whose density is far less than that of the ambient fluid. These encouraging results certainly justify further efforts along the lines of approximating a separated deadwater region by an inviscid flow. After all, on an airfoil viscosity causes circulation, but we do very successful analysis by neglecting it.

There are other possibilities. Klineberg and Steger [32] have judiciously combined finite-difference methods for the transonic inviscid flow equation and integral methods for the boundary-layer part and produced good results for separation at the rear of a biconvex airfoil. Just at the time of this writing the author received Reference 33, which claims to have good success with calculating separated flow in a diffuser.

12. BUFFET

Because of coverage elsewhere in this series, the author will do no more than make some reference to the work in [24]. This report contains a figure that summarizes and vividly shows the complexity of the transonic maneuvering and buffeting problem. Buffeting and maneuvering of course are inseparable, because as extreme conditions are reached buffeting is part of the motion. The data apply to the F-4 fighter and were taken in connection with study of leading-edge devices to improve transonic maneuvering and buffeting. The figure is reproduced here as Figure 37. Along the edge are listed and illustrated some of the factors that help determine the final motion. The complete airplane problem, indeed, is complicated. The center rectangle shows flight recorder data. If one reads the scales he sees that the pilot had quite a ride.

Reference [24] gave a good deal of attention to Thomas's theory of buffet onset [34] [35]. In Thomas original theory he stated that buffet would commence when separation at the rear of the airfoil moved forward to the shock, at which time the flow would get unsteady and buffet develop. The theory is interesting because as Mach number increases, separation if any, will likely move forward and the shock will move back. Later in [35] Thomas suggested that buffet would occur when separation moved forward to the 90%-chord line. This criterion seems little different from that which goes back to Pearcey, where he suggested that in wind-tunnel tests buffet would begin when there was a break in trailing-edge pressures as a function of angle of attack. Thomas' first method was evaluated in [24]. On conventional airfoils it was found to predict very well but on aft-loaded airfoils the predictions were poor. The theory nevertheless is attractive, because when the shock wave and separation are nearly coincident a situation favoring unsteadiness exists. Other buffet prediction methods have nothing about them that is directly related to unsteadiness. Pearcey's method which observes a break in pressures at the trailing edge is successful only because a separated flow always seems to have unsteadiness.

A very good paper on the state of the art of buffet theory and testing has recently been published by Mabey [36]. It covers test techniques, dynamics, aerodynamics and even describes a buffet rating system. Figure 38 from [24] is a useful summary of the considerable variety of methods for detecting buffet onset from either wind tunnel or flight test.

13. THREE-DIMENSIONAL EFFECTS

Since a picture is supposed to be worth a thousand words we shall start out by showing a good set of photos of tuft and oil flow patterns on an attack wing having a rather conventional peaky section. Figures 39 through 44 show the series. The flow is symmetrical so that we see the same flow marked by two different methods. At low angles of attack not much is seen except the expected outboard flow near the trailing edge. At 8.8° angle of attack a shock can easily be seen outboard near 30% chord, and of course the spanwise flow is increased. The oil and talc were emitted through small orifices in the nose of the airfoil. The oil flow and tufts were fluorescent and made visible by ultraviolet light.

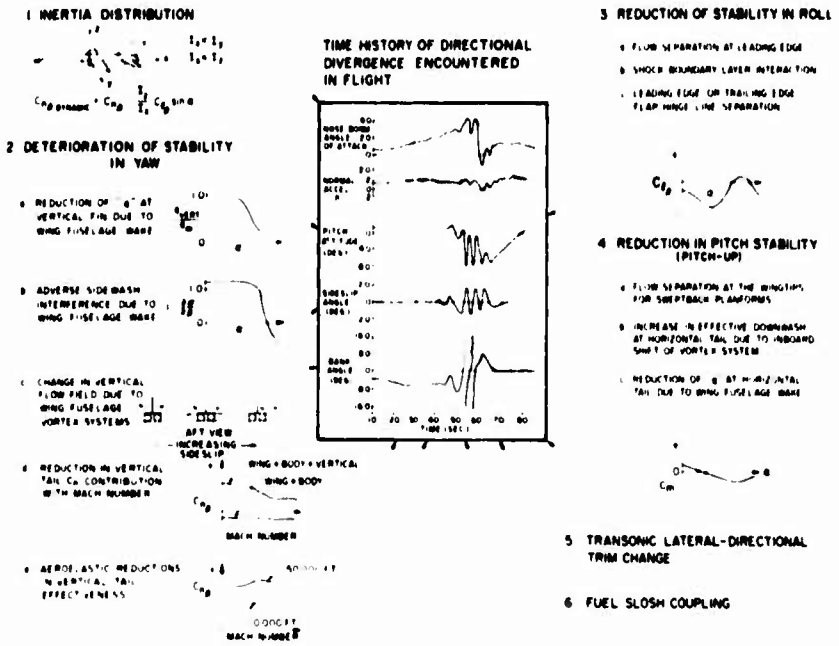

Figure 37. Factors influencing transonic stability at large lift coefficients. F-4 flight-test data.

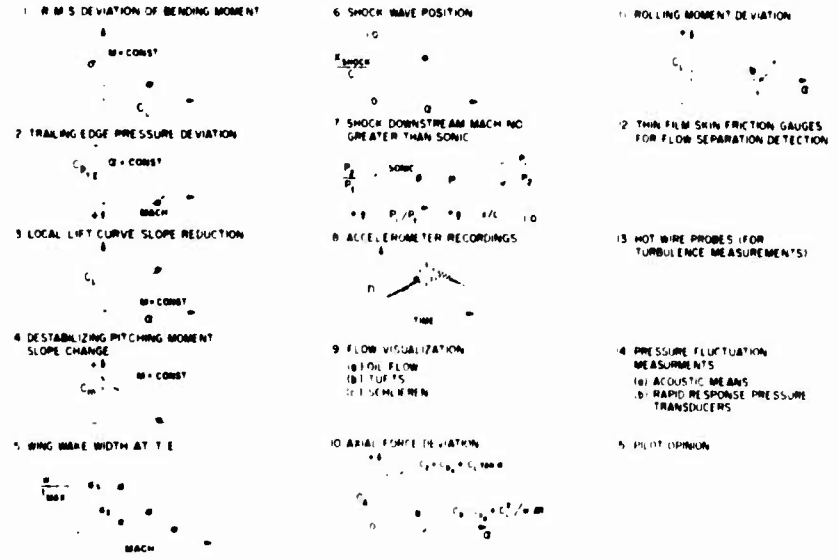

Figure 38. Methods of buffet/flow separation detection.

In Figure 42 the shock is even more strongly evident. It is clearly shown by the tufts as well, which suddenly turn at right angles. At , = 12.6° the tufts show that some separation has developed and this and the final photo show very wild oil flow patterns. They indicate the tremendous complexity of a true three-dimensional boundary-layer flow.

At the present time so long as all velocities are subsonic the entire potential flow for shapes like this or worse can be calculated very well up to the first separation, for example, the Douglas-Neumann Program. Work is actively under way to analyze such wing shapes at transonic speeds but because of the

Figure 39. An attack wing with conventional airfoil section. $M_\infty = 0.78$, $\alpha = 6.1°$, $C_L = 0.40$.

Figure 40. An attack wing with conventional airfoil section. $M_\infty = 0.78$, $\alpha = 7.4°$, $C_L = 0.51$.

Figure 41. An attack wing with conventional airfoil section. $M_\infty = 0.78$, $\alpha = 8.8°$, $C_L = 0.61$.

Figure 42. An attack wing with conventional airfoil section. $M_\infty = 0.78$, $\alpha = 10.1°$, $C_L = 0.71$.

Figure 43. An attack wing with conventional airfoil section. M_∞ = 0.78, α = 12.6°, C_L = 0.79.

Figure 44. An attack wing with conventional airfoil section. M_∞ = 0.78, α = 16.0°, C_L = 0.89.

nature of the transonic equations they require some kind of finite-difference method. This is much slower and whether it can handle a complicated shape with the necessary combination of precision and computing time remains to be determined. The boundary-layer aspect is in about the same state, at least for the more complicated flows. But for flows like those just shown at the lower angles of attack good turbulent boundary-layer methods are imminent. Computation time does not appear to be a problem. But at higher angles of attack where we wish to know separation patterns and where we wish to predict the oil flow swirls, practical calculation methods would seem to be at least five years away.

The literature and detail knowledge on three-dimensional wing flow is very large and generally available. Therefore, we shall only mention a few documents that help lead one into the subject. The first is by Kuchemann [12], which still stands an an accurate exposition of the involved flow processes that may occur on a swept wing. Another, by Foster [37] brings the subject up to date.

Three very useful U.S. documents on the subject of three-dimensional swept wing aerodynamics are [38], [39] and [40]. The first is a comprehensive review of a very wide variety of data including fuselage and tail effects, all at good Reynolds numbers. It is a 149 page report. The second is a more recent report that is especially concerned with stall characteristics. The third is unusual, for it reports on a systematic series of eleven wings at Mach numbers from 0.23 to 0.94. The models were all instrumented to measure wing-root bending moments and hence buffeting. Axial force was found to provide the best conventional indication of buffet onset. This report, too, is large. It contains 265 pages, much of it tabulated data.

14. REFERENCES

1. Chang, P.W.: Separation of Flow. Pergamon Press, New York, 1970.

2. Jones, B.M.: Stalling. J. Roy. Aero. Soc., Vol. 38, pp. 753-770, 1934.

3. Anon: Fluid Dynamics of Aircraft Stalling. AGARD Conf. Proc. No. 102, Nov. 1972.

4. Anon: Separated Flows. AGARD Conf. Proc. No. 4, May 1966.

5. Chappell, P.D.: Flow Separation and Stall Characteristics of Plane, Constant-Section Wings in Subcritical Flow. The Aero. J., Vol. 72, pp. 82-89, Jan. 1968.

6. Callaghan J.G.: Aerodynamic Prediction Methods for Aircraft at Low Speeds with Mechanical High Lift Devices. AGARD Lecture Series No. 67, May 1974.

7. Smith, A.M.O. and Cebeci, T.: Numerical Solution of the Turbulent Boundary-Layer Equations. Douglas Aircraft Co. Report No. DAC 33735, May 1967. AD656430

8. Rosenhead, L. (ed.): Laminar Boundary Layers. Oxford Univ. Press, 1963.

9. Smith, A.M.O.: High-Lift Aerodynamics. 37th Wright Brothers Lecture, AIAA Paper No. 74-939, Aug. 1974.

10. Mayer, J.P.: A Limit Pressure Coefficient and an Estimation of Limit Forces on Airfoils at Supersonic Speeds. NACA Research Memorandum RM No. L8F23, 1948.

11. Smith, A.M.O.: Aerodynamic Lifting Potentialities of Aircraft in Subsonic Flight. Douglas Aircraft Co. Report No. ES 20930, 1947.

12. Kuchemann, D.: Types of Flow on Swept Wings. J. Roy. Aero. Soc., Vol. 57, pp. 683-699, Nov. 1953.

13. Smith, A.M.O. and Clutter, D.W.: Solution of the Incompressible Laminar Boundary-Layer Equations. AIAA J., Vol. 1, No. 9, pp. 2062-2071, Sept. 1963.

14. Cebeci, T., Mosinskis, G.J. and Smith, A.M.O.: Calculation of Separation Points in Incompressible Turbulent Flows. J. of Aircraft, Vol. 9, No. 9, p. 618, Sept. 1972.

15. Loftin, L.K., Jr. and von Doenhoff, A.E.: Exploratory Investigation at High and Low Subsonic Mach Numbers of Two Experimental 6-Percent Thick Airfoil Sections Designed to have High Maximum Lift Coefficients. NACA RM L51F06, 1951.

16. Smith, A.M.O.: Aerodynamics of High-Lift Airfoil Systems. In Fluid Dynamics of Aircraft Stalling, AGARD-CP-102, 1972.

17. Stratford, B.S.: The Prediction of Separation of the Turbulent Boundary Layer. J. Fluid Mech., Vol. 5, pp. 1-16, 1959.

18 Cebeci, T. and Smith, A.M.O.: Analysis of Turbulent Boundary Layers. Academic Press, New York, N.Y., 1974.

19. Thain, J.A.: Reynolds Number Effects at Low Speeds on the Maximum Lift of Two-Dimensional Aerofoil Sections Equipped with Mechanical High Lift Devices. Rept. No. DME/NAE 1973(3), in Quarterly Bulletin of the Div. of Mech. Eng. and the Nat. Aero. Est., Ottawa.

20. Jaffe, N.A. and Smith, A.M.O.: Calculation of Laminar Boundary Layers by Means of a Differential-Difference Method. Progress in Aerospace Sciences, Vol. 12 Pergamon Press. Oxford, 1972.

21. Morduchow, M.: Review of Theoretical Investigations on Effect of Heat Transfer on Laminar Separation. AIAA J., Vol. 3, No. 8, pp. 1377-1385, Aug. 1965.

22. Wooten, L.R.: The Effect of Compressibility on the Maximum Lift Coefficient of Aerofoils at Subsonic Airspeeds. J. of the Roy. Aero. Soc., Vol. 71, pp. 476-486, July 1967.

23. Faulkner, S.M., Hess, J.L., Smith, A.M.O. and Liebeck, R.H.: Charts and Formulas for Estimating Velocity Fields in Incompressible Flow. Douglas Rept L.B. 32707, 1968, AD772233.

24. Gentry, A.E. and Oliver, W.R.: Investigation of Aerodynamic Analysis Problems in Transonic Maneuvering. Vol. I, Final Report, Douglas Aircraft Co. Report No. MDC J5264-01, Sept. 1971 (AD737 293).

25. Gentry, A.E. and Oliver, W.R.: Investigation of Aerodynamic Analysis Problems in Transonic Maneuvering. Vol. II, Airfoil Analysis Computer Program, Douglas Aircraft Co. Report No. MDC J5264-02, Sept. 1971 (AD740 124).

26. Gaster, M.: The Structure and Behavior of Laminar Separation Bubbles. In Separated Flows. AGARD Conf. Proceedings No. 4, Pt. 2, May 1966.

27. Horton, H.P.: A Semi-Empirical Theory for the Growth and Bursting of Laminar Separation Bubbles. ARC CP 1073, 1967.

28. Jacob, K.: Theoretische Berechnung von Druckverteilung und Draftbeiwerten für Beliebige Profile bei Inkompressibler Strömung mit Ablösung, AVA Bericht 67A62, 1967.

29. Jacob, K.: Berechnung der abgelösten inkompressiblen Strömung um TragflugelProfile und Bestimmung des maximalen Auftriebs. Zeitschrift. f. Flugw. Bd 17 pp. 221-230 (1969)

30. Lang, T.G. and Daybell, D.A.: Water Tunnel Tests of Three Vented Hydrofoils in Two-Dimensional Flow. J. Ship Research, Vol. 5, No. 3, pp. 1-15, Dec. 1961.

31. Fabula, A.G.: Thin-Airfoil Theory Applied to Hydrofoils with a Single Finite Cavity and Arbitrary Free-Streamline Detachment. J.F.M., Vol. 12, pp. 227-240, 1962.

32. Klineberg, J.M. and Steger, J.L.: Calculation of Separated Flows at Subsonic and Transonic Speeds. Proc. 3rd Int. Conf. on Numerical Methods in Fluid Mechanics, Vol 2, Paris, July 1972, Springer Verlag.

33. Wooley, R.L. and Kline, S.J.: A Method for Calculation of a Fully Stalled Flow. Report. MD-33, Thermosciences Div., Stanford Univ., Nov. 1975.

34. Thomas, F.: Determination of Buffet Limits of Airfoils in the Transonic Velocity Range. Transl. of "Die Ermittlung der Schuttelgrenzen von Tragflugeln im Transsonischen Geschwindigkeitsbereich." In Jahrbuch 1966 der DGLR, Friedrich Vieweg and Son Gmbh, pp. 126-144.

35. Thomas, F., Pedeker, G.: A Method for Calculating the Transonic Buffet Boundary Including the Influence of Reynolds Number. Paper No. 3 in AGARD Conference Preprint No. 83, Gottingen, April 1971.

36. Mabey, D.G.: Beyond the Buffet Boundary. The Aero. J., pp. 201-215, April 1973.

37. Foster, D.N.: The Low-Speed Stalling of Wings with High-Lift Devices. In Fluid Dynamics of Stalling. AGARD Conf. Proceedings No. 102, April 1972.

38. Furlong, G.C. and McHugh, J.G.: A Summary and Analysis of the Low Speed Longitudinal Characteristics of Swept Wings at High Reynolds Number. NACA Rept. 1339, 1957.

39. Harper, C.W. and Maki, R.L.: A Review of the Stall Characteristics of Swept Wings. NASA TN D-2363, 1964.

40. Ray, E.J. and Taylor, R.T.: Buffet and Static Aerodynamic Characteristics of Systematic Series of Wings Determined from a Subsonic Wind-Tunnel Study. NASA TN D-5985, June 1970.

PREDICTION AND ANALYSIS OF THE LOW SPEED STALL CHARACTERISTICS OF THE BOEING 747

by

William McIntosh
John K. Wimpress

The Boeing Company
Seattle, Washington
98124 U.S.A.

SUMMARY

It is important to estimate accurately the stall speed of a modern high-speed transport since take-off and landing performance, which has a large impact on the airplane's economic success, is based on this parameter.

The pre-flight estimates for the Boeing 747 were based on wind tunnel data obtained at a Reynolds number of approximately 1 million. These test results were adjusted to full scale flight values using correlation factors developed from other Boeing transport airplanes. As an independent check, high lift data were obtained in a pressurized wind tunnel up to a Reynolds number of 7.5 million and extrapolated to the full scale value of 40 million.

Flight results show that the correlation factors were moderately successful in predicting stall speeds. However, extrapolating the pressure tunnel data to full scale Reynolds numbers predicted the flight value of maximum lift coefficient with reasonable accuracy.

The empirical approach taken to predict the 747 stall speeds does not lead to any fundamental understanding of the physics of the stall. Therefore, a further analysis was undertaken that showed that the inclusion of aeroelastic and airplane dynamics in a stall analysis can explain quite well the demonstrated flight test speeds, and in particular the gross weight effect on the stall lift coefficient.

The wind tunnel data at all Reynolds numbers predicted satisfactory handling characteristics throughout the stall that were confirmed during flight testing.

1. INTRODUCTION

Modern jet transport airplanes normally fly at speeds well separated from their low speed stalls. There is no need for them to perform extreme maneuvers at low or moderate speeds or at high altitudes that might force them near their maximum lift coefficient. Only during take-off and landing, where the lowest possible speed is desired, does the stall become a matter of concern in the design. In these two critical phases of flight, the operational speeds must be such that adequate margin exists for atmospheric turbulence and piloting tolerance and that sufficient lift is available for necessary maneuvering. The magnitudes of these margins have been established through many years of experience and are defined, with but minor variations, by the various certificating agencies throughout the world, both military and civil. Usually, the operational speeds for take-off and landing are defined in terms of the stall speed of the airplane in the same configuration.

These operational speeds in turn define the useable take-off and landing field lengths of the airplane. The useable field lengths have a large impact on the economic usefulness of the transport, so much effort is exerted in making the operational speeds as low as possible. Thus, there is a desire to make the stall speed low and also to predict it accurately early in the design stages when the initial sales guarantees are being made. The initial predictions will be made several years before the airplane flies, and even the detail predictions for the final production configuration will be made some two years before the airplane is certified.

The importance of making the stall speed prediction accurately is demonstrated by considering the case where the airplane is designed to land with a full payload in exactly the field length available at its destination. In this case, an error of only 5 percent in predicting the stall speed will result in a 38 percent loss in payload capability and an even more dramatic 55 percent loss in the potential profit available to the operator on this particular mission.

The initial estimate of the stall speed of the 747 was made early in 1966 during negotiations with Pan American World Airways, the original buyer. These predictions were steadily refined during the design development of the airplane. Development of the low speed configuration involved some 4000 hours of wind tunnel testing over a period of 2-1/2 years. Many different configurations were considered, but this paper will discuss only the final configuration selected for production and the methods used to predict and analyze the full scale performance.

The methods used to predict the full scale flight performance, starting from the wind tunnel data of the final configuration, were not particularly elegant from the standpoint of theoretical aerodynamics. They involved no detailed analysis of the boundary layer or effect of Reynolds number on the various high-lift components. The approach used was one of practical engineering, limited in scope by the usual restrictions of time, people, and money. At the time the 747 was being developed, Boeing had already built and tested a series of jet transport having sweptback wings, different engine installations, and largely varying gross weights. This experience provided a great bank of flight data that could be correlated with the corresponding wind tunnel data as a function of configuration, center of gravity position, and wing loading. These correlations served as the primary bridge between the wind tunnel data and the predicted full scale performance of the 747.

However, the 747 had a leading edge flap that was markedly different from those on other Boeing airplanes, and therefore, it was felt necessary to evaluate the effects of Reynolds number on these leading-edge flaps. High Reynolds number tests were made that extended the wind tunnel data from a Reynolds number of approximately 1 million up to 7.5 million, based on the wing mean aerodynamic chord.

The flight test results shown in this paper are those obtained during the Federal Aviation Agency (FAA) certification of the 747. A total of 636 instrumented stalls were conducted to get stall speed data at all flap settings and gross weights and to completely evaluate the handling characteristics during the stall maneuver. A remote sensor of static pressure trailing behind the airplane was used for all air speed measurements. Accelerometers and rate and position gyros were used to establish the airplane motions, and a calibrated fuselage-mounted vane was used for measuring angle of attack.

Subsequent to the 747 flight tests an analysis was undertaken to determine if some of the anomalies inherent in the prediction versus test results correlation could be explained in a rational manner. The approach taken was to start from the same low Reynolds number wind tunnel data used in the prediction method and apply corrections for Reynolds number, Mach number, aeroelastic deflections and stall maneuver dynamics. The results from this analysis process were then compared with the flight test results.

2. DESCRIPTION OF THE 747 HIGH LIFT SYSTEM

A diagram of the 747 high lift system is shown in Figure 1. The wing has an aspect ratio of 7 and is swept back 37-1/2 degrees at the quarter chord. Both leading-edge and trailing-edge high lift devices are used. The leading-edge devices cover the entire span of the wing except for a small region next to the body. Inboard of the inboard nacelle is a flat Krueger flap with a rounded nose similar to that used on the 707. Between the nacelles, and outboard of the outboard nacelle, the Krueger flap is more sophisticated. As the flap is extended, a mechanical linkage bends the skin to form a continuous curve throughout its length. Also, the flap moves far enough forward to create a slot between it and the wing leading edge. This installation was the first time such a curved, slotted, Krueger flap had been used on a Boeing airplane.

The trailing-edge flaps extend from the body to approximately 70 percent of the span. The flap is divided into two major components separated to allow clearances for the jet efflux of the inboard engine. This space on the trailing edge is used for the inboard high-speed aileron. The trailing-edge system is triple-slotted, similar to that used on the 727 and 727, but tailored to the long-range mission of the 747. For take-off, the flap setting, as measured by the angle of the mid-segment, varies between 10 and 20 degrees, depending on take-off weight. The motion includes a great deal of Fowler action before much angular deflection occurs. For landing, the flap is extended to its full 30 degree deflection.* The various settings were selected after consideration of both the lift and drag, and the corresponding effects on field length performance, post-take-off climb, and go-around after a refused landing.

During the design of the 747 flap system, it was recognized that flap system design would be subject to some aeroelastic deflections, particularly on the leading edge devices which are basically flexible fiberglass panels. The flaps were designed so that under load they conformed to the angles and shapes defined during the wind tunnel development of the 747.

3. THE BASIC WIND TUNNEL DATA

The basic low-speed wind tunnel data were obtained in the University of Washington Aeronautical Laboratory wind tunnel, which has an 8 foot by 12 foot closed test section vented to the atmosphere. The model, shown in Figure 2, was an .04 scale replica of the 747 having a wing span of approximately 8 feet. This model duplicated carefully all the flap supports and fairings as well as all the contours, gaps, and slots that exist on the production airplane.

The wing was also twisted to simulate the aeroelastic deflections encountered during flight. Particular care was taken, since our experience has shown that many of the discrepancies between wind tunnel and flight, often blamed on scale effects, are in fact caused by an inadequate representation of the details of the flight configuration by the wind tunnel model. The data for representing the airplane flying near to the ground were obtained using a fixed ground plane.

An example of the data obtained from this model is shown in Figure 3. Normal wall and blockage corrections have been applied. Data is shown for a landing flap configuration of 30 degrees and typical take-off positions of 10 degrees and 20 degrees.

4. THE STALL ENVELOPE

Several full scale parameters must be estimated from this lift and pitching moment data as indicated in Figure 4, which shows the flight records obtained during a typical flight test stall. The principle item to be estimated is the Federal Aviation Regulation (FAR) stall speed. This speed is defined as the minimum speed obtained during a full stall that is approached at the rate of 1 knot per second. This minimum speed occurs during a dynamic maneuver and the airplane usually will be somewhere between .2g and .4g's at the time this minimum speed is reached. This FAR stall speed is used by the FAA as one consideration in determining take-off and landing speeds for airplanes certified within the United States. The corresponding FAR $C_{L_{Stall}}$ is defined at $C_{L_{Stall}} = \frac{W}{1/2\rho V^2_{Stall} S} = \frac{W}{qS}$ without considering the reduced load factor existing at the time V_{Stall} occurs. Another stall speed is the 1 g stall speed which is defined as that speed which occurs just as the normal acceleration breaks to a reduced value. This speed also is measured during a dynamic maneuver and may not occur at exactly 1 g normal acceleration. This 1 g stall speed is used as the basis for setting the take-off and landing speeds by the U.S. Air Force. The corresponding C_L historically has been used as $C_{L_{max}}$ in the structural analysis of the airplane. Also to be estimated, is the true $C_{L_{max}}$ achieved during the stall maneuver, where C_L is defined as $\frac{W}{qS}$. This maximum lift coefficient usually occurs at a speed below the 1 g stall speed and is the flight $C_{L_{max}}$ most nearly corresponding to the one measured in a wind tunnel test.

5. CORRELATION CURVES AND FLIGHT TEST RESULTS

5.1 FAR $C_{L_{Stall}}$ and $C_{L_{max}}$

Figure 5 summarizes the high-lift flight and wind tunnel data for a series of Boeing airplanes by showing the ratio of the FAR $C_{L_{Stall}}$ to the wind tunnel $C_{L_{max}}$. The data shows appreciable scatter between airplanes and the solid line was chosen as the value of the parameter to be used in estimating the 747 performance. The 747 flight test results generally lie somewhat below this estimated value. The data points shown in the upper part of the chart are for the airplanes at the maximum weights tested. The lower plot presents the trend of the stall speeds as a function of airplane wing loading, and shows that increasing cross weight decreases slightly the stall lift coefficient. This wing loading effect has been consistent throughout the history of Boeing airplanes. The values of wind tunnel $C_{L_{max}}$ used to develop these plots differs slightly from those shown in Figure 3. The reason is that there were no blockage corrections used in reducing the 747 wind tunnel data shown here. This was done in order to compare with the previous tests of the Boeing family, made before blockage corrections were a normal part of the wind tunnel data reduction procedure.

* Called "position 20" in the flight handbook

A similar summary of the 1 g $C_{L_{Stall}}$ is shown in Figure 6. Again, there is appreciable scatter in the data, and the solid line represents the value used in making the 747 pre-flight estimate. The 747 flight test results gave 1 g $C_{L_{Stall}}$'s as much as 8 percent below the original estimate. This fact is particularly surprising since a test installation of the 747-type leading-edge flap on a 707 gave a correlation factor well above the other airplanes. The 1 g $C_{L_{Stall}}$ showed the same trend with wing loading as was indicated for the FAR $C_{L_{Stall}}$.

At the time these estimates were being made, it was recognized that the 747 had a leading-edge device that might render past wind-tunnel-to-flight-test correlations inaccurate. Past Boeing airplanes had a leading-edge device, either Krueger flap or slat, that was relatively sharp, creating high pressure peaks and rapid pressure recoveries which would make the flow sensitive to Reynolds number effects. The 747, on the other hand, had a leading-edge device that was carefully designed using aerodynamic theory to produce a smooth pressure distribution having no severe gradients at high angles of attack. With the gradient selected to give no separations at low Reynolds number, no appreciable increase in lift should be expected as Reynolds number is increased.

In order to evaluate these considerations, a wind tunnel test was made in the 12 foot pressure tunnel at the Ames Aeronautical Laboratory of the NASA where the Reynolds number could be varied from approximately 1.2 million up to 7.5 million. These data, shown in Figure 7, are in good agreement at low Reynolds number with the data obtained in the University of Washington wind tunnel when corrected to the forward center of gravity position used in this figure. The increase in $C_{L_{max}}$ with Reynolds number was relatively modest, and the data showed enough linearity to allow extrapolation to the full scale Reynolds number of 30 to 40 million. The flight test data shown are the maximum C_L's achieved in the stall $\left(C_{L_{max}} = \frac{nW}{qS}\right)$ and indicate an agreement within 2 percent or less of the extrapolated wind tunnel values.

5.2 C_L's for Minimum In-Stick Speed

FAA certified lift-off speeds are related to the minimum speed that the airplane can demonstrate a complete take-off, called V_{MU}. The lift coefficient for this condition can be limited by either $C_{L_{max}}$ or by the angle of attack existing when the aft body contacts the ground. Therefore, it is necessary to estimate both the lift curve shape and the $C_{L_{max}}$ in ground effect. The basic data for making this estimate were obtained in the wind tunnel using a fixed ground plane modified to allow unusually high pitch attitudes, as shown in Figure 8. The lift curve so established was checked at high Reynolds number and found to be essentially unchanged. Since angle of attack is such an important parameter under these conditions, the model used for this test had the wing twisted to represent the aeroelastic distortion of the actual airplane during heavy weight, flaps down, flight. These wind tunnel data were then corrected by correlation factors obtained on previous Boeing aircraft similar to those shown for the free-air conditions. Resultant pre-flight estimates and subsequent flight data are shown in Figure 9. The data shows a scatter of ± 5 percent, typical of flight test information taken during the take-off phase. However, it does straddle very well the pre-flight estimate. A picture of this rather dramatic flight testing for $C_{L_{max}}$ in ground effect is shown in Figure 10.

5.3 Pitching Moments

The static longitudinal pitching moments play an important role in determining the handling characteristics of the airplane during the stall maneuver. The influence of aeroelastic deflections and local separations on a swept wing can have large effects on wing pitching moments.

Separations on the wing, body, and nacelles can influence the tail contribution to stability. Since these separations can be sensitive to Reynolds number effects, it is difficult to predict the airplane's full-scale behavior if the wind tunnel data indicate a situation that is marginal in any way. At Boeing, our philosophy has been for many years to design for good pitching moment characteristics under low Reynolds number conditions to assure good characteristics in flight. A small pitch-up in the stall is permissible and tends to hold the airplane to a slightly lower speed before it pitches down out of the stall. This permissible pitch-up must cause only a limited excursion in angle of attack, say 4 to 6 degrees, involve essentially no increase in C_L once the pitch-up begins, and must be followed by strong pitch-down to assure a good clean break away from the stall.

The wind tunnel pitching moment data at both low and high Reynolds number and the corresponding flight data are compared in Figure 11. There is practically no change in wind tunnel pitching moment data with Reynolds number probably a result of the cambered leading-edge flap. The flight data show slightly superior stability at stall entry than the wind tunnel data indicate. They also show that the wind tunnel predicted quite accurately the flight values for the angle of incipient pitch-up and the angle of recovery. These pitching moment characteristics produced an airplane extremely easy to fly throughout the stall maneuver.

6. STALL MANEUVER ANALYSIS

6.1 Stall Parameters

While the stall speed prediction method used for the 747 was moderately successful such a procedure does not lead to any fundamental understanding of the physics of the stall. Consequently an analysis was undertaken to get some appreciation of the factors involved in the stall. The parameters that have been considered in the 747 stall analysis are:

1. Reynolds number
2. Mach number
3. Aeroelastic effects
4. Pitchup characteristic
5. Pitch inertia
6. Stall entry rate
7. Stall technique

The influence of the last four items of the list can only be assessed in a dynamic stall simulation. A three degree of freedom digital simulation was undertaken to determine these effects.

6.2 Reynolds and Mach Number Effects

The Reynolds number effects were assessed by using the low Reynolds number data obtained at the University of Washington wind tunnel and extrapolating to full scale using the higher Reynolds number data obtained in the 12 foot pressure tunnel at the Ames Aeronautical Laboratory of the NASA. This extrapolation was augmented by some two dimensional high Reynolds number data obtained on the 747 flap system at the 5 x 5 foot variable density tunnel of the National Aeronautical Establishment (NAE) in Ottowa, Canada. This two dimensional data was taken over a Reynolds number range of 1.25×10^6 to 13.0×10^6. These data confirm the trend shown in Figure 7 which indicates quite a modest Reynolds number effect on $C_{L_{max}}$. This mild Reynolds number sensitivity for the 747 is due to the careful design which produced a smooth pressure distribution on the flaps having no severe gradients at high angles of attack. Reynolds number effects on earlier flap systems with severe gradients can be much larger as shown on Figure 12.

The basic low Reynolds number data at the University of Washington tunnel were obtained at a relatively low Mach number of M = .16. During a flight test stall the Mach number may be as high as M = .30. Due to the very high negative pressure coefficients involved on the flaps at high lift this discrepancy in Mach number could be quite serious. Therefore as a part of the test program at the NAE variable density tunnel in Canada the influence of Mach number on $C_{L_{max}}$ was also investigated. It was found that flap systems which did not take care to protect against severe pressure peaks and gradients at high angles of attack can have rather severe Mach number effects as shown on Figure 13. Because of the flap design philosophy, the influence of Mach number on the 747 $C_{L_{max}}$ is very mild.

6.3 Effect of Aeroelasticity

The influence of aeroelasticity on the stall was included by correcting the aerodynamic coefficients for aeroelastic deflections. The basic linear unstalled portion of the aerodynamic coefficients were corrected using terms derived from structural programs which use linear aerodynamics to supply the airloads.

The most difficult parameters to obtain are the aeroelastic effects near the stall. The basic 747 wind tunnel data was obtained with a wing which incorporated the aeroelastic twist for a critical flight loading case, namely the condition for a heavy weight airplane but with only partial wing fuel capacity. This condition corresponds approximately to the heavy weight stall conditions. To see the effect of the weight and fuel loading on the aeroelastic deflections consider the following cases:

	WEIGHT LBS	WING FUEL LBS	UNRELIEVED WEIGHT LBS
1.	335,000	0	335,000
2.	440,000	50,000	390,000
3.	699,000	150,000	549,000

Case 1 represents the minimum operating weight while case 2 is approximately the light weight stall conditions encountered in the 747 flight test. Case 3 is about the weight and fuel conditions encountered in the heavy weight flight test stalls. The difference in the weight deflecting the wing is quite apparent. The aeroelastic deflection associated with these loads cause a difference in span loading which on the 747 and several other Boeing airplanes causes a reduction in $C_{L_{max}}$ with increasing weight on the wing. This $C_{L_{max}}$ variation with loading should be determined by testing wind tunnel wings which have the twists and deflections associated with these loadings. Data exactly of this form are not available, however the trends do exist in the wind tunnel testing of the 747. Evidence of the aeroelastic effects are apparent in the 747 flight test data. By looking at the actual $C_{L_{max}}$ values achieved in the stall tests, a difference in maximum lift capability is apparent as shown on Figure 14. Note that the $C_{L_{max}}$ is not a function of the stall entry rate. The difference in $C_{L_{max}}$ cannot be explained in terms of Reynolds number or Mach number effects. These aeroelastic effects at the stall are part of a very complex system which is sensitive to a large number of variables and cannot be attacked except through wind tunnel testing of the range of variables involved.

To determine the total aeroelastic influence at least three cases must be evaluated, the rigid jig position wing, and at least two other deflected wings corresponding to the heavily and lightly loaded cases. The procedure used on the 747 analysis can only evaluate the increment between light and heavy loading with the total aeroelastic effect starting from the jig wing still unidentified.

6.4 Effect of Stall Dynamics

The influence of stall dynamics on stall speed was investigated using a three degree of freedom simulation which included the effects of variations in Reynolds number, Mach number and aeroelastic deflection during the stall maneuver. The simulation equations of motion are defined in Figure 15.

The FAR stall speed is specified at a stall entry rate of 1 knot per second. This entry rate is defined as follows:

$$\text{FAR entry rate} = \frac{V_{min} - 1.1V_{min}}{T_{V_{min}} - T_{1.1V_{min}}}$$

The flight test procedure is to perform several stalls using a consistent technique with entry rate as a variable and to plot stall speed versus entry rate to determine the FAR stall speed. The effects of stall technique, pitch inertia and pitchup were evaluated using the dynamic simulation and the FAR stall speed definition.

Using the definition of FAR stall speed it is apparent that any number of curves will pass through the points defined by V_{min} and 1.1 V_{min} and it is for this reason that stall technique is important. Two of the many possible curves are shown on Figure 16. The "slow" stall is characterized by a fairly uniform deceleration into the stall that is obtained by a gradual elevator application to a prescribed angle of attack at which the elevator is held fixed. The fast stall is characterized by a slower initial entry rate followed by a higher final entry rate. This type of stall is obtained by a slightly slower initial elevator application to some angle of attack at which full elevator is applied and held through the stall.

Two types of elevator application were devised for evaluation of the stall technique and were programmed for the simulation in order to systematically study the effect of stall entry rate and technique. A series of stall computations were then performed on the simulator to investigate the influence of gross weight, pitch up, pitch inertia and aeroelasticity on FAR stall speed. One of the simulations included the elevator input from a flight test stall to determine if the simulation was adequate. The comparison shown on Figure 17 indicates that the stall calculation simulates the flight test quite well.

6.5 Stall Simulation Results

Typical speed time histories from the simulation are shown on Figure 18 for the two types of stall entry technique with an elastic airplane. The minimum speeds and corresponding lift coefficients have been extracted and are shown plotted against stall entry rate on Figure 19. It is apparent from these data that the stall speeds are quite sensitive to both the entry rate and stall technique, but since the FAR stall is at a specified entry rate only the speed and lift coefficient at this rate are used. Similar data was obtained at lighter weights and the effects of gross weight and stall technique are shown on Figure 20. Also shown on Figure 20 are the 747 flight test results which are in reasonable agreement with the simulator generated levels.

The indicated gross weight effect on the stall lift coefficient includes the aeroelastic effects on $C_{L_{max}}$ previously shown. In order to separate the aeroelastic influence from the dynamics of the stall the flight weight simulation was repeated but without the aeroelastic lift effect. The results shown on Figure 21 indicate that virtually all of the gross weight effect on the stall is due to the change in lift attributed to aeroelastic deflections.

The variation of Reynolds number, Mach number and their effects on the $C_{L_{max}}$ during the stall are shown on Figure 22. It can be seen that while there is an effect of these parameters on the $C_{L_{max}}$ neither Reynold's number nor Mach number variations are dominant factors within the stall and if the aeroelastic effect is removed both configurations achieve approximately the same lift levels.

For a given gross weight and center of gravity a considerable range of pitch inertias may be obtained. To examine the effect of this parameter on the stall the pitch inertia was changed + 25% from the nominal value. The results indicate that the pitch inertia variations investigated have negligible effects on the FAR stall speeds. The data does indicate however that slightly faster elevator inputs are required to achieve the 1 knot per second entry rate and an effect could be found if the elevator becomes limiting.

As shown previously the pitchup at the stall is difficult to predict and some variation in the pitchup should be anticipated.

To examine the sensitivity of the FAR stall speed to the amount of pitchup, a series of simulations were performed with the pitching moments shown on Figure 23. The resulting FAR stall lift coefficients are shown on Figure 24. Over the range of pitching moments investigated, increasing the amount of pitchup has a negligible effect on the stall speeds while decreasing the amount of pitchup results in a rather serious loss in stall lift coefficient. The conclusions could be expanded into a more general statement that pitchup characteristics are not a dominant factor in the FAR stall speed determination unless the elevator capability is insufficient to develop the final stall entry rate. However, the stall characteristics at the aft center of gravity may limit the allowable pitch up and a strong pitch down after the initial pitch up must exist to assure a good clean break away from the stall.

The same simulations used to examine the FAR stall speeds were analysed to evaluate the 1 g stall speed correlation. The analyzed data presented on Figure 25 show again quite good correlation with the flight test data with the aeroelastic contribution accounting for the gross weight sensitivity. The 1 g stall speeds show a sensitivity to stall entry rate similar to the FAR stall speeds, and comparing the $C_{L_{1g}}$ values with the previously shown $C_{L_{max}}$ values it becomes apparent that the 1 g stall speeds are not obtained at unit load factor. The 1 g stall speeds are the result of the dynamics of the stall maneuver just as the FAR speeds are but at a load factor closer to unity.

A summary build up of the predicted FAR stall lift levels from low Reynolds number wind tunnel maximum lift data is shown on Figure 26. The predicted levels compare quite favorably with the values obtained during the certification flight tests. The key item is to start with a carefully designed low Reynolds number wind tunnel model twisted to a specified loading. The increments shown on Figure 26 indicate that for the 747 airplane the major influences in the buildup are the aeroelastic effect and the effect of the dynamics of the stall maneuver.

7. CLOSING REMARKS

The methods used to estimate the stall characteristics of the 747, based on the previous experience of Boeing transport airplanes, predicted the FAR stall lift coefficients within about 5 percent. This is well within the confidence band expected during the preliminary design phase of an airplane, but as shown in the introduction this is not adequate during the development and guarantee phase. A subsequent analysis considering the effects of Mach and Reynolds numbers, pitch inertia, pitchup characteristic stall technique, aeroelastics and stall dynamics has led to a better understanding and a more accurate prediction procedure for the future. The analysis has also pointed out some gaps in the data required to obtain a rational stall lift prediction.

One must conclude that the prediction of the stall lift coefficient remains a difficult engineering problem. Based on the results of the analysis of the 747 airplane much progress can be made to better understanding the physics of the stall maneuver. However there are still parts of the analysis in the area of aeroelastic effects and understanding the aerodynamics of stalled flows that should be examined in further detail to arrive at a more scientific stall prediction technique. The data required for this more scientific approach will in general not be available during the preliminary design phases of the development of an airplane and therefore the empirical procedure used for the 747 tempered with engineering judgement will still serve as a useful and reasonably accurate method for prediction.

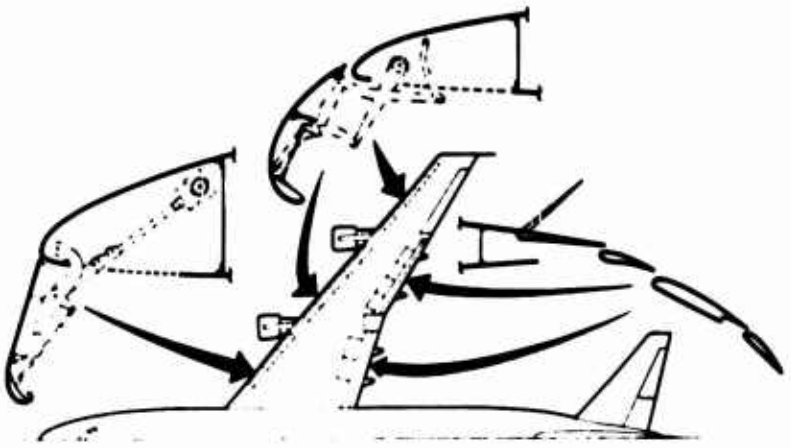

FIGURE 1: 747 HIGH LIFT SYSTEM

FIGURE 2: 747 HIGH LIFT WIND TUNNEL MODEL

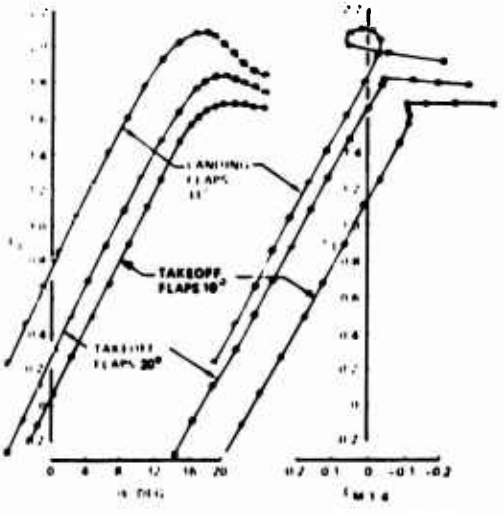

FIGURE 3: HIGH LIFT WIND TUNNEL DATA (LOW REYNOLDS NUMBER)

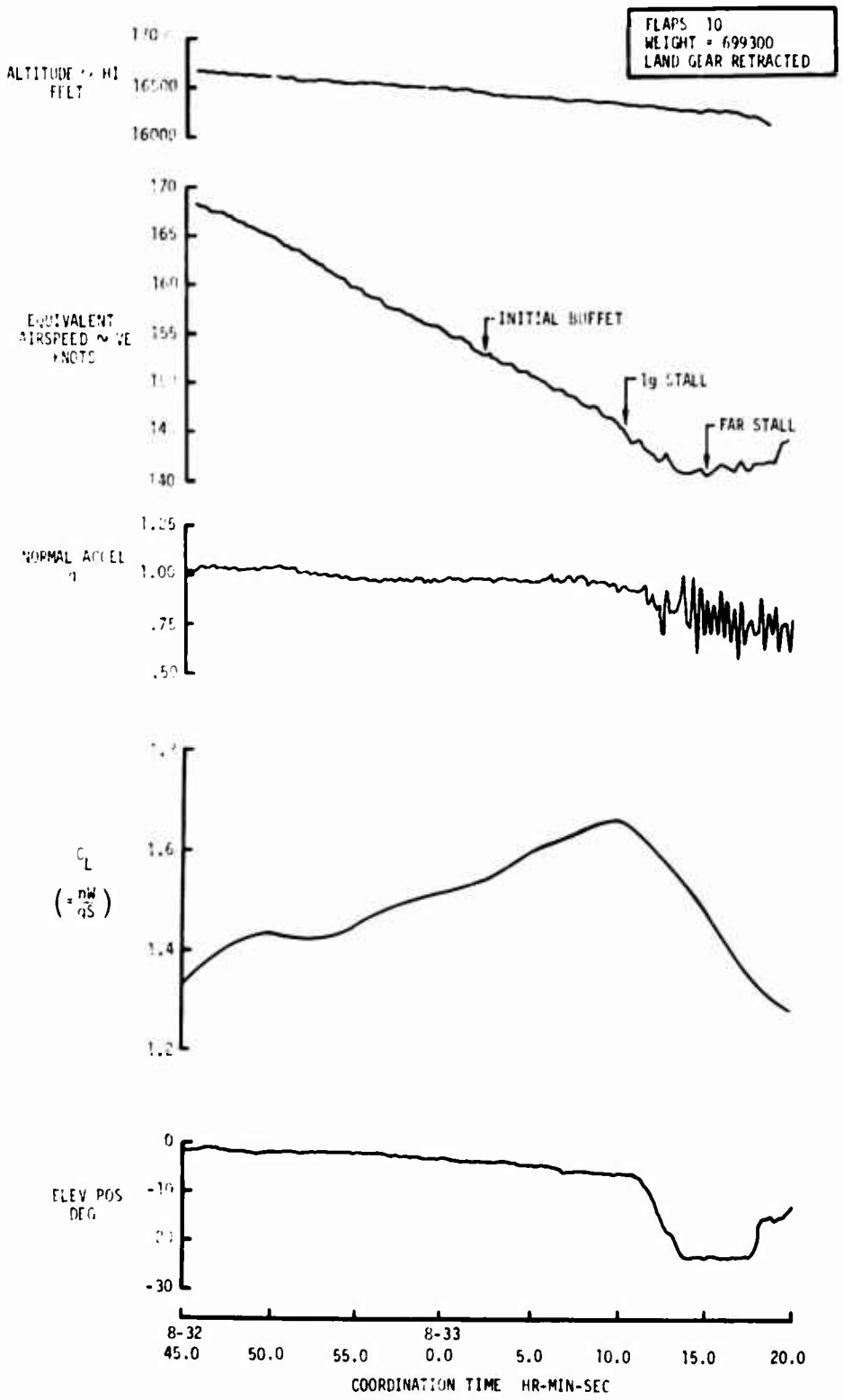

FIGURE 4: FLIGHT RECORD OF A STALL MANEUVER

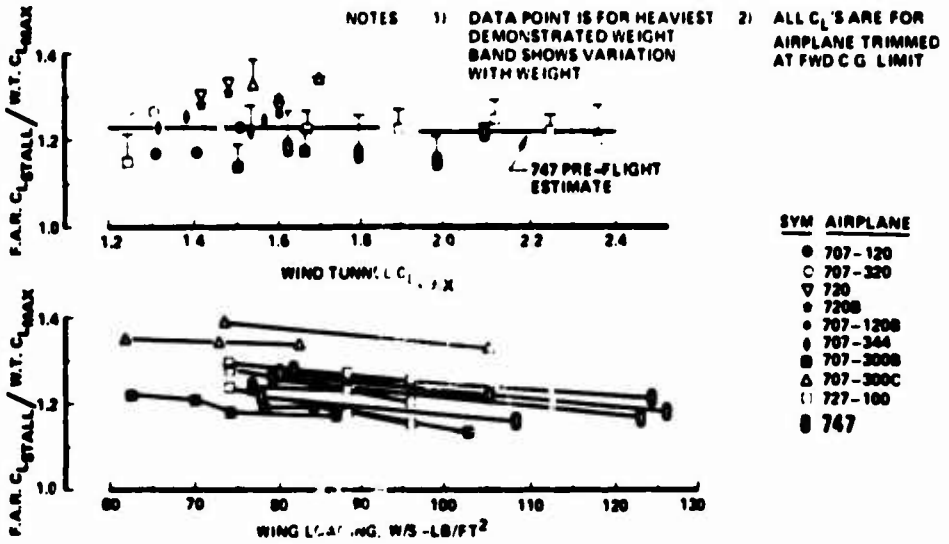

FIGURE 5: COMPARISON OF FLIGHT FAR $C_{L_{STALL}}$ AND WIND TUNNEL $C_{L_{MAX}}$

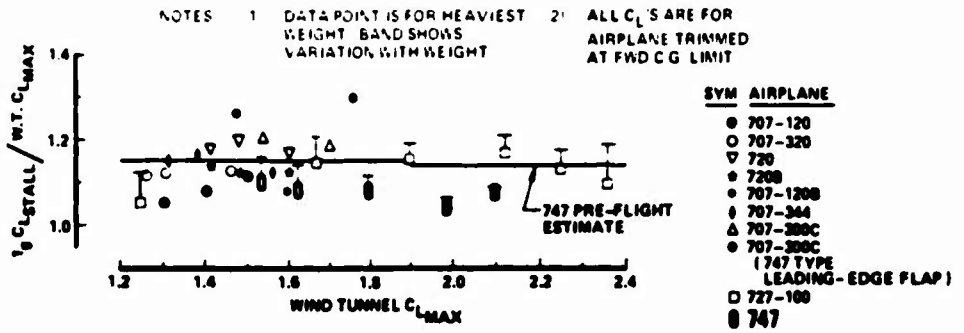

FIGURE 6: COMPARISON OF FLIGHT $^1gC_{L_{STALL}}$ AND WIND TUNNEL $C_{L_{MAX}}$

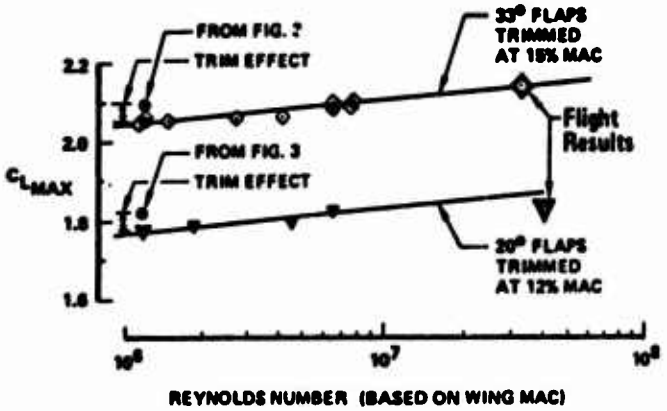

FIGURE 7: HIGH REYNOLDS NUMBER DATA

FIGURE 8: TEST FOR $C_{L_{MAX}}$ IN GROUND EFFECT

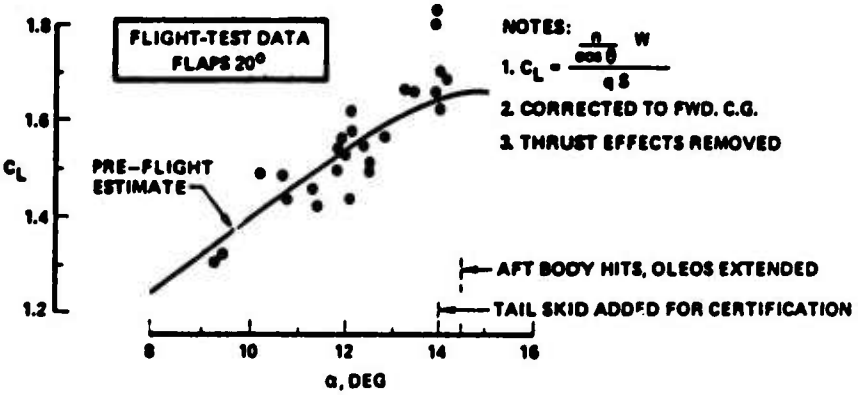

FIGURE 9: LIFT CURVE IN GROUND EFFECT

FIGURE 10: V_{MU} FLIGHT TEST

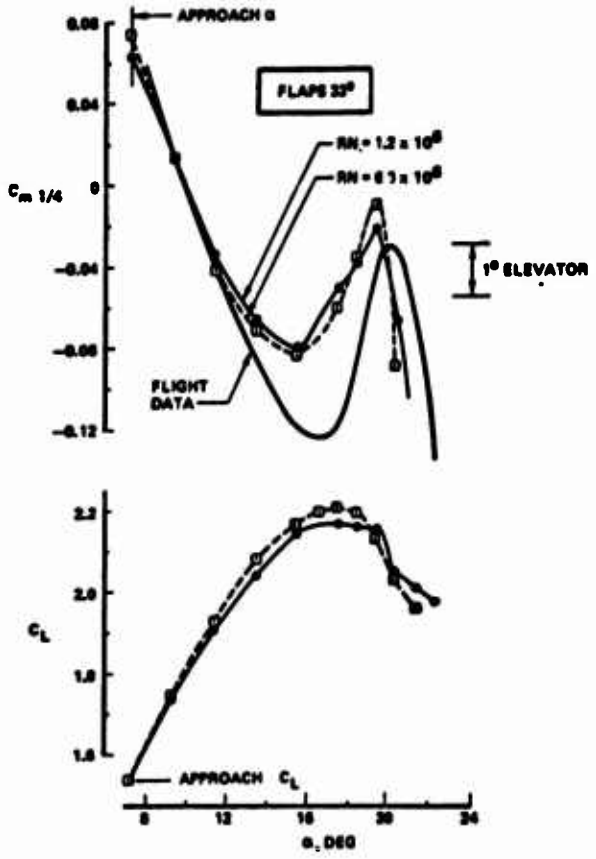

FIGURE 11: PITCHING MOMENTS IN THE STALL

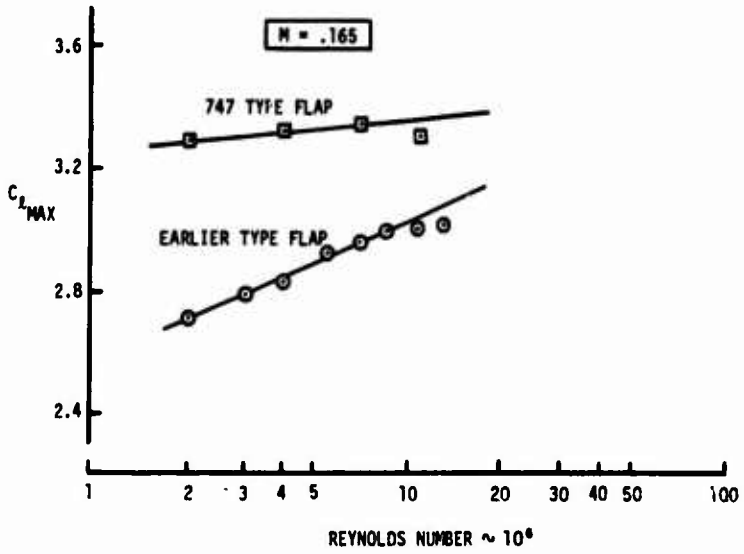

FIGURE 12: EFFECT OF FLAP TYPE AND REYNOLDS NUMBER ON TWO DIMENSIONAL MAXIMUM LIFT

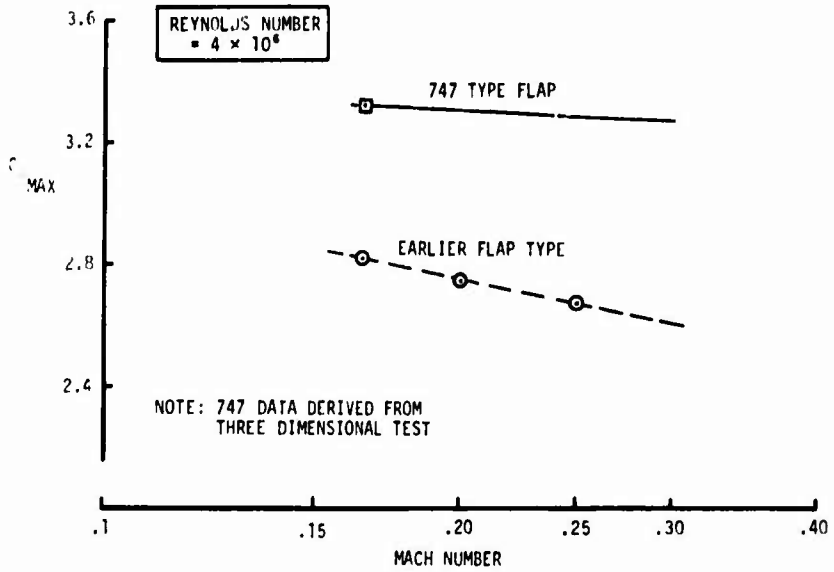

FIGURE 13: EFFECT OF FLAP TYPE AND MACH NUMBER ON TWO DIMENSIONAL MAXIMUM LIFT

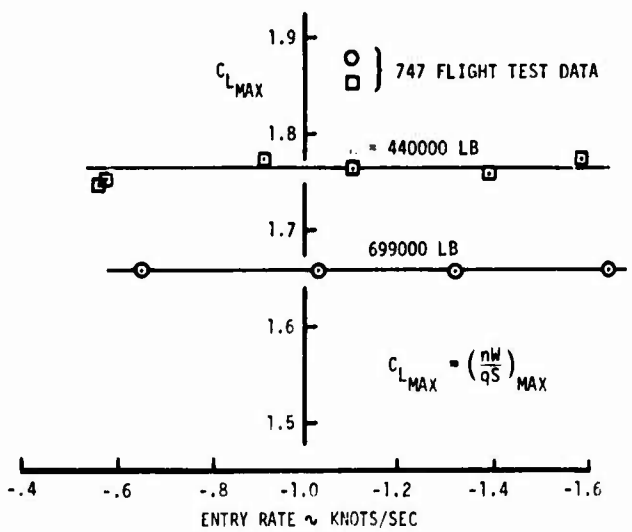

FIGURE 14: EFFECT OF GROSS WEIGHT AND ENTRY RATE ON $C_{L_{MAX}}$ ACHIEVED IN STALL

LIFT:

$$L - \frac{W}{g} V \dot{\gamma} - W \cos \gamma + T \sin (\alpha_B + i_T) = 0$$

DRAG:

$$T \cos (\alpha_B + i_T) - D - W \sin \gamma - \frac{W}{g} \dot{V} = 0$$

PITCHING MOMENT:

$$M_{ACG} + TZ_T - I_{yy} \ddot{\theta} = 0$$

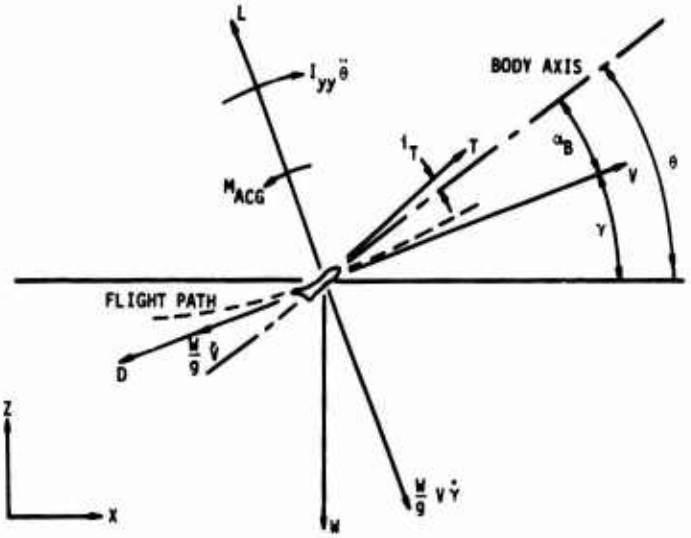

FIGURE 15: DEFINITION OF TERMS IN EQUATIONS OF MOTION

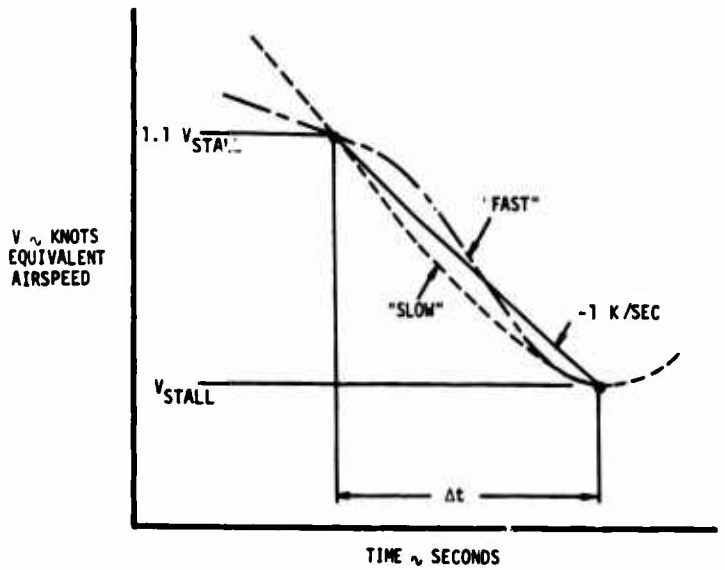

FIGURE 16: TWO TYPES OF STALL ENTRY RATE USED FOR STALL DYNAMICS STUDY

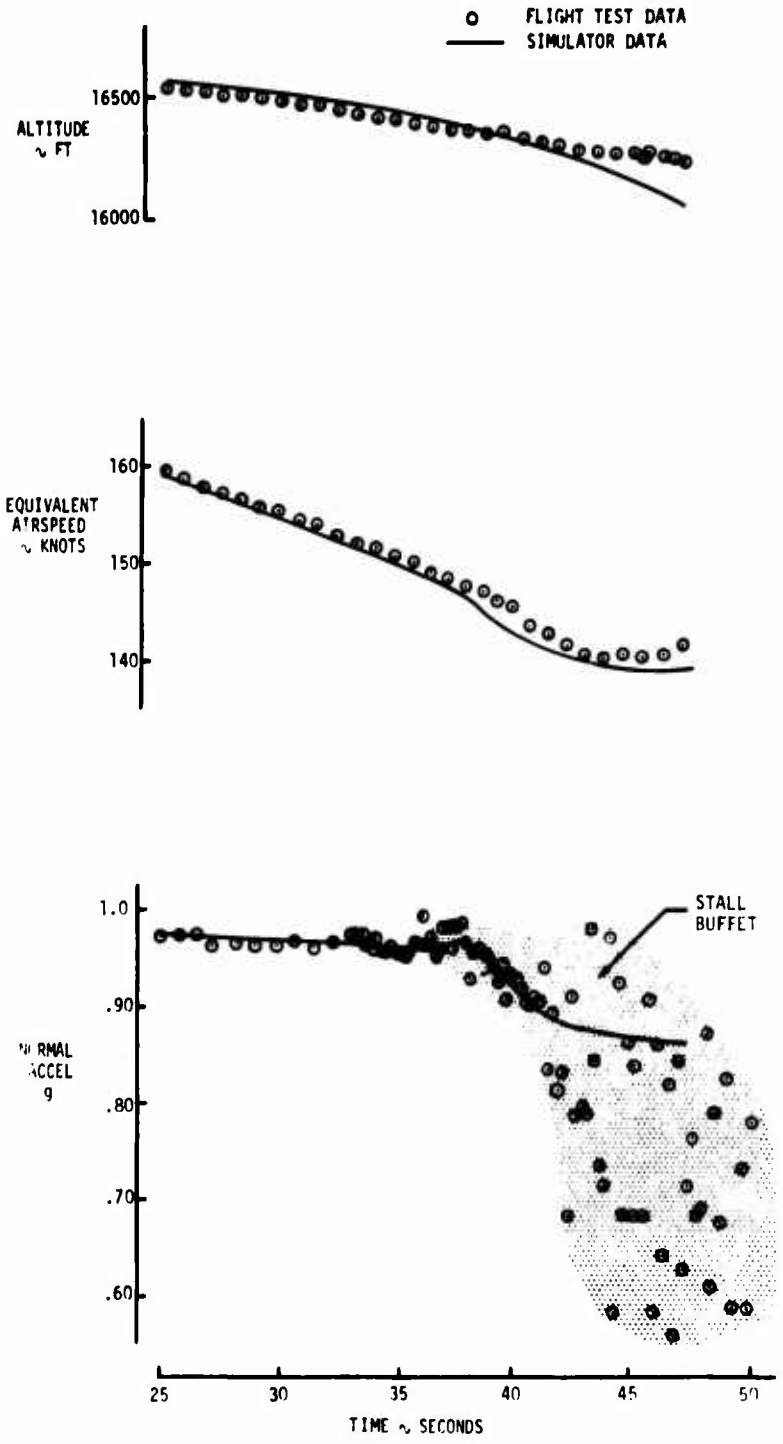

FIGURE 17: COMPARISON OF SIMULATION AND FLIGHT TEST RESULTS

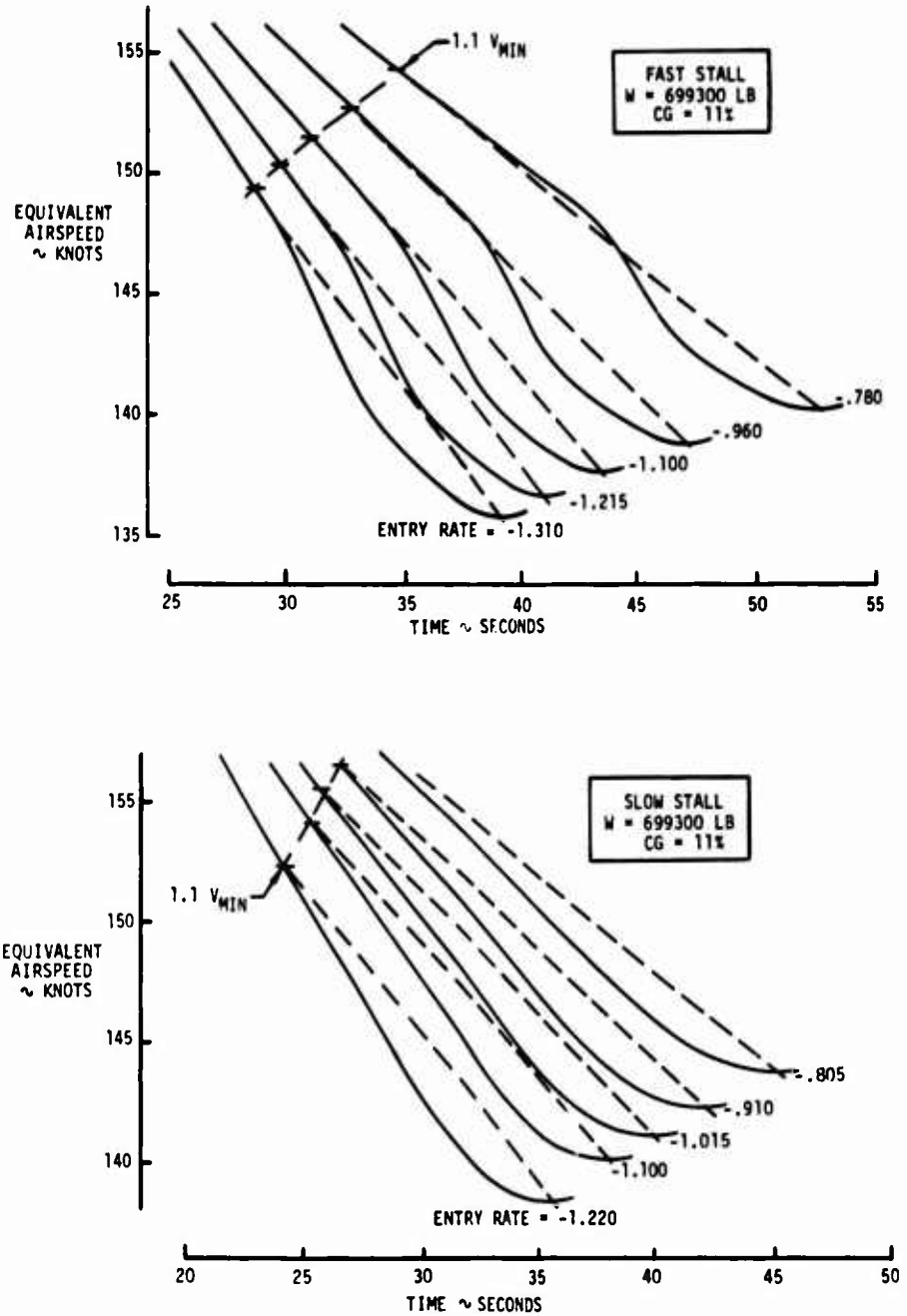

FIGURE 18: TYPICAL VELOCITY TIME HISTORIES FOR TWO TYPES OF STALL TECHNIQUE

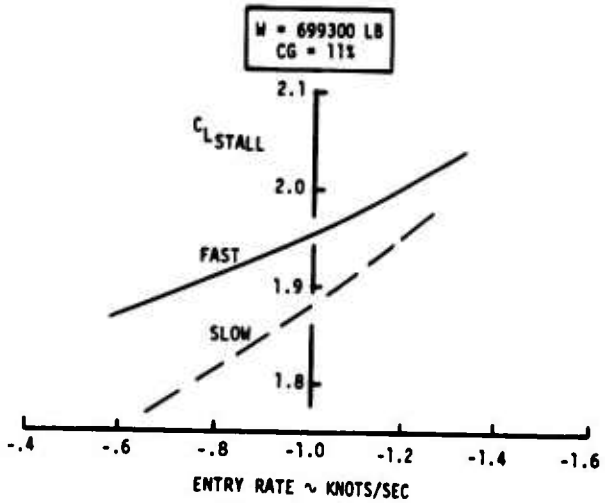

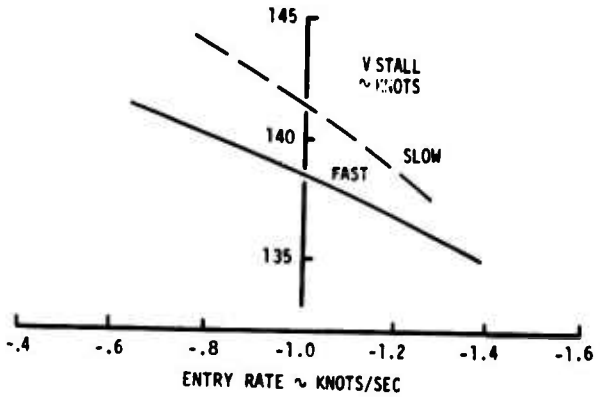

FIGURE 19: EFFECT OF STALL TECHNIQUE AND ENTRY RATE ON STALL SPEED AND LIFT COEFFICIENT

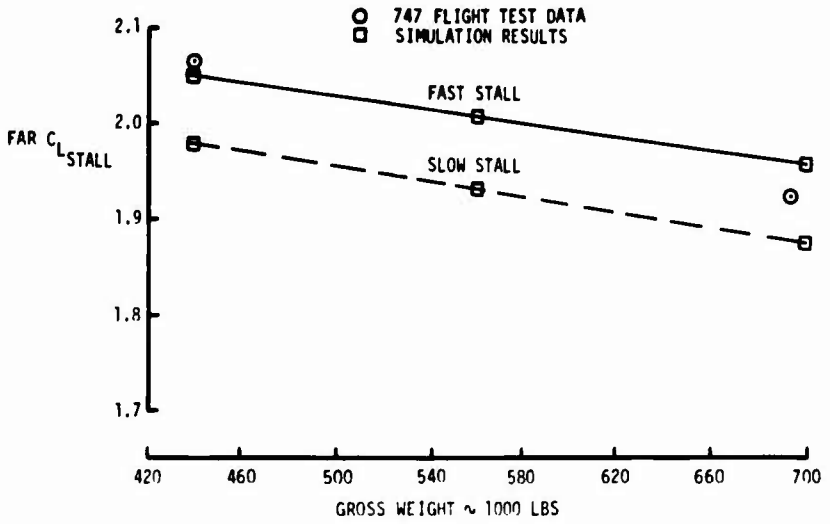

FIGURE 20: EFFECT OF STALL TECHNIQUE AND GROSS WEIGHT ON STALL LIFT COEFFICIENT

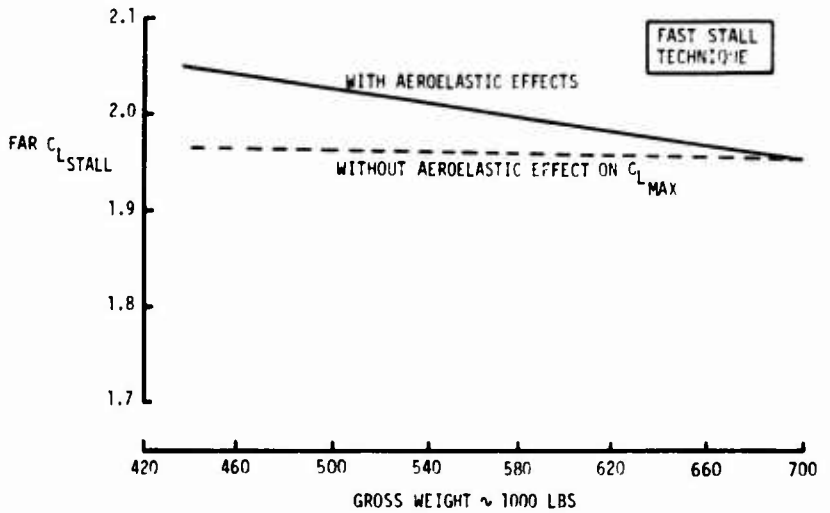

FIGURE 21: EFFECT OF AEROELASTIC LIFT INCREMENT ON STALL LIFT COEFFICIENT

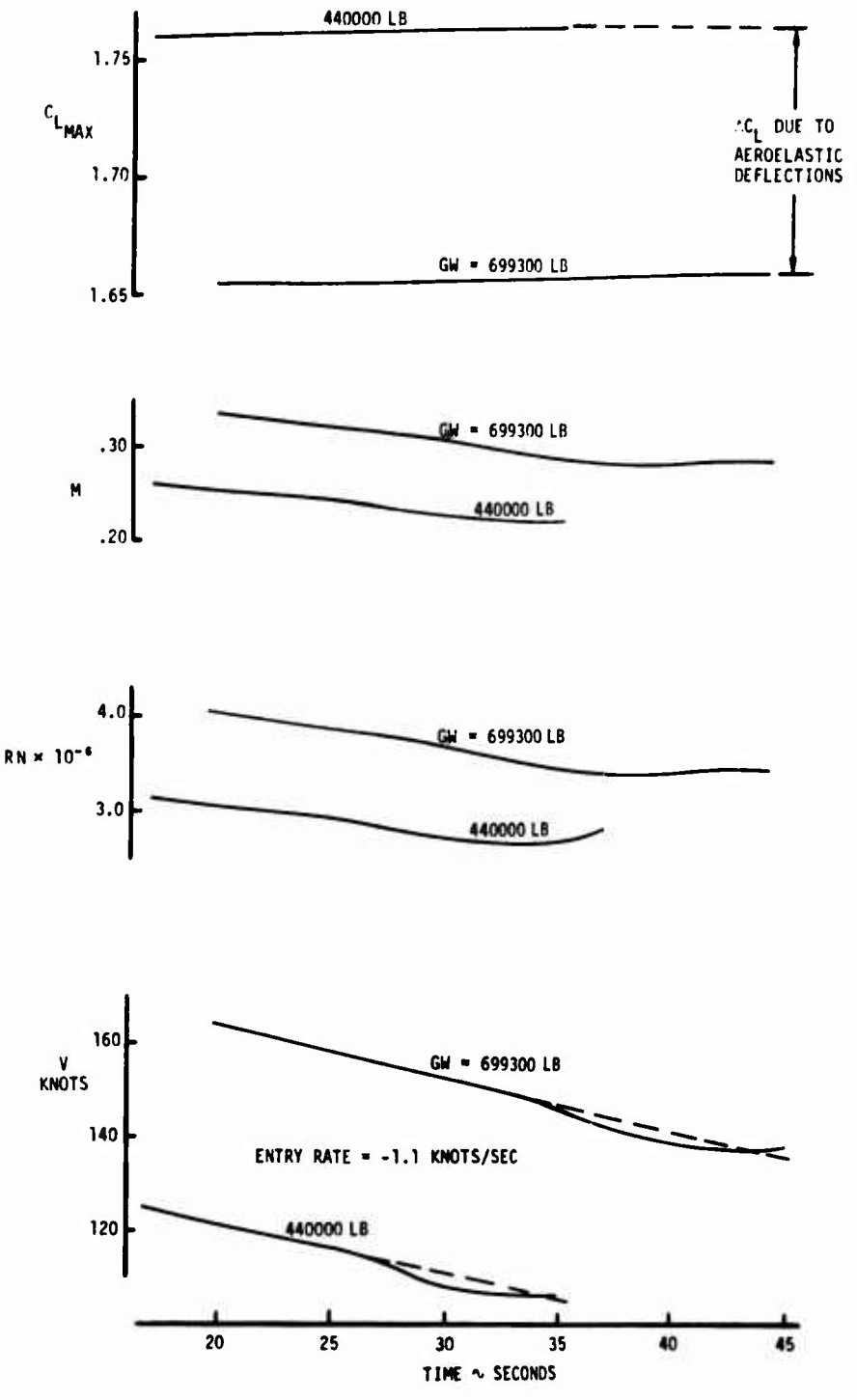

FIGURE 22: VARIATION OF MACH AND REYNOLDS NUMBER DURING TYPICAL STALL AND EFFECT ON $C_{L_{MAX}}$

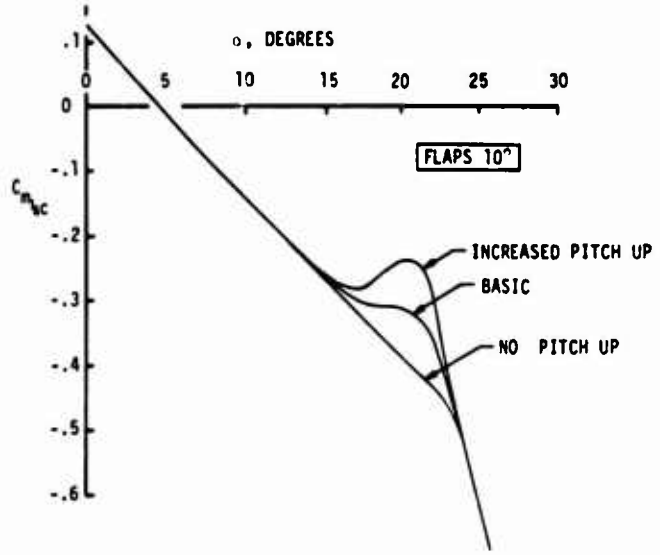

FIGURE 23: PITCHING MOMENTS INVESTIGATED IN STALL SIMULATION

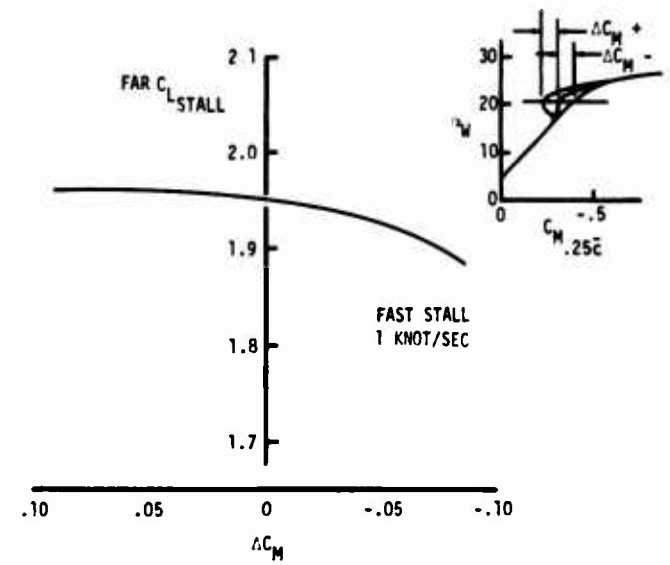

FIGURE 24: EFFECT OF PITCH UP ON STALL LIFT COEFFICIENT

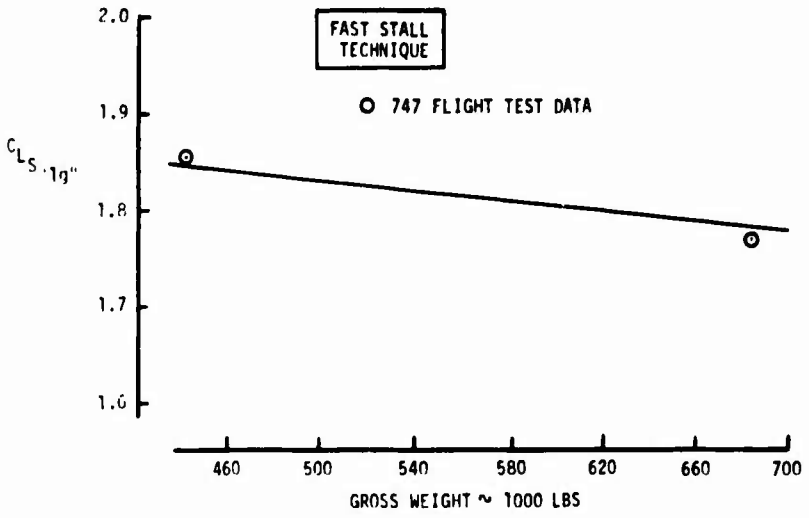

FIGURE 25: EFFECT OF GROSS WEIGHT ON "1g" STALL LIFT COEFFICIENT

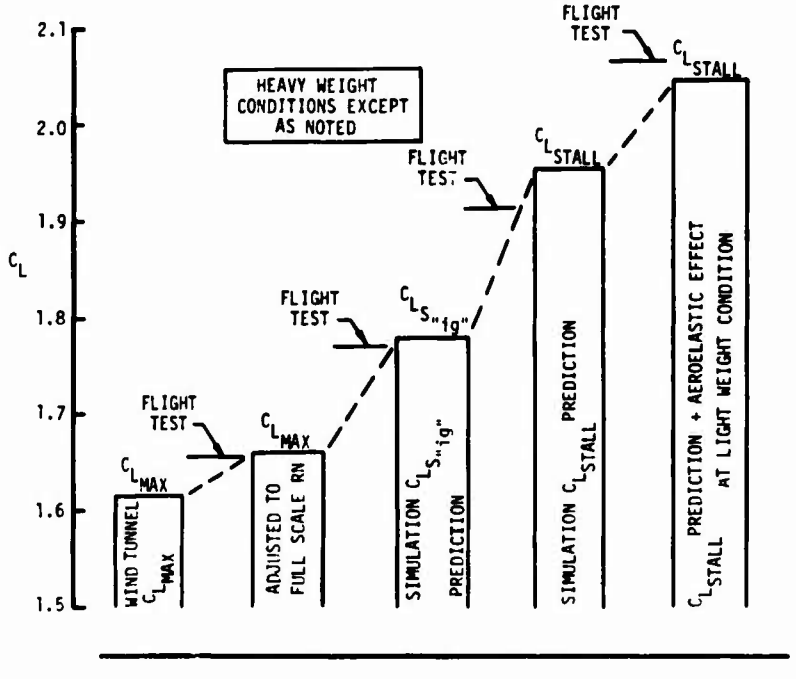

FIGURE 26: SUMMARY BUILDUP OF FAR STALL LIFT COEFFICIENT FROM LOW REYNOLDS NUMBER TUNNEL DATA

DECOLLEMENT ET EXCITATION AERODYNAMIQUES AUX VITESSES TRANSSONIQUES

B.Monnerie
Office National d'Etudes et de Recherches Aérospatiales
29, Avenue de la Division Leclerc
92320 Chatillon, France.

RESUME

Le décrochage et le tremblement sont des phénomènes liés à l'apparition et au développement sur les véhicules aériens, de zones d'écoulements décollés. Ces décollements sont le siège de remous qui produisent des fluctuations de pression et excitent la structure. Les décollements apparaissent sous l'action des gradients de pression positifs intenses, ils jouent donc un rôle important dans le régime transsonique qui provoque des recompressions très brutales par les chocs qu'il engendre.

Les fluctations de pression dans les décollements ont une intensité 10 à 100 fois supérieure à celles qui sont présentées dans les couches limites attachées. La prévision par le calcul de l'intensité du buffeting nécessite la connaissance du champ des pressions instationnaires ce qui est un probleme extrêmement ardu à aborder par voie purement théorique. La voie suivie actuellement consiste à évaluer les caractéristiques statistiques du champ de pression en les mesurant. Le probleme qui se pose alors est celui de savoir dans quelles conditions les relevés effectués au cours des expériences sur maquettes sont représentatifs de ce qui se passe à l'échelle réelle.

FLOW SEPARATION AND AERODYNAMIC EXCITATION AT TRANSONIC SPEEDS

SUMMARY

Stalling and buffeting are phenomena in connection with the birth and growth of separated flow areas on the aerospace vehicle surface. These areas are loci of turbulence which produce high level pressure fluctuations and excite the vehicle structure. Separation occurs due to strong positive pressure gradients and so plays an important role in the transonic regime which provokes steep recompressions with the shocks it creates.

The level of pressure fluctuations in a separated flow area is 10 to 100 times more intense than in attached boundary layers. The computation of buffeting intensity requires a knowledge of the unsteady pressure field which is very difficult to obtain by purely theoretical means. The method used at the present time is to measure the statistical characteristics of the unsteady pressure field. The problem which then arises is to know how measurements made on the model correspond to what occurs on the full-size vehicle.

1 - INTRODUCTION -

Le décrochage et le tremblement sont des phénomènes apparentés qui, l'un et l'autre, limitent les possibilités d'utilisation des avions et autres véhicules aériens.

Le décrochage d'un avion peut être défini comme l'ensemble des phénomènes qui apparaissent lorsque l'on cherche à faire croître la portance au-delà d'une certaine limite en augmentant l'angle d'incidence.

On constate alors que, contrairement à ce que prévoirait une théorie supposant que l'air est un fluide parfait, la portance, non seulement cesse de croître, mais finit par s'effondrer plus ou moins brutalement et qu'il s'ensuit évidemment de graves désagréments pour le véhicule et pour son pilote : perte d'altitude, difficultés considérables pour contrôler l'attitude etc... Ce phénomène est, on le sait, lié au fait que l'air est un fluide visqueux et, qu'en conséquence, les particules d'air au voisinage des parois de l'avion ne se contentent pas de s'écarter provisoirement pour laisser passer l'avion mais ont tendance à être entraînées. Les particules ainsi influencées sont contenues dans une zone généralement très voisine de l'avion qui est la couche limite. En simplifiant, on peut dire que ce que peut prévoir une théorie de fluide parfait, ce sont les caractéristiques de l'écoulement autour de l'avion déformé par la présence de sa couche limite.

Or, il se trouve que, dans certaines conditions, et notamment lorsque l'on cherche à obtenir des portances élevées, un évènement survient -le décollement de la couche limite- qui augmente considérablement l'étendue de cette couche limite et, par conséquent, modifie, de façon importante, la forme de l'ensemble avion + couche limite. On comprend qu'un calcul ne tenant pas compte de cette modification soit en contradiction avec l'expérience. Le décrochage de l'avion est donc provoqué par le décollement de la couche limite et, dans ces conditions, la portance est très inférieure à ce que prévoit une théorie de fluide parfait.

Le buffeting est un autre type de limitation qui a fondamentalement la même cause que le décrochage : l'existence de zones d'écoulement décollé. Il consiste en des vibrations de l'avion, ressenties par le pilote et les passagers, qui se produisent dans certaines conditions de vol.

Un vol avec un niveau de buffeting important est inacceptable aussi bien pour les passagers qui sont secoués que pour la structure dont la durée de vie en fatigue est limitée et qui pourrait même parfois être soumise à des charges dépassant la charge de rupture. C'est pourquoi le domaine de vol est nécessairement limité par l'apparition d'un certain niveau de buffeting.

Le buffeting, on le sait, est un problème pour les véhicules aériens dans le domaine transsonique mais il n'est pas exclusif du domaine transsonique car, par exemple, il accompagne le décrochage des avions aux basses vitesses. Si on en parle beaucoup plus souvent en transsonique c'est que, dans ce cas, il peut apparaître pour des niveaux de portances assez faibles, bien avant le décrochage, et avoir une intensité considérable.

Ainsi qu'on va le voir, le buffeting est le résultat de l'excitation de la structure de l'avion par les fluctuations de pression aérodynamique associées à la présence des zones d'écoulements décollés ; c'est donc un phénomène fort complexe faisant intervenir à la fois la structure et l'aérodynamique.

L'évaluation par le calcul des caractéristiques de buffeting des avions est, de ce fait, très difficile et fait l'objet de recherches et de travaux très nombreux sur lesquels le point sera effectué au cours de cette "lecture series". L'objet de cette conférence est plus particulièrement d'analyser le phénomène fondamental à l'origine du buffeting : le décollement de l'écoulement et les fluctuations de pressions qu'il engendre.

Un des points importants pour pouvoir adopter une schématisation réaliste mais aussi simple que possible du phénomène est de mettre en évidence dans quelle mesure le mouvement de la structure influence l'aérodynamique.

Cette question, nous le verrons, est encore ouverte et n'a pas encore reçu de réponse définitive.

Le plan de l'exposé est le suivant :

1 - introduction
2 - les divers types de buffeting
3 - les décollements
  3.1 - généralités
  3.2 - circonstances d'apparition
  3.3 - les décollements en transsonique
4 - les aspects instationnaires
5 - les moyens d'étude
6 - Conclusions.

2 - DIVERS TYPES DE BUFFETING -

Avant d'aller plus loin dans l'analyse des phénomènes, donnons quelques exemples et rappelons quels sont les types principaux de buffeting susceptibles d'être rencontrés.

Ainsi que le signale Mabey dans un papier récent où il fait le point sur les problèmes du buffeting [1], le terme de buffeting apparaît pour la première fois dans la littérature en 1930, lors de l'accident survenu à un monoplan Junkers à la suite d'une rupture de l'empennage pouvant être attribuée à une excitation intense provoquée par l'entrée de ce dernier dans le sillage fortement turbulent de l'aile en configuration décollée.

Plus récemment, plusieurs échecs lors des premières expériences spatiales ont révélé que les véhicules spatiaux pouvaient connaître des problèmes graves de buffeting à la traversée du domaine transsonique. Ces problèmes ont la même origine que le buffeting des avions : l'existence de zones d'écoulements décollés.

Le buffeting apparaît donc comme la réponse de structure à une excitation aérodynamique trouvant son origine dans les décollements.

Les principaux types de buffeting qu'on peut dégager sont, par suite, liés aux formes de structure et de décollement qui peuvent se présenter ; on distingue :

- le buffeting des ailes : dans ce cas la zone d'écoulement décollé apparaît sur l'aile,
- le buffeting des empennages dans le cas où l'empennage se trouve placé dans le sillage d'une aile décollée,
- le buffeting de cavité lorsque le décollement ne résulte pas de conditions aérodynamiques particulières mais simplement est provoqué par l'interruption volontaire de la continuité de la paroi,
- le buffeting des lanceurs, enfin, qui n'est pas différent de celui des ailes sur le plan fondamental mais qui possède des particularités propres compte tenu des formes allongées et de révolution des lanceurs.

3 - LES DECOLLEMENTS -

3.1 - Généralités -

Lorsqu'on étudie le mouvement relatif d'un fluide réel et d'un obstacle, on peut, en général, négliger le fait que les fluides sont visqueux sauf dans les portions d'écoulement qui ont été ou sont au voisinage immédiat des parois de l'obstacle. On désigne par couche limite la faible épaisseur de fluide qui est au contact des parois et dans laquelle la viscosité joue un rôle prépondérant. Emportées loin de l'obstacle par suite du mouvement relatif, ces couches limites forment ensuite le sillage.

Lorsqu'on s'éloigne de la paroi, dans la couche limite, la vitesse relative du fluide par rapport à la paroi passe assez rapidement de zéro au contact de la paroi à une valeur V_e dite vitesse extérieure, à la frontière de la couche limite, point au-delà duquel la vitesse est quasi constante.

Les théories de couche limite conduisent à des équations plus simples que les équations générales des fluides visqueux ou équations de Navier Stokes. Elles permettent d'expliquer que, pourvu que l'épaisseur de la couche limite soit petite vis-à-vis des rayons de courbure de la paroi, le gradient de pression statique normal à la paroi est nul. Elles permettent également de calculer le développement des couches limites et de prévoir leur comportement lorsqu'il existe un gradient de pression longitudinal. On trouve que si les gradients de pression négatifs n'ont qu'une influence modérée sur les divers paramètres caractéristiques de la couche limite, il n'en est pas de même pour les gradients de pression positifs qui sont présents lorsque l'écoulement extérieur se ralentit.

Les gradients de pression positifs font évoluer rapidement la forme du profil et l'épaisseur de la couche limite. S'ils sont suffisamment intenses, ou s'ils agissent suffisamment longtemps, ils conduisent à son décollement. Le décollement s'explique par la perte d'énergie cinétique des particules fluides les plus voisines de la paroi, freinées à la fois par l'action du frottement et par l'effet du gradient de pression ; elles finissent par s'immobiliser en un certain point au-delà duquel l'écoulement est dirigé en sens inverse. Pour assurer la continuité de débit, la couche limite est alors contrainte de quitter la paroi devenant ainsi une couche de sillage.

Au point de décollement, la pente à l'origine du profil de vitesse est nulle $\left(\frac{du}{dy}\right)_0 = 0$.

La figure 1 donne, à titre d'exemple, l'évolution du profil de couche limite lors du décollement.

3.2 - Circonstances d'apparition -

Les décollements apparaissent à chaque fois que la couche limite est soumise à des gradients de pression positifs suffisamment intenses. Ceci a tendance à se produire à la partie arrière des corps se mouvant dans un fluide ou lorsque la paroi présente des discontinuités ou des changements de pentes brutaux.

Par ailleurs, lorsqu'une onde de choc rencontre la paroi de l'obstacle, que cette onde soit due à la forme de la paroi ou à toute autre cause, il y a une augmentation brutale de pression à la traversée du choc et, par suite, une possibilité de décollement fonction de l'intensité du saut de pression, de l'état et de la nature de la couche limite à cet endroit.

Lorsque la couche limite a décollé de la paroi, elle peut y recoller un peu plus loin si le gradient de pression le permet ; en cas contraire, le recollement se produit dans le sillage, à l'aval, sur la nappe fluide qui est passée de l'autre côté de l'obstacle.

Selon que le point de décollement ou de recollement est situé ou non au voisinage immédiat d'un point singulier de la paroi on dit que le décollement ou le recollement est fixé ou libre.

En associant les diverses possibilités pour les points de décollement et de recollement on arrive à établir un tableau général des cas qui peuvent se présenter [figure 2].

Après ces généralités, voyons en quoi le domaine des vitesses transsoniques pose des problèmes particuliers.

Pour cela, il est nécessaire d'entrer un peu dans le détail de l'aérodynamique transsonique.

3.2 - Les décollements en transsonique -

3.2.1 - Cas du bidimensionnel -

A cause de la complexité des phénomènes transsoniques il est utile d'aborder le problème en examinant le cas d'un profil en écoulement plan. On peut avoir une première idée des phénomènes en observant figure 3 l'évolution de la distribution de pression sur un profil symétrique à incidence nulle lorsque le nombre de Mach croît à partir de zéro jusqu'aux valeurs transsoniques. Bien qu'une telle évolution soit fonction du type de profil choisi les grandes lignes de ce qui est constaté a un caractère général.

Aux faibles valeurs du nombre de Mach amont la répartition des vitesses sur le profil est entièrement subsonique. Il y a un point d'arrêt près du bord d'attaque, puis l'écoulement se détend et s'accélère jusqu'à un certain maximum, enfin il se recomprime et se ralentit à l'approche du bord de fuite. Pour une valeur du nombre de Mach amont appelée nombre de Mach critique la vitesse du son est atteinte en un point du profil. Pour des valeurs encore plus grandes du nombre de Mach une petite zone supersonique se développe autour de ce point. Au début la recompression peut être isentropique mais assez vite elle s'effectue au moyen d'une onde de choc. Ce choc se déplace vers l'aval à mesure que le nombre de Mach augmente, et en général, en même temps, son intensité augmente.

Lorsque le profil est placé en incidence, on constate un décalage entre l'évolution du choc d'intrados et celle du choc d'extrados. Pour un profil de type classique en incidence, lorsque le nombre de Mach amont croît un choc apparaît d'abord à l'extrados, mais celui qui apparaît un peu plus tard à l'intrados recule plus rapidement et atteint donc le bord de fuite avant le choc d'extrados. Il en résulte une perte de portance localisée à l'arrière du profil et corrélativement un moment cabreur important. A des nombres de Mach voisins de 1 le choc d'extrados rejoint le bord de fuite et le moment cabreur diminue. La raison pour laquelle le choc d'extrados ne recule pas régulièrement et rapidement vers l'aval, ce qui finalement est la cause du moment cabreur constaté, c'est que la couche limite ne peut supporter la recompression imposée par le choc et qu'il se produit un décollement.

Il apparaît ainsi que les décollements sont amenés à jouer un rôle très important dans les écoulements transsoniques. Les principales configurations de décollement qui peuvent être rencontrées sur un profil sont présentées figure 4 extraite de la référence 2 dans laquelle a récemment été effectuée une présentation générale des problèmes posés par les écoulements transsoniques :

a) décollement laminaire de bord d'attaque sans choc qui est fondamentalement analogue à ceux qui peuvent se produire en écoulement incompressible ;

b) décollement généralisé depuis le bord d'attaque ;

c) décollement de la couche limite turbulente produit par le choc et suivi d'un recollement ;

d) décollement de la couche limite turbulente produit par le choc et non suivi de recollement ;

e) décollement au pied du choc suivi de recollement, mais la couche limite très épaissie par le processus précédent décolle de nouveau à l'approche du bord de fuite ;

f) plusieurs types de décollement sont simultanément présents.

3.2.2 - Effet du nombre de Mach et de l'angle d'incidence -

La figure 5 extraite de [2] d'après [3], montre l'évolution de la distribution de pression avec le nombre de Mach et les configurations d'écoulement correspondantes. Le développement d'une région décollée au bord de fuite n'empêche pas le mouvement du choc vers l'arrière mais ralentit sa progression.

L'évolution typique de la distribution de pression avec l'angle d'incidence, à nombre de Mach fixé, est de façon similaire présentée figure 6. Lorsque l'angle d'incidence augmente, dans un premier temps le choc recule et devient plus intense. A cause de l'intensité plus grande du choc un bulbe de décollement se forme et se développe au pied du choc et ceci provoque un épaississement de la couche limite et du sillage. Lorsque le bulbe de décollement s'est développé jusqu'au bord de fuite le choc se met à avancer. Cette situation peut être obtenue soit par l'extension vers le bord de fuite du décollement induit par le choc ou par le développement vers l'amont d'un décollement qui a pris naissance au bord de fuite. Pour des angles d'incidence encore plus grands l'écoulement décolle depuis le bord d'attaque.

Il doit être noté que dès qu'un bulbe de décollement de dimension sensible a été formé, la pression statique au bord de fuite, qui jusqu'alors restait à un niveau constant, se met à diminuer. Ce phénomène est utilisé pour détecter l'apparition des décollements et par suite celle du buffeting, on l'appelle "divergence de la pression de bord de fuite".

3.3.3 - Interaction choc - couche limite et effet du nombre de Reynolds -

Dans les évolutions précédentes en fonction du nombre de Mach ou de l'incidence, on a vu que des chocs, parfois intenses se déplaçent sur le profil. Ces chocs agissent sur la couche limite et les effets qui en résultent, dépendent des caractéristiques de la couche limite (épaisseur, paramètre de forme) et de l'intensité du choc.

Dans tous les cas la couche limite est épaissie par l'interaction avec le choc. Si le décollement ne se produit pas les effets sont relativement faibles, mais s'il se produit, même dans le cas où il y a recollement, les conséquences peuvent être importantes. La couche limite à l'aval du recollement se retrouve déstabilisée et fortement épaissie et donc dans une situation défavorable pour pouvoir supporter la recompression à l'approche du bord de fuite.

Indirectement ceci explique pourquoi l'effet du nombre de Reynolds peut être si grand sur les écoulements transsoniques et pourquoi il n'est pas facile d'améliorer la situation en utilisant des dispositifs de déclenchement de la transition : pour pouvoir simuler de façon convenable ce qui se passe en vol à des nombres de Reynolds élevés il faut être capable de reconstituer une couche limite ayant une épaisseur et un paramètre de forme convenable particulièrement à l'endroit des chocs. Si on utilise des dispositifs de déclenchement il peut être nécessaire de les ajuster en position et dimension pour chaque condition de vol définie par un nombre de Mach, un nombre de Reynolds et un angle d'incidence.

La figure 7 montre l'évolution de la distribution de pression en fonction du nombre de Reynolds pour un profil symétrique à incidence nulle. Pour le nombre de Reynolds le plus bas il y a une interaction choc - couche limite laminaire typique avec un décollement au pied du choc assez étendu. La recompression, de ce fait, s'étend sur près de 40 % de la longueur de la corde. A plus grand nombre de Reynolds ($0{,}66.10^6$) l'étendue de la zone d'interaction diminue. Pour des nombres de Reynolds encore plus grands il y a une interaction choc - couche limite sans décollement et la répartition de pression devient indépendante du nombre de Reynolds.

Les effets du nombre de Reynolds peuvent encore être plus spectaculaires dans les cas où l'écoulement est sur le point de décoller à l'approche du bord de fuite. Dans cette situation la position du choc, qui est fonction de l'étendue de la zone décollée au bord de fuite est aussi dépendante du nombre de Reynolds.

3.3.4 - Les écoulements tridimensionnels -

Même en se limitant au cas des ailes il est très difficile de présenter des considérations générales sur les écoulements tridimensionnels parce que presque chaque cas est un cas particulier par suite du grand nombre de paramètres nécessaires pour caractériser complètement une aile : allongement, effilement, angle de flèche, loi d'épaisseur, de cambrure et de vrillage. Les ailes peuvent, cependant, être classées en trois grandes catégories, en fonction de l'un des paramètres les plus importants, l'angle de flèche moyen ; ce sont :

- les ailes à flèche faible ou nulle (a)
- les ailes en flèche (b)
- les ailes élancées ou à très forte flèche (c).

Des valeurs typiques d'angles de flèche pour chaque catégorie peuvent être données, par exemple 5, 30 et 60 degrés, mais il est impossible de définir des limites précises parce que pour les valeurs intermédiaires de l'angle de flèche c'est la considération des autres paramètres comme l'allongement ou l'angle d'incidence qui alors détermine le type d'écoulement.

a) Sauf dans le cas des allongements faibles et des ailes vrillées, les ailes à faible flèche ont des configurations d'écoulement qui sont pratiquement bidimensionnelles [4]. Tout ce que l'on vient de décrire dans les paragraphes précédents s'applique donc à ce type d'aile.

b) Pour les ailes en flèche la situation est beaucoup plus compliquée car elle comporte un mélange inextricable et apparemment imprévisible d'ondes de choc, de tourbillons et de décollements. Cependant, grâce à de nombreuses et patientes études en soufflerie reposant sur la mesure des répartitions de pression et sur l'utilisation des visualisations pariétales, on a pu obtenir une assez bonne compréhension des phénomènes dans certains cas [5].

Le schéma typique de l'écoulement pour des ailes en flèche à des angles d'incidence modérés est montré figure 8 extraite de [2]. C'est une configuration à trois chocs. Dans la partie interne de l'aile, du côté de l'emplanture, il y a deux chocs : le choc de tête qui part obliquement de l'apex de l'aile vers l'extrémité et le choc arrière qui émane sensiblement du bord de fuite de la section d'emplanture et qui remonte légèrement l'écoulement en se dirigeant vers l'extrémité. Ces deux chocs se rencontrent et se rassemblent pour former un seul choc plus intense, le choc externe.

Lorsque l'incidence croît le choc de tête se déplace vers l'aval tandis que le choc arrière se déplace vers l'amont de sorte que leur point d'intersection se rapproche de la section d'emplanture et que la fraction de l'aile intéressée par le choc externe augmente. Ceci est très important car, à cause de son intensité, le choc externe produit un décollement de l'écoulement qui s'étend en général jusqu'au bord de fuite (cas c et d de la figure). Ainsi lorsque l'angle d'incidence augmente, la région d'écoulement décollée derrière le choc externe s'étend-elle progressivement de l'extrémité vers l'emplanture de l'aile. Pour des angles d'incidence encore plus élevés la ligne de décollement s'avance jusqu'au bord d'attaque (cas b de la figure) et la région décollée tend à s'organiser en un tourbillon. Enfin à grande incidence l'écoulement est complètement décollé et organisé en un tourbillon qui part de l'apex de l'aile.

c) Pour les ailes à forte flèche à bord d'attaque aigu même à faible incidence, l'écoulement décolle dès le bord d'attaque et s'enroule pour former un tourbillon à l'aval auquel il y a recollement. le décollement est stable et bien organisé jusqu'à ce que, à des incidences très élevées, le tourbillon éclate au niveau de l'aile.

4 - LES PHENOMENES INSTATIONNAIRES -

Compte tenu de sa complexité, le problème du buffeting a longtemps été étudié d'une façon globale. D'ailleurs très souvent on se limitait à caractériser les circonstances de son apparition, liée on le sait à celle des décollements.

Actuellement pour concevoir des machines optimisées ayant des performances sans cesse améliorées, on souhaite aller plus loin et être capable de prévoir l'intensité du buffeting qui peut se produire avec une configuration donnée. Pour cela il faut pouvoir utiliser les modèles sophistiqués mis au point pour décrire la dynamique des structures et donc connaître ce qui est à l'origine même du buffeting, les fluctuations de pression dans l'écoulement.

Ce problème qui dans sa généralité est sans doute l'un des plus compliqués qu'on puisse imaginer en aérodynamique n'a réellement été qu'abordé jusqu'à présent. Cependant les nombreux travaux en cours actuellement sur le sujet devraient dans un proche avenir améliorer de façon sensible la compréhension des phénomènes.

4.1 - Fluctuations de pression dans les couches limites -

Bien que d'un niveau très faible vis-à-vis des fluctuations de pression provoquant le buffeting, les fluctuations de pression dans les couches limites sont intéressantes à étudier comme point de comparaison avec celles qui se produisent dans les décollements ; par ailleurs elles sont la cause d'une bonne partie du bruit aérodynamique engendré par l'écoulement. Pour les caractériser on a l'habitude d'utiliser :

- leur valeur efficace $\sqrt{\tilde{p}^2} = \frac{1}{T}\int_0^T \tilde{p}^2 dt$

- leur spectre de puissance $G(f)$ qui est la transformée de Fourier de la fonction d'auto-corrélation $R(\tau)$

$$R(\tau) = \frac{1}{T}\int_0^T \tilde{p}(t)\ \tilde{p}(t+\tau)\, dt$$

$$G(f) = \frac{2}{\pi}\int_0^\infty R(\tau)\cos(2\pi f\tau)\, d\tau = \lim_{\Delta f \to 0} \frac{1}{\Delta f\, T}\int_0^T \tilde{p}(t, \Delta f)^2\, dt$$

- les corrélations spatio-temporelles qui permettent de juger de la cohérence des fluctuations en divers points de la surface :

$$R(x, y, \tau) = \frac{1}{T}\int_0^T \tilde{p}(x,t)\cdot\tilde{p}(y, t+\tau)\, dt$$

Dans le cas des couches limites non décollées les résultats de provenances diverses rassemblés par G.F. Coe et W.J. Chyu [6] montrent que la valeur efficace des fluctuations est proportionnelle à la pression dynamique de l'écoulement extérieur de sorte que $\sqrt{\tilde{p}^2}/q_\infty$ n'est pratiquement fonction que du nombre de Mach (figure 9).

M.V. Lowson [7] avait proposé une loi $\sqrt{\tilde{p}^2}/q = 0{,}006 / (1 + 0{,}1\, M^2)$ pour représenter cette dépendance mais les résultats obtenus à M = 3 et 3,5 à Ames invalident cette représentation pour des nombres de Mach supérieurs à 2,5.

Il est à remarquer que les tentatives pour relier $\sqrt{\tilde{p}^2}$ à une grandeur caractéristique de l'état de la couche limite à l'endroit de la mesure (le frottement de paroi τ_p par exemple) conduisent à une corrélation plutôt moins satisfaisante des résultats [7].

Les spectres d'énergie qui indiquent comment l'énergie des fluctuations est répartie suivant la gamme des fréquences sont corrélés en terme de nombres de Strouhal c'est-à-dire en considérant les fréquences et les densités spectrales réduites $f\ell/v$ et $Gv/q^2\ell$, v, ℓ et q étant respectivement une vitesse, une longueur et une pression caractéristique de référence.

Pour les couches limites il est commode d'utiliser l'épaisseur de la couche limite, la vitesse et la pression dynamique à l'extérieur comme éléments de réduction.

La figure 10 extraite de [6] donne un résultat typique obtenu à Ames. On remarque un gonflement du spectre vers les basses fréquences de sorte que la formule proposée par M.V. Lowson [7]

$$\frac{G v}{q^2 \delta} = \frac{1}{8} \times \left(0{,}006 / 1 + 0{,}14\, M^2\right)^2 / \left[1 + \left(\frac{2\pi f \delta}{8 u}\right)^2\right]^{3/2}$$

ne peut convenir pour les fréquences réduites inférieures à 0,1.

Les corrélations spatiales exploitées par M.K. Bull [8] sous forme normalisée

$$R_{pp}(r_1, r_3, \tau) = R(x, x+r, \tau) / R(x, x, 0)$$

sont présentées figure 11. Elles montrent qu'au voisinage immédiat du point de référence ($r < \delta^*$) le champ est isotrope.

Les corrélations spatio-temporelles correspondant à des déplacements dans le sens de l'écoulement toujours extraites de [8] mettent en évidence figures 12 et 13, l'existence d'une vitesse de convection légèrement variable avec la distance et qui tend vers $0{,}625\ U_\infty$.

4.2 - Fluctuations de pression dans les décollements -

Des études fondamentales ont été entreprises sur des modèles relativement simples en écoulement bidimensionnels plan ou de révolution.

C.F. Coe et W.J. Chyu, dans le but d'arriver à une méthode de calcul des vibrations de paroi en présence de décollement, ont étudié de façon approfondie en supersonique les fluctuations dans les décollements en amont de marches ascendantes de formes diverses. Les résultats des mesures effectuées sur des configurations de révolution ou en écoulement plan présentés figure 14 montrent que les niveaux de fluctuations sont très élevés spécialement au voisinage des points de décollement et de recollement et qu'ils n'évoluent pas de façon sensible avec le nombre de Mach entre 1,7 et 3,5. Les spectres correspondant aux mêmes configurations, réduits comme précédemment pour les couches limites, se regroupent de façon très satisfaisante, spécialement vers les hautes fréquences [figure 15].

L'analyse détaillée de l'effet du nombre de Mach sur ces spectres indique une décroissance de la densité spectrale lorsque le nombre de Mach croît pour les fréquences réduites inférieures à 0,3 et une augmentation pour les fréquences supérieures.

Enfin en utilisant la méthode des moindres carrés C.F. Coe et W.J. Chyu [6] montrent qu'il est possible d'adopter une formule de décroissance exponentielle pour représenter l'évolution spatiale des densités spectrales croisées ce qui leur permet d'exprimer sous forme analytique les caractéristiques du champ de pression instationnaire.

D.G. Mabey [9] a étudié les fluctuations dans les bulbes de décollement. Dans ce cas ni le point de décollement ni le point de recollement ne sont fixés et par conséquent la position même du bulbe est susceptible de fluctuer. Compte tenu de l'allure même des courbes de recompression il en résulte une fluctuation importante de la pression au niveau du recollement (figure 16 extraite de [1]). Par ailleurs l'évolution de l'épaisseur de la couche de mélange conduit aussi à prévoir un maximum de fluctuation au niveau du recollement.

Un temps caractéristique pour la propagation d'une perturbation d'une extrémité à l'autre du bulbe est ℓ / U_s, ℓ étant la dimension du bulbe et U_s la vitesse de l'écoulement extérieur au niveau du bulbe (vitesse plateau). Dans ces conditions Mabey indique que la valeur de la fréquence réduite $n = f\ell/U$ formée avec la vitesse amont pour laquelle la densité spectrale est maximale, doit être voisine de 0,6 ce qui est effectivement confirmé par l'expérience (figure 17 extraite de [1]).

Les études concernant des configurations tridimensionnelles d'ailes réelles sont beaucoup plus récentes que les précédentes et les résultats publiés sont encore très peu nombreux et fragmentaires.

Dans un premier temps il est nécessaire d'étudier l'écoulement moyen de façon à bien connaître l'apparition et le développement des zones décollées. La référence [10] est un exemple de ce genre d'étude appliquée à une aile de flèche modérée. La corrélation entre l'apparition du buffeting et celle des décollement y est clairement mise en évidence. Ensuite l'analyse du champ de pression instationnaire nécessite l'utilisation d'un grand nombre de capteurs de pression instationnaire et un traitement très complet et très lourd des informations. Plusieurs opérations de ce genre sont en cours actuellement et des progrès sont certainement à attendre pour un proche avenir.

5 - LES MOYENS D'ETUDE -

Compte tenu de la complexité des phénomènes il n'est pas possible à l'heure actuelle d'obtenir par voie théorique les caractéristiques statistiques concernant les fluctuations de pression. Leur connaissance repose donc sur l'expérience.

La technique consiste à équiper la maquette d'un grand nombre de capteurs de pression instationnaires, à bande passante aussi large que possible, qu'il est impératif de placer à l'endroit même de la mesure pour éviter que la canalisation d'amenée de la pression n'introduise des déphasages ou un certain filtrage, l'idéal étant que la membrane même du capteur constitue la paroi de la maquette. Bien que le traitement en temps réel soit possible au moins lorsque le nombre d'information est petit on prévoit généralement un enregistrement analogique des signaux, ce qui permet ultérieurement d'effectuer tous les dépouillements souhaités. A ce stade le principal problème se situe au niveau de la définition de la structure de la maquette.

Idéalement puisque le buffeting est essentiellement une réponse de structure à une sollicitation aérodynamique, il serait nécessaire d'assurer une parfaite similitude dynamique entre la structure de la maquette et celle de l'engin que l'on veut étudier. Indépendamment des questions de coût et de délais pour obtenir ce genre de maquette, la similitude rigoureuse est généralement impossible à réaliser, il faut donc essayer de se rendre compte dans quelle mesure en régime de buffeting les répartitions de pressions instationnaires sont dépendantes du mouvement de la maquette.

Jusqu'à présent cette question n'a pas reçue de réponse définitive et générale. Tantôt il ne semole pas qu'une modification du mode de suspension de maquette provoque des modifications décelables au niveau du spectre des pressions dans les régions décollées alors qu'elle modifie de façon très nette la réponse structurale [10]. Tantôt au contraire des expérimentateurs signalent qu'ils ont retrouvé dans les spectres en régime buffeting des raies caractéristiques des modes structuraux. Compte tenu de l'importance de ce problème de nombreuses recherches sont actuellement en cours qui devraient permettre dans un proche avenir de trancher la question.

6 - CONCLUSIONS -

Le décrochage et le tremblement sont des phénomènes liés à l'apparition et au développement sur les véhicules aériens, de zones d'écoulements décollés. Ces décollements sont le siège de remous qui produisent des fluctuations de pression et excitent la structure. Les décollements apparaissent sous l'action des gradients de pression positifs intenses, ils jouent donc un rôle important dans le régime transonique qui provoque des recompressions très brutales par les chocs qu'il engendre.

Les fluctuations de pression dans les décollements ont une intensité de 10 à 100 fois supérieure à celles qui sont présentes dans les couches limites attachées. La prévision par le calcul de l'intensité du buffeting nécessite la connaissance du champ des pressions instationnaires ce qui est un problème extrêmement ardu à aborder par voie purement théorique. La voie suivie actuellement consiste à évaluer les caractéristiques statistiques du champ de pression en les mesurant. Le problème qui se pose alors est celui de savoir dans quelles conditions les relevés effectués au cours des expériences sur maquettes sont représentatifs de ce qui se passe à l'échelle réelle.

REFERENCES

[1] - MABEY, D.G. ;
Beyond the buffet boundary.
Aeronautical Journal N° 748 ; April 73.

[2] - GENRAY, A.E. and OLIVER, W.R. ;
Investigation of aerodynamic analysis problems in transonic maneuver
Douglass A/C Co Rpt MDC - J 5264-01 Vol. 1 ; Sept. 71.

[3] - PEARCEY, H.H. ;
Some effects at the shock and rear separation of turbulent boundary layers in transonic flow past aerofoils.
R & M N° 3108, 1959.

[4] - MOSS, G.F. ;
Some notes on the aerodynamic problems associated with the phenomenon of buffeting ;
Tech. Memo. Aero. 1293 ; February 71.

[5] - ROGERS, E.W.E. and HALL, I.M. ;
An introduction to the flow about plane swept-back wings at transonic speeds ;
Journal of the Royal Aeronautical Society, Vol. 64 ; August 60.

[6] - COE, C.F. and CHYU, W.J. ;
Pressure - fluctuation inputs and response of panels underlying attached and separated supersonic turbulent boundary layers ;
AGARD CP 113 ; Sept. 72.

[7] - LOWSON, M.V. ;
Prediction of boundary layer pressure fluctuations ;
WYLE LABORATORIES AFFDL - TR - 67 - 167.

[8] - BULL, M.K. ;
Wall-pressure fluctuations associated with subsonic turbulent boundary layer flow ;
J. Fluids Mechanics, vol. 28, part. 4, pp. 719 - 754 ; June 67.

[9] - MABEY, D.G. ;
Pressure fluctuations caused by separated bubble flows at subsonic speeds ;
RAE TR 71160 ; August 71.

[10] - MONNERIE, B. and CHARPIN, F. ;
Essais de buffeting d'une aile en flèche en transsonique ;
10ème colloque d'aérodynamique appliquée de la AAAF ; Novembre 1973 (to be published in the "Aéronautique et Astronautique" Journal).

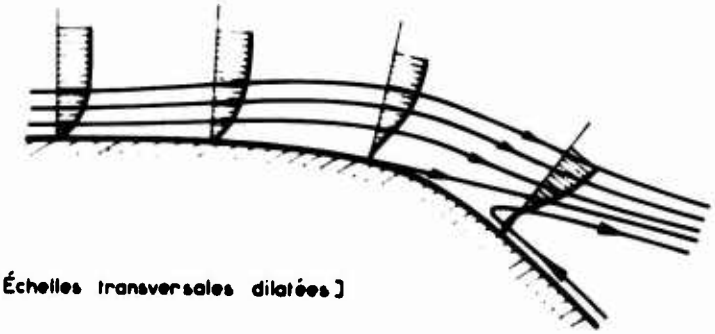

Figure 1 - Evolution du profil de couche limite lors du décollement.

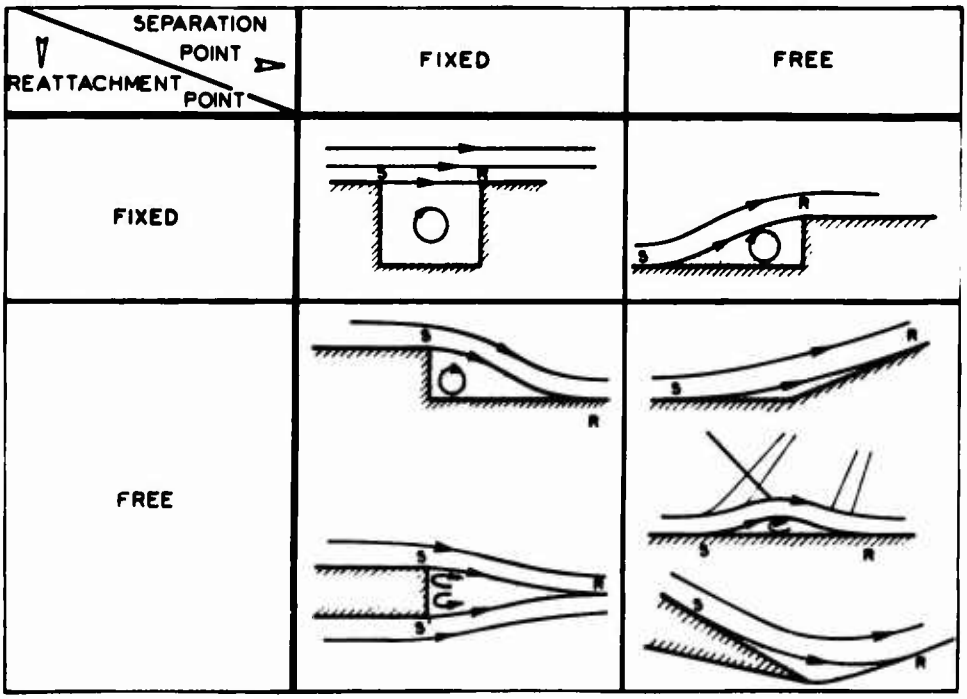

Figure 2 - Différents types de zones décollées.

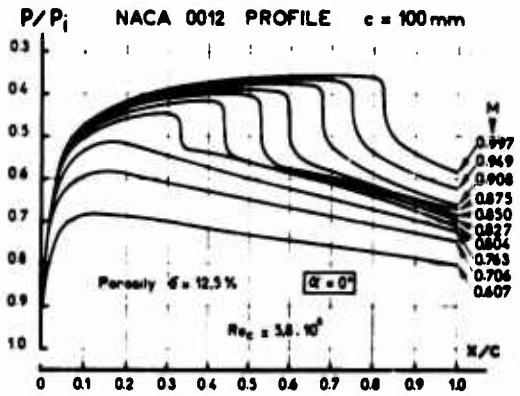

Figure 3 - Répartition de pression sur un profil à incidence nulle.

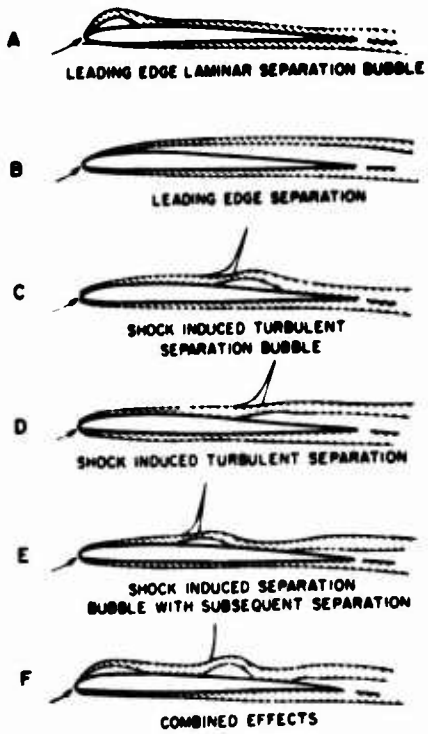

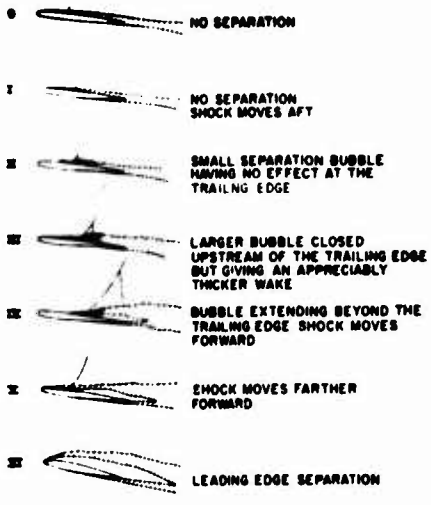

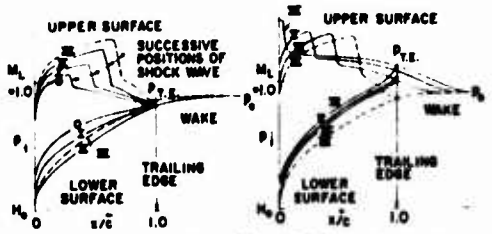

Figure 6 - Aperçu [illegible] sur un profil par différentes [illegible]

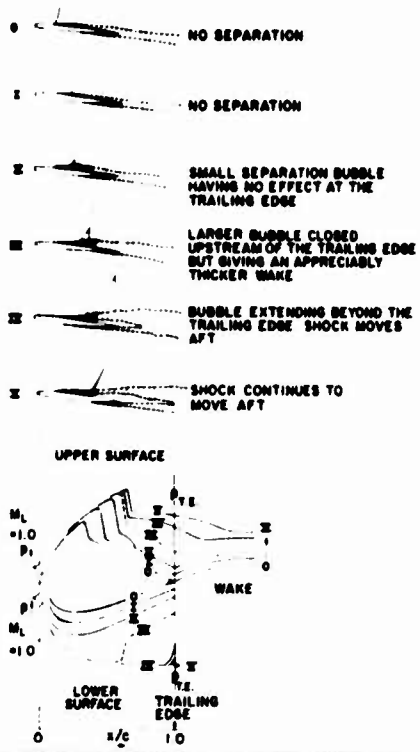

NOTE THE ORDINATE OF PRESSURE FOR THE LOWER SURFACE IS A MIRROR IMAGE OF THAT FOR THE UPPER SURFACE.

Figure [illegible] - [illegible]

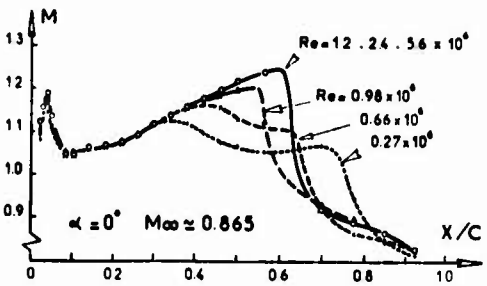

Figure 7 - Effet [illegible] nombre de Reynolds sur la répartition de pression.

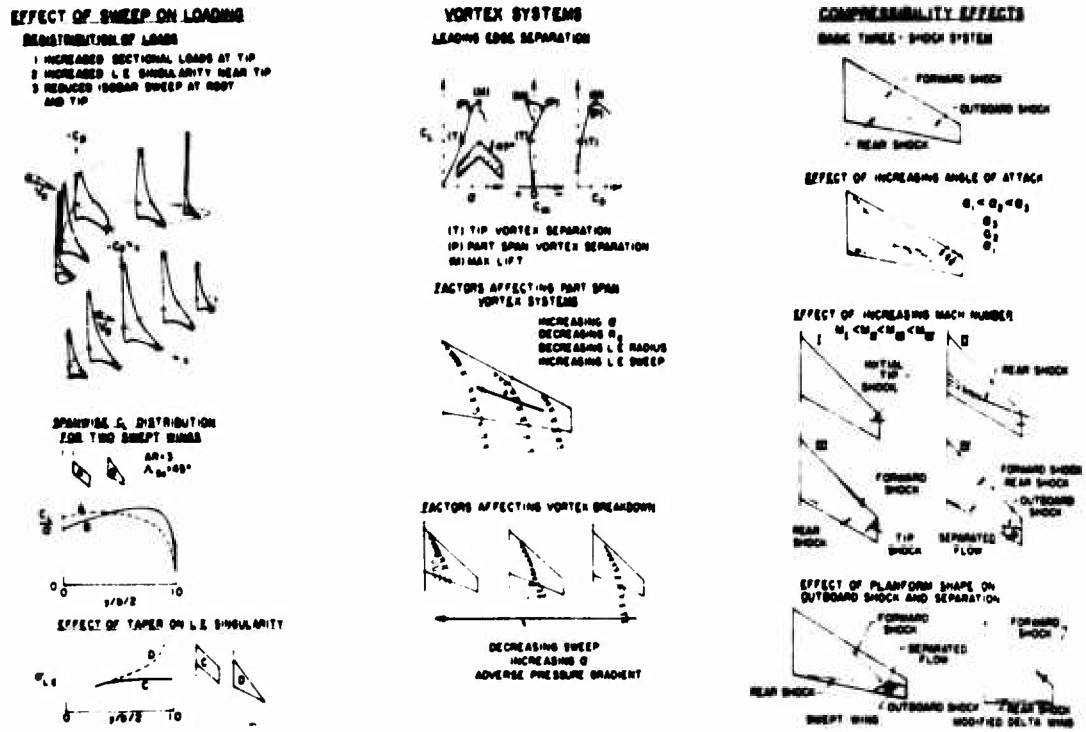

Figure 8 – Principa[illegible] l'écoul[illegible] ailes en flèche [illegible].

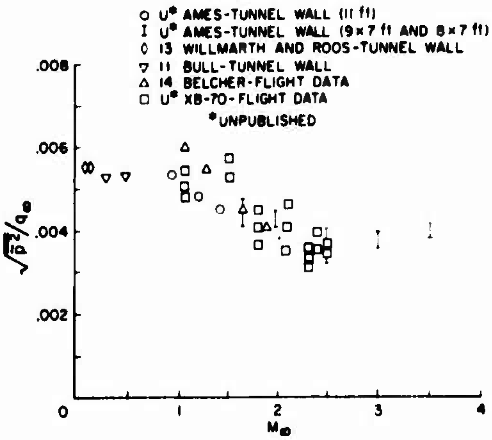

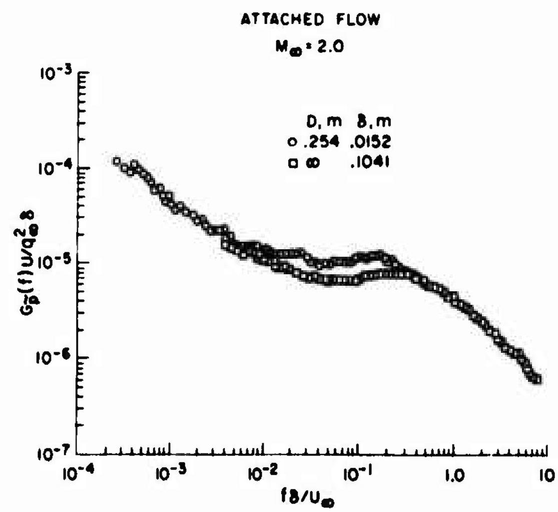

Figure 9 – Valeur efficace [illegible] fluctuations de pression [illegible] couche limite turbulente [illegible].

Figure 10 – Spectre [illegible] fluctuations de pression sous une couche limite turbulente [illegible].

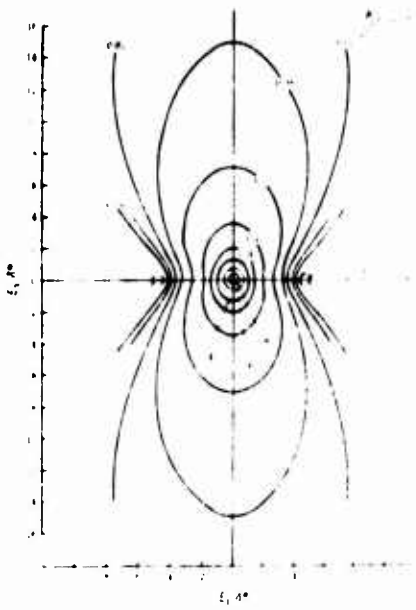

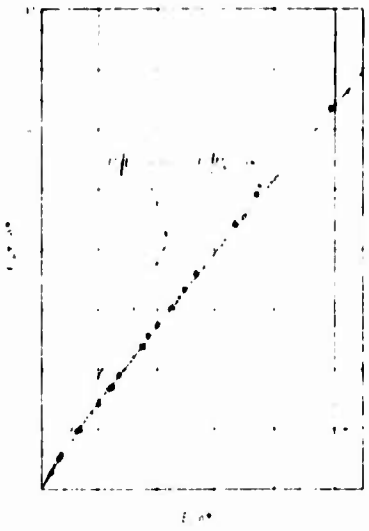

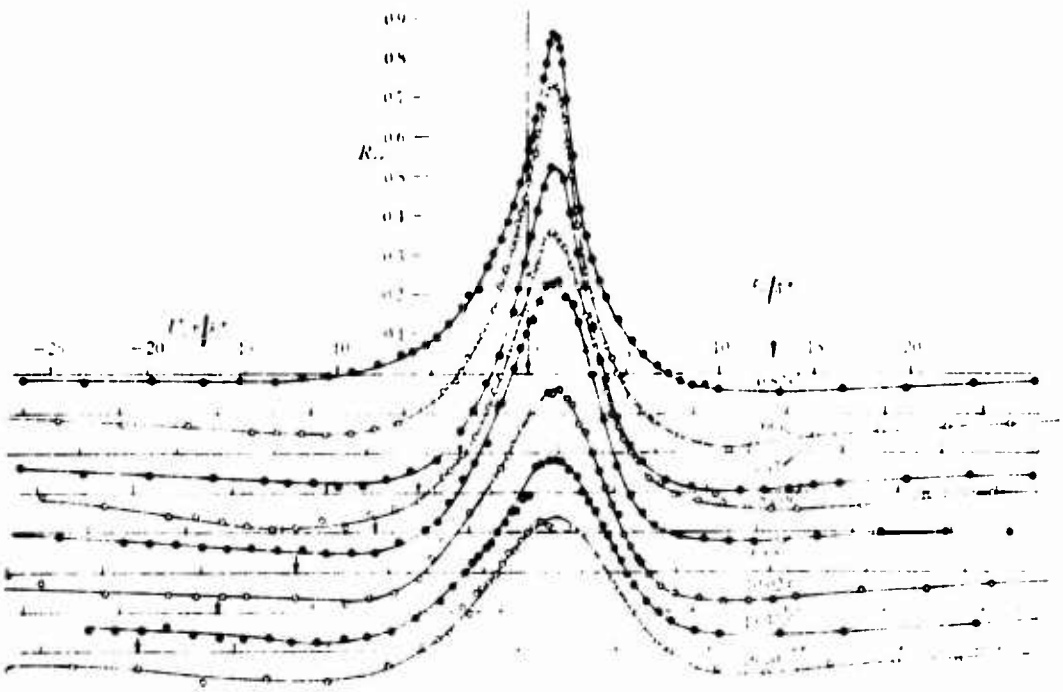

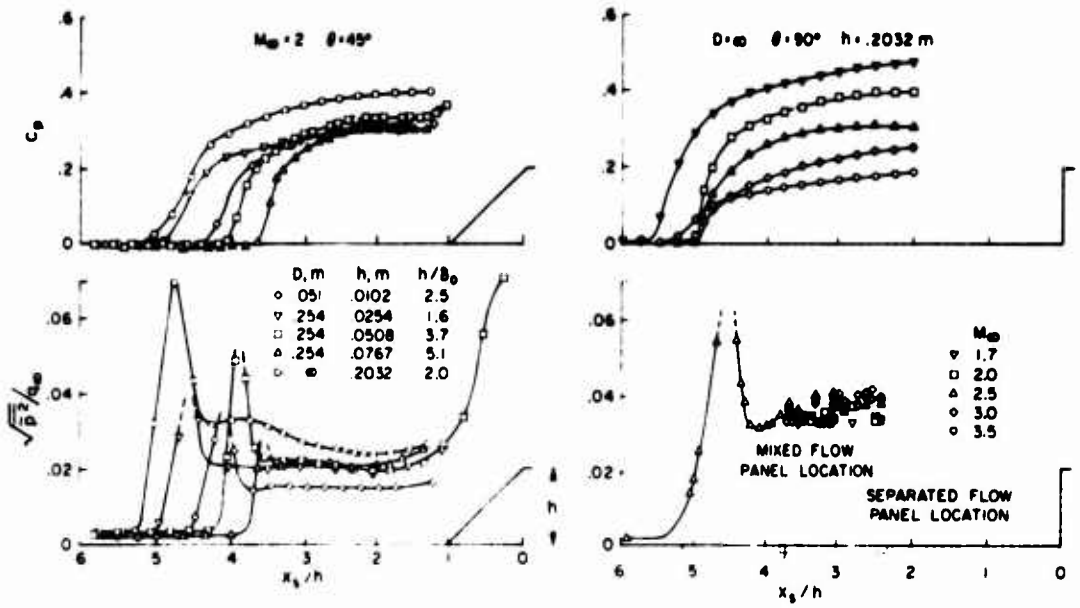

Figure 14 – Répartitions des pressions statiques et des valeurs efficaces des fluctuations de pression dans le décollement en amont de marches ascendantes [6].

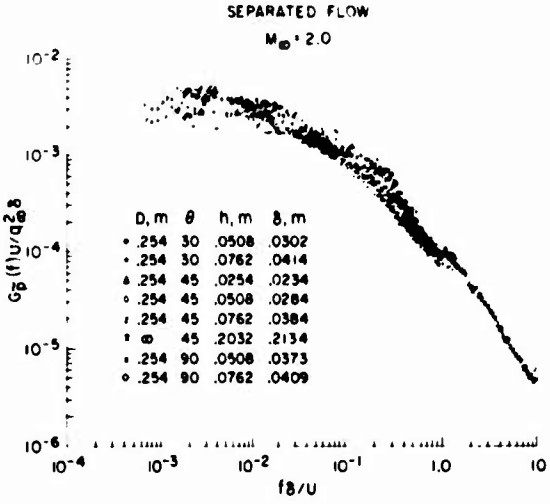

Figure 15 – Spectres des fluctuations de pression dans le décollement en amont de marches ascendantes [6].

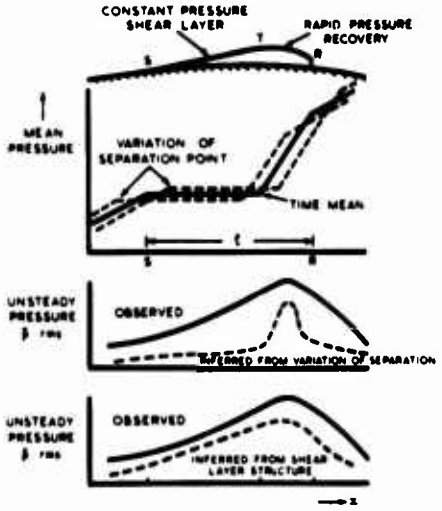

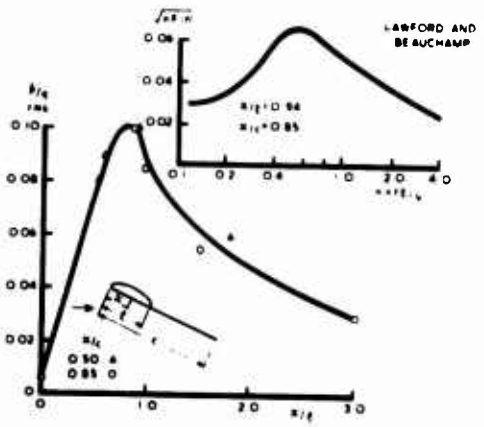

AIRCRAFT DYNAMIC RESPONSE ASSOCIATED WITH FLUCTUATING FLOW FIELDS

by

J. G. Jones
Royal Aircraft Establishment
Bedford, England

SUMMARY

An important feature of separated flow fields is their characteristic unsteadiness. This lecture is mainly concerned with the interactions between such fluctuating flow fields and the dynamic response of the aircraft structure generally known as buffeting. A basic feature of the dynamical analysis of buffeting is the closed-loop interaction between the fluctuating fluid motion and the motion of the wing surface. The problem of formulating an appropriate theoretical model for structural buffeting is discussed, together with the analogous situation involving response in rigid-body modes, including the oscillatory motion known as wing-rocking.

In illustration, buffeting measurements obtained from flight tests of a combat aircraft are presented. These illustrate the complexity of the structural response in terms of a wide range of vibration modes. The modal content varies both with position over the aircraft and with degree of penetration beyond buffet onset.

Other flight-test measurements illustrate the characteristics of unsteady pressure fields on a buffeting wing.

In the case of aircraft rigid-body motions, the possibility is discussed of relating those unsteady characteristics which adversely influence handling qualities and tracking ability to quantitative parameters in an analytical model.

1. INTRODUCTION

Previous lectures in this series have discussed the fluid mechanics of aircraft stall. In this lecture we shall be concerned with the manner in which the characteristic unsteadiness of separated flow interacts with the dynamic properties of the aircraft to produce fluctuating response in both structural and rigid-body modes.

Over the past few years, problems of buffeting behaviour and handling characteristics at high lift have received increased attention, particularly in the context of manoeuvrability of combat aircraft. As a consequence of the occurrence of regions of separated flow on the wing, the high-g performance of a combat aircraft may be limited either by vibration (buffeting), mainly associated with structural flexibility, or by degradation in handling characteristics. Phenomena in this latter category include 'wing-rocking', 'wing-dropping' and 'nose-slice'. For example, Fig.1 illustrates a typical penetration to high normal force coefficient C_N of a fighter aircraft, such as might occur during a 'high-g' turn. Two types of oscillatory response are apparent. One is in the filtered wing-tip acceleration trace, predominantly at the frequency (of order 10 Hz) of the first symmetric wing-bending mode and known as buffeting. The other is primarily in the roll-rate trace, at a frequency of about 1 Hz, in a rigid-body fluctuating motion usually referred to as wing-rocking. Both types of response, one in a structural and the other in a rigid-body mode, are associated with unsteady separated flow conditions above the wing. As aircraft speed is increased from subsonic into the transonic range, the angle of attack at which these undesirable features occur tends to decrease; indeed, at transonic speeds steady conditions may not exist even in the case of flight at 1 g (straight and level in the mean). Since such forms of fluctuating motion clearly have an adverse effect on the manoeuvre capability of high performance aircraft, it is of great practical interest to be able to understand and predict these characteristics.

Historically, work on buffeting dates back to the investigation of an accident in 1930 which led to wind-tunnel testing of tail vibration at high angles of attack due to immersion in the separated stalled-wing flow. Originally the expression 'buffeting' was applied to such tail vibrations, and early work concentrated on what we now call 'tail buffeting'. Subsequently, interest shifted to the excitation of the wing itself by the fluctuating stalled flow above it, and this is what is currently meant by the term 'buffeting'. More recently, in the context of manoeuvres of combat aircraft at high subsonic speeds, buffeting associated with shock-induced separations has become of primary importance. A related problem, mainly associated with work on high performance compressor and helicopter blades, is the oscillatory motion of a stalled wing in such a way that the nature of the flow separation differs at different instants in the cycle, possibly switching from attached to separated flow or from a leading-edge to a trailing-edge stall. This phenomenon, known as stall-flutter, is usually associated with a marked torsional (pitching) wing motion. The affinity between buffeting and stall-flutter has been discussed by Fung[1] who pointed out that there may be situations where it is difficult to make the distinction.

A basic feature of such fluctuating systems is the interaction between the fluid motion, involving separated flow, and the motion of the wing surface. We distinguish between two cases, differing in the nature of this interaction. The first we refer to as a FORCED VIBRATION. This consists of an irregular random motion in which 'turbulent' pressure fluctuations which are independent of wing motion produce an aerodynamic driving force, the consequent motion of the wing producing an additional, additive, motion-dependent pressure field. The appropriate analytical model in this case is 'non-autonomous', involving a random forcing term explicitly expressible as a function of time. The theoretical model describing the wing motion, for a prescribed random force of excitation, may often take the form of linear equations. However, nonlinearity plays an essential role in an overall view of the situation as it dominates the

process of energy transfer, within the airflow, by which energy is extracted from the mean flow and channelled into the fluctuations of the aerodynamic driving force.

The second case we refer to as NONLINEAR FLUTTER. Here, more-or-less regular oscillations of a stalled wing occur, in which the time-varying pressure field is essentially determined by the past history of the wing motion. The appropriate analytical model is 'autonomous' and involves no significant terms explicitly expressed as functions of time. This type of motion is also known as a limit-cycle, and a non-linear analytical model is essential. It includes stall-flutter as a particular case. In contrast to 'forced vibration', the nonlinear mechanism of energy transfer from the mean airflow now involves the motion of the wing in addition to the unsteady motion of the air. The essential distinction between the two phenomena is that in the former case we may say that the wing motion is 'forced' by the fluctuating flow field, whereas in the latter case the joint motion of wing and flow field arises as a mutual interaction.

In some situations the amplitude of wing motion is a relevant parameter, motion of small amplitude leaving the turbulent fluctuations in the separated flow similar to those that would occur in the flow past a rigid wing but leading to an additive, motion-dependent, pressure field. As the amplitude of wing motion is increased, however, the possibility arises of the 'entrainment' of the larger-scale irregular flow fluctuations into a deterministic relationship with the wing motion. This type of resonance is of course most likely if the frequency of wing motion (Strouhal number) is close to some natural frequency of vorticity shedding in the separated flow.

Whilst it is customary to regard wing structural buffeting as an aerodynamically forced vibration, in which the forcing term can in principle be obtained from measurements on a rigid wing, more basic research is required to determine the limits of applicability of this approach. Even in cases where the buffeting wing is appropriately regarded as aerodynamically forced, the relationship between the forces on the structurally-responding wing and on a geometrically similar but rigid wing is not necessarily straightforward. In particular, there is the possibility that the motion of the wing may interfere with the nonlinear process by which energy is transferred from the mean flow to the fluctuating fluid motion and thus modify the statistical characteristics of the aerodynamic exciting force. The clarification of these topics is of considerable practical importance in that they determine the circumstances in which rigid wind-tunnel models may be used as the basis for estimation of intensity of buffeting of full-scale aircraft.

An analogous problem concerning the choice of appropriate theoretical model occurs in connection with wing-rocking. Should a state of steady wing-rocking be regarded as aerodynamically forced or in terms of limit-cycle oscillations of a closed-loop system whose motion remains bounded through the action of amplitude-dependent nonlinear forces? In the latter case a unified treatment of wing-rocking and the divergent motions known as 'wing-dropping' and 'nose-slice' may be possible, the distinction arising primarily in the nature of the (nonlinear) forces at large amplitude, stabilising in the case of wing-rocking but not in the other cases. An important area of current work is the determination of appropriate characteristics that may be identified using wind-tunnel models to indicate the onset of wing-rocking of the full-scale aircraft. Two types of criteria are possible, one based on the appearance of a significant random FLUCTUATING component in the aerodynamic forces (or moments) and the other, based on the MEAN component of the aerodynamic forces, indicating either a loss of dynamic stability for small perturbations about some high-lift equilibrium condition, or a loss of equilibrium due to asymmetry. For example, one might expect the appearance of fluctuating forces or moments on a rigidly-mounted wind-tunnel model to correlate in general with a dynamic situation appropriately modelled as an aerodynamically forced vibration. Conversely, we might expect the measurement of mean aerodynamic forces that indicate a loss of dynamic stability or equilibrium to correlate with a dynamic divergence or, under the action of appropriate amplitude-dependent forces, with fluctuating motion of the limit-cycle, or nonlinear flutter, type. However, exceptions to this association of onset criteria with types of dynamic motion can occur. For instance, the appearance of random fluctuating forces on a rigidly-mounted model may correlate with a dynamic situation in which the fluctuations in the flow field become deterministically related to wing motion, leading to nonlinear flutter. Moreover, it is quite possible for the two types of criterion to be satisfied simultaneously, fluctuating aerodynamic forces occurring in conjunction with destabilising changes in the mean force or moment curves.

2. MATHEMATICAL MODELS OF AIRCRAFT RESPONSE ASSOCIATED WITH UNSTEADY FLOW

A common element of the buffeting and wing-rocking phenomena discussed in the previous section is the interaction between the unsteady fluid motion, involving separated flow, and the motion of the wing. In this section we clarify the ways in which a mathematical formulation of these and related phenomena may be made.

We begin by considering the influence of time-varying boundary conditions, applied at the surface of a wing, upon a rotational flow field. Two cases can be distinguished:

(a) Random flow field

Substantially different flow time histories follow from nominally identical realisations of the boundary conditions. Thus, corresponding to given boundary conditions, there exists a whole family of compatible flow fields. Quantitative analysis is concerned with statistical properties, such as means and correlations, of such a family.

(b) Deterministic flow field

The flow field at any instant depends uniquely upon the past history of boundary conditions. A separated flow field of this type depends upon the orderly shedding of vorticity from the boundary.

In the above distinction between random and deterministic flow fields the time-varying boundary conditions may either be externally imposed, by forcing the wing to follow some prescribed time history, or

may arise through the structural response of the wing to aerodynamic forces. In the latter case the wing motion becomes one of the unknowns in the dynamic equations and we have a 'closed-loop' interaction.

The interaction between fluid motion and wing motion may be described in 'systems analysis' terms (Fig.2). The simplest 'closed-loop' system representation arises when the flow field is deterministic, depending uniquely on the past history of wing motion. As illustrated in Fig.2a there are in this case two independent deterministic relationships between the wing motion and the aerodynamic force (a generalised force, appropriate to the mode of response in question, taking the form of a weighted integral of pressures over the structure). One relationship is obtained from the equations of motion of the structure; and since the flow field is uniquely dependent upon the past history of wing motion we can, in principle, deduce a second relationship between wing motion and aerodynamic force from the equations of motion for the fluid. The joint time variation of wing motion and aerodynamic force may then be deduced as that compatible with these two independent relationships. The closed-loop system may be referred to as 'autonomous' or 'self-excited' and the motion takes the form of a limit cycle. Whilst the structural response can often be adequately defined using linear equations, the fact that two INDEPENDENT functional relationships exist between aerodynamic force and wing motion requires that the aerodynamic feedback loop be nonlinear (we exclude the trivial case where the closed loop fluctuations take the form of sinusoidal oscillations of a linear system in neutral equilibrium). We will refer to all such types of motion as NONLINEAR FLUTTER.

A second representation of the interaction between fluid motion and wing motion arises in the case where the flow field is random, differing flow time-histories following from identical realisations of wing motion. The appropriate system formulation then takes the form illustrated in Fig.2b where two components of aerodynamic force are shown separated, one determined by, and one independent of, wing motion. Two particular cases of this formulation may be distinguished. In the first case the combination (indicated in Fig. 2b by a dashed line) of structural response and motion-dependent aerodynamic force forms a stable system which, left to itself, would settle down to a state of equilibrium. In conjunction with the motion-independent component of aerodynamic force this is the FORCED VIBRATION model for the interaction. The motion-dependent aerodynamic force may be linear or nonlinear. In the second case the feedback loop itself produces self-excited oscillations (for which nonlinearity of the motion-dependent aerodynamic force is an essential condition) and we have the situation of an essentially autonomous system disturbed by random noise. Whilst this latter theoretical model is at present little used in practice it is required conceptually if we wish to consider a continuous transition between aerodynamically forced vibration and nonlinear flutter.

In practical applications of the forced vibration model (Fig.2b) several further assumptions are often made which require careful investigation. In the first place it is usually assumed that the aerodynamic excitation, or 'motion independent aerodynamic force', is relatively wide band and can be obtained from measurements on a fixed wing. This assumption may be justifiable for low amplitudes of structural motion but requires validation in the general case. For, whilst the aerodynamic excitation of the system illustrated in Fig.2b is motion independent in the sense that it may be regarded as an 'external noise generator', the STATISTICAL PROPERTIES (such as power spectral density) of this force may in fact depend on the mean amplitude of structural motion. This possibility appears to have been first discussed in Ref.2, where it was invoked as a possible explanation of a trend in the experimental results.

If we do make the assumption that the aerodynamic excitation may be obtained from measurements on a rigid wing and are also able to obtain numerical estimates for the motion-dependent aerodynamic force (of which, in the case of wing flexible response, the most significant component is usually aerodynamic damping) the forced-vibration model provides the basis of a method for predicting the amplitude of the closed-loop response on the basis of rigid-wing measurements. It is therefore also of practical importance to know whether the existence of separated flow significantly affects motion-dependent forces such as aerodynamic damping. There is now substantial evidence[3,4] that there may be a significant change of damping under these circumstances. For example, in the case of wing structural buffeting at high subsonic speeds measurements indicate[3] relatively large increases in aerodynamic damping around the buffet-onset condition (although a factor of 2 error in Fig.10 of Ref.3 exaggerates the effect). A possible mechanism to explain this phenomenon, in terms of the (quasi-static) variation with wing incidence of the area over which a leading-edge suction force acts, has been proposed in Ref.5.

The above review is largely taken from Refs. 6 and 7, where a more detailed discussion of the fluctuating response of an aircraft structure coupled to a separated flow field may be found.

3. STRUCTURAL BUFFETING OF A FLEXIBLE AIRCRAFT

3.1 Description of the phenomenon

The structural buffeting of a flexible aircraft involves interactions between complicated separated flow fields and complicated aircraft structures. In this section we illustrate this complexity with reference to a particular investigation[8] of the flight buffeting response of a combat aircraft (Fig.3) at subsonic and transonic speeds. The content of this sub-section is largely taken from the text of Ref.8.

A general conclusion is that many natural vibration modes can be excited during a manoeuvre in which wing flow separation occurs. Study of the many spectra obtained showed that the spectral character of the responses varies with the type of sensor, with the location on the aircraft and with the angle of attack beyond buffet onset. Thus it is clear that the changing nature of the aerodynamic forcing function is reflected in the structural response and that each response item varies in its own unique way.

A windup turn manoeuvre at M = 0.80 and h = 19,800 ft provided some particularly interesting results. Figures 4 to 7 show power spectra for a nominal indicated angle of attack of 12.2 degrees. The data sample length was 2 seconds. The right wing tip accelerometer data presented in Fig.4 shows how complex the response of the wing can be. Many peaks in the PSD values occur in the band of frequencies from 5 to 78 Hz. Ten of these peaks are labelled with associated natural vibration modes as identified from ground vibration test data obtained on other aircraft in the development program. There

are other peaks at higher frequencies which could not be clearly identified with particular vibration modes.

The accelerations measured on the fuselage show spectra that are considerably different from those at the wing tips. Figs. 5 and 6 present power spectra for vertical accelerations measured near the centre of gravity and at the pilot's seat, respectively. The c.g. data show little response at frequencies below 23 Hz and the major peaks occur at 23, 31, 36, and 50 Hz. The second antisymmetric wing bending, two horizontal tail pitch and the horizontal tail plus second wing torsion modes are associated with these peaks. A significant amount of power is also associated with responses at frequencies above 70 Hz at the centre of gravity. At the pilot's seat, the major responses occur between 16 and 50 Hz. At 16 and 18 Hz the modes are a wing-tail mode and the second symmetric wing bending mode, respectively. Some response in first wing torsion is apparent at 23 to 25 Hz. Very little response occurs above 40 Hz in contrast to the activity at the c.g. location. Neither the c.g. or pilot seat vertical accelerometers show much response at the first wing bending or first fuselage vertical bending frequencies at this angle of attack.

In the case of lateral acceleration responses at the pilot seat, the power spectrum presented in Fig.7 shows the major responses to be at 20 and 28 Hz and several frequencies above 55 Hz. The major peaks at the lower frequencies correspond to second fuselage lateral bending and second antisymmetric wing bending. The latter mode has a coupled motion with vertical tail torsion which probably accounts for the high response at 28 Hz.

It is thus apparent that the frequency content of the accelerations can be quite different depending on the location of the measurement and whether vertical or lateral accelerations are measured. The wing strain-gauge measurements also show different frequency content. Ref.8 presents power spectra of wing bending moments measured at three different spanwise locations on the right wing. At the inboard location the majority of the power is at the first wing bending frequency with much smaller responses at first wing torsion, second antisymmetric wing bending and two horizontal tail pitch modes. Further outboard there is still a large peak at first wing bending with some response at second symmetric wing bending but little response at higher frequencies. Near the wing tip the relative response at the two symmetric wing bending frequencies is small and the bulk of the power is in a range of frequencies between 23 and 37 Hz with the major peak at the second antisymmetric wing bending frequency. Thus, we see that the frequencies of response tend to increase as the measurements are taken at points located further and further outboard on the wing. The increase in frequency can be a major factor in determining fatigue damage in outboard or secondary wing structure. More details on the wing loads are given in Ref.8.

It was also found that the frequency content of the responses of many of the sensors changed with angle of attack above buffet onset. As an example, Fig. 8 shows spectra for the pilot's seat vertical accelerometer for two angles of attack. Slightly above buffet onset (circular symbols), the major response peaks are at the wing-tail, second symmetric and second antisymmetric wing bending modes. At the higher angle of attack (square symbols) the relative response has shifted to higher frequencies so that the dominant mode is second antisymmetric wing bending. Thus changes in response frequencies are attributed to changes in the aerodynamic flow field which occur with angle of attack. The fluctuating pressure field will change as the separated flow expands in the chord-wise and spanwise directions. The field can also change in intensity levels as a function of frequency and in the phasing relationships between different spatial locations also as a function of frequency. Examples of measured fluctuating pressures from flight tests are discussed in a later section.

3.2 Modelling of structural buffeting

It is usual to assume that, to model the structural buffeting of a flexible aircraft, a linear 'forced vibration' model is applicable, with aerodynamic excitation obtainable from rigid-wing measurements. In this section we review the manner in which the forced vibration theoretical model may be applied. Before doing so, however, we emphasise that the limits of applicability of this approach are in need of further experimental clarification. In particular, it is likely that the applicability of this type of theoretical model will be limited at high-subsonic and transonic speeds. In the case of flexible modes which cause significant wing-incidence variations, there is evidence[6] that oscillatory wing motion may in such situations couple in a nonlinear manner with fore-and-aft motion of the shock wave leading to a form of nonlinear flutter (requiring a limit cycle representation). For a wing at small sweep angles, this suggests that the model will probably be valid for wing bending but possibly not for wing-torsion modes. In the case of a highly-swept wing the situation is less clear-cut, as the bending and torsion modes may each contribute significantly to wing incidence changes.

The forced vibration linear analytical model for flexible aircraft response may be expressed in terms of generalised co-ordinates. The deformation of an aircraft structure may be represented quite generally by the superposition of preassumed vector mode functions, in the form[9]

$$u_i(P,t) = \sum_{r=1}^{\infty} q_r(t) f_{ir}(P) \quad , \quad (i = 1,2,3) \quad , \tag{1}$$

where $u_i(P,t)$ is the elastic deformation vector at point P and time t, the $q_r(t)$ are generalised co-ordinates, and $f_{ir}(P)$ are associated mode shape functions. Applying Galerkin's technique, the dynamic equations then reduce to a set of ordinary differential equations:

$$\sum_{r=1}^{\infty} \left[M_{rs}\ddot{q}_r(t) + D_{rs}\dot{q}_r(t) + K_{rs}q_r(t) \right] = Q_s(t) \quad , \tag{2}$$

where M_{rs}, D_{rs} and K_{rs} are generalised mass, damping* and stiffness matrices, and $Q_s(t)$ is a generalised force.

---

* We consider only viscous damping for the purpose of the present discussion

A considerable simplification may be obtained by eliminating the structural inertia and elastic cross-coupling terms. This may be achieved by choosing the modes to be the undamped natural vibration modes of the free system in a vacuum. There remains, however, cross-coupling of these modes due to structural damping, and due to aerodynamic inertia, damping and stiffness.

The coupling due to structural damping is usually both small and difficult to measure and consequently neglected. Provided that mode frequencies are relatively well separated, and the damping light, the aerodynamic cross-coupling terms will also be small and a single-degree-of-freedom analysis will be justified. However, since there are indications that aerodynamic damping of flexible modes may substantially increase under conditions of separated flow, the possibility that aerodynamic mode coupling may play a significant role in the dynamics of buffeting cannot be ruled out.

In the context of attached flow, aerodynamic cross-coupling terms can in principle be calculated - for instance using three-dimensional lifting surface theory. Indeed, such terms play a vital part in flutter calculations and are also sometimes used in predicting the response of flexible aircraft to atmospheric turbulence. Provided that the buffet excitation can be calculated as a generalised force vector, for instance on the basis of measured fluctuating pressures, there is no reason in principle why such calculations should not be applied in the context of buffeting. The practical difficulty in this case, however, is that we have at present no information concerning the effect of separated flow on the magnitude of the cross-coupling terms.

On the assumption that aerodynamic mode coupling may be neglected, we may express the forced vibration linear analytical model for response in a flexible mode in terms of a single generalised co-ordinate $Z(t)$, representing the displacement in that mode, and a generalised aerodynamic excitation $x(t)$ assumed to have no feedback from wing motion (see Fig.9). $Z(t)$ should be multiplied by the mode shape to obtain the displacement at an arbitrary point on the wing. The aerodynamic excitation $x(t)$ has a power-spectrum which depends on cross-spectra of fluctuating pressures over all pairs of points on the wing, weighted by mode shape. The power spectral density $\Phi_x(f)$ of $x(t)$ is assumed to be approximately constant in the neighbourhood of the mode natural frequency $f_0 = \omega_0/2\pi$. When relating measurements on a model in a wind tunnel to full scale, assumptions have to be made concerning the appropriate scaling factors. On the hypothesis that Reynolds number effects are negligible, the mean-square fluctuating force $\overline{x^2}$ scales like $(qS)^2$, where q is dynamic pressure and S wing area, and the appropriate length and velocity parameters for scaling frequency are a geometric length (e.g. mean wing chord $\bar{c}$) and true airspeed V.

On this basis the power spectral density of aerodynamic excitation may be expressed[6] in the form

$$\Phi_x = \frac{E^2\bar{c}}{V}(qS)^2 \quad , \tag{3}$$

where E is a non-dimensional aerodynamic parameter, a function only of wing incidence, Mach number and Reynolds number.

The response in the single-degree-of-freedom mode is defined by the differential equation:

$$m_1\ddot{Z} + 2m_1\zeta\omega_0\dot{Z} + m_1\omega_0^2 Z = x(t) \quad . \tag{4}$$

In equation (4), m_1 is the equivalent (generalised) mass of the mode, given by

$$m_1 = k_1 m \tag{5}$$

where m is the total mass of the aircraft and k_1 is a non-dimensional quantity that depends on wing geometry, mode shape, and mass distribution. The undamped natural frequency ω_0 (in rad s^{-1}) is assumed to be independent of aerodynamic forces (stiffness and inertia). This simplifying approximation, together with the neglect of aerodynamic coupling between modes, appears on the basis of experimental data to be acceptable in many practical buffeting situations. It assumes, of course, that we are well away from any boundaries of conventional flutter. ζ (equation (4)) is the total damping ratio,

$$\zeta = \zeta_a + \zeta_s$$

where ζ_a is aerodynamic damping ratio and ζ_s is structural damping ratio (this assumption of a viscous type of structural damping simplifies, but is not essential to, the analysis).

The aerodynamic damping ratio is given by

$$2m\zeta_a\omega_0 = k_2 a_1 \rho V S \quad , \tag{6}$$

where a_1 is effective lift-curve slope (evaluated at the non-dimensional mode frequency $n_0 = f_0\bar{c}/V$). k_2 is a non-dimensional quantity that depends on mode shape. ρ is air density.

The term $m_1\omega_0^2$ in equation (4) represents the structural stiffness.

Then a power-spectral-density (PSD), analysis gives the root-mean-square acceleration associated with the mode as

$$\sigma_{\ddot{Z}} = \frac{1}{2\sqrt{2}}\left(\frac{\bar{c}\omega_0}{V\zeta}\right)^{\frac{1}{2}} \frac{qE}{(m_1/S)} \quad . \tag{7}$$

If follows from equation (7) that the non-dimensional aerodynamic excitation parameter E is given by

$$E = \sqrt{2}\left(\frac{V}{\bar{c}\omega_0}\right)^{\frac{1}{2}}\left(\frac{m_1}{S}\right)\left(\frac{\zeta^{\frac{1}{2}}\sigma_{\ddot{Z}}}{q}\right) \quad . \tag{8}$$

The quantity $\zeta^{\frac{1}{2}}\sigma_z''/q$ thus appears as a useful measure of aerodynamic excitation derivable from measured acceleration response and total damping ratio. Equation (7) illustrates the quantities required in a theoretical buffeting prediction method based, for example, on wind-tunnel measurements. For an aircraft flying at given wing loading, speed and altitude, the aerodynamic-dependent quantities are E and ζ.

One method for the evaluation of E involves the measurement of fluctuating pressures on relatively rigid wind-tunnel models and the derivation of the generalised force by means of cross-correlation techniques[8,10,11]. This approach is discussed further in section 4.1. Alternatively, E may be derived from wind-tunnel tests on the basis of equation (8) using models for which the relevant mode shape is approximately correct (note that fully-scaled aeroelastic models are not necessary). To obtain E from equation (8), wind-tunnel measurements of σ_z'' and total damping ratio are required, together with a knowledge of mode natural frequency ω_0 and generalised mass m_1.

The other quantity required in a buffeting prediction method, based on equation (7), is the value of the total damping ratio appropriate to the full-scale aircraft. As mentioned in section 2, the investigation of effects of separated flow on the aerodynamic component ζ_a of damping ratio is a subject of current research. Perhaps the most promising approach to the problem of predicting aerodynamic damping, for use in conjunction with the forced-vibration model of buffeting, equation (4), is that based on the use of static experimental data as an input, as suggested in Ref.5. Qualitative agreement with measured changes in damping of the wing-bending mode in the vicinity of buffet onset have been shown using this approach, although good quantitative predictions have still to be demonstrated.

The least-well understood aspect of structural buffeting of a flexible wing concerns the response in wing torsion modes at high-subsonic and transonic speeds. There is some evidence that fore-and-aft shock motion tends to couple with torsional oscillations of the wing, providing a strong mechanism by which the flow fluctuations occurring on a rigidly-mounted wing might be fundamentally modified. Indeed, if the flow-field essentially 'locks-in' to the wing torsional motion, the forced-vibration type of analytical model for buffeting (equation (4), or, more generally, equation (2)) is no longer appropriate and the phenomenon becomes a type of nonlinear flutter. The appropriate model then takes the form of a limit cycle, probably with a significant amount of additive noise. This is an area where considerable further work remains to be done.

3.3 Response to transient buffet excitation

We end this outline of theoretical methods for the dynamic analysis of buffeting by mentioning that the 'forced vibration' model (Fig. 9) has been used[12] as a basis for the investigation of buffeting response occurring during a transient incursion into the buffet regime, due to either a gust or a manoeuvre. Using the theory of non-stationary random processes, observed lags in buffeting build-up and decay can be shown to be of similar size to the predicted delays in the response of wing structure. These delays in structural response are in addition to lags associated with unsteady aerodynamics. A particular application discussed in Ref.12 concerns the buffeting induced on a subsonic transport aircraft by a vertical gust. Such an aircraft often cruises quite close to its buffet onset boundary and, in severe turbulence, may be expected to intermittently penetrate beyond its buffet boundary due to fluctuations in incidence.

The dynamic analysis of this situation may be based on the model illustrated in Fig.9, in conjunction with the theory[13] for the transient response of a linear system excited by a random input. This theory may be used to evaluate the response of the system, in statistical terms, when an input signal such as $x(t)$ (Fig.9) is either suddenly switched on, or grows smoothly from zero amplitude in some prescribed manner.

For instance, suppose that $x(t)$, equation (4), takes the form

$$x(t) = \alpha(t)N(t) \quad ,$$

where $N(t)$ is 'white noise' of uniform spectral density Φ (per Hz) and $\alpha(t)$ is a prescribed function, related to the incidence penetration beyond buffet onset, satisfying

$$\alpha(t) = 0, t < 0 \quad .$$

Then it can be shown that the equation for the (ensemble) mean square response σ_z^2 at time t is given by

$$\sigma_z^2(t) = \left(\Phi/2m_1\right) \int_0^t \alpha^2(\tau)h^2(t-\tau)d\tau \quad ,$$

where $h(t)$ is the response of the system to a unit impulse. Practical applications of this result are described in Ref. 12, and include, for instance, the effect of the length of a gust on the alleviation of maximum buffeting response.

4. FLUCTUATING PRESSURES ON BUFFETING WINGS

In this section we consider the interpretation of measured fluctuating pressures on a wing, on the basis of the forced vibration buffeting model, and briefly review the manner in which measured fluctuating pressures may be used to predict buffeting amplitudes.

4.1 Measured fluctuating pressures on rigid wing

First we consider applications of measurements obtained using wind-tunnel models which are rigid in the sense that no model response mode occurs at frequencies in the vicinity of the (scaled) frequency at which buffeting intensity is to be predicted on the full-scale aircraft. By taking measurements at a sufficient number of points, and integrating pressures to obtain overall forces, it is in principle possible to use fluctuating pressures on a scaled model rigid wing in a wind tunnel as the basis of a statistical calculation of buffeting response. The basic quantity required for such a calculation is the power spectrum of the aerodynamic excitation $x(t)$ (Fig.9), which arises as an integrated product of the aircraft

structural mode shape and the cross spectra of pressure fluctuations. As a result, those fluctuating pressures which are correlated over distances of the order of a 'wavelength' of the structural mode will predominate in their contribution to the excitation. In the case of the first symmetric wing-bending mode, for instance, only those pressure fluctuations which integrate to provide significant fluctuations in circulation will be relevant. This situation is in contrast to the excitation of wing panels by regions of separated flow. In this latter case, the relevant pressure fluctuations are generated primarily in the shear layer and appear almost exclusively directly beneath the region of separated flow. We may refer to this as a direct effect of the separated flow. On the other hand, a significant component of fluctuating circulation may arise as an indirect effect of the separated flow, through its influence on the Kutta condition which determines the circulation. The basic unsteadiness in this case is in the potential flow, the viscous effects arising as a 'circulation control' mechanism, and we cannot necessarily assume that the associated pressure fluctuations are located only in the immediate vicinity of the separated flow region. Indeed, it is possible for the whole flow field around the wing to be inherently unsteady, and thus pressure fluctuations which contribute to fluctuating lift may occur at all points where there are large spatial mean-pressure gradients. Such regions appear beneath shock waves at transonic speeds and may arise in the vicinity of the leading edge at subsonic speeds.

On the assumption that the power spectrum of $x(t)$ is available from pressure fluctuation measurements on a rigid wing as outlined above, equation (4) may be used to calculate the amplitude of structural buffeting in the mode in question if an estimate is available for the total damping ratio ζ. This approach has previously been employed[14] to calculate buffeting of a slender wing with a leading-edge vortex. However, in the case of a swept wing at high subsonic speeds the possibility of using fixed-wing pressure fluctuations as a basis for the prediction of buffeting amplitudes requires critical investigation. The occurrence of separated flow on the wing not only leads to the appearance of a fluctuating aerodynamic excitation but may, in addition, significantly influence the aerodynamic component of damping ratio ζ_a. In Ref.5, flight-test results are described which indicate relatively large variations with C_N of aerodynamic damping on a buffeting wing, particularly large values of apparent damping ratio arising around the buffet onset condition. More information is required to see whether these results are of general applicability, but meanwhile they may imply a significant limitation on the quantitative use of pressure fluctuations measured on rigid wings.

4.2 Measured fluctuating pressures on structurally-responding wings

We turn now to the case where fluctuating pressures are measured on a buffeting wing which is structurally responding in a flexible mode. This situation arises in both full-scale flight experiments and in wind-tunnel experiments using models with properly scaled mode frequencies. The interpretation of such measurements, if taken in isolation, is in general complicated by the fact that the fluctuating pressure distribution is the sum of overlapping aerodynamic excitation and response fields (including aerodynamic damping). As advocated in Ref.6, considerably more information may be obtained from wind-tunnel tests if fluctuating pressures on structurally-responding wings and on rigid wings with similar geometry are compared.

Firstly, we note that high intensity pressure fluctuations of relatively high frequency originate from separated shear layers and can be measured on the wing surface directly beneath the separated region. Whilst having little relevance to the dynamics of wing buffeting, since high frequency pressure fluctuations make negligible contribution to fluctuating circulation and lift, such measurements can provide valuable indications regarding the extent of separated flow and, in conjunction with photography of wing tufts, can enable full-scale flow patterns from flight tests to be compared with those obtained in wind-tunnel experiments involving flow visualisation techniques such as oil flow.

The [illegible] to pressure fluctuations in the lower frequency range, directly related to the dynamics of lower order modes of wing flexible response, we suppose that wing buffeting is appropriately modelled as an aerodynamically forced vibration, in which case the fluctuating pressure $p(t)$ at an arbitrary point on the wing may be expressed as the sum of two components: a 'motion dependent' component $p_d(t)$ and a 'motion independent', or aerodynamic excitation, component $p_x(t)$. The power spectrum of $p_d(t)$ will consist of a narrow-band peak at the resonant frequency of response and the spectrum of $p_x(t)$ is assumed* to be relatively wide band. These differing characteristics allow a qualitative assessment of the relative contributions of the two pressure fields at an arbitrary point on the wing on the basis of measured power spectra. For instance, at points on the wing where the primary component of $p(t)$ is $p_d(t)$ (this probably includes points well separated in a spanwise direction from regions of separated flow) the spectrum of $p(t)$ will be dominated by a narrow-band peak. In general, however, the pressure fields $p_x(t)$ and $p_d(t)$ will overlap, and the shape of the spectrum of $p(t)$ in the vicinity of the resonant frequency will depend critically on the degree of correlation, and the phase-relationship, between these two components.

In Refs. 6, 7 it was shown that the total aerodynamic force $(y(t)$, Fig.9) on a structurally-responding wing with low structural damping contains relatively little power at the resonant frequency of response, (Φ_y, Fig.10). This is due to the cancellation of the aerodynamic excitation at this frequency by the corresponding motion-dependent aerodynamic force (including damping). Now, although this result has been derived for the generalised aerodynamic force associated with the structural mode in question, it is relevant to individual component pressures. If we consider the extreme case of aerodynamic excitation and response fields each of which consists of a pressure distribution varying in time but independent of spatial position at each instant (the limiting case of complete spatial correlation) then the instantaneous aerodynamic force is a constant multiple of instantaneous pressure and the energy cancellation apparent in Φ_y also arises in the spectra of individual pressure fluctuations. However, this result depends on complete correlation between aerodynamic forces and component pressures. At the opposite extreme of low correlation between aerodynamic force and individual pressures, such as arises when there is low correlation between individual fluctuating pressures at

---

* The assumption made here is that no purely aerodynamic resonance exists. An exception may arise in the case of flows with oscillating shock waves. In this latter situation the forced vibration hypothesis should be used with extra care, as there will be a strong possibility of the flow fluctuations locking in (to form a limit-cycle) with a structural response mode of similar frequency.

different points on the wing, there will also be little correlation between the component pressure fields $p_d(t)$ and $p_x(t)$ at any arbitrary point on the wing, and the power spectrum of $p(t)$ will then consist approximately of the sum of the component spectra, thus taking the form of a broad-band spectrum with superposed peak.

Thus, in general, the power spectrum of fluctuating pressure $p(t)$ at a point on a structurally-responding wing can in principle take any form between a wide-band spectrum with superposed narrow-band peak and a wide-band spectrum with a 'notch' similar to that in Φ_y, Fig.10. However, the latter phenomenon requires almost perfect correlation between the pressure $p_d(t)$ and the 'motion-dependent' aerodynamic force $x(t)$, and between $p_d(t)$ and the 'motion-dependent' aerodynamic force. Whilst the latter correlation is to be expected (since both $p_d(t)$ and the aerodynamic damping force are each highly correlated with wing motion) it is doubtful whether the correlation between $p_x(t)$ and $x(t)$ is ever sufficiently strong for this condition of pressure cancellation to be realised in practice on a three-dimensional wing.

In Refs. 6, 7, the above situation, in which energy cancellation occurs between the excitation and response pressure fields on a structurally-responding wing, is contrasted with that which occurs when the time history of wing motion is externally imposed by means of external forces (as a wing surface might be forced to follow some prescribed time history in a wind-tunnel experiment). In this latter case we refer to the wing motion as 'externally forced'. As an example, Fig.10 illustrates the difference between Φ_y, the spectrum of aerodynamic force on a structurally-responding wing, and $\Phi_{\bar{y}}$, the corresponding spectrum on an externally-forced wing, both associated with the same spectrum Φ_z of wing motion.

In illustration of the above discussion of fluctuating pressures on structurally-responding wings, pressure fluctuations measured during high g manoeuvres on a small combat-trainer aircraft are illustrated in Figs. 11a and 11b. In these figures power spectral density of fluctuating pressure p is expressed in terms of $(p/q)^2$ per unit bandwidth, q being the dynamic pressure. Following the qualitative method of interpretation described above, the dashed line in each case represents an estimate of the intensity of the local broad-band aerodynamic excitation and peaks rising significantly above this level are taken to be associated with motion-dependent aerodynamic pressures. In particular, by comparing the spectra at the inner upper-surface station and the lower-surface station, under conditions of medium (Fig. 11a) and heavy (Fig. 11b) buffet, it can be seen that the relative contributions to the motion-dependent aerodynamic force (including damping) of particular points on the upper and lower surfaces of the wing can depend strongly on the level of buffeting intensity.

Finally we note that whilst measured fluctuating pressures on a structurally-responding wing can provide useful information concerning the spatial extent of regions of separated flow, and qualitative information concerning the spatial distribution of aerodynamic excitation and damping fields, the quantitative separation of these two pressure fields, and subsequent integration to provide both generalised excitation and damping forces, poses severe problems. Assuming that the only effect of wing motion is to produce a linearly dependent pressure field, the properties of the excitation field may in principle be deduced from measurements at frequencies other than those of structural response. If the excitation field is then assumed to behave smoothly, in terms of frequency across structural resonances, its overall properties may be deduced by interpolation with respect to frequency, and results comparable to those described in section 4.1 (rigid wing) may be obtained. On the other hand there appears to be no satisfactory way of extracting the aerodynamic damping field. As explained earlier, the shape of the power spectrum of fluctuating pressure $p(t)$ in the neighbourhood of a structural resonance depends on the degree of correlation, and the phase-relationship, between the two component pressures $p_x(t)$ and $p_d(t)$. Thus the properties of the damping field $p_d(t)$ cannot be obtained from measurements of $p(t)$ alone. Moreover, the cross-correlation of $p(t)$ and the motion of the wing cannot provide a satisfactory means for separating $p_x(t)$ and $p_d(t)$, as wing motion is correlated with both pressure fields, the correlation with the damping field arising directly through the aerodynamic response and the correlation with the excitation field arising through the flexible response of the wing structure.

Throughout the above discussion we have assumed structural damping to have a negligible effect. Whilst on the basis of current information this appears to be a reasonable hypothesis for many flight conditions, there remains some uncertainty in this area. Estimates of structural damping are normally based on ground resonance tests, and such tests usually refer to wing loading equivalent to 1 g. At the high values of lift relevant to buffeting, however, the appropriate loading may be as high as 7 g, and in this situation structural damping is not generally measured. Nevertheless, whilst a large static load will probably have an effect on friction at joints, etc., there is no obvious physical reason why the structural damping should be systematically greater in this case.

5. FLUCTUATING RIGID-BODY MOTIONS OF AN AIRCRAFT

5.1 Introductory remarks

We turn now to aircraft fluctuating motion, associated with wing separated flow, in rigid-body response modes. The frequencies involved are lower than those associated with airframe flexible response, and can have a direct effect on the controllability of an aircraft and the ability to hold an accurate flight path. From the pilot's point of view, whereas aircraft flexible response may be said to influence 'ride-quality', rigid-body fluctuating motion also adversely influences 'handling-characteristics'. The most important example of rigid-body response in this context is the lateral fluctuating motion known as 'wing-rocking' which is known to have a detrimental effect on air-to-air tracking capability. In some situations, however, longitudinal rigid-body motion plays a significant role, either in the form of predominantly longitudinal motions or by coupling with the lateral degrees of freedom.

5.2 Longitudinal motion

Pilot descriptions of aircraft fluctuating motion at high lift include the expressions 'bounce' and 'porpoising'. These refer to types of longitudinal motion at frequencies primarily influenced by aircraft rigid-body modes. The former is a description of a type of motion perceived as fluctuations at about 2-3 Hz in normal acceleration. The latter, porpoising, probably involves both normal acceleration and

pitching motion and takes place at a rather lower frequency.

From the pilot's point of view there is probably no clear distinction between the types of motion mentioned above and aircraft buffeting that takes place primarily through the response of the flexible structure. However, for the purposes of theoretical analysis, the appropriate response mode for calculations of buffeting intensity (in terms of normal acceleration) depends upon the frequency range in which the response is to be evaluated. In section 3 we showed how buffeting in structural modes may be modelled as wing-flexible response. However, if we are concerned with response fluctuations at frequencies below that of the first wing-bending mode (say below about 7 Hz on a combat aircraft) it is more appropriate to consider aircraft rigid-body motion. Moreover, if we are concerned with buffeting in the vicinity of the nodes of the first wing-bending mode (and the pilot may sit at a point where the amplitude of wing-bending response is relatively small), a significant part of the energy in the frequency range up to approximately 10 Hz could appear as a rigid-body motion.

A simple approximation to longitudinal rigid-body aircraft motion may be derived by neglecting pitching motion and considering the response in heave (translation) only. Fig. 12 illustrates the block diagram for the heaving motion (of an aircraft with mass m and wing area S) modelled in this manner (a special case of Fig. 2b). The total aerodynamic force $F(t)$ is expressed as the sum of two components, a fluctuating aerodynamic excitation $F(t)$ having no feedback from aircraft motion, and an aerodynamic damping contribution expressed in terms of lift slope 'a'. The corresponding differential equation is

$$m\frac{dw}{dt} + \tfrac{1}{2}\rho VSaw = F(t) \quad , \tag{9}$$

where $w(t)$ is aircraft heaving velocity. The equivalent transfer function equation describing the effect of $F(t)$ on normal acceleration $\dot{w}(t)$ is

$$\dot{w} = \frac{s}{As + B} F \quad , \tag{10}$$

where $s = d/dt$

$A = m$

$B = \tfrac{1}{2}\rho VSa$.

A 'break frequency', related to the time constant of the above first order equation is given by

$$\bar{f} = \frac{1}{2\pi}\frac{B}{A} \quad . \tag{11}$$

For frequencies above $\bar{f}$, the effect of damping on the heaving acceleration dw/dt becomes small. Moreover, the effect of unsteady aerodynamics reduces the influence of damping still further at high frequencies. On the assumption that the power spectral density Φ_F of F is constant over the frequency range of interest, and introducing a dimensionless parameter E, dependent only on flow geometry, we may write

$$\Phi_F = \frac{\bar{c}}{V} E^2 (\tfrac{1}{2}\rho S)^2 \quad . \tag{12}$$

The root-mean-square intensity of acceleration corresponding to an arbitrary fixed pass band above frequency $\bar{f}$ then satisfies the proportionality:

$$\sigma_{\dot{w}} \sim \frac{1}{A}\sigma_F$$

$$\sim \left(\frac{\bar{c}}{V}\right)^{\frac{1}{2}} \frac{qE}{m/S} \quad . \tag{13}$$

As a numerical example, we take a typical small military aircraft, say

m/S	=	60 lb ft^{-2}
lift slope a	=	4.0
Mach number	=	0.7
altitude	=	10000 ft

then

$$\bar{f} \doteq 0.2 \text{ Hz} \quad .$$

At frequency $\bar{f}$ the effect of damping is to reduce the amplitude of fluctuating acceleration to about 66% of its value without damping. However, at frequencies above 1 Hz, the acceleration amplitude is at least 97% of its undamped value. Thus, in situations in which heaving motion makes a significant contribution to buffeting intensity, for example at positions very close to wing-bending nodes at frequencies in the range 1-10 Hz, the effect of aerodynamic damping is negligible and buffeting intensity satisfies equation (13). A particular consequence is that at a given value of E, for example for flight at constant incidence on the assumption that Reynolds number effects are negligible, the buffeting response, at fixed Mach number and within a fixed frequency range, is directly proportional to excitation and hence to q, and thus at constant true airspeed varies linearly with air density ρ. Allowing for changes in airspeed with altitude the variation is approximately with $\rho^{1.0}$. This contrasts[6] with the case of response in a flexible mode, where buffeting intensity at constant airspeed is proportional to ρ^{1}: allowing for changes in airspeed with altitude this becomes $\rho^{0.6}$.

The analysis presented in this section is the rigid-body equivalent of the forced-vibration type of analysis used for wing structural response in section 3.2. However, it should be noted that in the case of aircraft rigid-body motion it is more likely that the effects of nonlinear mean aerodynamic forces become significant. In particular, the regularity of the 'porpoising' motion suggests that the possibility of a limit-cycle (nonlinear flutter), in which the periodic fluctuations in the flow field become coupled deterministically to the motion of the wing, cannot be ruled out.

5.3 Lateral motion

The principal undesirable rigid-body motions in the context of handling characteristics of combat aircraft at high lift are the wing-rocking, wing-dropping, and nose-slice phenomena. Wing-rocking should be distinguished from wing-dropping and nose-slice in that, whilst the latter two may present a major hazard, possibly leading to loss of an aircraft in extreme circumstances, wing-rocking should generally be regarded more in terms of nuisance, degrading weapon aiming accuracy but not necessarily limiting sustained manoeuvres. Whereas wing-dropping and nose-slice are relatively well understood phenomena, taking the form of a divergence associated with loss of lateral or directional stability, the provision of an appropriate theoretical model for wing-rocking is an outstanding problem. A principal objective is a means for relating the dynamic motion of the full-scale aircraft to measurements that can be made using rigidly-mounted wind-tunnel models.

Two basic types of analytical model exist for wing-rocking, analogous to the systems illustrated in Figs. 2a and 2b, one representing an autonomous oscillation, or limit-cycle, and the other an aerodynamically forced response. If wing-rocking takes the form of an autonomous oscillation, the system is unstable over a limited range of amplitudes, but constrained to motion of finite amplitude through the existence of nonlinear aerodynamic forces. (We use the expression 'unstable' (above) in a broad sense to cover both dynamically-unstable equilibrium configurations and asymmetrical configurations which are not even in static equilibrium).

The simplest analytical models for the case of autonomous oscillations exclude hysteresis and/or time-lag effects and are related to a change from positive to negative damping. If it is required to model conditions of sustained wing-rock, in which the oscillations continue with approximately constant amplitude, a nonlinear model is called for. It may be necessary to include a source of additive noise as a means of introducing small perturbations about the basic limit cycle. If, however, it is required to model conditions of transient wing-rock, terminated by the pilot reducing the aircraft angle-of-attack, then it may be sufficient to employ linear equations (with negative damping) to describe the rate of growth of the amplitude of oscillations. The existence of additive noise is again likely to distort the oscillatory motion, particularly in the initial phase when the amplitudes are small. Tests with wind-tunnel models are in principle capable of predicting the onset of this class of motions through the indication of a loss of aerodynamic damping. For this application, the aerodynamic measurements should be made on a complete model so as to include effects of wing separated flow on the rear-fuselage or tail. However, the prediction of the nature of the motion subsequent to initial divergence is much more difficult. If it is desired to predict the complete wing-rocking motion as an autonomous oscillation then the aerodynamic forces (including those dependent on aircraft rates of motion) need to be known as functions of aircraft angular displacements, and account should also be taken of the possible existence of hysteresis, for instance in rolling-moment measurements. This type of prediction has not as yet been attempted, and indeed it is clear that a complete analysis would be one of some complexity.

The alternative possibility is that wing-rocking takes the form of an aerodynamically-forced vibration (in the technical sense outlined in section 2), excited by fluctuating aerodynamic forces which are independent of wing motion. Fluctuating rolling- and yawing-moments have in the past been observed on rigidly-mounted wind-tunnel models, but it is not known under what circumstances coupling (locking-in) between flow field and motion takes place in the corresponding dynamic situation. On the assumption that significant random force or moment components persist throughout the motion, the analytical model then resembles in general structure that used to describe buffeting (section 3.2), an aerodynamic excitation force, analogous to $x(t)$ in equation 4, producing fluctuations in the response of an essentially stable system. A variant of this model occurs in the case of 'critical fluctuations of a soft mode' (Ref.7), where the approach to a condition of disappearing stiffness leads to an amplification of the forced response.

Experience with a range of high-performance aircraft over the past few years has provided a wide variety of illustrations of the types of phenomena outlined above. Examples include loss of lateral stiffness, due largely to changes in the n_v derivative, leading to 'yaw-off' or 'nose-slice', loss of Dutch-roll damping (due for instance to changes in the l_p and n_p derivatives) leading to wing-rock[15], and a case of wing-rock where no loss of stability is apparent from the measured stability derivatives and the phenomenon has thus been regarded as a 'forced' motion, associated with a randomly fluctuating wing-flow field. It is clear that no single parameter, or combination of parameters, can provide a measure for aircraft handling qualities at high angle of attack. In some cases the phenomenon of wing-rock is regarded by pilots as non-repeatable, in the sense that the same aircraft flown by the same pilot in apparently the same conditions may or may not exhibit wing-rock. The explanation may be that rolling-moment behaviour is sensitive to small changes in sideslip angle of which the pilot is not aware. A further complication is the effect on stability of pilot control inputs. For example, in the absence of control forces the parameter controlling Dutch-roll stiffness is $n_v - \sin\alpha\, l_v i_z/i_x$, known as 'dynamic n_v'. However, the use of ailerons by the pilot, in an attempt to keep wings level, can lead to divergence at a lower angle of attack on account of the yawing moments introduced by aileron deflections.

6. RELATED TOPICS

The concepts used in prescribing appropriate analytical models for the fluctuating motion of a wing in the presence of separated flow are applicable in a more general range of situations. An instructive example is that of a circular cylinder, transverse to the mean-flow direction, shedding a regular vortex street. In the case of a rigidly-mounted cylinder, despite the high degree of order in the vorticity distribution, we have an example of a 'random' flow field, since the phase of the flow fluctuations is not determined by the boundary conditions. However, if the cylinder is mounted on elastic supports so that it is free to respond dynamically in a direction transverse to the flow, the phase of the flow fluctuations may

become deterministically related to the cylinder motion if the structural stiffness is chosen so that the cylinder natural frequency lies sufficiently close to the vortex shedding frequency. When this phenomenon occurs, the coupled motion is appropriately regarded as a limit cycle and measurements of pressures and forces on the rigidly-mounted cylinder cannot be sensibly related to the motion of the dynamically-mounted cylinder by 'forced-response' calculations.

In the above situation we may say that the cylinder is 'structurally responding'. A related experiment may be performed in which the cylinder is 'externally forced', by means of imposed constraints, to perform sinusoidal oscillations of prescribed amplitude and frequency. Again, if the amplitude of motion is sufficiently large, and the forcing frequency (Strouhal number) lies in the neighbourhood of the natural vortex-shedding frequency, the phase of the flow fluctuations may become controlled by the cylinder motion. This is an extreme example of the phenomenon that a changeover from a 'random' to a 'deterministic' flow field, and a corresponding necessary change in the nature of associated dynamic response calculations, can occur as the mean amplitude of structural motion increases.

Brief mention may be made here of the related topic (in that it involves flow fluctuations and wing motion) of panel vibration. Instead of fluid motion involving separated flow, the problem usually studied involves the motion of a panel in the presence of a fluctuating turbulent boundary layer. A commonly used procedure is to measure fluctuating pressures on a rigid panel, and to use these in conjunction with aerodynamic damping estimates to calculate the motion of a flexible panel as an aerodynamically-forced response. Alternatively, the panel oscillations sometimes occur as nonlinear flutter. These alternatives have been discussed in Ref.16. In the latter case the larger-scale boundary-layer fluctuations, which are random on the rigid panel, become coupled deterministically to the panel motion. The theory of Landahl[17], in which the large-scale turbulence components in a boundary layer on a rigid wall are calculated as the most lightly damped eigenmodes of the associated linear stability problem, suggests that a form of nonlinear coupling could arise in which the large scale fluctuating components in the tubulent flow past a flexible panel are related to the eigenmodes of the linear stability problem including wall flexibility. This is only to suggest possibilities, however, as the theory for large-scale turbulence fluctuations has not yet reached any generally accepted form, a fact which serves to emphasise that the type of problem discussed in this paper can at present only be treated by semi-empirical analytical theories.

7. CONCLUDING REMARKS

We have discussed ways in which the inherently unsteady nature of separated flow interacts with aircraft dynamic response, and reviewed the problem of formulating appropriate theoretical model structures for such conditions.

Practical examples include aircraft buffeting and wing-rocking. The importance of understanding these phenomena lies in the fact that modern high-performance aircraft often have to operate in such states in order to fully exploit their manoeuvre flight-envelope. Applications of theoretical models of the phenomena include planning and interpretation of appropriate wind-tunnel tests, as a basis for prediction of full-scale behaviour, and programming of ground-based simulations of manoeuvering conditions.

The mutual interaction between a dynamically-responding wing and a separated flow field can take two forms: in one the wing motion is 'forced' by the fluctuating flow field, in the other the joint motion of wing and flow field arises as a mutual interaction. The distinction is that in the former the nonlinear process of energy transfer from the free stream to the fluctuations is predominantly a flow-field phenomenon, the response of the wing possibly modifying but not fundamentally interfering with this process; in the latter case the nonlinear energy transfer mechanism depends fundamentally on the coupling between flow field and wing motion.

In the case of structural buffeting of a flexible wing it is usual to assume that a linear forced vibration model, with aerodynamic excitation obtainable from rigid-wing measurements, is applicable. We have reviewed the manner in which this type of analysis may be applied. At the same time, we have emphasised that the limits of applicability of this approach are in need of experimental clarification. It is likely that the limitations are greatest at high subsonic speeds and for flexible modes which contribute significantly to incidence variations, as there is evidence that the wing motion may in this situation couple in a nonlinear manner with fore-and-aft motion of the shock wave.

As there is an increasing trend towards the use of fluctuating pressure measurements for the study of buffeting, we have discussed the interpretation of such measurements. A conclusion drawn from this discussion is that measured pressure fluctuations on a structurally-responding wing, as in flight tests, are difficult to interpret on a quantitative basis, owing to the mutual cancellation of aerodynamic excitation and aerodynamic damping forces at the natural frequency of wing motion.

On the assumption that the forced-vibration analytical model for buffeting is appropriate, measured fluctuating pressures on a rigid wing may, in principle, be used in conjunction with estimates of aerodynamic damping in a response calculation for buffeting amplitudes. However, flight tests have indicated significant changes in aerodynamic damping as separated flow develops on the wing, indicating the need for further research in this area.

The possibility has been discussed of relating the wing-rock phenomenon, which is known to significantly degrade precision tracking ability, to measurable characteristics of a theoretical model. An important objective of this work is a means of relating degradation in aircraft handling characteristics under manoeuvering conditions to measurements that can be made using wind-tunnel models. Theoretical characteristics which are thought to have been associated in the past with oscillatory or divergent phenomena on a range of aircraft include loss of Dutch-roll damping, loss of Dutch-roll stiffness (dynamic n_β) and modified Dutch-roll response forced by a randomly-fluctuating wing-flow field. The conclusion has been drawn that no single parameter, or combination of parameters, can provide an overall measure for aircraft handling qualities at high angle of attack.

REFERENCES

1.	Y.C. Fung	An introduction to the theory of aeroelasticity John Wiley (1955)
2.	A. G. Rainey T. A. Byrdsong	An examination of methods of buffeting analysis based on experiments with wings of varying stiffness NASA TN D-3 (1959)
3.	J. G. Jones	The dynamic analysis of buffeting and related phenomena AGARD Specialist Meeting on Fluid Dynamics of Aircraft Stalling, Lisbon 1972. AGARD CP 102
4.	L. L. Erickson	Transonic single-mode flutter and buffet of a low aspect ratio wing having a subsonic airfoil shape NASA TN D-7346 (1974)
5.	L. E. Ericsson	Dynamic effects of shock-induced flow separation AIAA Paper No. 73-308 (1973)
6.	J. G. Jones	A survey of the dynamic analysis of buffeting and related phenomena Royal Aircraft Establishment, Technical Report 72197 (1972)
7.	J. G. Jones	Modelling of systems with a high level of internal fluctuations. AGARD Specialists Meeting on Methods for Aircraft State and Parameter Identification, NASA Langley, 1974
8.	D. B. Benepe A. M. Cunningham, Jr W. D. Dunmyer	A detailed investigation of flight buffeting response at subsonic and transonic speeds AIAA Paper No. 74-358 (1974)
9.	H. Försching	Dynamic aeroelastic calculations of aircraft based on ground-vibration test data Progress in Aerospace Sciences, Vol. 11, Pergamon Press (1970)
10.	C. Hwang W. S. Pi	Transonic buffet behaviour of Northrop F-5A aircraft. Northrop Corporation. Presented to 38th AGARD Structures and Materials Panel Meeting, Washington (1974)
11.	H. John	Critical review of methods to predict the buffet penetration capability of aircraft. Messerschmitt-Bolkow-Blohm GMBH 38th AGARD Structures and Materials Panel Meeting, Washington (1974)
12.	J. K. Zbrozek J. G. Jones	Transient buffet loads on wings J. Sound Vib., 5 (2), (1967)
13.	J. G. Jones	Evaluation of the transient response of a linear system excited by a random input Royal Aircraft Establishment, Technical Report 69092 (1969)
14.	C. G. D. Mitchell	Calculation of buffeting of slender wing aircraft at low speed Royal Aircraft Establishment, Technical Report 68165 (1968)
15.	A. J. Ross	Determination of aerodynamic derivatives from transient responses in manoeuvering flight AGARD Flight Mechanics Panel Specialists Meeting on Methods for Aircraft State and Parameter Identification, NASA Langley (1974)
16.	E. H. Dowell	Noise or flutter or both? J. Sound Vib., 11 (2), (1970)
17.	M. T. Landahl	A wave-guide model for turbulent shear flow J. Fluid Mech., 29 (1967)

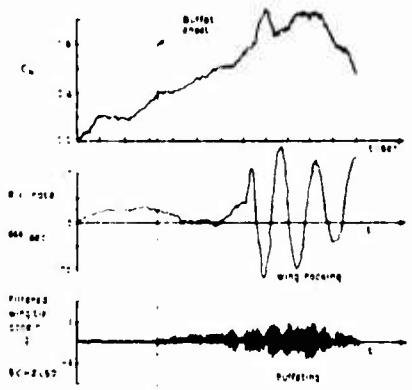

Fig. 1 Typical penetration to high $C_{L_{max}}$ of fighter-type aircraft (schematic)

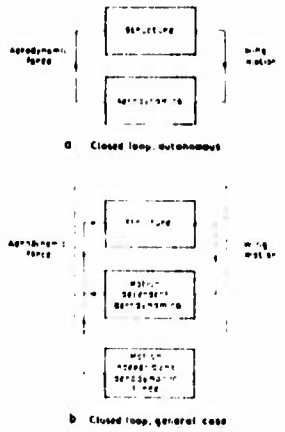

Fig. 2 System analysis relationships for aeroelastic flight simulation

KEY	POD DESCRIPTION
1	First Symmetric Wing Bending
2	Symmetric Fin-Tail
3	Second Symmetric Wing Bending
4	Third Fuselage Vertical Bending + First Symmetric Wing Torsion
5	Second Antisymmetric Wing Bending
6	Horizontal Tail Pitch
7	Horizontal Tail Pitch
8	Horizontal Tail + Second Wing Torsion
9	Horizontal Tail Pitch
10	Horizontal Tail

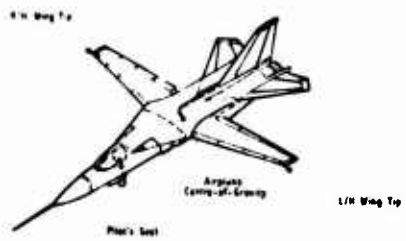

Fig. 3 Acceleration measurements

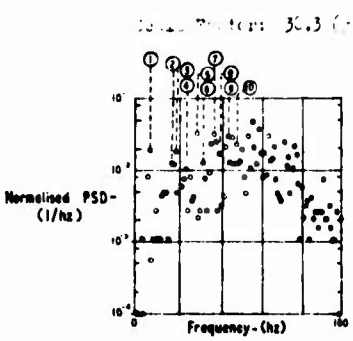

Fig. 4 Spectrum - Wing Tip Acceleration
M ≈ 0.8, h ≈ 20,000 ft., α_i = 12.2°

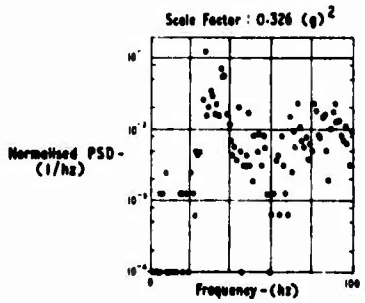

Fig. 5 Spectrum - C.G. Vertical acceleration,
M ≈ 0.80, h ≈ 20,000 ft., α_i = 12.2°

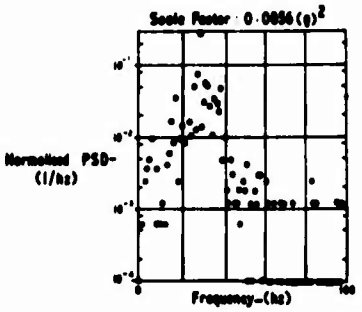

Fig. 6 Spectrum - Pilot seat vertical acceleration, M ≈ 0.80, h ≈ 20,000 ft., α_i = 12.2°

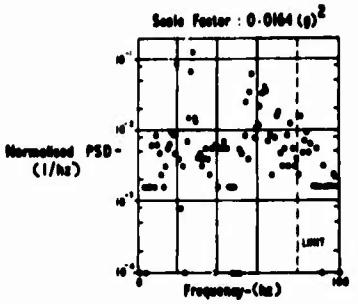

Fig. 7 Spectrum - Pilot seat lateral acceleration, M ≈ 0.80, h ≈ 20,000 ft., α_i = 12.2°

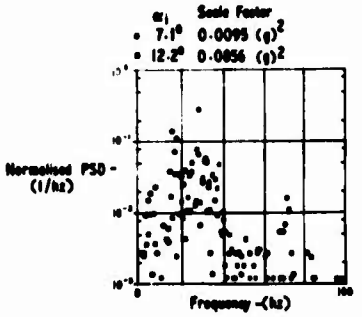

Fig. 8 Effect of angle of attack on modal content - pilot seat vertical acceleration, M ≈ 0.80, h ≈ 20,000 ft., α_i = 12.2°

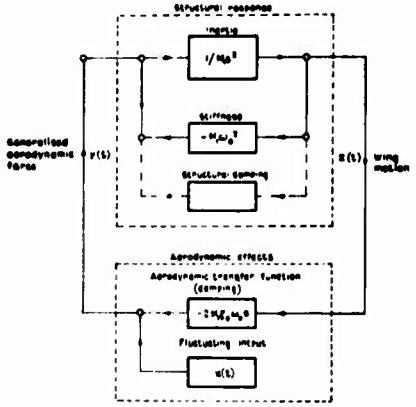

Fig. 9 Forced-vibration model of structural buffeting, representing response in a flexible mode

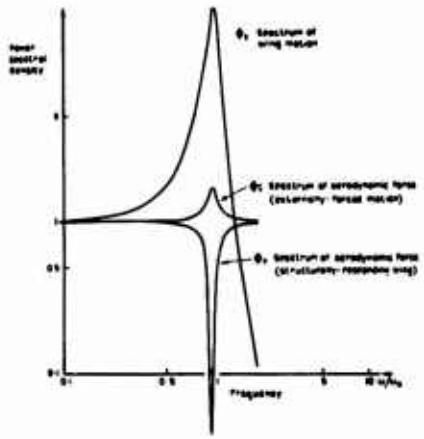

Fig. 10 Power spectra of aerodynamic forces on externally-forced and structurally-responding wings

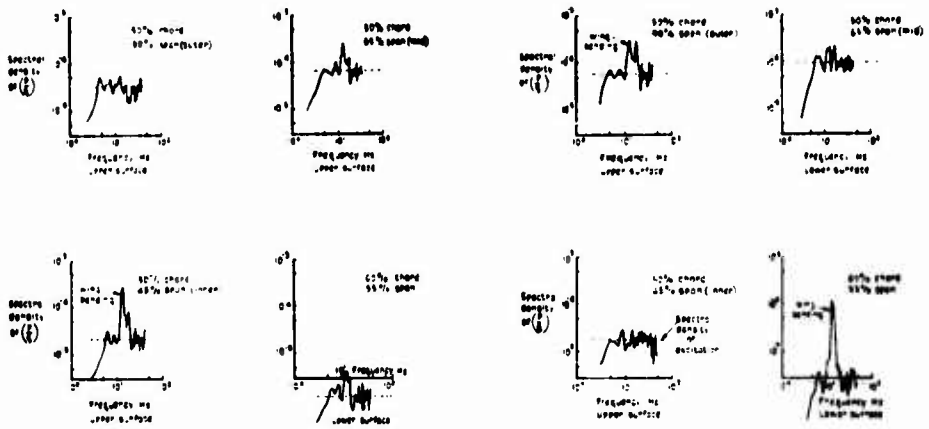

(a) Case 1, medium buffet (b) Case 2, heavy buffet

Fig. 11 Structural buffeting of small combat wing. Power spectra of measured pressure fluctuations, M = 0.7

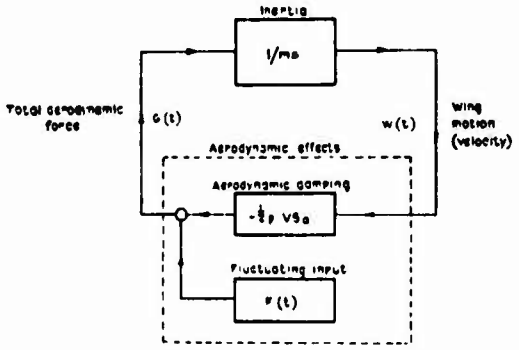

Fig. 12 Forced-vibration model for "buffet time" response with rigid-body wave mode

PRE-STALL BEHAVIOUR OF COMBAT AIRCRAFT

by: D.E. Shaw,
Principal Aerodynamicist,
Aerodynamics Department,
BRITISH AIRCRAFT CORPORATION LIMITED,
Military Aircraft Division,
Warton Aerodrome,
WARTON. Nr. Preston, Lancs.
PR4 1AX

SUMMARY

The general "state of the art" with regards to high-incidence pre-stall behaviour is discussed in terms of fluid flow characteristics and the corresponding flight dynamic phenomena. Particular attention is focussed on the results of recent work undertaken in the U.K. on two very different phenomena, each separately described by pilots as "wing rock". The first is associated with a "collapse" of the dutch roll characteristics to a divergent rolling oscillation and the second with the rigid airframe response in the dutch roll mode to the low frequency content of wing buffet.

CONTENTS

NOMENCLATURE

A	Rolling inertia or aspect ratio
b	Wing span
c	Characteristic length
C	Yawing inertia
C_L	Life coefficient (of whole wing)
C_{LL}	Local lift coefficient
ΔC_p	Incremental pressure coefficient
f	Frequency [Hz]
f(t)	Time dependant forcing function
i_A	Non-dimensional rolling moment of inertia $\left[= \frac{A}{M\left(\frac{b}{2}\right)^2}\right]$
i_C	Non-dimensional yawing moment of inertia $\left[= C/M\left(\frac{b}{2}\right)^2\right]$
i_E	Non-dimensional cross coupled moment of inertia $\left[= E/M\left(\frac{b}{2}\right)^2\right]$
l	Separation bubble length
l_p	Rolling moment due to rate of roll-non-dimensionalise
l_v	Rolling moment due to side slip
l_ξ	Rolling moment due to roll control deflecting
M	Aircraft total mass
n	Non-dimensional frequency $\left(= \frac{fc}{V}\right)$
$\sqrt{NF(N)}$	Power Spectral density ($= \bar{p}/q\sqrt{e}$ where e = bandwidth of measuring apparatus, $\Delta f/f$ and $\bar{p}$ = RMS pressure fluctuation in that band)
n_η	Yawing moment due to rate of yaw
n_v	Yawing moment due to side slip
n_ξ	Yawing moment due to roll control deflection
p	Pressure or roll rate
$\bar{p}$	RMS pressure fluctutations
q	Dynamic head $(= \frac{1}{2}\rho V^2)$
η	Yaw rate
RMS	Root mean square
S	Wing (reference) area
t	time (seconds)
V	Free stream velocity
y_v	Side force due to side slip
z	Displacement
α	Incidence to free stream
ω_o	Natural frequency
ζ	Relative damping
ρ	Free stream density
τ	Aerodynamic time constant $\left(= \frac{M}{\rho SV}\right)$.
Λ	Sweep
ϵ	Phase angle
β	Side slip
λ	Taper ratio and wing
η	Non-dimensional spanwise ordinate - based on semi-span, $b/2$

1. INTRODUCTION

Many current combat aircraft have very similar wing planforms in terms of sweep, aspect ratio, and taper. These similarities lead to a number of corresponding similarities in their stalling and buffeting characteristics. Work recently undertaken in the U.K. at the R.A.E. and B.A.C. - M.A.D. (British Aircraft Corporation, Military Aircraft Division), has extended our knowledge of the phenomena involved.

The fluid motion characteristics of the type of flow met on combat aircraft wings at high incidence will be discussed briefly.

This will be followed by a general description of some of the flight dynamic phenomena associated with flight at high incidence.

The main part of the paper deals with two particular phenomena, each separately described as "wing rock".

The first is associated with a development of the negative "dynamic nv" concept suggested in the U.S.A. as an explanation of "nose slice". For only slightly different variations of the lateral derivatives with incidence, it is possible for the dutch roll damping to collapse without a significant change in the "dynamic nv". This results in a divergent oscillatory rolling motion with significantly different phase relationships between yaw and roll than in a conventional dutch roll. This can be interpreted by pilots as wing rock.

The second phenomenon is associated with a possible "rigid airframe" response to the low frequency content of wing buffet. The case studied was the dutch roll response to buffet of an aircraft with low roll inertia. The buffet levels were taken from published experimental data, and the buffet spectrum was approximated to that of "white noise".

The paper will be concluded with remarks on possible improvements. In the first place these will be directed at control of the flow development. However, improvements to the automatic control systems will also be briefly discussed.

2. FLOW MECHANISMS INVOLVED IN PRE-STALL BEHAVIOUR (freely adopted from Ref. 1)

2.1 Initial Assessment

When we consider the flow development on wings with moderate sweep, (say, up to 50°, as on Eagle, Jaguar or later marks of Mirage), the two-dimensional sectional characteristics lose their significance. With increasing angle of sweep-back the flow must be regarded as a three-dimensional phenomenon rather than a piece-wise collection of two-dimensional characteristics. However, the main three-dimensional effects are at the wing root and near the wing tips, and the mid semi-span region behaves somewhat like a sheared infinite wing - at least in terms of the type of pressure distribution developed before shocks and separation occur.

The main factors which affect the flow development are:

(i) Tapered swept planforms produce the highest aerodynamic loading outboard. The effects of sweep and taper on the spanwise loading are shown in Figures 1 and 2 respectively. In addition the root effects are such that for given local C_L's in the region near the root, the suction pressures on the upper surface are shifted rearwards from the neighbourhood of the leading edge. The opposite occurs in the region of the wing tips.

(ii) The normal wing body interaction at moderate to high subsonic Mach number is to produce the conventional "three-shock system" (Figure 3). The inboard aft shock is dominated by the compression waves caused by the restraint of the body on the wing flow. This shock can be reduced in strength by suitable body-and wing-root shaping which can achieve largely isentropic recompression in the root. The forward and outer shocks are more difficult to control except at specific design points. They are analogous to the shock found on a 2-Dimensional section.

(iii) The boundary layer outflow and relatively high outboard local C_L's at high incidence tend to make the separation occur earlier outboard. This outflow which occurs inside the boundary layer is due to the pressure gradient normal to the free stream direction, (or indeed local stream direction), caused by the sweep on the isobars which is there even for constant C_L along the span and obviously for the more general case where C_L increases outboard along the span.

All these points tend to cause the flow on the outboard part of the wing to separate or "stall" first. Thus, as separation starts to develop there is a noticable change in the wing dominated pitching moment and the lateral derivatives - in particular l_p and l_v, (rolling moment due to roll or side slip), as there are grossly affected by the loading changes at or near the wing tip.

In addition the separated flow is characteristically unsteady. Oscillatory or time dependent near step-function forces and moments may result.

Obviously, we must look at the flow mechanisms involved in a little more detail.

2.2 Initial Wing Tip Separation - The Possible Flow Mechanisms at Low Speed

The preceeding discussion suggests that stall begins at the tip at a certain incidence and then moves inboard with further increases of incidence. Once initial separation has occurred there will

obviously be attached flow over the inboard sections and "stalled" flow over the outer sections.

The flow and the development of the flow in the outer stalled region can take several forms, depending on the section, sweepback angle, taper and "three-dimensional treatment" such as twist. One form is a type of long bubble met with on thin sharp nosed sections in two-dimensions. Boundary layer separation occurs near the leading edge with re-attachment occurring some way downstream. As the incidence increases, the length of the bubble increases until separation occurs at the nose with no re-attachment.

The "dead air" region has small mean velocities. Dead air implies air where there has been a significant loss in momentum or total head.

A second form is akin to the trailing edge-type of 2-D stall where separation occurs and the separated (dead air) region continues into the wake. A third form occurs at moderately high sweeps when the separation occurs near the leading edge and the shed vorticity rolls up into a concentrated vortex. In this case there is no "dead air" region, (i.e. large region where there is a loss in total head), and consequently there is no loss of lift in the tip region. In fact the lift increases because of the additional suction on the wing surface just underneath the concentrated vortex. This form is often called "part span vortex" flow and often dominates the flow development on the wing up to quite high subsonic Mach numbers. Probably the best known aircraft with this type of flow is the Anglo French Concorde.

Returning to the first and second types of tip "stall" where there is an appreciable "dead air" region, either in a long bubble or in the separated flow near the trailing edge, there must be a vortex sheet between the inner attached flow and the outer dead air region. It is not known exactly how this vortex sheet arises and arranges itself in the neighbourhood of the wing, but above the wing and behind the wing the vorticity must tend to align itself in the stream direction. This must not be confused with the part span vortex discussed above, (as often occurs in the literature). This shed vorticity has an important influence on the flow, since it stabilises the stall pattern. In the unstalled inboard region downwash velocities are induced, reducing the effective angle of incidence. Conversely, the effective incidence is increased outboard giving incidences well above the sectional stalling angle.

2.3 Mach Number Effects - Wing Flow

As implied in our previous discussions (2.1) the development of the shock wave pattern for increasing free stream Mach number is a complex procedure.

For the class of wing of interest, the effect of high local C_L's and the bias in the pressure gradients in the tip region is to cause a small shock normal to the free stream. Although this shock moves slightly rearward and inboard with increasing Mach number, the situation soon becomes dominated by the rear shock caused by the compression waves arising at the wing root. These eventually coalesce along the span to form the rear shock. At slightly higher angles a third shock appears, known as the forward shock, this shock is akin to the sectional shock which would occur on the infinite sheared wing. These two shocks combine to form the three shock system as shown (Figure 3). At higher incidence the outer shock moves forward as for the 2-D case. As can be imagined the interaction of this shock system with the separated flow phenomena, described above for low speeds, is complex.

The most common situation is a mixture of part span vortex separation and the three shock system. It may be expected that the part span vortex can only exist inboard of the forward shock, since the mere existence of a forward shock implies that ahead of it the leading edge separation has been suppressed by the expanding supersonic flow.

Separation can and usually does occur behind this forward shock.

However, the forms of separation are as varied as those met in two dimensions (Figure 4 - Reference 2).

These vary from:

(i) Pearcey Class A where a small bubble, (separation and re-attachment a short way down stream), at the foot of the shock developing rather like a long bubble until separation spreads right from the foot of the shock into the wake.

to

(ii) Pearcey Class B where the "short" bubble at the foot of the shock does not develop but trailing edge separation does. The ultimate flow picture is the same but the intermediate stages are significantly different and could cause a significant difference in the buffeting and rigid body response.

It is easy to imagine that there can be a complex picture of part span vortices, shed vorticity, shocks, trailing edge separation, long bubbles and short bubbles.

An excellent introduction to the general subject of flow development on swept wings can be found in Reference 3. More particular discussions are available in References 4, 5 and 6.

2.4 Basic Interference Effects

The incidence effect on the basic derivatives and on fin effectiveness have been discussed elsewhere in detail. For example, Reference 7. Some of these effects are illustrated in Reference 6.

The reduction of fin effectiveness is in itself an interesting (and vital) problem. If the reduction with incidence is greater than expected, or if differences exist between various tunnel tests, diagnosis can be a time consuming task. The causes are many, but can be subdivided into dead air and vortex-type interferences.

The dead air type can be caused by fuselage and/or canopy separation effects reducing the effective dynamic head ($\frac{1}{2}\rho V^2$) in the vicinity of the fin, particularly near the root.

Vortex interference can be caused by the reduction of the effective local side slip in the vicinity of the fin by the action of a vortex system generated from the fuselage, intakes or wings. An excellent introduction to this subject can be found in Reference 8.

6.5 Oscillatory Pressures (General Background)

Obviously, we are well outside anything that can be treated in a theoretical manner, (at least this side of 1960?), although our understanding of each phenomenon on its own in well controlled conditions is currently very much on the increase. An excellent review of the situation can be found in Reference 9. I will use this assessment as a basis for our discussions on the nature of the oscillatory forcing phenomena which could be the root cause behind buffeting, and the class of pseudo rigid modes such as wing rocking and bucking that we are interested in.

One important cause of the oscillatory pressures is found in bubbles. Flight test on the Venom with a sharp leading edge and the canard control of the XB-70 showed buffet onset corresponded with the formation of a long bubble. The buffeting then increased steadily as the bubble extended downstream, until the re-attachment point approached the trailing edge and the trailing edge pressure diverged. This point corresponded with heavy buffet. However, we are more interested in establishing buffet characteristics before heavy buffet is reached and hence it is worth considering what data there is for flow associated with separation bubbles.

Mabey has collected data from a number of sources covering:

Leading edge bubbles
Bubbles downstream of spoiler
Bubbles downstream of steps
Bubbles upstream of steps
Bubbles downstream of sudden expansion in pipes
Bubbles within shallow cavities

This data correlates very well and implies the general conclusions drawn will have application to a wide class of flows (Figure 5). Data studied at various Mach numbers, (flow down a step and also on an aerofoil), tend to support this conclusion except that the unsteadiness appears to decrease at supersonic speeds.

The data shows r.m.s. values of ΔC_p reaching as much as 10 although 5% to 6% appears more common. This peak, as can be seen, occurs near or just in front of about 0.8 x/l, the reduced frequency being based on free-stream velocity and bubble length. Little data extends below f l/v of 0.1.

6.6 Oscillatory Pressures (Wing Flow)

Some time ago, Moss and Mundell undertook some limited tests in the R.A.E. 8' x 6' transonic tunnel on an early B.A.C. variable sweep project. Limited results from these tests are presented in Reference 9.

The type of flow involved is shown in Figure 6 at "moderate buffet" conditions (Mach number was 0.860). The r.m.s. variation of oscillatory pressure coefficient with incidence is shown in Figure 7. The outboard shock continues to move back until about 5°, pause, then it moves forward. Whilst the shock is moving back, we can surmise that the slow steady increase in pressure fluctuations are the combined effect of shock oscillation and the attached boundary layer growing under an increasingly adverse pressure gradient. As the shock passes the point in question the fluctuations increase rapidly presumably due to the shock wave oscillation and hence of a local nature. Shortly after this point, the boundary layer separates under the shock, which starts to move forward. At this stage, buffeting is detected by the wing-root-strain gauges. The "local" fluctuations reduce and level off at a roughly constant value. Any variations there are will be due to the increasing strength of the fluctuations in the lengthening bubble and the relative position of the point to the bubble. What is significant is the fact that this fluctuation is probably spread over a large part of the wing ir and behind the long bubble. Equally significant is the rather flat frequency spectrum (Figure 8) which spreads right across the wing panel modes, (40 to 200 Hz aircraft scale), through the wing structure modes, (2 to 10 Hz), and possibly down to the rigid body modes at less than 1 Hz. Obviously, we are dealing with a long bubble phenomenon where separation is caused by the outboard shock. A short bubble would excite frequencies too high to be relevant except for panel flutter.

Dr. H. John in the next lecture will also present tunnel data on a design of rather more current interest. The measured power spectra shows a flat content down to 5 to 6 Hz (model). A peak is evident at very high frequency, (about 1.5 scaled), which is probably associated with a short bubble at the foot of the shock passing across that pressure point.

However, probably the most interesting experimental data published is that by Lemley and Mullans on the Phantom. This includes data from both tunnel and flight (Reference 10).

To quote their concluding remarks:

"Model data obtained from wind tunnel tests of a 10% scale YF-4E airplane have been analysed and compared with full scale results. Random signal analysis was performed on fluctuating pressure transducer outputs which were then studied for spatial and spectral effects, and for Mach number and angle of attack variation.

Validation of wind tunnel pressure measurements made on the model was accomplished by comparison with flight data. Although limited by the small number of flight transducers, these comparisons showed good agreement in the spectral shapes. In general, the model r.m.s. levels were somewhat higher. Aircraft response predictions are therefore expected to be somewhat conservative.

Several pertinent conclusions drawn from the test data include the following:

- At high angles-of-attack the flow pattern over a highly swept wing with a leading edge snag is quite complex. The flow close to the upper surface is strongly affected by a vortex system consisting of leading edge, tip, and snag vortices causing abrupt changes in flow direction over the surface. The regions of high fluctuating pressures seem to be associated with these vortices, particularly the snag and tip vortices.

- No discernible single "convection" mechanism for the transport of the fluctuating pressures was evident such as the downstream convection reported in studies of slender spacecraft launch vehicles. Disturbances seemed to emanate from multiple sources simultaneously and propagated in a complex manner.

- Correlation is small between points on the wing that are separated by more than about one-fourth of the mean aerodynamic chord.

- The fluctuating pressure spectrums frequently exhibited peaks at frequencies believed to be associated with vortices. The frequency associated with the snag vortex was generally about half that of the leading edge and tip vortices. These frequencies, scaled to the flight vehicle, were at the higher end of the vehicle's primary structural resonances.

- Maximum buffet intensities occurred at the high subsonic Mach numbers diminishing abruptly to small values at sonic and supersonic speeds.

- Maximum r.m.s. wing root bending moments caused by buffet were of the order of 7% of the corresponding steady bending moments.

- Maximum fluctuating pressure coefficients were generally of the order of $P_{rms} = 0.2$.

The measurements from this model were used to establish a buffet spectral response method for computing wing vibrations; encouraging agreement with flight measurement was obtained."

Having set the scene, I will leave the subject of buffeting to Dr. John.

2.7 Oscillatory Effects - Conclusion

However, all the buffet and general oscillatory pressure data have a significant frequency content below the airframe mode resonant frequencies and possibly with sufficient energy to cause some response through the rigid airframe modes. We will return to this point later.

3. THE FLIGHT DYNAMIC IMPLICATIONS

3.1 General Discussion

Current aircraft requirements in the combat/strike field lay great emphasis on the manoeuvrability of the aircraft, particularly at high subsonic speeds. Real and simulated combat experience has shown that the critical speed range is round about 0.8/0.9 Mach number, where it can be shown that rate of turn at a given altitude is at a maximum for most aircraft. Unfortunately, as we have discussed, this region is also one of the most complicated from a fluid dynamics point of view. As recently as early 1971, the then head of the R.A.E. Dynamics Division (L.J. Beecham) listed this subject as a number one priority. It has subsequently featured high in R.A.E. activities and Ministry-sponsored research. To paraphrase his comments:

> In general terms the problem is concerned with dynamic behaviour of the flexible aircraft under conditions of flight associated with high angles of incidence and can manifest themselves in many forms separately or in combination. In one form or another, such problems have bedevilled aircraft design over many years. In spite of this, there has been little development in our fundamental understanding of the underlaying causes and none in the ability to relate cause and effect in a quantitative manner. Almost without exception solutions have been reached in an empirical way through Wind Tunnel studies guided by an often all too inadequate qualitative understanding.

Those in industry involved in the problem would agree with almost all of Beecham's comments, but view with doubt the chances of using tunnel rather than flight experiments in reaching a "final solution". A considerable amount of effort has been spent in diagnosing both flight dynamic and fluid mechanic aspects and although work remains to be done, the problems are less of a mystery.

3.2 Pilot Work Load and Pilot Opinions

The lift limits will obviously vary from one type of aircraft to another and will also vary from one type of task to another. It appears frequently to vary from pilot to pilot. With regards this last point - if pilot A claims, (and the flight records substantiate), higher C_L's than pilot B, this can be due to skill; familiarity; or a different interpretation of the task in hand. Tact is required in sorting out differences.

To illustrate the problem of pilot opinion consider two types of manoeuvre.

Collision Avoidance (Figure 9a)

The pilot will only have one thing on his mind. His total attention will be on pulling the maximum 'g' available. The aircraft and flight path must obviously be under the pilot's control, but nobody will expect the aircraft to be easy to fly. The aircraft may well be shaking, bucking, and rocking, but as long as the pilot can "stay with it" he will be "happy" at least after the event - even if the aircraft suffers some structural damage and the aircrew all need a good stiff drink!

Normal Manoeuvring Flight (Figure 9b)

The pilot will find a somewhat lower lift limit than the above for normal flying maximum usable lift limit. Handling can be poor and the aircraft could be wing rocking and buffeting. However, under normal - no panic - flying, this is a limit that the pilot would pull to without hesitation. The pilot will use it for aerobatics, rapid changes in flight direction, and so on.

Other more demanding limits can and do exist, involving combat missions including Guided Weapons firing or gun firing.

3.3 Notes on Theoretical Models of Vehicle Dynamics

In any attempt to establish the causes of complex vehicle dynamic behaviour such as wing rock it is necessary to assess the various possible theoretical models. J.G. Jones has discussed these in some detail in the previous paper of this lecture series. However, the main points relevant to this current exercise are summarised as follows:-

The phenomena discussed in this paper and in particular "wing rock" involve a possible closed-loop interaction between the unsteady fluid motion involving separated flow and the motion of the aircraft. If we ignore buffet then the conventional psuedo-rigid airframe assumptions can be made. The various models can be illustrated using a single degree of freedom equation, thus:

$$M \ddot{z} + 2 M \zeta \omega_o \dot{z} + M \omega_o^2 z = f(t) \qquad (1)$$

(a) Autonomous Oscillations

Consider the case when there is no "external" forcing function, i.e. $f(t) = 0$ and where $\zeta < 1$, i.e. the system dynamics are oscillatory.

The simple case is when the damping derivative, (coefficient of the term $\dot{z}$), and stiffness derivative, (coefficient of the z term), are constant. This is the description of the so-called "linear system" which is unstable (divergent) if $\zeta < 0$.

However, in the general case, these derivatives will not be linear. The non-linearity can take many forms, including hysteresis effects and low amplitude unstabilities. These non-linearities can, and often do, lead to limit cycle phenomena.

(b) Force Oscillations

Reintroducing the term $f(t)$. This can take many forms, from the simple single frequency sinusoidal oscillation, through more complex oscillatory shapes and step functions, to complex inputs with a wide range of frequencies.

The situation can become very complex and difficult to assess if the forcing function, $f(t)$, itself is affected by the vehicle response $z(t)$ to any great extent.

3.4 Longitudinal Handling Characteristics

Longitudinal stability and control problems have been with the aircraft designers for a long time. These days they are either designed out in the initial stages or special care is needed in designing control systems, autostab systems and stall warning devices to allow the design to be optimised using a configuration which inherits this type of problem.

(a) Pitch Up

This is an almost classical problem. It in due to the development of outboard separations discussed previously. If large sweep and aspect ratios are used in combination the separations cause a marked forward shift in lift, a positive nose up pitching moment and hence a sudden increase in incidence.

(b) Wing Wake to Tailplane Interference

Wing to tailplane interference effects can cause both stability and control problems. In particular, this can happen if the tailplane is mounted relative to the wing so that the wing

wake hits the tailplane in a particular incidence range. If the thick wing wake, (or wing body junction wake), which occurs after separation of the wing boundary layer hits the tailplane the problems can be very severe.

(c) Bucking and Tuck

Bucking is officially described in the rather terse expression "uncommanded pitch oscillations".

Tuck, on the other hand, is almost a mirror image of pitch-up. It is the uncommanded and sudden decrease of incidence whilst flying at low or negative lift at high subsonic speeds. This is very dangerous phenomena to occur on ground attack aircraft for obvious reasons, and must be designed out, even if this compromises the cruise efficiency of the aircraft. It can be caused by using too much wing twist (wash out) so that the wing tips have negative lift on them. It is not surprising that the high speed (shock) stall characteristics of an aerofoil with camber are not very good when "upside-down".

7.5 Lateral Stability Characteristics

Three different phenomena are often mentioned by pilots when they are discussing the lateral handling characteristics as they affect usable lift limits. These are:

(a) Nose Slice: An uncommanded roll yaw motion, viewed by the pilot primarily as a divergence in yaw. Frequently, the expression "yaw off" is used.

(b) Wing Rock: An uncommanded roll yaw motion viewed by the pilot primarily as roll oscillation but with significantly different characteristics to a normal dutch roll.

(c) Wing Drop or Flip: An uncommanded roll yaw motion, viewed by the pilot primarily as a divergence in roll.

The main common factor of these phenomena, (and indeed of the equivalent longitudinal phenomena already discussed), is that they are rigid body modes. That is, the motion in question is a motion of the whole aircraft. Obviously, aeroelastic effects change the pressures round the aircraft, but in the main these effects can be allowed for by modifying the aerodynamic derivatives etc. Thus as with most S & C work we are discussing a situation described aptly as psuedo-rigid.

The causes of all these phenomena vary according to the aircraft configuration and are dependent on the effects of flow separation on the wing and the steady deterioration of the lateral stability characteristics with incidence.

A word of warning - pilots assess the phenomena after retrospective thought based on the motion of the aircraft. It is not uncommon to find similar pilot comments applying to different phenomena - due to the very wide class of motions which can be included within the definitions. It is also not uncommon to find different pilot opinions about the same phenomena.

Let us now isolate possible causes of these phenomena.

7.5.1 Unstable Dutch Roll

As discussed previously, at high incidences combat aircraft are affected by a marked change in the dominant lateral derivatives. The increasing amounts of wing separation can cause a marked deterioration in the wing rolling derivatives, in addition to the steady reduction in weather-cock stability (fin effectiveness). Obviously, no two types of aircraft behave in the same manner - see for example a comparison between the LTV A-7 and the McD-D F-4 (Ref. 11).

It is probable that non-linear aerodynamic characteristics, i.e. hysteresis and "dead spots", play an important part in determining the exact nature of the phenomena. However, work in the U.S.A. and the U.K. indicate that very full and satisfactory explanations of a number of phenomena can be found within the frame-work of linear aerodynamics.

The approximate formulae for the dutch roll frequency, (using the notation common in the U.S.A.), is:

$$\omega_o^2 = \frac{2V}{b\,\tau\,i_c}\left(n_v + \frac{i_x}{i_A}\,l_v\right)$$

$$\tau = \frac{M}{\rho\,SV} \qquad i_c = \frac{C}{M\,(b/2)^2}$$

Whilst the damping is given by:

$$\zeta_d\ \omega_o = \frac{-1}{2\tau}\left(y_v + \frac{n_r}{i_c} + \frac{l_p}{i_A}\right)$$

at least for high incidences.

The existing correlations published (5, 6 and 11) suggest that the critical parameter is the frequency, i.e. dynamic $n_v\left(n_v + \frac{I_\Sigma}{I_A} l_v\right)$ or stiffness derivative.

However, at least two combat aircraft do not suffer from a collapse of the stiffness derivative but still have what the pilots describe as "wing rock". One example has been, or will be used by both my co-lecturers - Figure 10. The second is shown in Figure 11, both are "typical" cases of wind up turns that might occur with autostabilisers switched off.

Figure 12 shows the variation of the dominant stability derivatives for a typical combat strike aircraft, whilst Figure 13 shows the major parameters describing the dutch roll for the aircraft in question without autostabilisers. The dominant factors are the damping, the ratio of roll to yaw and the phase angle between roll and yaw.

Returning to Figure 11, which shows a typical flight trace of a "wing rock" oscillation which occurred as the pilot was undertaking a "wind up turn". Analysis of this trace shows it to be a "divergent dutch roll" although not easily recognised as such. Figure 13 shows the comparison of the in-flight factors with the predicted values. (In addition the factors measured from a conventional dutch roll - deliberately induced, are shown). For the case in question, the pilot clearly identified this phenomena as an absolute lift limit and nobody would argue with him, however, the pilot description is often affected by pilot familiarisation. We have had a specific case where the pilot identified the divergence and initiated recovery at the same flight condition, with descriptions which were, on face value, contradictory. However, deeper thought shows that within the context they were reasonable and helpful comments. His first description was "yaw off". He initiated recovery almost as soon as the motion started. In his next encounter with the phenomena he allowed slightly over one cycle of the oscillation to occur before recovery. This he diagnosed as wing rock. Due to the high roll/yaw ratio this is not surprising. The third time he held it for about a cycle and a half and described it as a "divergent dutch roll".

Flight simulation studies show that this type of phenomena involving a collapse of the dutch roll damping is not as serious as the alternative where the stiffness derivative collapses.

3.5.2 External Forcing Functions

In cases where flow separation develops in an asymmetric manner, rolling moments can be induced in a symmetric (zero sideslip) situation. Bore (Reference 4) has described how this phenomena affected the Kestrel and the good correlation between flight behaviour and wind tunnel rolling moment measurements - to paraphrase - if the on-line pen recorders oscillated continuously at a constant incidence, then the aircraft experienced wing rock - whereas a steady excursion of rolling moment corresponded with "wing low" in flight.

Recent investigations on this wing rock phenomena has shown that this is a psuedo-rigid airframe response to an external forcing function.

The external forcing function in question can be found in the low frequency content of the oscillatory pressures acting on the wing usually associated with buffeting. The low frequency content found for example on the Phantom was described in Reference 10 and discussed here previously. The type of small amplitude wing rock shown in Figure 11, prior to the large amplitude wing rock, can be attributed to such a response for aircraft with low roll inertia. The characteristics are a rather random rolling oscillation with no dominant frequency and no recognisable corresponding yawing motion.

One example is shown in Figure 14, where the response to a random rolling moment input is shown. A more rigorous statistical approach using an input with representative frequency content gives a rolling motion with a root mean square very close to that observed in flight with autostabs inoperative.

3.6 Lateral Control Characteristics

The above description has been grossly over simplified because the subject of stability is so inter-related with control as to make sensible analysis of each separately impossible. Apparently poor aircraft stability can sometimes be caused by direct intervention by the pilot as he attempts to control the situation. This can be if, for example, the attempted roll control results in large yawing moments. On the one hand the yawing moment can give sideslip which produces a rolling moment that offsets the roll control (adverse yaw); and on the other, sideslip produces a rolling moment that augments the roll control (proverse). Either can make the vehicle difficult to control. Incidence effects can change the basic characteristics to give either effect depending on the type of roll control.

Another control problem can be caused by the loss of effectiveness of wing-mounted roll control devices - either spoiler or ailerons at high incidences. If, as discussed above, the roll damping also reduces with incidence, the steady state roll rate does not necessarily decrease and although the handling may be "acceptable" the pilot will not consider the situation in a very favourable light. However, if the roll damping does not collapse with incidence, the roll control could be totally inadequate.

Many detailed investigations into this complicated problem have been undertaken. For example, the work undertaken by System Technology Inc. in the mid-60's (Reference 12). A useful and more up-to-date reference is the AGARD Conference Proceedings - "handling criteria" (Reference 13).

Before leaving this very brief mention of lateral control characteristics, mention should be made of a problem often met when the roll control has adverse yaw characteristics, coupled with low lateral

stability (n_v) and still negative roll due to sideslip (l_v). A rather simpler approach to that of Reference 12 can show the characteristics of the problem:

Consider the case where the pilot is stabilising bank angle by use of roll control, (roll rate zero), and assume no rudder input. Under these circumstances the lateral equations of motion can be rearranged (by eliminating ζ) and an equivalent lateral stiffness derivative emerges, (analogous to dynamic n_v), thus ($n_v - l_v {}^{n}\zeta/l_\zeta$), with proverse yaw. This second term augments the lateral stability, but with adverse yaw the term is de-stabilising and obviously can dominate if n_v is numerically small. Under these circumstances a divergence can occur which is pilot induced but may not be recognised as such. Pilot description can be "mild yaw off" (or nose slice? in the States).

4. POSSIBLE IMPROVEMENTS

4.1 Fluid Mechanic

Manipulation of the configuration to arrange for acceptable variations of the basic sideslip derivatives has been a way of life for a number of years - ever since the first model gliders. As the flight envelope, (in terms of Mach number and incidence), has increased, so have the tricks to keep acceptable derivatives. These include anhedral or dihedral on wing or tailplane and also ventral or twin dorsal fins.

Manipulation of the configuration to delay the collapse of the roll damping is much more difficult. It is the natural tendency for wings of the type of interest to "stall" first at the tips and it is this development of separation which must be controlled.

This can be done by sophisitcated section design coupled with wing twist and assisted by the usual arrays of fences, vortex generators, notches and sawteeth. One very expedient method has been to use the low speed high lift leading edge devices such as slats at an intermediate position.

4.2 Control System

However, it is often more pragmatic to depend on automatic control systems which, (even with low authority), can be very useful in improving the high incidence characteristics. The only complexity required even with simple scheduled gain systems is to allow adequately for the incidence effects. For example, Dutch Roll stability can be improved by a yaw damper at low incidence but will probably require a roll damper at high incidence.

REFERENCES

1. Problems of aircraft behaviour at high angles of attack.
   AGARD-ograph 136 G.J. Hancock April, 1969.

2. The interaction between local effects at the shock and rear separation - a source of significant scale effects in wind tunnel tests on aerofoils and wings.
   AGARD Conference Proceedings No. 35. A.H. Pearcey J. Osborne A.B. Haines September, 1968.

3. An introduction to the flow about plane swept-back wings at transonic speeds.
   Vol. 64 (August, 1960). The Journal of the Royal Aeronautical Society. E.W.E. Rogers, and I.M. Hall.

4. Post/Stall aerodynamics of the "Harrier" G.R.I.
   AGARD Conference Proceedings No. 102. C.L. Bore April, 1972.

5. On airflow separation and buffet onset during fighter aircraft manoeuvring.
   AGARD Conference Proceedings No. 102. P.J. Butkewicz April, 1972.

6. Manoeuvre and buffet characteristics of fighter aircraft.
   AGARD Conference Proceedings No. 102. E.J. Ray, L.W. McKinney, and J.G. Carmichael April, 1972.

7. Design considerations for the satisfactory stability and control of military combat aeroplanes.
   AGARD Conference Proceedings No. 119. B.R.A. Burns November, 1972.

8. Some effects of shed vortices on the flow fields around stabilising tail surfaces.
   AGARD Report No. 108. R.W. Stone Jnr. and E.C. Polhamus April - May, 1957.

9. Beyond the buffet boundary.
   Supplementary paper - Aeronautical Journal. R.Ae.S. D.G. Mabey April, 1973.

10. Buffeting pressures on a swept wing in transonic flight.
    Comparison of Model and full scale measurements.
    AIAA Paper 73-311. C.E. Lemley and R.E. Mullans March, 1973.

REFERENCES (Cont.)

11. Aerodynamic design and flight test of U.S. Navy Aircraft at High Angles of Attack.
AGARD Conference Proceedings No. 107. W.H. Burris and J.T. Lawrence April, 1972.

12. A study of conventional airplane handling qualities requirements.
Technical Report AFFDL-TR-65-138. I.L. November, 1965.
Part I Roll Handling Qualities
Part II Lateral Directional Oscillatory Handling Qualities.

13. Handling Qualities.
AGARD Conference Proceedings No. 106.

FIGURES

1. Effect of wing sweep on spanwise loading due to incidence.
2. Effect of taper ratio on local lift distribution.
3. Development of the three shock system.
4. Types of aerofoil shock induced separation.
5. Types of bubble flow.
6. Example of flow separation patterns on a wing of moderate sweep at buffeting conditions.
7. Local buffet on a swept wing M = 0.9.
8. Spectra of excitation on a swept wing M = 0.85.
9. Pilot work load.
10. Typical "pull up" response. Aircraft "A".
11. Typical "pull up" response. Aircraft "B"
12. Lateral Derivatives. Aircraft "B"
13. Comparison of predicted and flight "dutch roll" characteristics. Aircraft "B".
14. Reponse to random rolling moment input.

FIG 1. EFFECT OF WING SWEEP ON SPANWISE LOCAL LIFT DISTRIBUTION

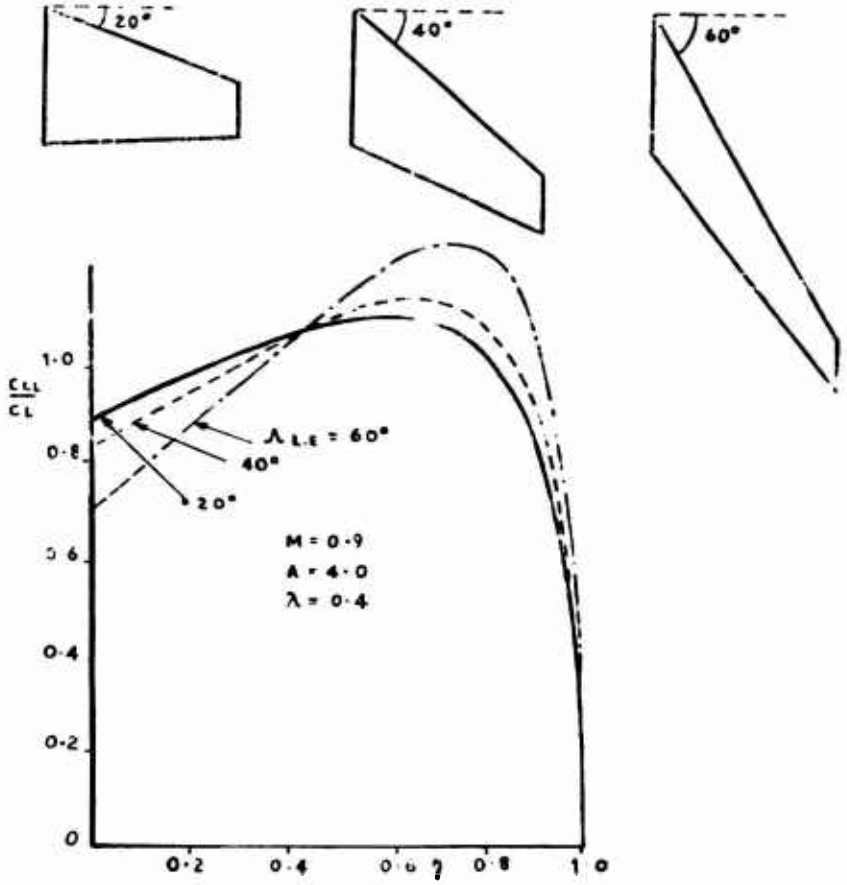

FIG. 2. EFFECT OF TAPER RATIO ON LOCAL LIFT DISTRIBUTION

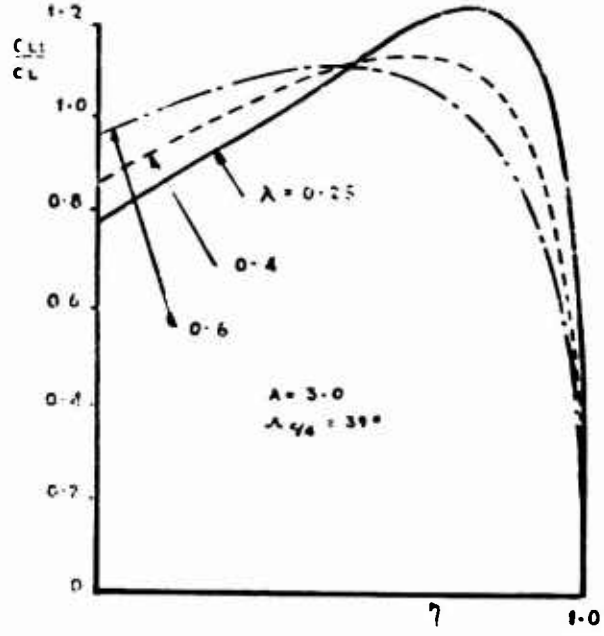

FIG 3. DEVELOPMENT OF

THE THREE-SHOCK SYSTEM

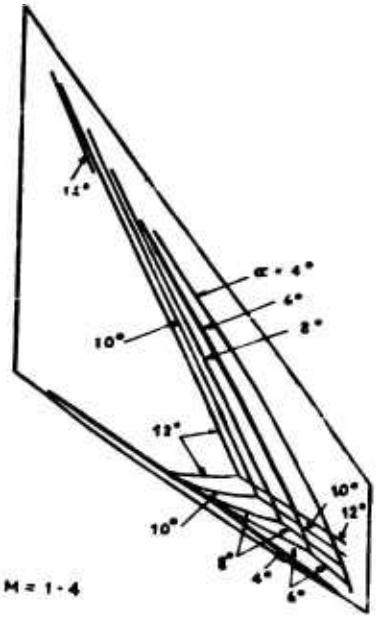

M = 1·4

FROM REF. 3.

FIG 4 FLOW DEVELOPMENT FOR SHOCK-INDUCED SEPARATION OF THE TURBULENT BOUNDARY LAYER WITH INCREASING INCIDENCE OR FREE-STREAM MACH NUMBER (REF 2)

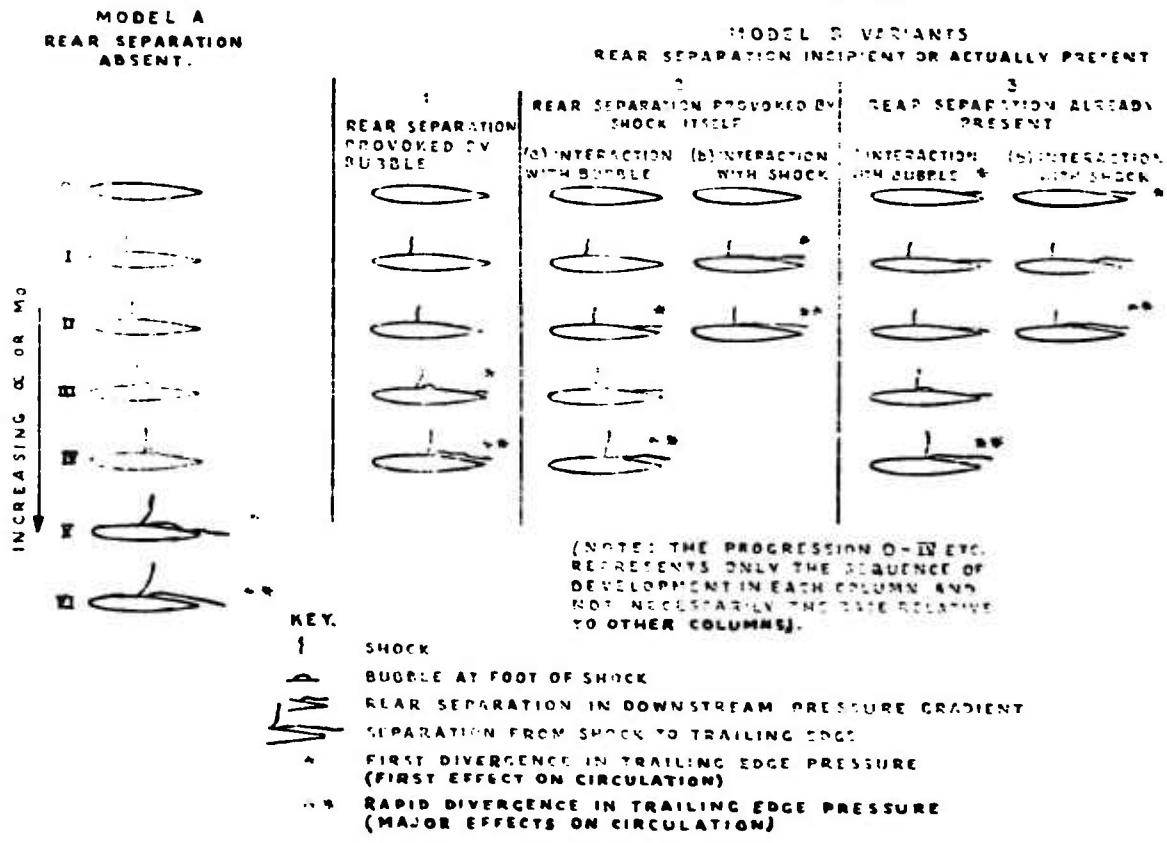

FIG.5. TYPES OF BUBBLE FLOW.

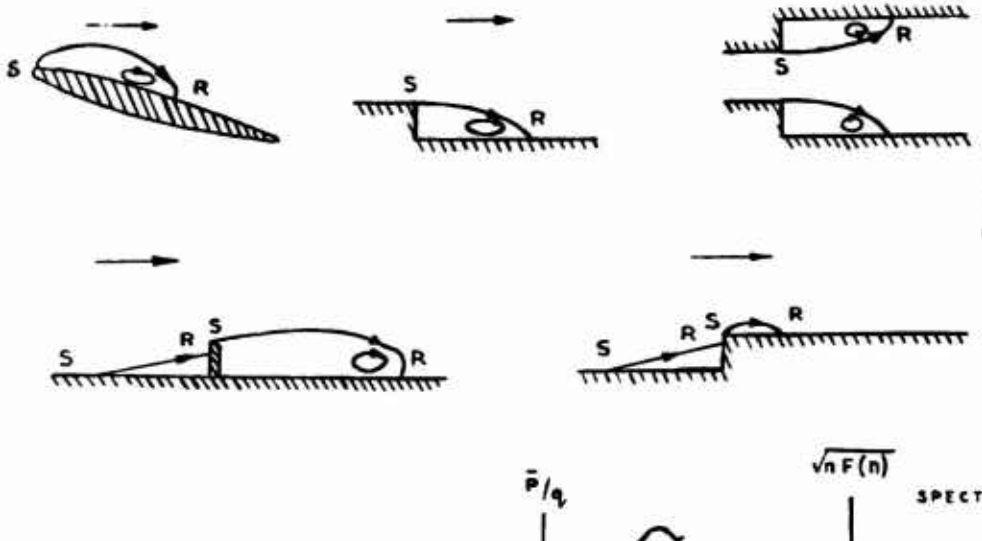

FIG.6 EXAMPLE OF FLOW SEPARATION PATTERN ON A WING OF MODERATE SWEEP AT BUFFETING CONDITIONS.

R A E 8FT. x 6FT TRANSONIC TUNNEL TEST8

M = 0·8

α = 8·3°

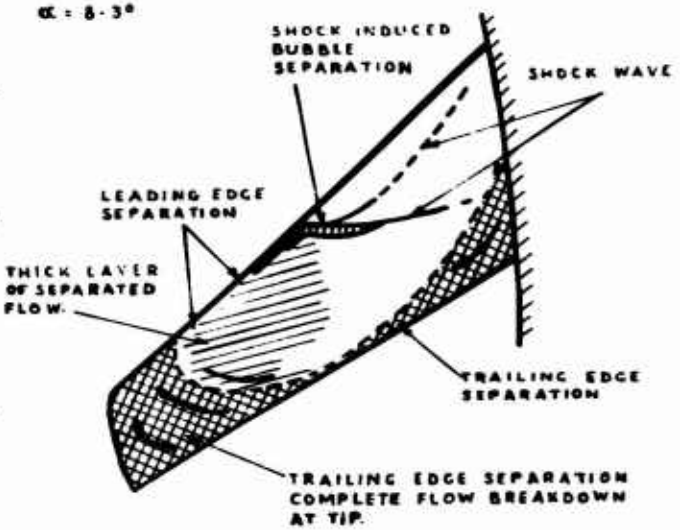

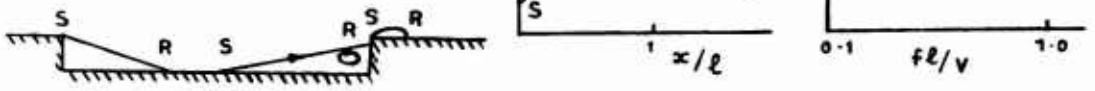

FIG 7 LOCAL BUFFET ON A SWEPT WING, M=0·8

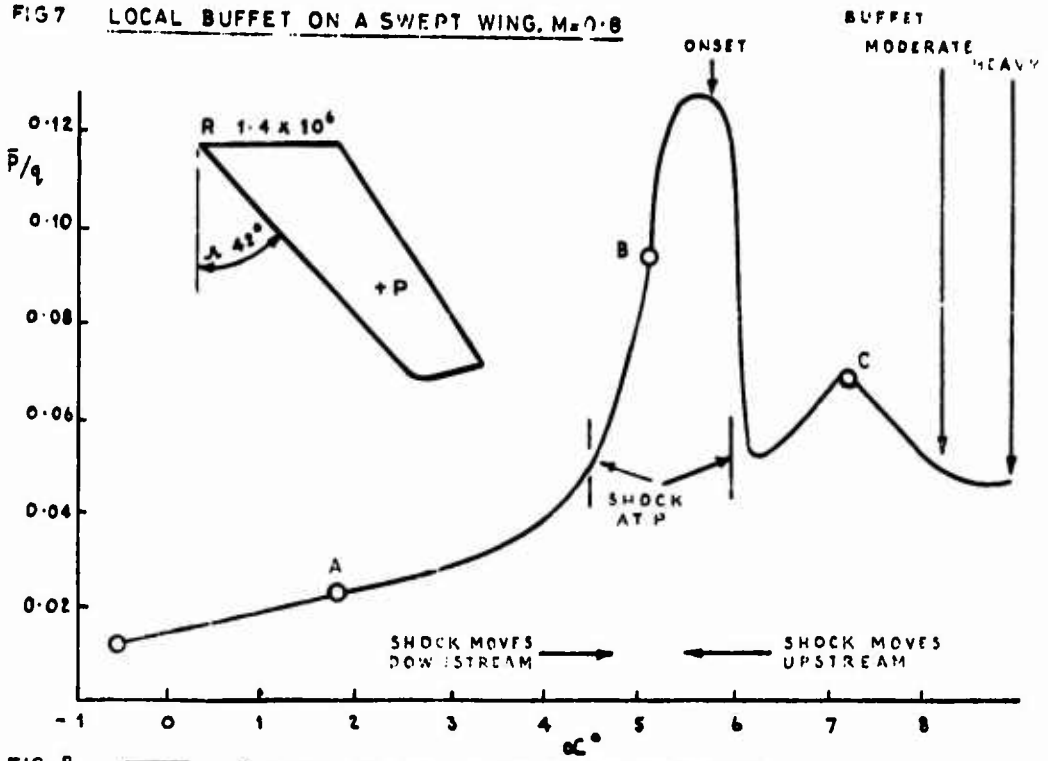

FIG. 8. SPECTRA OF EXCITATION ON A SWEPT WING

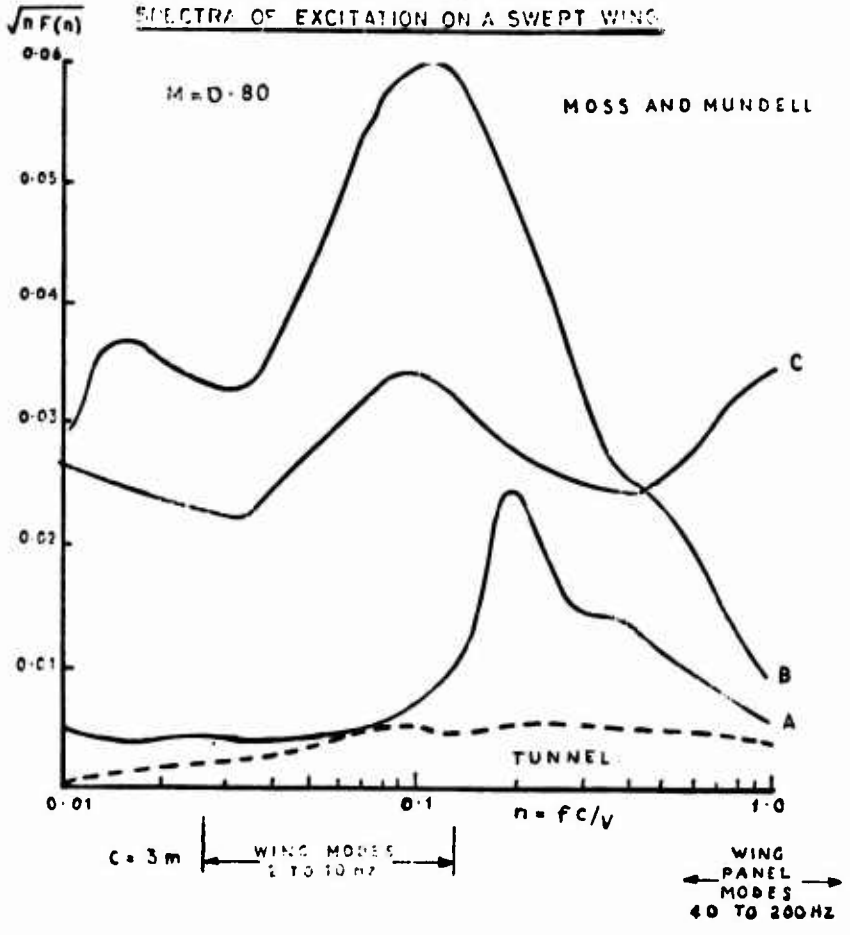

9a. COLLISION AVOIDANCE

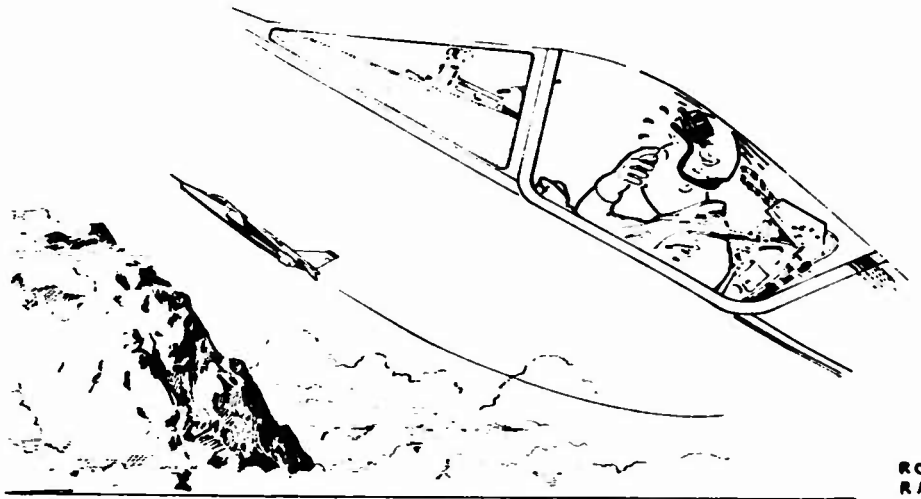

9b. NORMAL MANOEUVRING FLIGHT

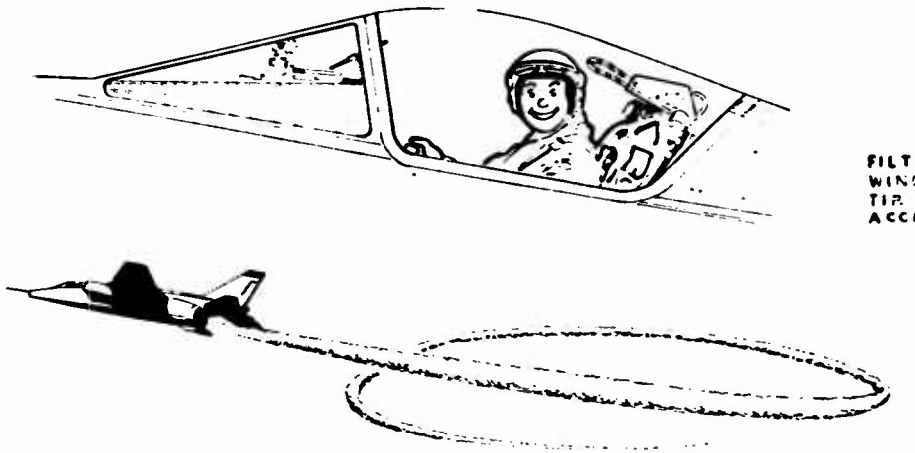

FIG 12 TYPICAL "PULL UP" RESPONSE
AIRCRAFT A

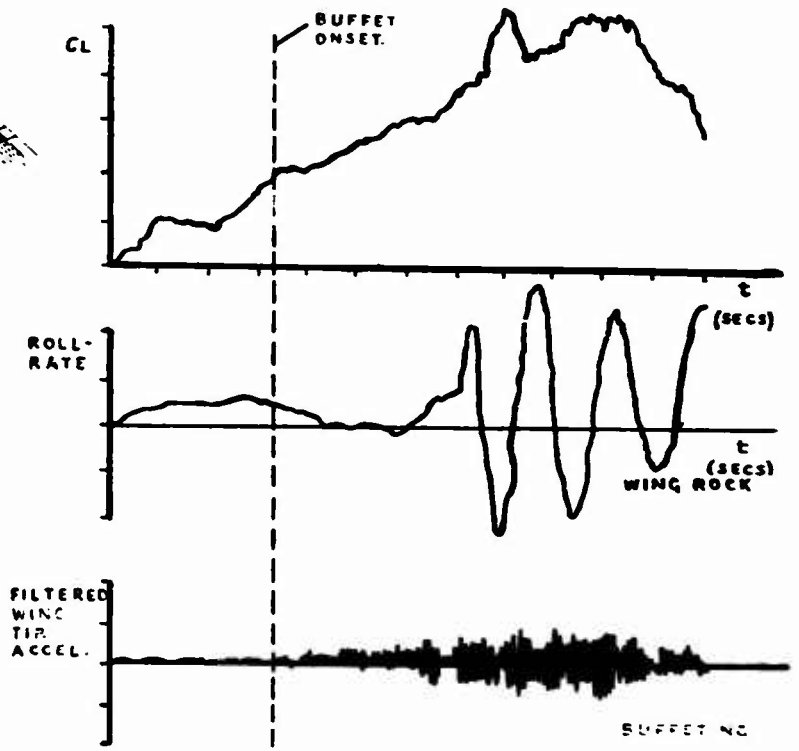

FIG 11 TYPICAL "PULL UP" RESPONSE
AIRCRAFT B

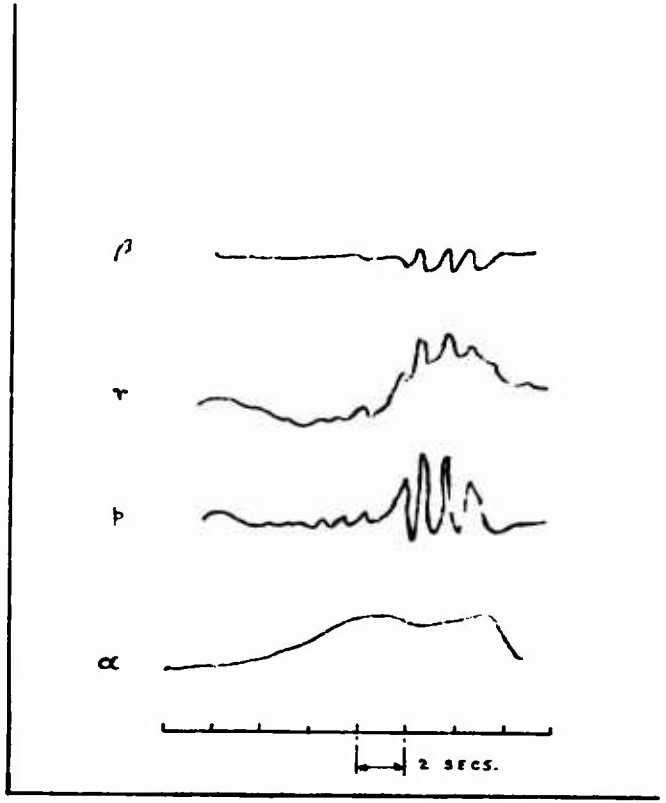

FIG 12 LATERAL DERIVATIVES
AIRCRAFT B

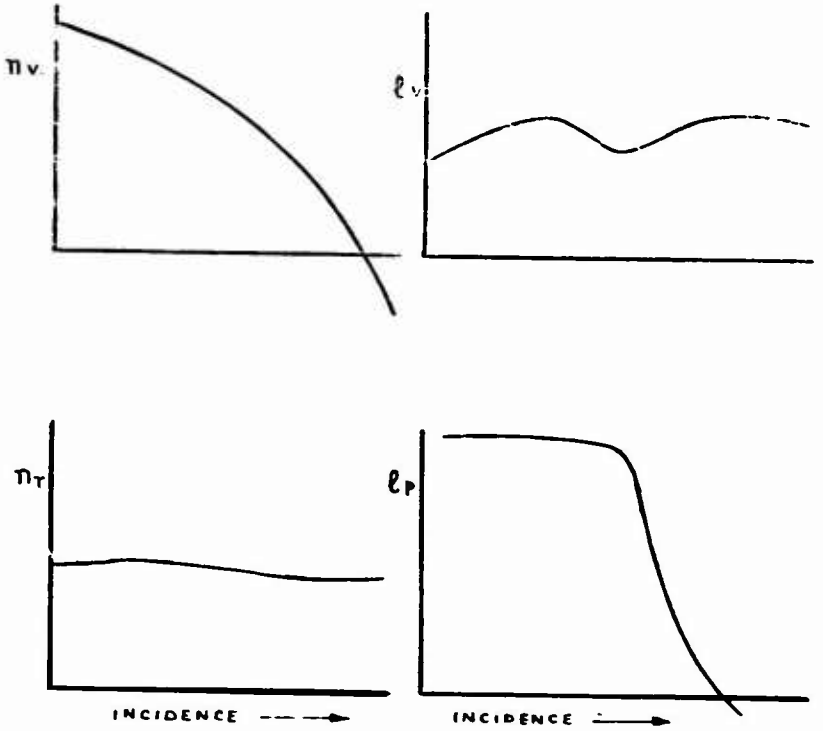

FIG.13.

COMPARISON OF PREDICTED AND FLIGHT "DUTCH ROLL" CHARACTERISTICS AIRCRAFT B

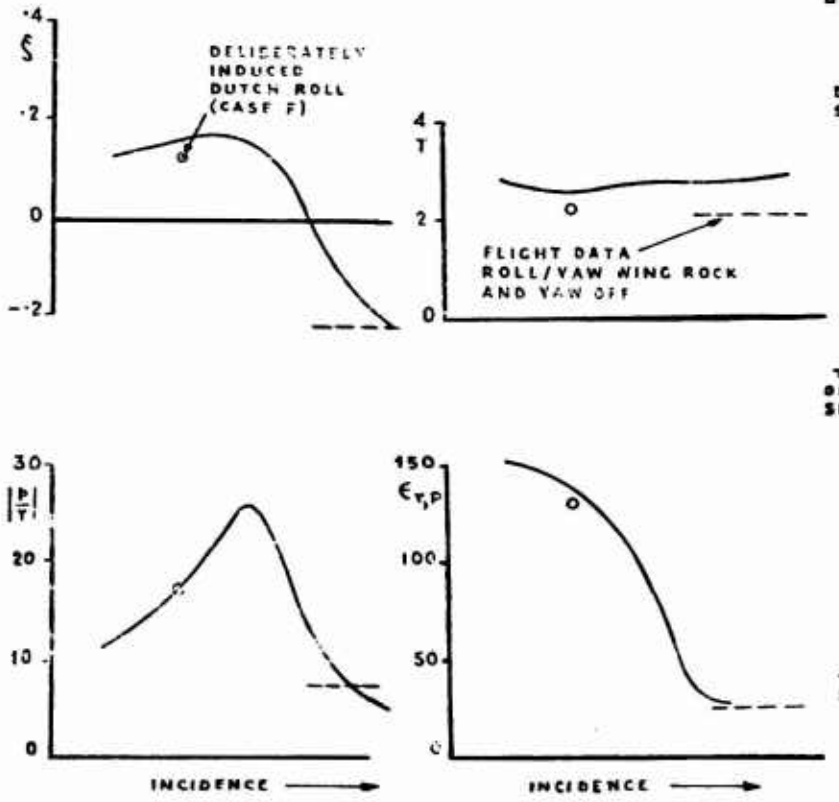

FIG 14 RESPONSE TO RANDOM ROLLING MOMENT — INPUT

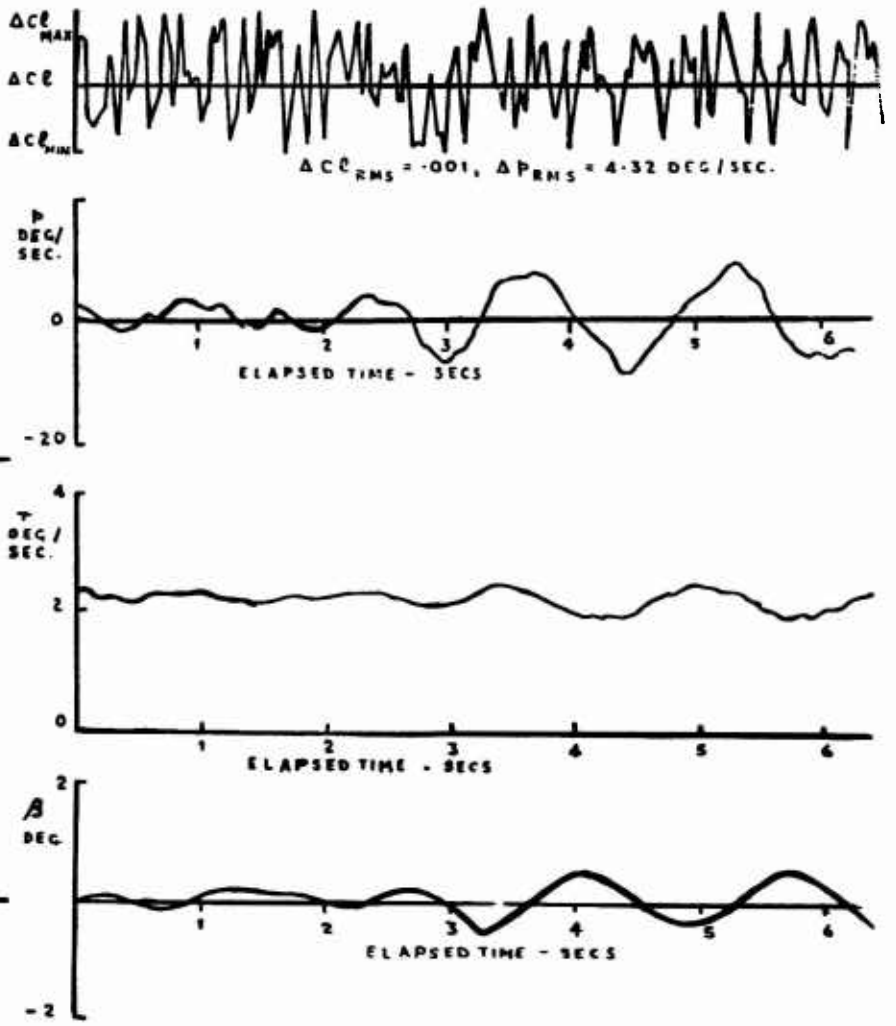

CRITICAL REVIEW OF METHODS TO PREDICT THE BUFFET PENETRATION CAPABILITY OF AIRCRAFT

by

Dr. Helmut John
Messerschmitt-Bölkow-Blohm GmbH, Munich,
Germany

SUMMARY

According to the nature of buffeting as the wing-flexible response to the fluid motion, including exciting forces of separated flow, the most favourable test technique implies the use of dynamically scaled flexible models. Nevertheless, a number of techniques are based on the use of semi-rigid models and yield good results in comparison with flight tests. Methods covered in this critical review are: the possible relation - ship between buffeting intensity and mean loads; the dynamic analysis of unsteady wing root bending moments, and the use of fluctuating pressure measurements to predict the buffet penetration capability of aircraft.

This report contains a survey of methods which are in use in European countries.

NOTATION

c	chord
$\bar{c}$	mean aerodynamic chord
d_n	total damping
f	frequency
g	gravitational constant
k_n	reduced frequency
p	pressure
q	dynamic pressure
s	semispan
x,y,z	coordinates
c_L	lift coefficient
c_M	pitching moment coefficient
c_D	drag coefficient
c_B	Buffeting coefficient
c_p	pressure coefficient
A	aspect ratio
C	stiffness
D	damping
K	transfer function or constant of proportionality
M	mass
M_o	Mach number
P	force
S	wing area
α	incidence

η	fraction of semispan
ϱ	density
σ	strain
ω	circular frequency
Λ	sweep angle

Indices

n	number of mode
r	ratio
TE	trailing edge

Abbreviations

PSD	Power Spectral Density
RMS	Root Mean Square Value
SEP	Specific Excess Power

1 INTRODUCTION

1.1 General

The object of this paper is to present a general survey of methods for predicting the buffet penetration capability of aircraft which are used at present in the various European countries with aeronautical interests. In the past ten years, novel practical techniques have been developed and employed, and it has become necessary to make a critical review of their respective capabilities and of the specific conditions of their use.

The increased attention that is being given to studies of buffet characteristics by aerodynamicists is resulting from the present trend in combat aircraft development. This trend is currently demanding greater manoeuverability in the transonic flight regime. The performance of a transport aircraft and the manoeuvre capability of a combat aircraft can be severely limited by flow seperations on the wing, which causes buffeting and which can be accompanied by a variety of adverse effects, such as, for example, increase in drag, losses in lift and stability, pilot impairment, reduced tracking ability and fatigue problems.

Figure 1 illustrates the influence that these limiting factors can have on the performance of a fighter. This figure also shows the sensitivity of turn rates to typical boundaries at subsonic, transonic and supersonic speeds. The shaded area represents the region where the manoeuvre performance is reduced as a result of buffeting. Figure 1 also includes an agility plot which shows specific excess power (SEP) versus turn rate.

Not only the aerodynamic performance in terms of turn rates or g-levels is affected by buffeting, but also structural aspects need to be considered. In view of the fatigue life of the structure for the pilot in his cockpit environment, for weapons aiming and for systems like gyros etc., knowledge of amplitude ratios, vibration levels and predominant frequencies is of vital necessity for designers, and should be the objective of a project orientated evaluation with high priority.

1.2 Definition of Buffeting and Related Phenomena.

As a consequence of the occurrence of regions of separated flow on the wing at a certain incidence, the performance of an aircraft might be limited either by vibration or by degradation in handling characteristics. To this latter category belong phenomena like "pitch up", "wing dropping", "nose-slice" and "wing rocking". In Figure 2 a comparison of the predicted wing-drop boundary with the moderate buffet boundary is shown for a swing-wing fighter at 25° and 45° degrees of sweep. The estimation is done on the basis of coefficients $c_{n\beta}$ and $c_{n\delta}$, taking the point where in the incidence range at small side slip angles, these coefficients change sign. As can be expected for $\Lambda = 25^{\circ}$, the three boundaries compare very well, due to the 2-dimensional character of the flow. At $\Lambda = 45^{\circ}$ where a "mixed type of flow" is encountered, a more gradual development of separation is to be expected, and the difference between the quoted criteria is obvious, leaving room for speculations up to which boundary the aircraft can be handled.

The highly undesirable rigid body motions of aircraft at incidences above separation onset are referred to in the longitudinal motion as "bouncing", "pitch-up" and "porpoising", while for the lateral motion "wing rocking", "wing dropping" and "nose-slicing" phenomena are known. The phenomena of "pitch-up", "wing-dropping" and "nose-slicing" are relatively well understood, resulting in a deficiency in longitudinal, lateral or directional stability, possibly leading to loss of an aircraft in extreme situations. The phenomena of "bouncing","porpoising" and "wing rocking" are a degradation in handling but not necessarily a limitation to sustained manoeuvres. While "wing bouncing" is typically associated with a rigid body heaving mode of the aircraft for "porpoising" and "wing rocking", an appropiate model is not yet established. It may either be an autonomous oscillation, better known as "limit cycle", in which nonlinear mean aerodynamic forces become significant, or an aerodynamically forced response to fluctuating pressures. There also exists the possibility of a limit cycle oscillation in which the periodic fluctuations in the flow field are coupled deterministically to the motion of the wing. Typically, the motion referred to as "wing rocking" is, as shown in Figure 3, primarily occurring in the roll-rate trace at frequencies lower than those associated with airframe flexible response in a fluctuating rigid body motion. Therefore, those phenomena of the second category belong to the flight mechanical problem area, and do have a direct effect on controllability and the ability to hold an accurate flight path. Phenomena of the first category, mentioned above, and which are associated with flexible modes of the aircraft structure can be said to influence "ride quality", and are referred to as "flight in turbulence" and "buffeting". The difference between turbulence and buffet is given by the basic difference of the driving force, while the structural behaviour of the elastic system is the same. The driving force of turbulence is embedded in the on-coming free air-stream and can be defined by a finite wave length and spectrum. Turbulence, therefore, can be encountered at any incidence and flight condition.

Any elastic system fed with energy is subject to instabilities, and for an aircraft in flight, the energy is provided by the propulsion system which maintains the relative airflow around the exposed components of the aircraft. The instability

phenomenon of the structure is known as "flutter". The instability phenomenon of the relative airflow is associated with separation and produces the driving forces known as buffet, while buffeting is the flexible response to the fluid motion. The vibration level or buffeting intensity, defined by local accelerations or displacements at either natural or forced frequencies, is the result of the perturbation of the system and the energy loss of the oscillating component due to damping. If the energy gain is larger than the damping forces, a rapid failure of the structure will occur, and the integrity of the structure will be lost.

An excellent survey of the phenomena discussed above, is given by Jones (1), wherein theoretical models and differential equations in use are also discussed.

This present report concentrates on wing buffeting at transonic speeds only.

1.3 Theoretical Aspects

Of major importance in buffeting investigations are aerodynamic disturbances that produce driving forces for the airframe structural response, called buffeting, which finally establishes the attained vibration level. Theoretical structural models defining the dynamic properties of the structure have been used for years to provide informations on flutter speeds and gust analysis. Starting from stiffness and mass distributions, the so-called modal analysis allows the calculation of natural frequencies, mode shapes and generalized masses. Those results can be compared and corrected using ground vibration tests.

With regard to buffet forces, the situation is completely different. The presence of any sizable separated flow region provides a strong and sufficient energy source for airframe disturbance. The flow field around wings becomes extremely complex in the transonic flight regime, when complicated shock systems interact with the viscous flow field. The influence on separation can be very dominant if the shock strength is sufficiently large to cause a bubble-type separation, which is known as shock-induced separation. Regions of mixed vortex flow with embedded separated areas and unstable shock waves that are present in a 3-dimensional wing flow field at transonic speeds, form the greatest difficulties in describing and defining a precise flow model. Therefore, nearly all investigations involve wind tunnel tests to predict buffet forces.

1.4 Objectives

Because of the complexity of the buffet problem, considerable emphasis is placed on test techniques to obtain various types of wind tunnel data. The target is to provide buffeting boundaries for designers to establish the performance of the aircraft and to produce information about buffeting loads for stressing purposes.

Typical results of buffeting boundaries for a fighter and a transport aircraft are shown in Figure 4. For the fighter, boundaries are defined by buffet onset, which corresponds to the first indication of boundary layer separation. Light buffeting or pilot's onset is defined by the first appearance of a sizable vibration. Moderate buffeting can be said to represent a boundary for a stable weapon platform or a limit for pilot's impairment. Above a boundary, defined by heavy buffeting, the integrity of the aircraft structure is questionable. For a fighter aircraft, the margin to moderate buffeting represents the manoeuvrability in terms of a "n.g" instantaneous pull up or in turn rates (see Figure 1).

With regard to a transport aircraft, a 1.3 g separation from buffet onset to cover light manoeuvres defines the cruise altitude and thus influences the performance of the aircraft considerably. During a normal cruise, the aircraft may encounter a strong gust which carries the aircraft beyond the buffet threshold. Therefore, a 1,6 g separation from maximum penetration, or a definite gust velocity -- for example a normal velocity of 12.5 m/s and a corresponding wave length of 33 m -- must be applied to provide a safety margin for the aircraft structure.

This information can be provided from wind tunnel tests using normal semi-rigid models. The application, however, of the wind tunnel data to establish local buffet loads, vibration levels at any station of the aircraft, predominant frequencies and amplitude ratios for the full scale aircraft, requires some means of accounting for the effects of flight Reynolds number and aircraft structural response, effects which can only be simulated adequately during a wind tunnel test by use of dynamically scaled full aeroelastic models in high density tunnels. In this case, it would be necessary only to record vibration levels via accelerometers at points of interest, and extrapolate the results for the full scale aircraft using similarity rules. Such tests have been performed in the USA by P.W. Hanson (2), Langley Research Center, on a F-111 type model. Although the tests mentioned are done in the USA, one main point is taken from this report, and that is the extrapolation formula, as shown in Figure 5. As mentioned in the report by Hanson (2), parameters k_{n_r}, d_{n_r} and $\left[c_{L,n}\,(k_n)\right]_r$ should be unity. Small differences in structural or aerodynamic damping can produce differences in the comparison of aircraft to model response. These quantities must be monitored carefully. This statement is one of the central themes in this paper.

It is not clear whether such a model can be designed in Europe in the near future. The problems involved are the design and construction of a model that can withstand large static and dynamic loads at high incidences and high wind tunnel shut down loads. Furthermore, such models are expensive and not readily available.

For these reasons, nearly all European techniques are based on the use of semi-rigid models, and include flight-tunnel correlation factors. Methods covered in this critical review are discussed in subsequent chapters.

2 PREDICTION OF BUFFETING INTENSITY ON THE BASIS OF MEAN AERODYNAMIC LOADS

2.1 Principle

The earliest concepts of deriving buffeting boundaries from normal wind tunnel tests with some reliability were developed by Pearcey and Holder (3, 4). The principles for these methods are derived from the close study of buffeting characteristics of different aircraft in comparison to wind tunnel tests. The conclusion was that the most frequent cause of buffeting is not a localized response to fluctuating pressures, but the result of the direct effects which any kind of separation on a wing exerts on the total loading. The effects on mean loads are, in turn, closely connected with the variation of mean pressure at the trailing-edge through the wing circulation.

The mechanism acting on an airfoil or a wing can be described in brief as follows: if separation on the upper surface of the wing -- due to leading edge, trailing-edge, or shock induced separation, whichever first occurs at relevant Mach number and incidence -- has developed sufficiently to thicken the boundary layer at the trailing-edge position and hence does influence the wake, a rapid fall in pressure on the upper trailing-edge will happen. However, on the lower surface there are no comparable changes in the viscous flow that can give the reduced pressure and that would be necessary on the two sides of the wake, because the wake cannot, in general, support a pressure difference across it. The same pressure as on the upper edge can, in fact, only be achieved by a reduction in circulation. Such a change does provide increased velocities and decreased pressures over the whole lower surface.

Accordingly, the assumption taken by Pearcey and Holder (3, 4) is that the unsteady loads triggered by separation are proportional to the change of the mean aerodynamic loading, i. e., the loss in lift compared to the linear variation with incidence for attached flow as indicated in Figure 6. Locally, the onset of unsteadiness can be derived from the rapid divergence of the trailing-edge pressure compared to the linear variation for attached flow as shown in Figure 6.

The driving buffet force is defined by a lift loss Δc_L or a mean trailing-edge pressure divergence Δc_{PTE}. Structurally, the assumption is made that the aircraft can be treated in a rigid body heaving mode, or that most of the aircraft behave very similar in their elastic response characteristic to a certain degree of excitation, and that the buffeting intensity can be obtained by calibration from flight tests.

2.2 Analysis

2.2.1 Kinkology

Following the hypothesis of Pearcey an Holder (3, 4), outlined above, kinks -- defined by slope changes, rather than by arbitrary irregularities -- in the slope of c_L or c_M versus incidence, are used:

to estimate for

1. Kink = buffet onset
2. Kink = Moderate buffet (2.1)
3. Kink = Heavy buffet

A justification for using the second kink to define moderate buffeting is proven by the fact that the separated flow often rolls up into a vortex. As soon as the vortex influences a sufficient large portion of the wing due to the accompanying lift loss or due to a backward shift of the local c. p. position, either a pitch up or pitch down c_M - kink occurs, which also results in a sudden increase in drag. Thus, the variation in axial force versus α or c_L also can be used as an indication. Figure 7 shows a typical example for those kinks. Although the second kink does not allow the establishment of a quantitative value for buffeting intensities, it gives, in many cases, good correlation to pilot's opinion. It appears that in those cases, the severity of buffeting is not the limiting factor, so that pilot's tend to fly right up to a handling boundary, such as pitch up or wing dropping, which are likely to occur beyond the second kink, as already discussed (see Figure 1).

2.2.2 Simplified Buffet Response Calculation

In Reference (5) C.L. Bore postulates that buffet response is to be measured by peak acceleration (B.g)* suffered by the mass of the aircraft and the fluctuating forces causing buffeting are taken to be proportional to the decrement of lift coefficient as outlined in para 2.1. The expected intensity of buffet response can be estimated from the simple formula

$$B = K \cdot c_B \Big/ \frac{W}{q \cdot S} \qquad (2.2)$$

using the equivalence $\Delta c_L = c_B$, as shown in Figure 8 a, where W is the aircraft weight, S is wing area, q is dynamic pressure and K is the constant of proportionality.

The peak acceleration criteria used for various degrees of buffeting are as follows:

Buffet onset	$B \rightarrow 0$ negligible	
light	$B = \pm$ 0.2 g peak to peak	
moderate	$B = \pm$ 0.6 g " " "	(2.3)
heavy	$B = \pm$ 1.0 g " " "	

Correlations are presented in Reference (5); an example is shown in Figure 8 b for the Harrier GR1. For this airplane, K = 1 has been found satisfactory. Bore's method does not take into account either the effects of aerodynamic damping or of wing elasticity. The fluctuating force is representing a total aerodynamic force independent of wing motion, and the aircraft response is calculated on the basis of a rigid-body heaving mode.

The analysis presented by Jones (1), which starts from the differential equation for the heaving mode, proves that under certain conditions a heaving response calculation is appropriate. This is possible only when the heaving motion contributes significantly to pilots' impairment, for example, at positions very close to bending nodes at frequencies of 1 - 10 Hz. Then the effect of aerodynamic damping is negligible and vibration intensities satisfy the equation given by Bore (5). Consequently the response is directly proportional to the excitation and likewise to q. Thus at constant true airspeed the response varies linearly with air density ϱ (see Figure 8 b).

2.2.3 Method Based on Trailing-Edge Pressure Divergence

The first suggestion that trailing-edge pressure divergence may be used to predict buffet loads was made by J.C. Winnpenny in the discussion of the paper, Ref. (4). An attempt to predict buffet onset from a divergence of $\Delta c_{p_{TE}} = 0{,}04 - 0{,}05$ at a semispan position of $\eta = 0.85$ is certainly too simplified. Husk (6) shows good comparisons, but this is obviously only true for wings that are designed using the same principles. In Figure 9 an example is shown, but the comparison is poor.

A better approach is proposed by Bore (7). The method is based on an analogy of a buffet force coefficient with the normal force coefficient giving:

$$c_N = \frac{N}{q \cdot S} = \frac{1}{0.7 \cdot M_o^2} \frac{n \cdot W}{p_o \cdot S}$$

$$c_B = \frac{B}{q \cdot S} = \frac{1}{0.7 \cdot M_o^2} \frac{b \cdot W}{p_o \cdot S} \qquad (2.4)$$

Where N is the normal force, B is the peak oscillatory normal force; $(n.g)^{*)}$ is normal acceleration and $(b.g)^{*)}$ is the peak oscillatory acceleration. Taking a number of simplifying assumption, Bore used this equation,

$$c_B = \int_0^1 \Delta c_{p_{TE}} \cdot \frac{c}{\bar{c}} \cdot d\eta \qquad (2.5)$$

which is a strip-theory analogy to the steady flow relations-ship. The integral can be evaluated graphically for given values of α, and M_o and c_B can be cross-plotted in a c_L against M_o diagramm.

---

* Read: B in fractions of gravitational constant.

*)Read: n or b in fractions of the gravitational constant.

Values for B can then be calculated by the use of equation (2.2). As outlined for equation (2.3) moderate buffeting is then attributed to a value of B = ± 0.6. A schematic example is shown in Figure 10. In applying this method, care must be taken to allow for all the exceptions that can influence the trailing-edge pressure, such as the presence of supersonic flow at the trailing-edge or vortices, which is described in more detail in Ref. (3).

Reliable buffet loads can not be obtained by either of these methods presented in paragraph 2.2.

2.3 Critical Remarks

The methods discussed are a good first approach for defining buffeting boundaries, especially in the lower Mach number area and in cases where no other information is available. Also, in cases where a 2-dimensional type of flow is predominant, the results will be good, because there is almost no margin between buffet onset, moderate buffet and c_{Lmax}. Limitations come in at higher Mach numbers, and in cases where assumptions taken for the dynamic characteristic of the structure are no longer valid.

The following main problems can be defined:

1. The determination of buffet onset on the basis of kinks often leads to too optimistic results. This observation is in accordance with recent experiments of Ray and Taylor (8) on a large number of wings. A possible explanation is that the initial onset of separation that causes a lift loss on one area may be compensated by an increase in lift resulting from a sudden extent of a local supersonic region in an other area of the wing (see Figure 11).

2. If the flow separation starts at the leading edge and extents slowly downstream, then it is obvious that trailing-edge pressure divergence and lift loss due to an overall change in circulation will occur significantly later than buffet onset.

3. Bore's assumption that the aircraft can be treated in its rigid body heaving mode is a limitation which can be adopted only for small fighters with low aspect ratio wings. It must be clearly stated that the elastic behaviour of the structure and the effect of damping can not be neglected in establishing vibration levels. This can be seen from theoretical considerations that in cases where aerodynamic damping is dominant in one mode, then the attained vibration level should be proportional to $\sqrt{\varrho}$ of air density and not directly to ϱ as would result from equation (2.2). But there is a possibility to replace the constant K of equation (2.2) by a transfer function, which will allow the inclusion of such a dependency on damping.

2.4 Theoretical Methods

Following the principles outlined in paragraph 2.1, Pearcey and Holder (3) proposed a procedure for calculating the buffet onset boundary. The first successful attempt to evaluate transonic buffet limits in a theoretical approach was reported by Thomas (9). Thomas predicted buffet onset assuming that it occurs when shock position and separation - only rear separation can be treated - coincide. According to the availability of theoretical methods, including shocks, Thomas applied only two-dimensional methods. Recently an extension to sheared wing flow was presented by Redeker (10). The application of these methods is limited to wings with a predominant 2-dimensional flow.

A disadvantage in the use of the above methods is that they predict rather large Reynolds number increments in cases where wind tunnel results show little or no influence of Reynolds number. The assumption of Thomas and Redeker (10) that there exists a linear relationship between buffet and the region of separated flow is obviously no longer valid at high Mach numbers and for small thickness ratios.

Since it is, at present, impossible to calculate boundary layer and exciting forces for separated flow, it is impossible to evaluate buffeting intensities.

3. Prediction of Buffeting Intensity on the Basis of the Dynamic Response of Semi-Rigid Models

3.1 Principle

Since buffeting is the dynamic response to an unsteady load, a number of dynamic test techniques and evaluation procedures have been developed during the last few years. Huston (11) suggested a method for predicting the onset of buffeting and flight buffeting loads from measurements of unsteady wing root bending strain performed on semi-rigid wind tunnel models. In order to obtain unsteady wing root bending moments, strain gauges are cemented near the root of the wing on the flexural axis. The method assumes that the reduced frequency of the wing fundamental bending mode is about the same for model and aircraft.

$$f \cdot c_{model} = f \cdot c_{aircraft} \qquad (3.1)$$

Normally on a model, this mode is only slightly damped. Therefore, about 80 % of the total RMS of the wing root bending strain is concentrated near this frequency and can be easily analyzed. During a normal test run, the wing root strain signal is recorded and filtered on the basic mode to eliminate influences of the rigging system. *) RMS values can be generated either on line to monitor the test, or after the tests using digital computers, if more and more accurate information is wanted. In Figure 12 a typical plot of the RMS value of the wing root bending strain versus incidence is shown. Up to a certain incidence, $\sqrt{\sigma^2}$ is nearly constant, and from the incidence of buffet onset onward, the signal is rising, comparable to the divergence of trailing-edge pressure.

In this way, buffeting tests can be made simultaneously with conventional force measurements. This method is generally accepted as the most consistent and reliable method of assessing buffet onset from model tests (12, 13, 14). Many flight/tunnel comparisons of buffet onset are available (12, 13, 15). The correlation is in general good to fair, and the method is widely used for comparative tests during the early stages of project studies or for wing design purposes. In order to obtain information about the severity of buffeting, which is closely connected to the post separation onset behaviour of the flow over the wing and the dynamic response of the structure to this excitation, one is left with the problem of scaling the buffeting loads from the model to the aircraft. This problem is difficult to solve because it involves the correct knowledge of the excitation and the transfer function of the elastic system in terms of their quantitative values. In an early stage of a project, this information is not available.

One attempt to overcome those problems is to by-pass the uncertainties and to use the buffeting measurements on semi-rigid models and derive dimensionless buffeting coefficients, and correlate them directly with buffet penetration achieved in flight. Such a method has been developed and presented by Mabey (15), and is in common use in Europe for estimating the buffet penetration capability of aircraft.

3.2 Description of the Mabey Technique

The unsteady RMS value of the wing root strain signal, filtered around the wing fundamental frequency is divided by the dynamic pressure q to give values of

$$c_B\ (\alpha) = \sqrt{\sigma^2}/q \qquad (3.2)$$

which can be plotted against incidence at a given Mach number, (see Figure 12). Mabey assumes that there is a substantial range of incidence at the lower test Mach numbers for which the flow over the wing is attached and for which c_B is constant. This value is denoted c_{Bo}, and can be related to the tunnel flow unsteadiness parameter $\sqrt{n \cdot F(n)}$ * at the appropriate Mach number and frequency. The basic hypothesis of Mabey is that $\sqrt{n \cdot F(n)}$ is the exciting force to c_{Bo}, and can be used for calibration, thus it can be written.

$$c_{Bo} = K \cdot \sqrt{n \cdot F(n)} \qquad (3.3)$$

A dimensionless coefficient can then be obtained

$$c'_B\ (\alpha) = \frac{1}{K} \cdot c_B\ (\alpha) \qquad (3.4)$$

and the relation exists

$$c'_{Bo} = c_{Bo/K} = \sqrt{n \cdot F(n)} \qquad (3.5)$$

This evaluation implies that a certain tunnel unsteadiness is necessary, and that the tunnel used must be calibrated with respect to $\sqrt{n \cdot F(n)}$. A typical variation of this quantity with Mach number at constant frequency is plotted in Figure 13. The buffeting coefficient $c'_B\ (\alpha)$ is a direct measure of the generalized force acting in the wing fundamental mode due to any distribution of pressure fluctuations on the wing. The scaling factor K can be regarded as a transfer function representing the dynamic behaviour of the structure in the wing fundamental mode. K is, of course, different for every model and depends on mass, stiffness distribution and total damping of the fundamental wing mode and on details of the instrumentation. Mabey assumes that K is invariant with Mach number. At higher Mach numbers. when even at α = 0 some separation on the wing can occur, c'_{Bo} will show an increase relative to $\sqrt{n \cdot F(n)}$ (compare Figure 14) but until then, the two curves should be similar, and it is recommended to check the trend with Mach number.

*) for example the sting heaving mode.

* $\sqrt{n \cdot F(n)} = \frac{\bar{p}}{q} \cdot \sqrt{\varepsilon}$; $\bar{p}$ = unsteadiness in pressure

$\varepsilon = \Delta f / f$ analyzer bandwidth

In order to achieve a coefficient $c''_B = 0$, which corresponds to buffet onset, a reduction to

$$c''_B\ (\alpha) = \sqrt{c'^2_B\ (\alpha) - n \cdot F\ (n)} \qquad (3.6)$$

is proposed by Mabey; however, this is often ill defined, due to a premature creep in the variation of c_B with incidence prior to the rapid build-up of buffet. In order to prove the validity of his method, Mabey has performed a number of tests on a variety of research models at different scale, but always the same planform geometry. The models were built from different material, and had different values for total damping and fundamental frequencies. They were tested at different levels of tunnel unsteadiness but at the same Reynolds number, and he obtained almost the same buffeting coefficients. Mabey then proposed on the basis of flight-tunnel comparisons and based on pilots' opinion, that for any aircraft one can plot c_L against Mach number boundaries defined by:

Mabey criteria

Fighters		Transport aircraft	
$c''_B = 0$	buffet onset	$c''_B = 0$	buffet onset
$c''_B = 0{,}004$	light buffeting	$c''_B = 0{,}006$	max. penetration
$c''_B = 0{,}008$	moderate "		
$c''_B = 0{,}016$	heavy "		

A typical comparison is shown in Figure 15. The poor correlation at $M = 0.6$ and above can be due to a number of reasons; they are not discussed by Mabey.

The application of the discussed method involves a number of assumptions, and some recommendations are given in Ref. (15), which should be followed to obtain conclusive results. The extrapolation of buffet loads for the full scale aircraft on the basis of buffeting coefficients is explained in Ref. (1), or classical methods (11, 14, 16) can be applied.

A surprising fact in the correlation established by Mabey is that the buffeting boundaries can be obtained in most cases by a dimensionless buffeting coefficient. In these cases it is obviously not necessary to evaluate dimensional local accelerations by use of mode shape factors, nodal line position, generalized masses and damping, although it is doubted that those parameters can be neglected completely. Some "theories" exist with regard to this phenomenon: The most simple one is that nearly all aircraft behave structurally very similiar due to the fact that flutter specialists have carefully designed the structure to the same common principles in order to obtain flutter speeds well outside the flight envelope. The numbers presented in equation (3.7) thus include most of the structural particularities. The difference between maximum penetration of a fighter and of a transport aircraft already accounts for the fact that a pilot on a transport aircraft is more off the nodal line of the fuselage than on a fighter.

Since the dimensionless buffeting coefficient represents a generalized aerodynamic excitation, it is, in any case, possible to produce design charts which show at least trends of the influence on aerodynamic excitation of the main design parameters like section form, sweep back, wing form, wing thickness, and possible improvements by use of manoeuvre slats and /or flaps. Such design charts can well assist the designer in his early project evaluation. A typical example of the influence of sweep on buffeting contours of a swing wing fighter is shown in Figure 16 and of the increments due to well designed manoeuvre slats in Figure 17.

3.3 Critical Remarks

Tunnel results obtained by this method are, in general, good to fair and extremely useful for project studies and comparative tests. The problems associated with the use of the Mabey technique are those which either result from models and the tunnel, or which are by-passed by using statistical correlations and pilots' opinion:

1. Sometimes poor repeatability must be stated. Whether or not this is due to differences in rigging or differences in transition fixing is unclear.

2. Establishing an appropriate K-factor at higher Mach numbers and/or in cases where c'_{Bo} and $\sqrt{n \cdot F\ (n)}$ do not show a unique trend, causes considerable difficulties.

3. The imperfections of the model structure can have a negative influence on results. Large changes in mid frequency (see Figure 18) can be reported, which causes problems in establishing proper RMS values. The resulting c''_B is extremely spiky and shows an irregular variation with incidence. Plateaus, spikes and predivergence creep etc., cause considerable difficulties in the interpretation.

4. On a model, one will find purely structural damping. Imperfections of the model, like a large number of joints, can result in a variation of structural damping with either static or dynamic load (see Figure 18). Since the variation of structural damping on those models which form the basis of Mabeys tunnel-flight correlation is not known, it is unclear whether results obtained with varying damping must be corrected or not.

5. In flight, most of the buffeting at the pilot's station, (see Ref. 2), is in second and third structural modes, because the total damping in those modes is smaller than for the first wing bending mode. This fact casts some doubt on the assumption of Mabey that there exists a linear correlation of intensities between pilot's station and the wing root fundamental bending strain. In cases where unstable shocks at frequencies outside natural ones produce large amounts of energy, a forced mode can be established. This effect can even be found on semi-rigid models, as is shown in Figure 19. This forced mode is however not taken into account by the Mabey technique due to the application of a filter around the fundamental mode.

4. Methods Using Fluctuating Pressure Measurements

4.1 Principle

Methods discussed so far give relatively good results about exciting forces, but the structural problems are either oversimplified or by-passed by using statistical correlations. Thus the extrapolation to the full scale aircraft is in many cases questionable. There are two fundamentally different methods of predicting the buffeting intensity composed from the main modes starting from wind tunnel measurements on models. The first one uses dynamically scaled aeroelastic models. This has been discussed already in paragraph 1.4. The second one starts from measurements of the pressure fluctuations on a semi-rigid model and then calculates the dynamic response, when these pressures act on the flexible structure. A survey of the problems involved in this second possibility of an approach is given by Moss (17). The first attempt to perform such calculations was done by Mitchell (18) on a Concorde type of wing. No flight to calculation comparison has been published by Mitchell.

A detailed analysis of the different possible concepts for this approach is given by Jones (1). According to the principles outlined by Jones, the difficulty that arises is encountered in the difference in dynamics of the structure of a quasi-rigid wing (model), having small amplitudes only and in the full scale aircraft having rather large amplitudes at buffeting conditions. Two main cases can be distinguished:

1. Forced vibration model

   This consists of random pressure fluctuations, which are independent of wing motion. The motion in turn produces an additional pressure field (oscillating pressures), which provides the aerodynamic damping. The appropriate model is "nonautonomous" and a linear analytical formulation is adequate.

2. Non-linear flutter model

   Here the driving forces depend in a deterministic way on the motion of the wing. The appropriate model is "autonomous" and a nonlinear analytical formulation is essential.

The main problem that arises for the theoretical approach is the fact that the transition from the first case to the second is fluent, and the amplitude of the wing motion is a relevant parameter.

4.2 Theoretical Model and Assumptions

A software package for the application of PSD concepts for buffeting analysis is presently under development in Germany, and is monitored by the author (19, 25). Details of the recording system and the equations used can be taken from Ref. (19, 25). A brief verbal description is presented here only, due to the rather complicated equations; on the other hand there is nothing new about the application of statistical concepts, like correlation functions, power spectral density (PSD) and RMS values in aerodynamics.

A linear theory, the so-called "forced vibration model", (see Figure 20) has been adopted to be applied in the area up to moderate buffeting only, assuming that on the aircraft up to this limit the amplitude of the wing motion is small (see above). The calculation is starting from the differential equation of motion

$$M \cdot \ddot{x} + D \cdot \dot{x} + C \cdot x = P_{\ddot{x}} + P_{\dot{x}} + P_{x} + P_{Buffet}, \qquad (4.1)$$

where the left hand side represents the structure and the right one the aerodynamic quantities. M is the equivalent mass, D a viscous damping, C the stiffness, x the amplitude and the dotes the derivatives with time. P with index is the appropriate aerodynamic force and P_{Buffet} represents the exciting force due to buffet. The structural model is equivalent to those used for gust response calculations. The

solution of equa. (4.1) is, therefore, well known and typically reported in (19,24).

For a semi-rigid model, the assumption can be made that the amplitudes are negligibly small, so that buffet forces are acting on the surface only, which can be recorded via dynamic pressure pick-ups. For the investigation, fluctuating pressures have been recorded using a 5th scale half model, as shown in Figure 21. A half model was selected to provide sufficient thickness for installing the total equipment, as there was: 44 static pressure tappings, 19 unsteady pressure pick-ups, 6 accelerometers and a wing root strain gauge. The following pictures will show some typical results. In general, it can be stated that the power spectral density is flat, dropping at a distinct frequency (see Figure 22). In cases where unstable shocks appear, the spectrum is showing a local maximum, and the accelerometers indicate a forced mode at this frequency, often near the natural torsion mode (see Figure 23 and 19). In Figure 27 a comparison is shown of normalized PSD-plots of unsteady pressures taken at different Reynolds numbers, which have been recorded during a test phase in the 8' x 8' RAE pressurized tunnel. This figure shows a clear trend, but it is difficult to judge the overall trend from those records, because there is no unique trend for all stations.

Using pre-established mode shapes for a number of natural frequencies, generalized forces can be generated using such records. The next step is to calculate autocorrelation and cross-correlationfunctions for use with the structural model. As a final result, power spectral densities of local accelerations in fractions of the gravitational constant can be obtained at any station of the aircraft. From the response calculation at the station of the pilot, an assessment of the pilot's impairment can be achieved using the ISO-Standard method (20). Another approach to assess the pilot's limitations is to accummulate signals of the different frequencies using weight factors for different frequencies according to Ref. (20) and calculate a total RMS buffeting acceleration. This value can be transformed to a peak-to-peak normal buffeting acceleration, using a criterium according to equation (2.3), buffeting boundaries can be established. Three typical results of local PSD plots -- at wing tip, strain gauge position and pilots seat --are to be seen in Figures 24, 25, 26.

Up to now, the calculations are simplified insofar as a wing-body combination can be treated only.

The brief description given above does already indicate that an extensive computation effort is needed. Hence, a limited number of measurements and calculations are available only.

4.3 Damping

For the final calculation, oscillating pressures due to the motion of the wing and denoted in equa. (4.1) $P_{\ddot{x}}$, $P_{\dot{x}}$, P_x, must be introduced, and a number for the structural damping of each mode, must be adopted. For the investigations mentioned above, the structural damping is varied between 3 % and 5 %, and can be finally assessed from ground vibration tests of the aircraft. Oscillating pressures are calculated according to a method described by Laschka (21) assuming attached flow. The aerodynamic damping, as obtained by theory for attached flow, is considered to be linear; that means the coefficient of damping is a constant for all amplitudes of oscillation.

Flight test results performed recently by Jones (22) on a fighter aircraft indicate, as can be seen from Figure 28, a large variation of "apparent" damping in the wing fundamental mode with incidence. Test results reported by Rainey (23) on harmonically excited models also show a variation with incidence, although not to the same extent as given in Figure 28. When it is recalled that the increase occurs beyond buffet onset where steady force coefficients are also nonlinear, it is unlikely that the assumption of linear characteristics during buffeting will be valid. Thus, the calculation will be pessimistic with regard to the fundamental wing mode.

4.4 Remarks

Up to now, only theoretical approaches and discussions are published. Mitchell (18) has never circulated results of Concorde flight tests. The lack of correlation information with which one could obtain the accuracy of the method is certainly a disadvantage. On the other hand, it is obvious that measured pressure fluctuations on a structurally responding wing - as on a flying aircraft - are difficult to interpret on a quantitative basis, owing to mutual cancellation of aerodynamic excitation and aerodynamic forces at the natural frequency of wing motion. Thus, vibration levels and buffeting design loads can be correlated only.

Due to a number of uncertainties and simplifications, some short comings must be expected. Nevertheless one can perform a number of comparative studies in a parametric way and gain in experience about the behaviour of an aircraft beyond the buffet boundary. An example of such a comparative calculation, wherein the influence of wing fuel on buffeting was studied (see Ref. 25), is shown in Figure 29. The result presented in Figure 29 gives an indication about the scatter which can be expected from fight tests depending on the amount of fuel carried in the wing.

5. Conclusions and Objectives for Future Research Work

Several methods -- for some various techniques of analysis - - are thus available to the specialist interested in buffeting information. Particular considerations in each case will guide the individual choice: availability of models or appropriate tunnels and means of analysis.

The most favourable, but most expensive test technique implies obviously the use of dynamically scaled flexible models. The required information, however, will come relatively late in a project stage and will not influence the configuration directly. For early design phases and comparative tests on alternative wing designs, the application of the Mabey technique is recommended. The extensive computing facilities that are needed to obtain buffeting levels and loads using the PSD-concept will limit this method to an application for check out in critical areas or for specific design problems only. The relation between buffeting intensities and mean loads is restricted to relatively rigid aircraft. An extension to include dynamic response characteristics of the structure is wanted.

Of major importance for all methods discussed is the influence of damping on the attained vibration level. It is recommended, therefore, to monitor the possible variation of damping with incidence on models and on aircraft to provide detailed information and means of correlation. More research work is wanted in this area to eliminate contradictory conclusions.

For many years it is known that separation has a derogatory effect on aircraft performance. Therefore, much effort has been concentrated on improving theoretical methods of wing design to avoid early separation. Possibilities to control the growth of separation beyond buffet onset and to obtain by such means a more gradual development of buffet forces with incidence, are not studied in sufficient depth. Most of our knowledge about fences, notches, vortex generators etc., has been obtained through trial and error and has proven to be successful. As there is an increased trend toward the use of fluctuating pressure measurements for the study of buffeting, a research program should be initiated to investigate means of controlling the growth of separation. This would help to put our understanding of the phenomenon on a firmer footing.

Furthermore, high Reynolds number test facilities are needed to eliminate the uncertainties which arise in the extrapolation to the full scale flow conditions.

Finally it must be stated here that a method to predict tail buffeting loads in turbulent wake flow is practically nonexistent.

6. References

1. Jones, J.G. — A Survey of the Dynamic Analysis of Buffeting and Related Phenomena. RAE Tech. Rep. 72197, 1973

2. Hanson, P.W. — Evaluation of an Aeroelastic Model Technique for Predicting Airplane Buffet Loads. NASA-TND-7066, 1973

3. Pearcey, H.H. Holder, D.W. — Simple Methods for the Prediction of Wing Buffeting from Bubble Type Separation. NPL Aero Rep. 1024; ARC 23,884, 1962

4. Pearcey, H.H. — A Method for the Prediction of the Onset of Buffeting and other Separation Effects from Wind Tunnel Tests on Rigid Models. AGARD Rep. 223, ARC Rep. 20,631, 1958

5. Bore, C.L. — Post-Stall Aerodynamics of the Harrier GR1. AGARD-CP-102, Paper 19 "Fluid Dynamics of Aircraft Stalling", 1972

6. Husk, D.I. — The Influence of Major Design Parameters upon Buffet Boundaries of a Wing. Paper Presented at the 14th AGARD Meeting of Structures and Materials Panel, Paris 1962

7. Bore, C.L. — Estimation of Buffet Boundaries Using Wind Tunnel Trailing Edge Pressure Measurements. Unpublished Work at Hawker Aircraft Ltd., 1962 Description included in Ref.

8. Ray, E.G. Taylor, R.T. — Buffet and Static Aerodynamic Characteristics of a Systematic Series of Wings Determined from a Subsonic Wind Tunnel Study. NASA TND - 5805, 1970

9. Thomas, F. — Die Ermittlung der Schüttelgrenzen von Tragflügeln im transsonischen Geschwindigkeitsbereich. Jahrbuch der WGLR 1966, S. 126 - 144.

10. Redeker, G. — Die Berechnung der Schüttelgrenzen von Pfeilflügeln ZFW, 1973, Heft. 10

11. Huston, W.B. — A Study of the Correlation Between Flight and Wind Tunnel Buffet Loads. AGARD Rep. 111, 1957

12. Mabey, D.G. — Comparison of Seven Wing Buffet Boundaries Measured in Wind Tunnels and Flight. ARC CP 840

13. Hollingworth, E.G. Cohen, K. — Comparison of Wind Tunnel and Flight Test Techniques for Determining Transonic Buffet Characteristics on the McDonnel F4 Airplane. AIAA Paper No 70-584, 1970

14. Vanino, R. Wedemeyer, E. — Windtunnel Investigations of Buffet Loads on Four Airplane Models. Facilities and Techniques for Aerodynamic Testing at Transonic Speeds and High Reynolds Number. AGARD Conf. Proc. 83 Paper 34, 1971.

15. Mabey, D.G. — An Hypothesis for the Prediction of Flight Penetration of Wing Buffeting from Dynamic Tests on Wind Tunnel Models. RAE Tech. Rep. 70189, 1970

16. Davis, D.D. Huston, W.B. — The Use of Wind Tunnels to Predict Flight Buffet Loads. NACA RM L57 D 25, 1957

17. Moss, G.F. — Some Notes on the Aerodynamic Problems Associated with the Phenomenon of Buffeting. RAE Tech. Memo Aero 1293

18. Mitchell, C.G.B. — Calculation of the Low-speed Buffeting of a Slender Wing Aircraft. RAE Paper No 4 prepared for Proceedings of the Symposium on Structural Dynamics Loughborough University March 1970

19. John, H. — Calculation of Buffeting Intensity Using Fluctuating Pressure Measurements. Part I: Theory MBB Report to be published

20. ISO Standard — International Organization for Standardization. "Evaluation Exposure of Humans to Whole Body Vibration." ISO/TC 108/WG1 (Secr.-8)

21. Laschka, B. — Zur Theorie der harmonisch schwingenden tragenden Fläche bei Unterschallströmung. ZFW Heft 7, Juli 1963

22. Jones, J.G. — The Dynamic Analysis of Buffeting and Related Phenomena. AGARD Conference CP 102 Paper "Fluid Dynamics of Aircraft Stalling.", 1972

23. Rainey, A.G. — Measurements of Aerodynamic Forces for Various Mean Angles of Attack on an Airfoil Oscillating in Bending with Emphasis on Damping in the Stall. NACA Rep. 1305, 1957

24. Hoblit, F.M. et al. — Development of a Power-Spectral Gust Design Procedure for Civil Aircraft. FAA-ADS-53, January 1966.

25. Becker, J. — Buffetvoraussage mit Hilfe der PSD-Analyse MBB-UFE 1128, Dez. 1974

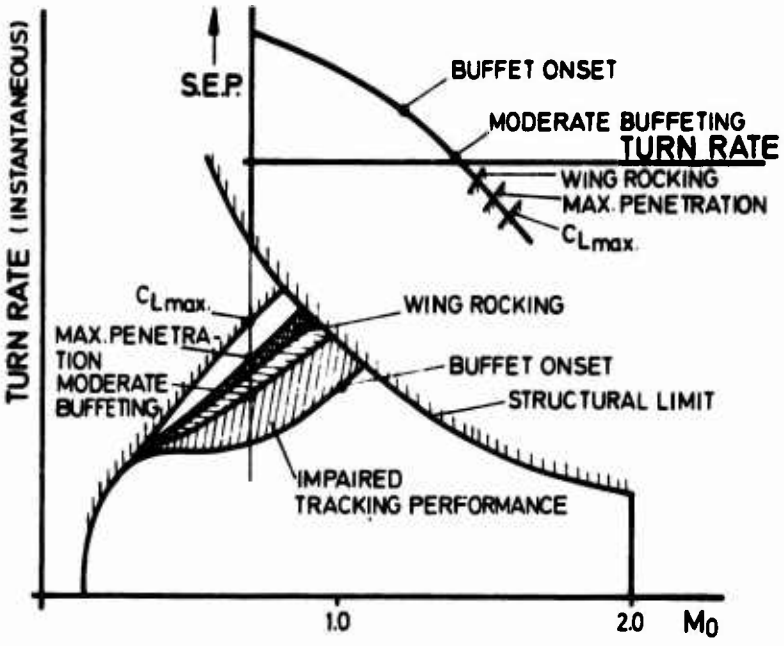

Fig. 1: Principle of Manoeuvre Boundaries for a Fighter Aircraft

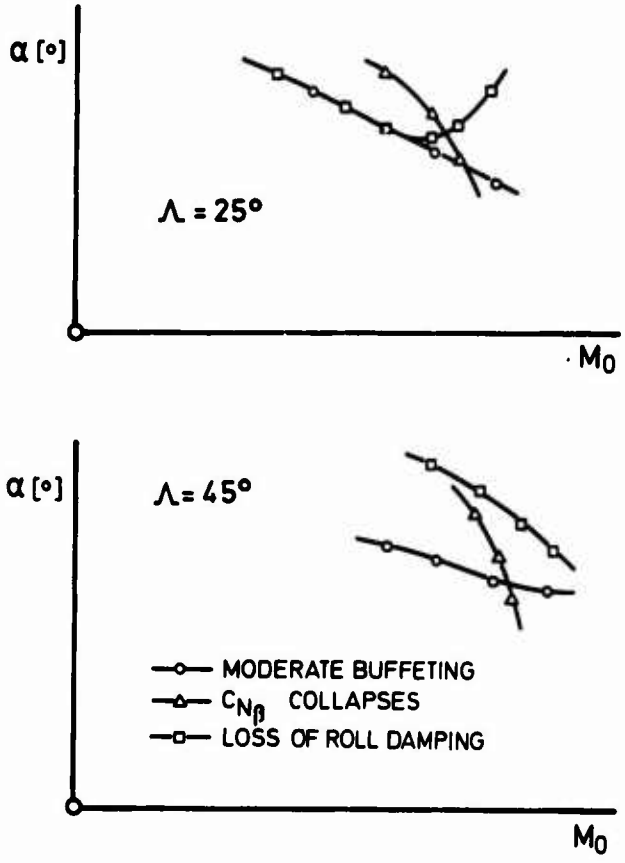

Fig. 2: Summary of Manoeuvre Limiting Phenomena

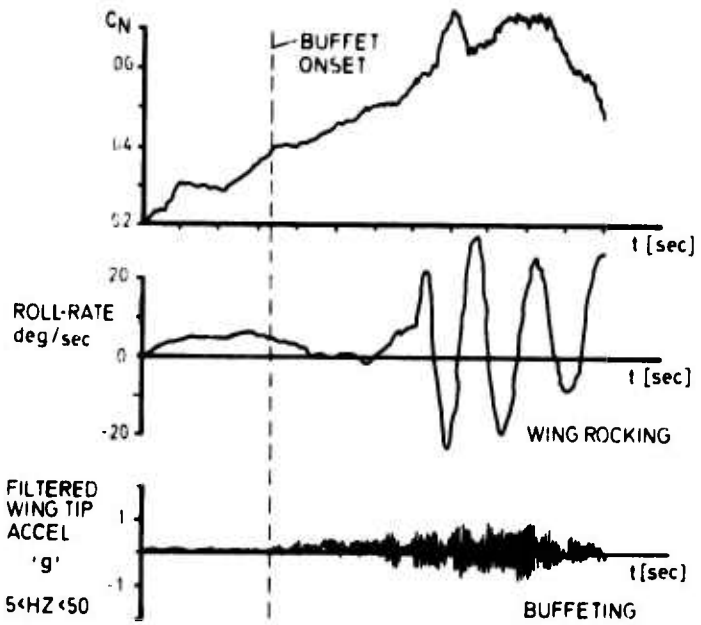

Fig. 3: Typical Penetration to High c_N of Fighter Type Aircraft

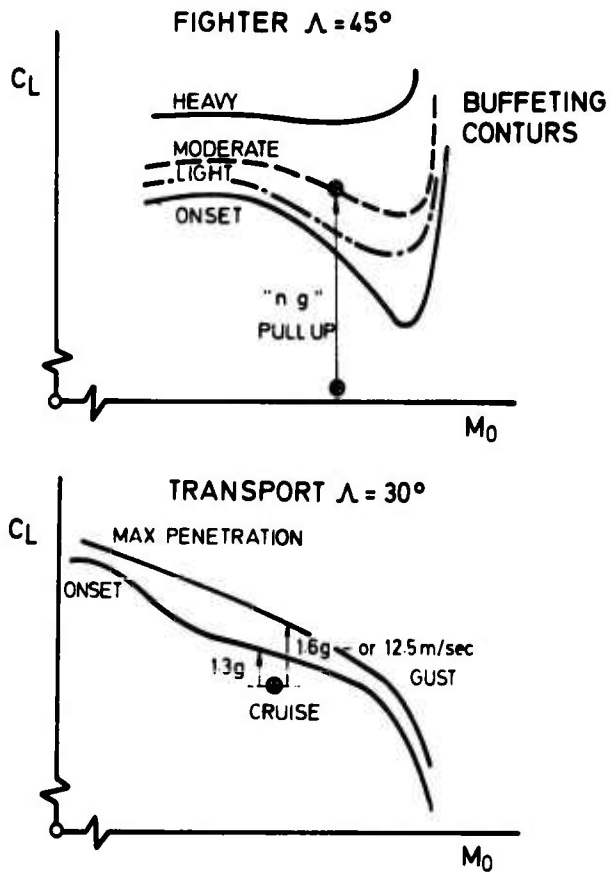

Fig. 4: Buffeting Criteria

$$a^2(\eta_0)_{T,A} = b_r^4 q_r^2 \sum_{n=1}^{\infty} K_{n,r} \frac{1}{m_r^2} \cdot \frac{d_{n,M}}{d_{n,A}} \cdot \left[\hat{C}_{L,n}(K_n)\right]_r a^2(\eta_0)_{n,M}$$

NOTATION :

$a(\eta_0)_{T,A}$	AIRPLANE TOTAL ROOT-MEAN-SQUARE BUFFET ACCELERATION AT PARTICULAR LOCATION.
b_r	SCALE FACTOR .
q_r	AIRPLANE TO MODEL DYNAMIC PRESSURE RATIO
$K_{n,r} = \frac{b_r \cdot \omega_{n,r}}{V_r}$	REDUCED FREQUENCY A/M-RATIO FOR nth NATURAL VIBRATION MODE.
$\left[C_{L,n}(K_n)\right]_r$	A/M-RATIO OF POWER SPECTRUM OF EFFECTIVE RANDOM AERODYNAMIC LIFT COEFFICIENT.
$d_n = \left[\left(\frac{C_a}{C_{cr}}\right)_n + \left(\frac{C_s}{C_{cr}}\right)_n\right]$	SUM OF AERODYNAMIC AND STRUCTURAL DAMPING IN nth VIBRATION MODE
$a(\eta_0)_{n,M}$	MODEL RMS BUFFET ACCELERATION IN nth VIBRATION MODE AT PARTICULAR LOCATION.

Fig. 5: Extrapolation Formula for Buffet Loads

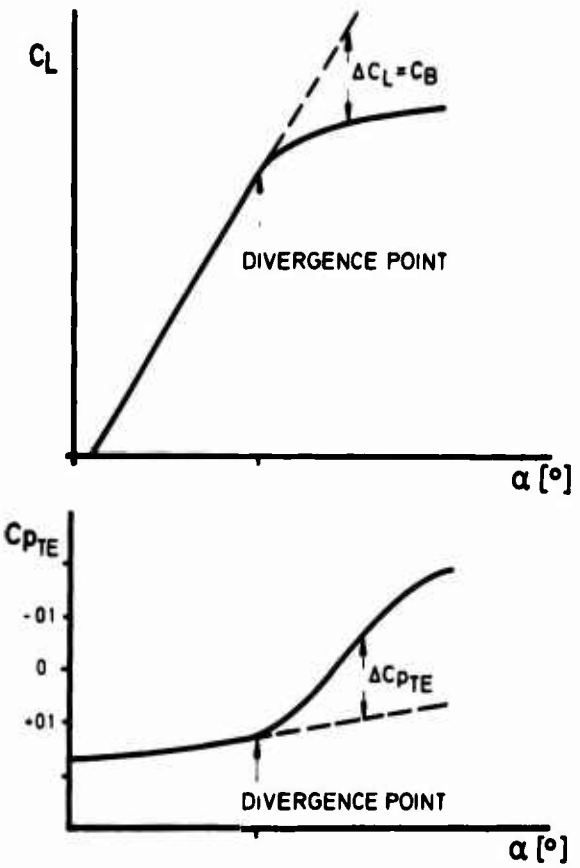

Fig. 6: Correlation between Divergence in Trailing-Edge Pressure and Lift Coefficient Variation.

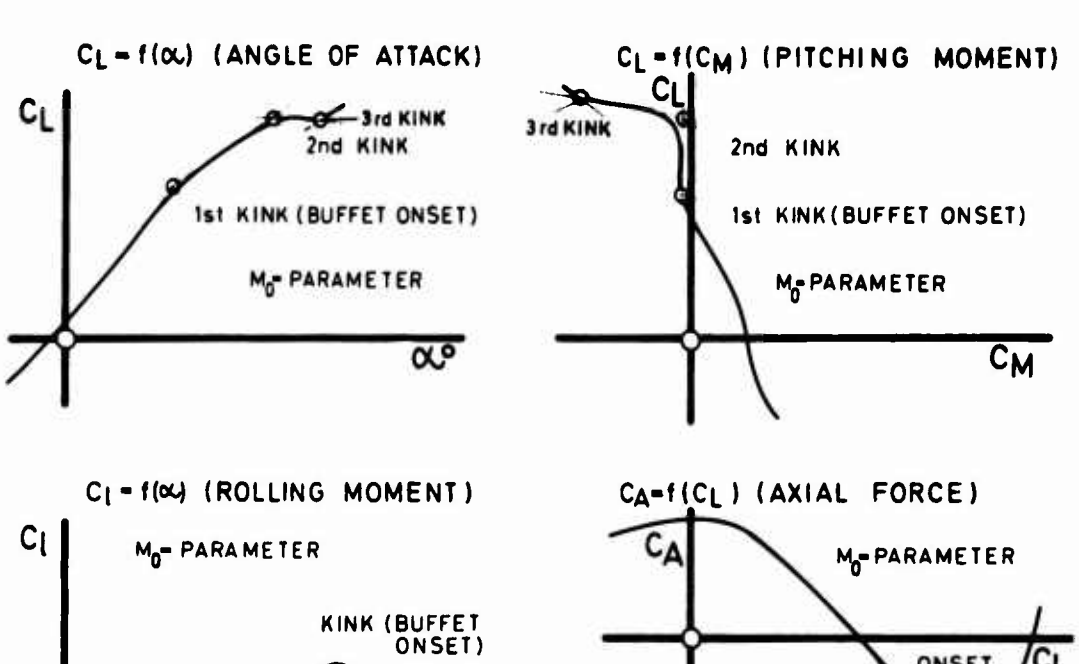

Fig. 7: Definition of Kinks

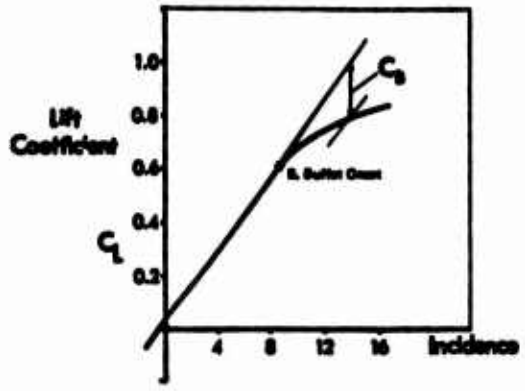

$$B = K C_B / \left(\frac{W}{q \cdot S}\right)$$

MODERATE BUFFETING $B = \pm 0.6\,g$

WHERE W IS THE AIRCRAFT WEIGHT, S IS WING AREA, q IS DYNAMIC PRESSURE AND K = 1 HAS BEEN FOUND SATISFACTORY FOR THE CONSTANT OF PROPORTIONALITY

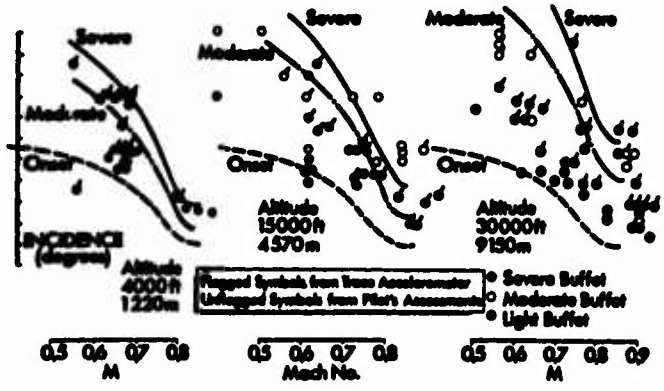

TAKEN FROM REF. 5

Fig. 8: Simplified Buffet Response Calculation

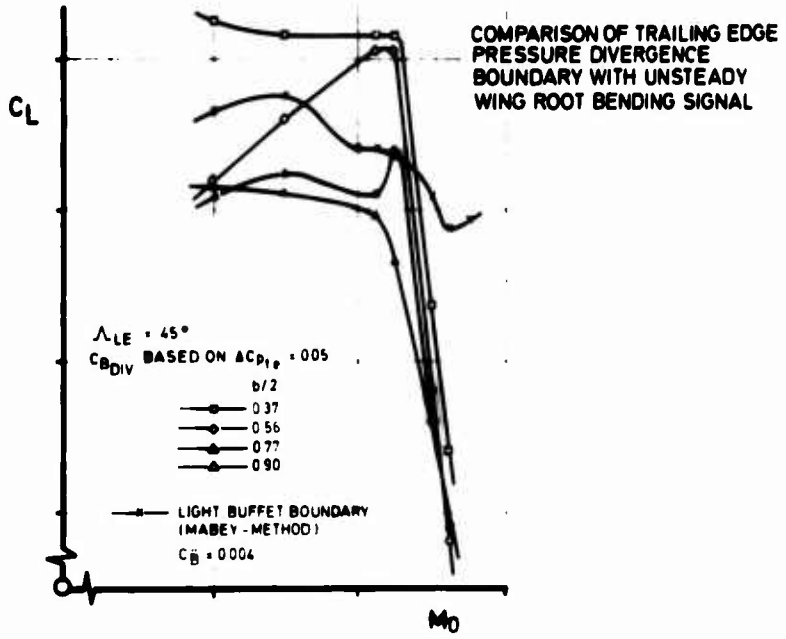

Fig. 9: Definition of Buffet Onset

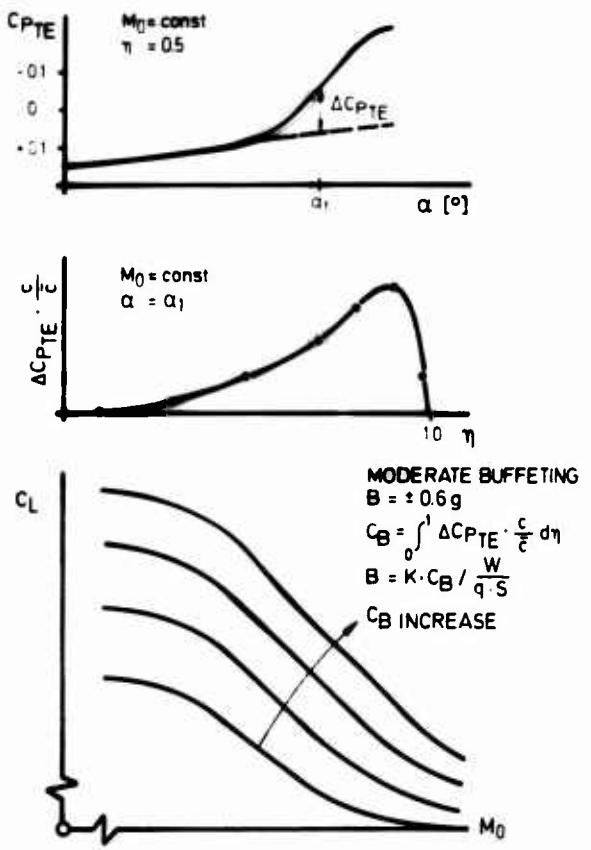

Fig.10: Buffet Response Calculation by Use of Trailing-Edge Pressure

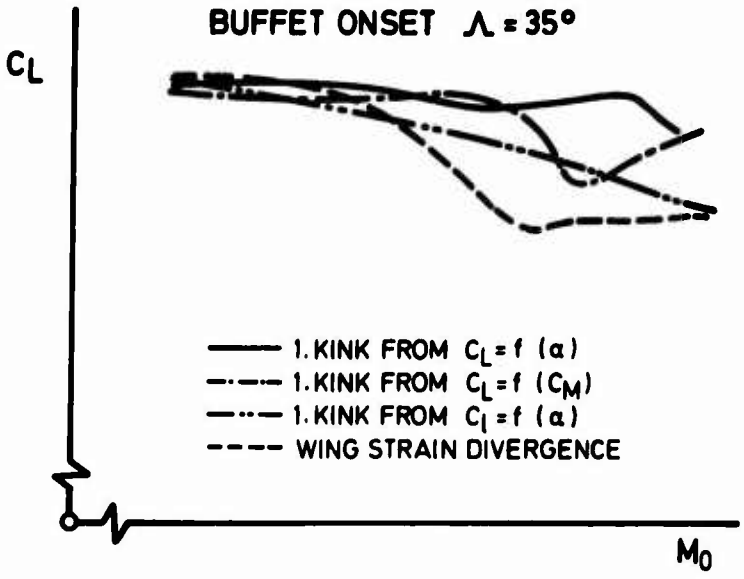

Fig.11: Comparison of Different Buffet Onset Criteria

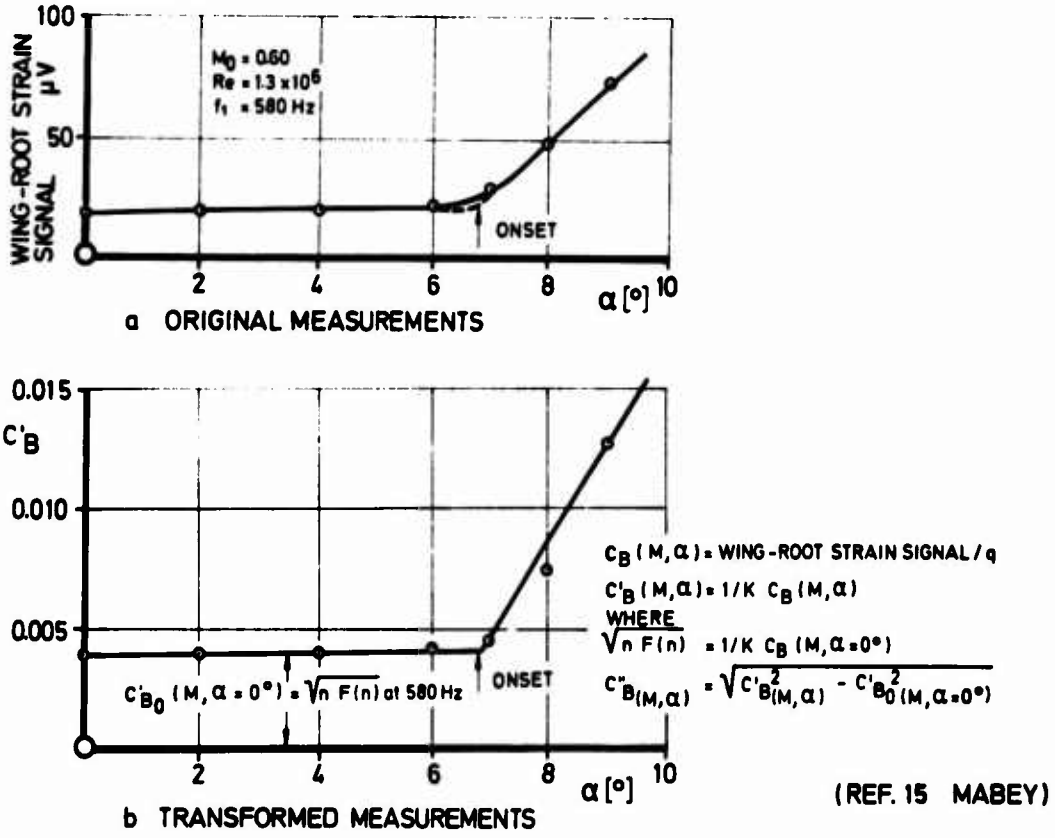

Fig. 12: Definition of Buffeting Coefficients

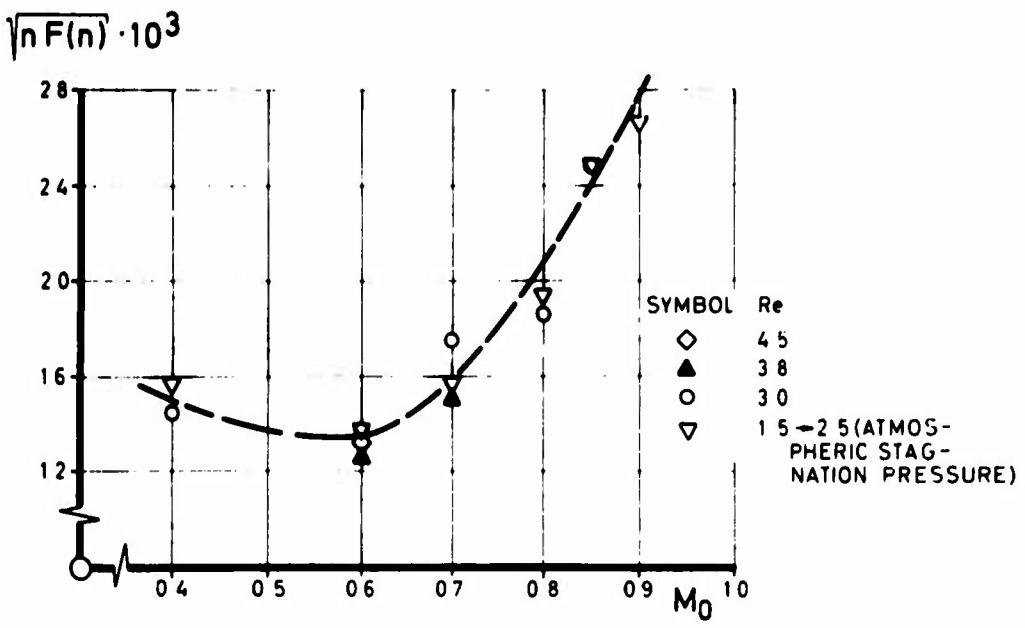

Fig.13: Typical Variation of Tunnel Unsteadiness with Mach-Number and Tunnel Stagnation Pressure

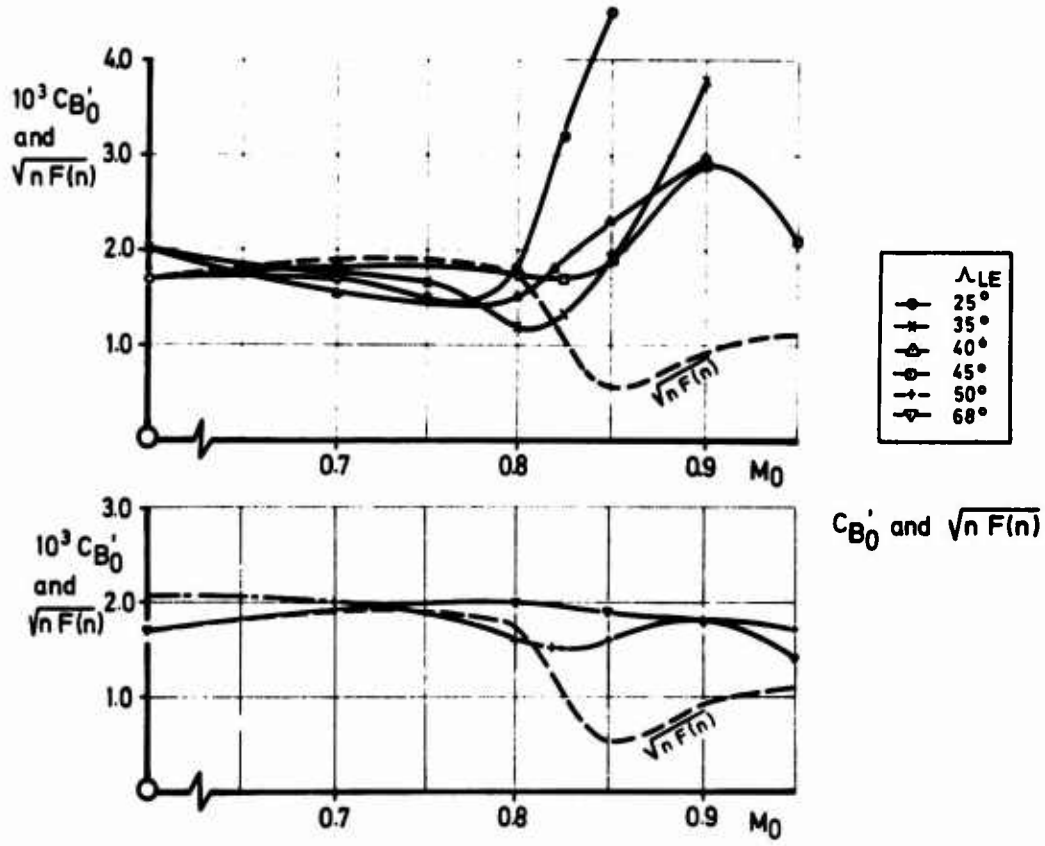

Fig.14: Low Level Buffet and Tunnel Noise

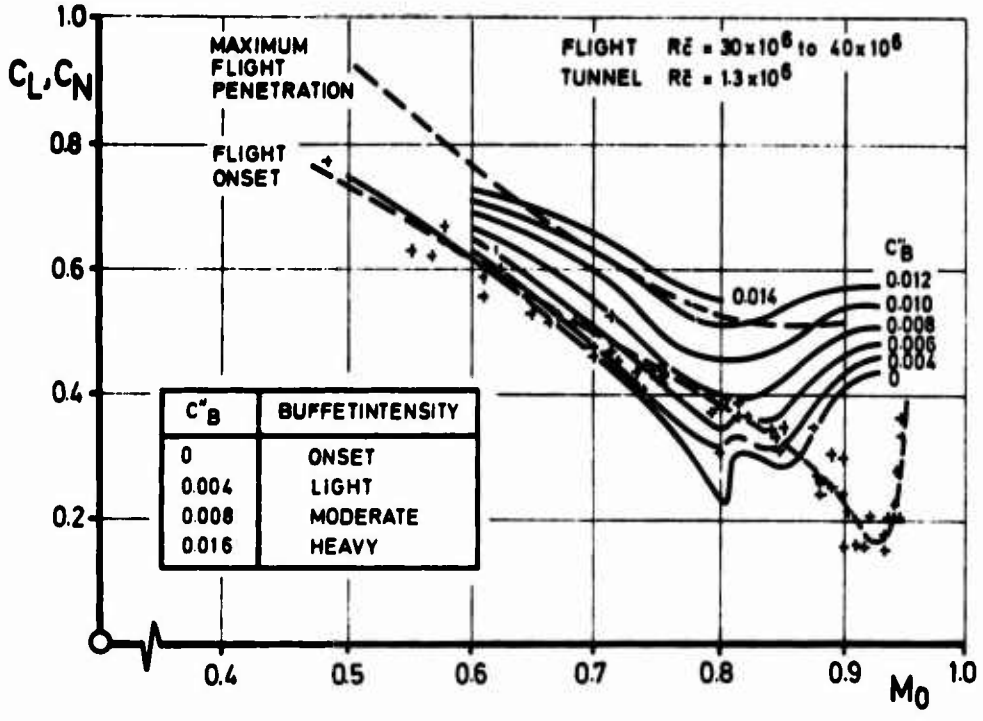

Fig.15: Correlation of Model Buffeting Coefficient with Flight Data

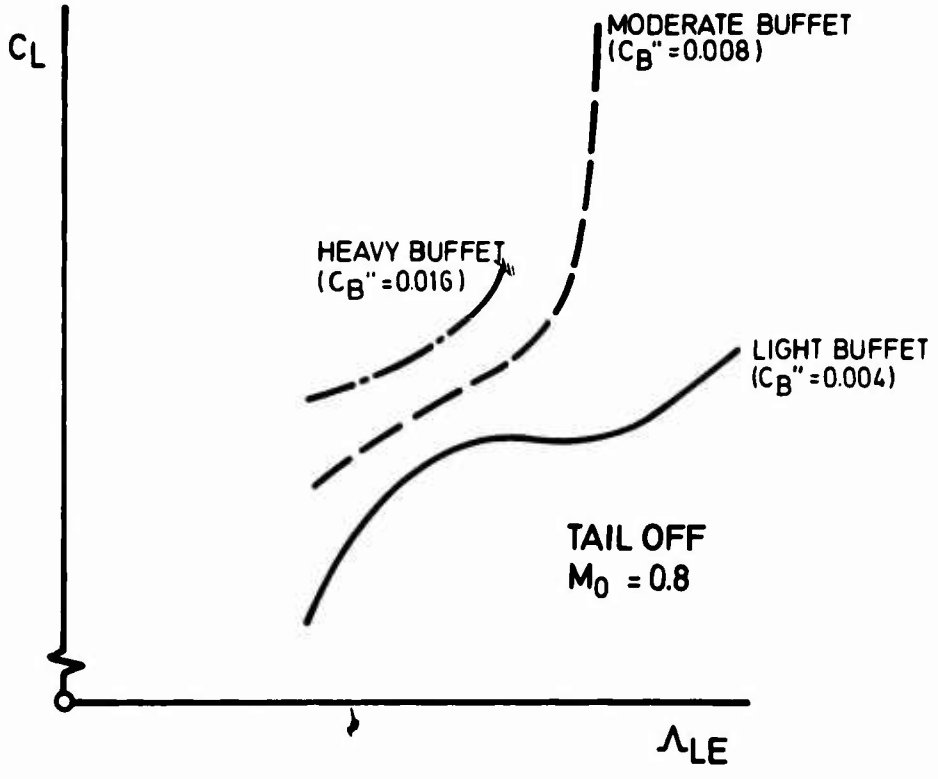

Fig.16: Effect of Wing Sweep on Buffeting Penetration

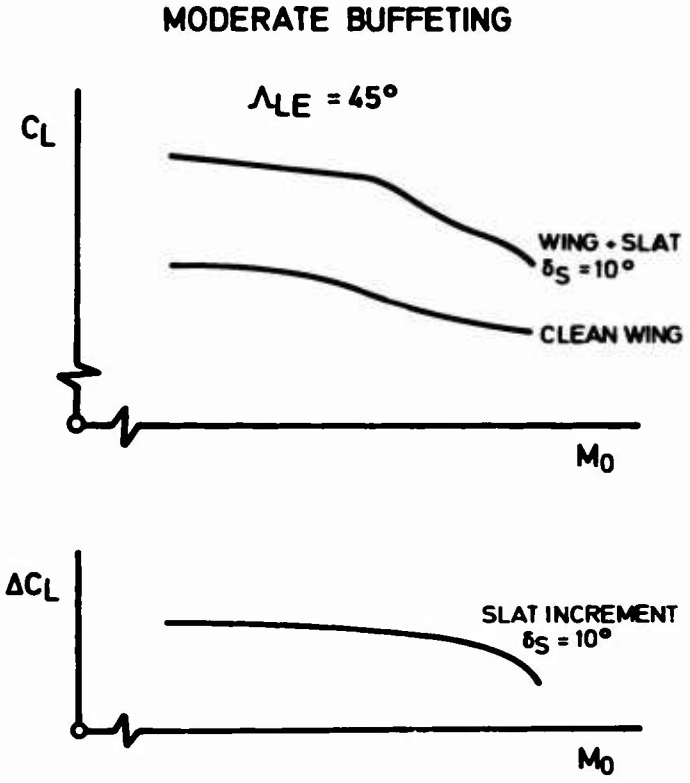

Fig.17: Effect of Manoeuvre Slat

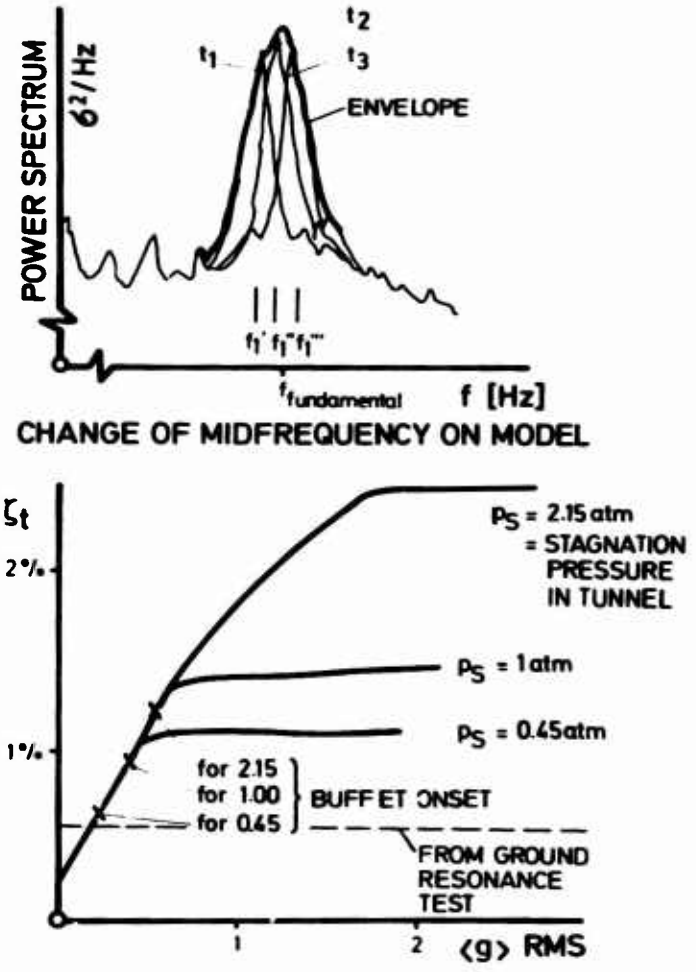

Fig.18: Total Damping versus Acceleration Level on Model

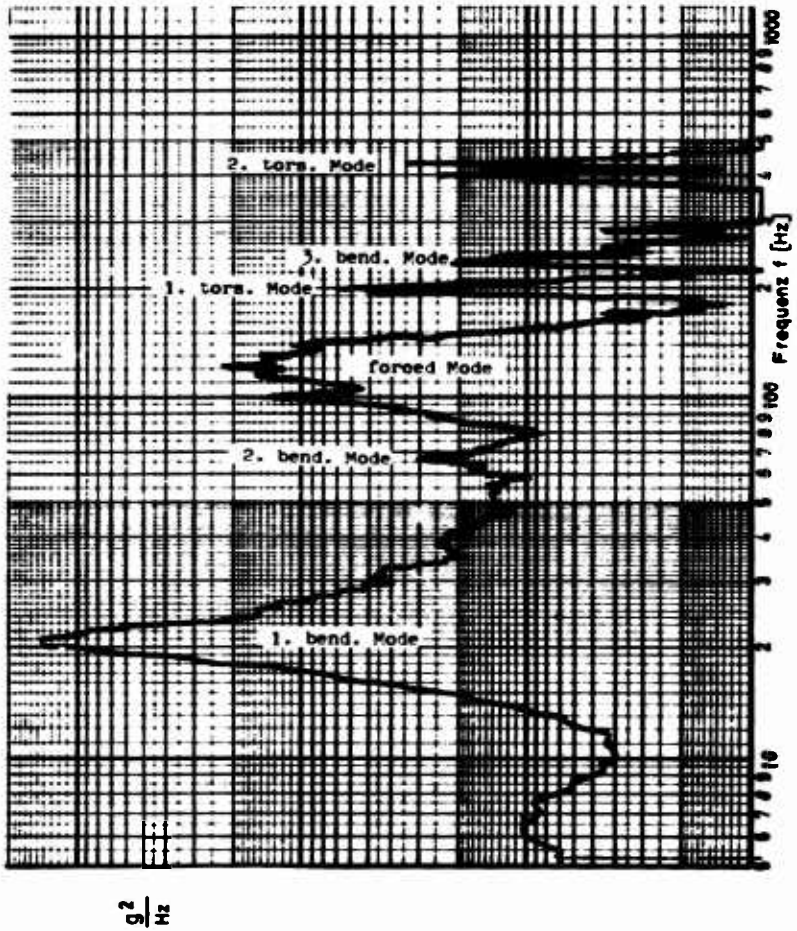

Fig.19: Power Spectrum of Accelerometer on Model

$$M \cdot \ddot{x} + D \cdot \dot{x} + C \cdot x = P_{\ddot{x}} + P_{\dot{x}} + P_x + P_{Buffet} \qquad (4.1)$$

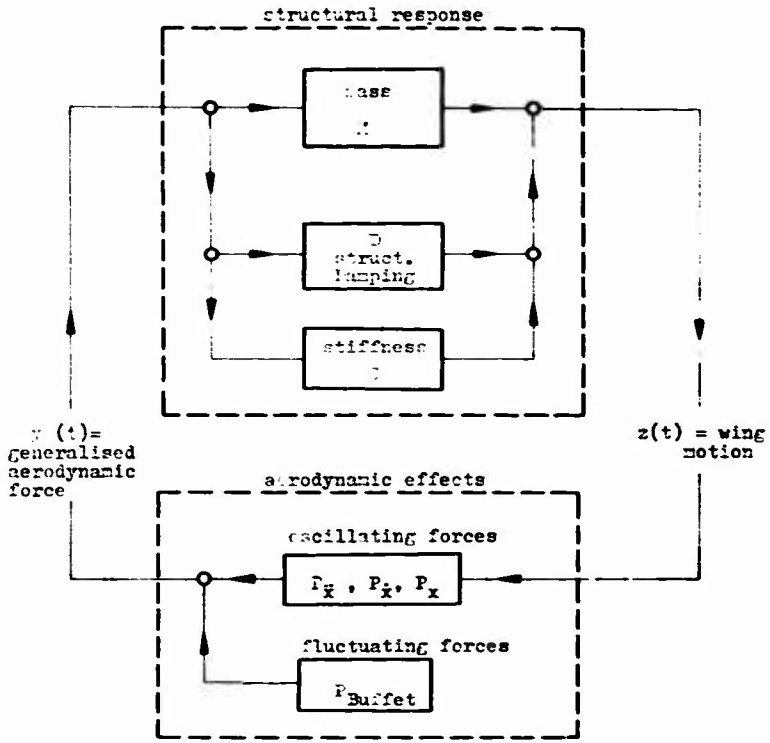

Fig.20: Block Diagram for Structural Buffeting, Representing Response in Flexible Mode.

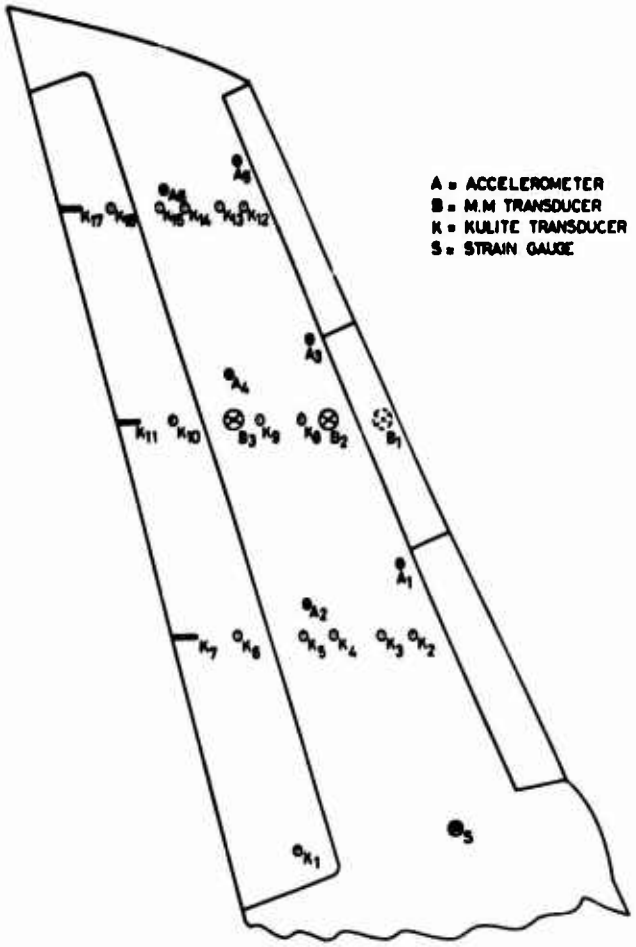

Fig.21: Clean wing Upper Surface with Transducer Positions.

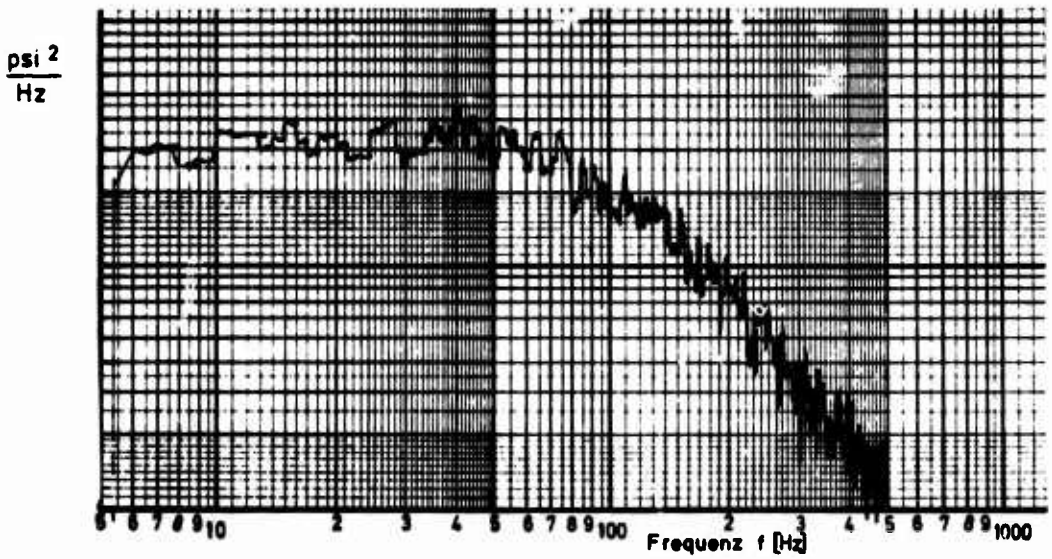

Fig.22: Power Spectrum of Pressure Fluctuation on Model at Midspan.

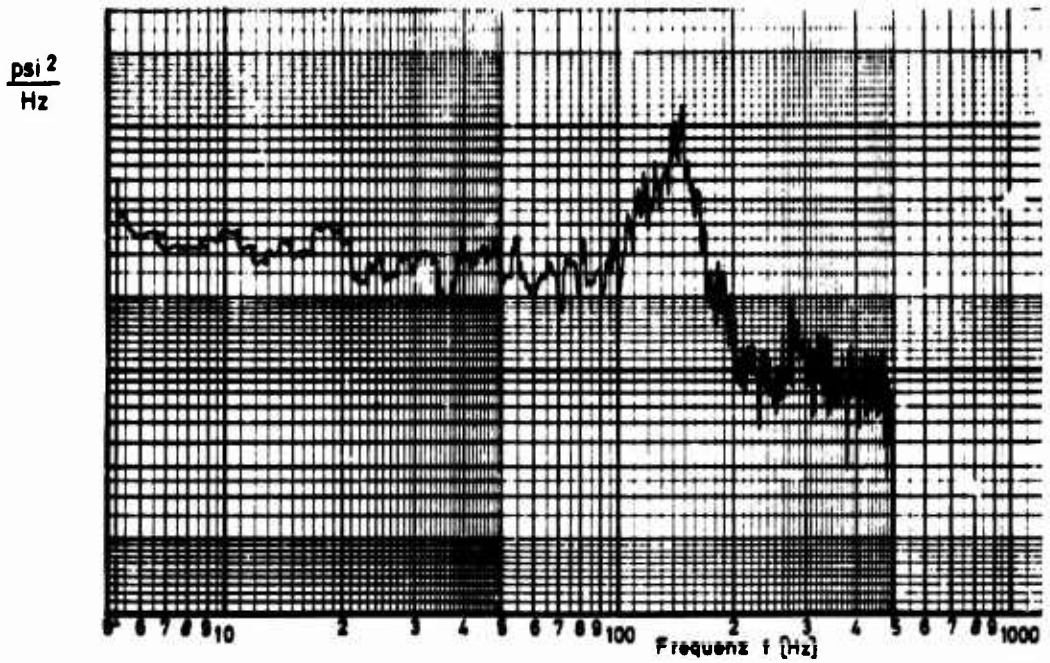

Fig.23: Power Spectrum of Pressure Fluctuation on Model near Tip.

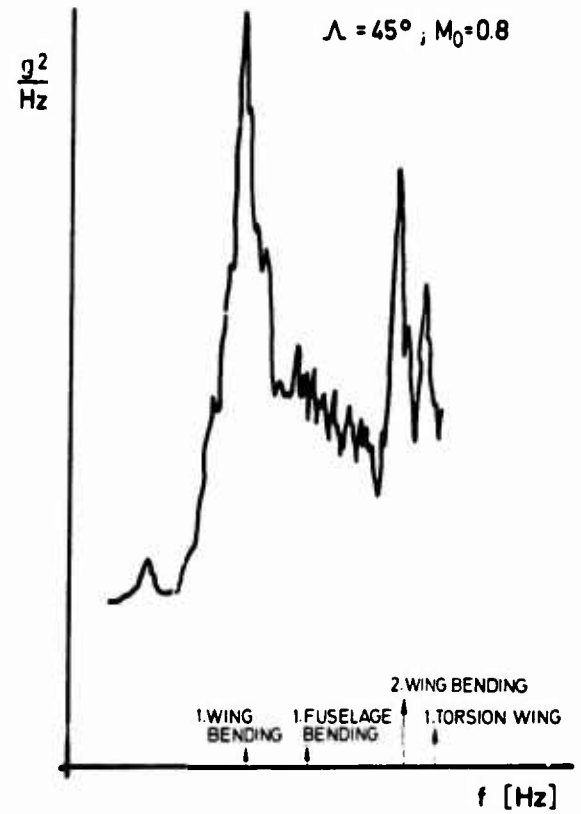

Fig.24: Buffeting Response Calculation.
Power Spectrum at Wing Tip.

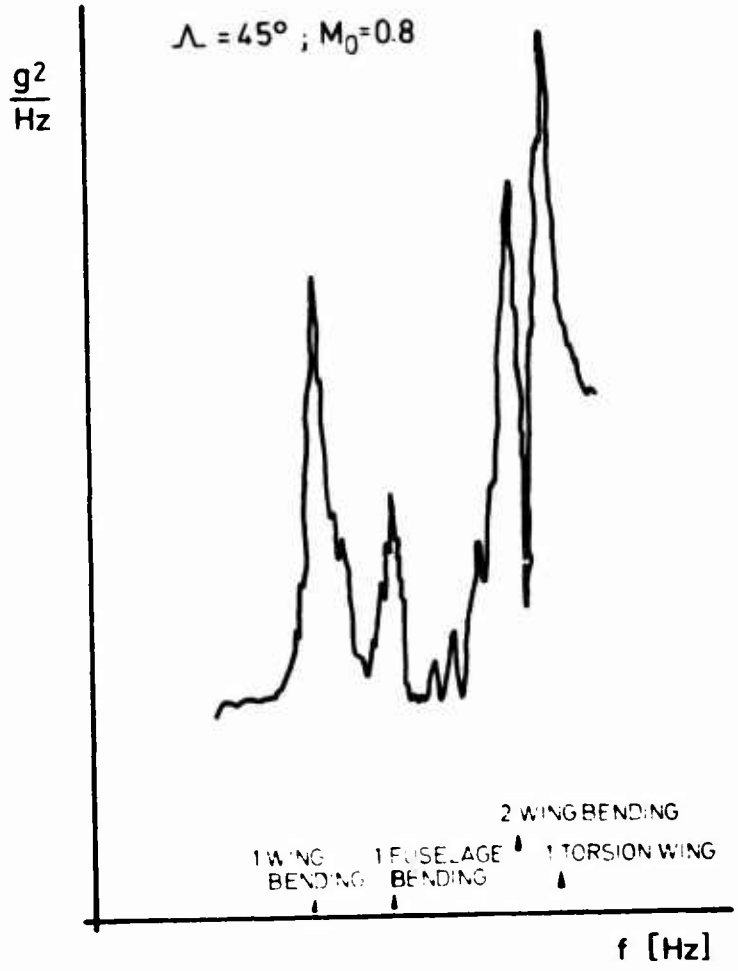

Fig.25: Buffeting Response Calculation.
Power Spectrum at Wing Root.

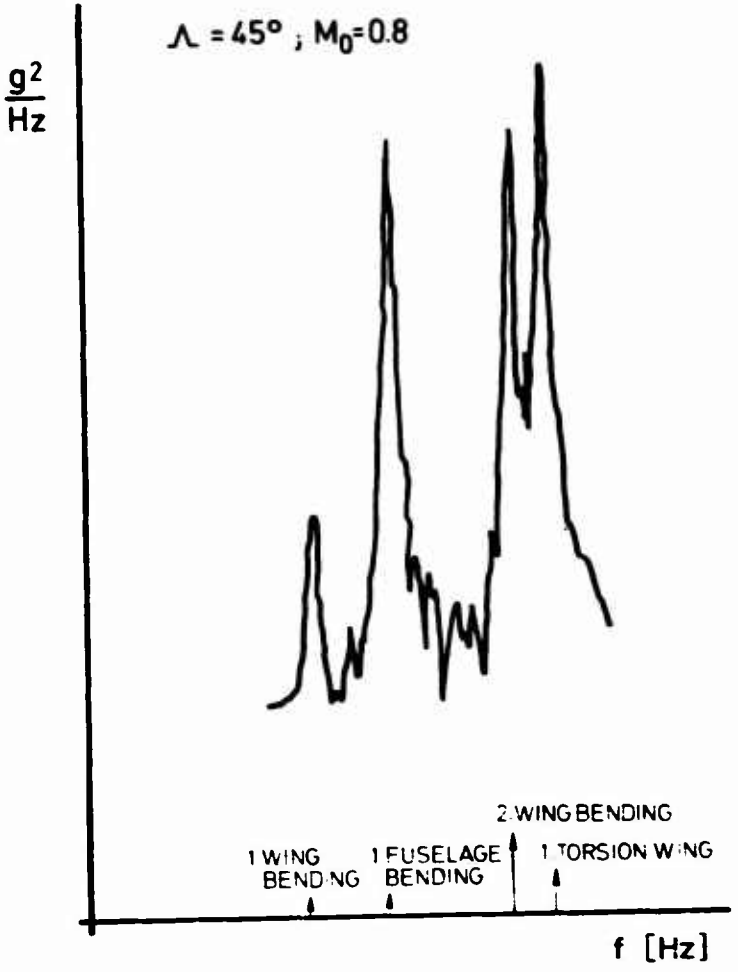

Fig.26: Buffeting Response Calculation
Power Spectrum at Pilot Station.

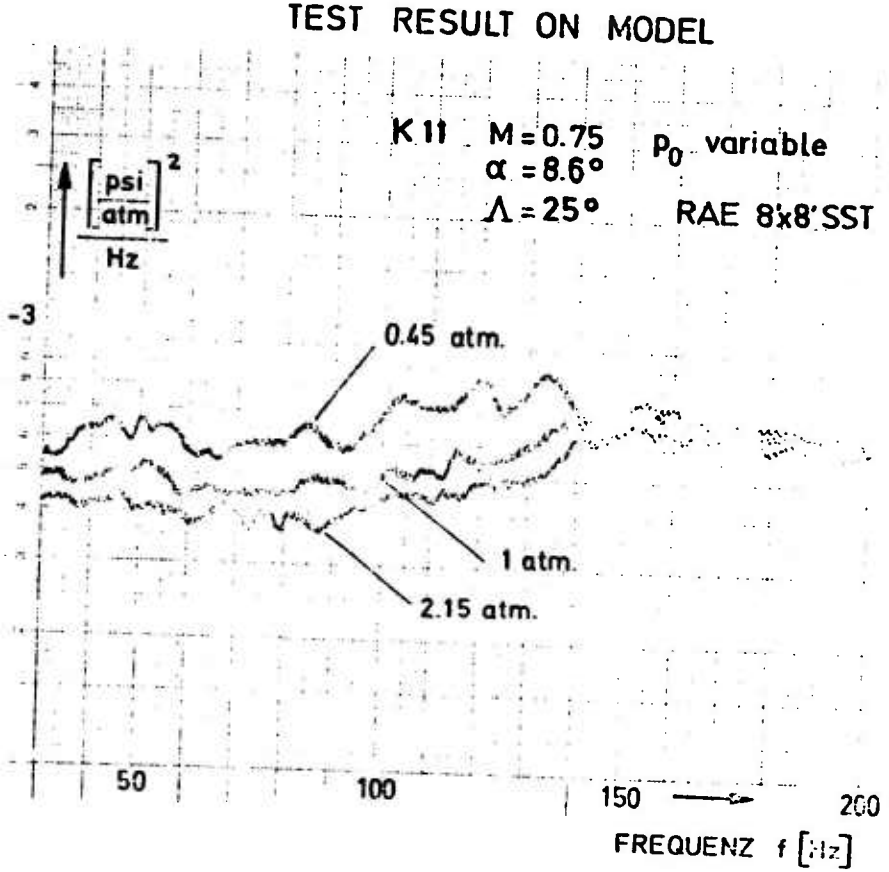

Fig.27: Influence of Reynolds Number on Power Spectrum of Pressure Fluctuation on Model at Wingspan.

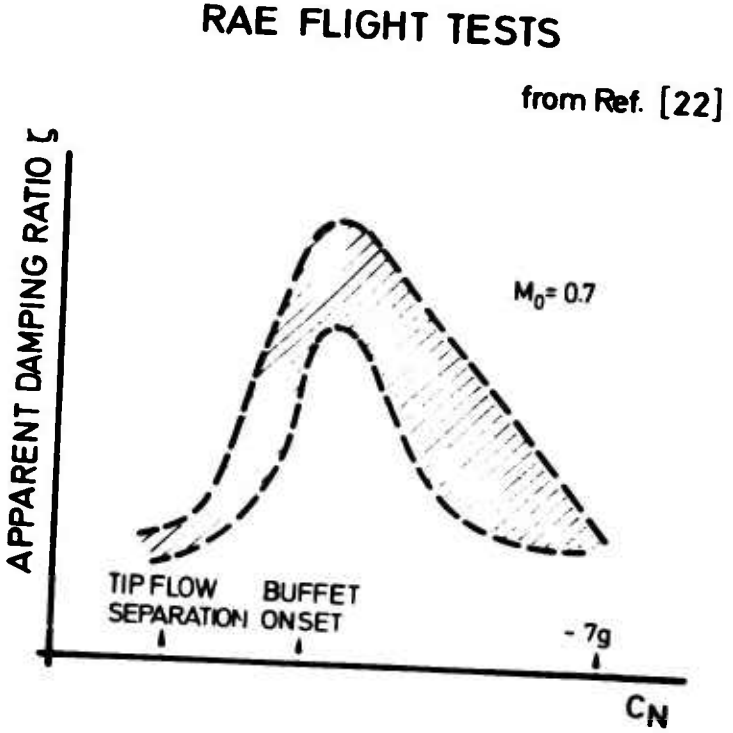

Fig.28: Damping in Wing Fundamental Mode During Buffet Penetration.

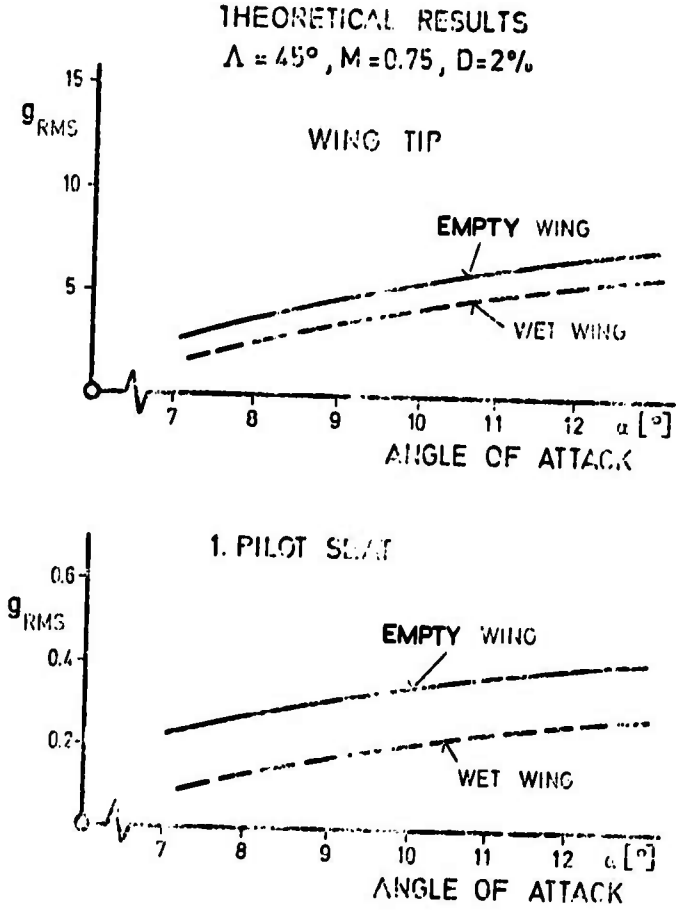

Fig.29: Buffeting Response Calculation;
Comparison of RMS-Acceleration Level
Between Empty Wing and Wing Full of Fuel.

Bibliography on Aircraft Stalling

N74-13709
Dynamic Stall
P. Crimi and P.F. Yaggy, ed. Nov. 1973, 41 p, refs
Advisory Group for Aerospace Research and Development, Paris (France)
NASA-CR-136473; AGARD-AG-172

N74-13674
Reynolds Number Effects at Low Speeds on the Maximum Lift of Two-Dimensional Aerofoil-Sections Equipped with Mechanical High Lift Devices
J.A. Thain
Natl. Res. Council of Can. Quart. Bull. of the Div. of Mech. Eng. and the Natl. Aeron. Estab. 30. Sep. 1973, p 1-24, refs.

N73-30935
The Lift and Stalling Characteristics of a 35 deg Swept Back Wing Designed to have Identical Chordwise Pressure Distributions at all Spanwise Stations when near Maximum Lift
D.S. Woodward and D.E. Lean, 1973, 135 p, refs
Royal Aircraft Establishment, Farnborough (England), Aerodynamics Dept.
ARC-R/M-3721; RAE-TR-71050; ARC-33417

N73-30050
Experimental Investigation of Wake Velocity Fluctuations behind Stalled Wings at Reynolds Numbers up to 4.8 Million, Final Report, Feb. 1971-1973
Robert F. Smiley, Feb. 1973, 62 p, refs
Allied Research Associates, Inc., Newton Upper Falls, Mass.
AD-763468; ARA-9G87-F

N73-21042
Aerodynamic Forces Computation and Measurement on an Oscillating Aerofoil Profile with and without Stall
J.J. Philippe and M. Sagner
In: AGARD, Aerodyn. of Rotary Wings, Feb. 1973, 13 p, refs
AGARD-CP-111

N73-18023
Technical Evaluation Report on Fluid Dynamics Panel Specialists Meeting on Fluid Dynamics of Aircraft Stalling
R.C. Pankhurst, Nov. 1972, 11 p, refs
Advisory Group for Aerospace Research and Development, Paris (France)
AGARD-AR-49

N73-17000
Adjustment of Flying Qualities by Wind Tunnel Testing
Tj. Schuringa
In: AGARD, Stability and Control, Nov. 1972, 7 p
AGARD-CP-119

N73-16023
Post-Stall Testing of Aircraft with a Wind Tunnel Captive System, Final Report, Feb.-Jun. 1972
J.R. Milillo, Nov. 1972, 21 p, refs
ARO, Inc., Arnold Air Force Station, Tenn.
AD-751461; ARO-PWT-TR-72-115; AEDC-TR-72-126

N73-15016
Predicting the Low Speed Stall Characteristic of the Boeing 747
John K. Wimpress
In: AGARD, Fluid Dyn. of Aircraft Stalling, Nov. 1972, 9 p
AGARD-CP-102

N73-15015
Aerodynamics of Wing Stall of the Fokker F28
Tj. Schuringa
In: AGARD, Fluid Dyn. of Aircraft Stalling, Nov. 1972, 5 p
AGARD-CP-102

N73-15014
Post-Stall Aerodynamics of the Harrier GR1
Cliff L. Bore
In: AGARD, Fluid Dyn. of Aircraft Stalling, Nov. 1972, 7 p, refs
AGARD-CP-102

N73-15013
Stall/Post-Stall Characteristics of the F-111 Aircraft
Charles A. Anderson
In: AGARD, Fluid Dyn. of Aircraft Stalling, Nov. 1972, 9 p
AGARD-CP-102

N73-15012
Flight Development of the Stalling Characteristics of a Military Trainer Aircraft
W.D. Horsfield and G.P. Wilson
In: AGARD, Fluid Dyn. of Aircraft Stalling, Nov. 1972, 9 p
AGARD-CP-102

N73-15011
A Practical Look at the Stall and High Lift Operation of Externally Blown Flap STOL Transport Configurations
David J. Moorehouse
In: AGARD, Fluid Dyn. of Aircraft Stalling, Nov. 1972, 13 p, refs
AGARD-CP-102

N73-15010
The Effect of Leading Edge Geometry on High Speed Stalling
G.F. Moss, A.B. Haines and R. Jordon
In: AGARD, Fluid Dyn. of Aircraft Stalling, Nov. 1972, 16 p, refs
AGARD-CP-102

N73-15008
The Low Speed Stalling of Wings with High Lift Devices
D.N. Foster
In: AGARD, Fluid Dyn. of Aircraft Stalling, Nov. 1972, 12 p, refs.
AGARD-CP-102

N73-15002
Airfoil Stall Prediction in Incompressible Flow
Michel Vincent DePaul
In: AGARD, Fluid Dyn. of Aircraft Stalling, Nov. 1972, 15 p, refs
AGARD-CP-102

N73-15000
Some Research on Two Dimensional Laminar Separation Bubbles
E. Dobbinga, J.L. Vanlngen and J.W. Kooi
In: AGARD, Fluid Dyn. of Aircraft Stalling, Nov. 1972, 8 p, refs
AGARD-CP-102

N73-14999
Role of Fluid Dynamics in Aircraft Stall and Poststall Gyrations
G.J. Hancock
In: AGARD, Fluid Dyn. of Aircraft Stalling, Nov. 1972, 16 p, refs
AGARD-CP-102

N73-14998
Fluid Dynamics of Aircraft Stalling
Nov. 1972, 342 p, refs
AGARD-CP-102

N72-26251
Review of MIT Research on Airfoil Dynamics Stall 1964-1971
Norman D. Ham, Sep. 1971, 33 p, refs
Massachusetts Inst. of Tech., Cambridge, Aeroelastic and Structures Research Lab.
AD-738610; ASRL-TR-130-3; AROD-4846:13-E

N72-26003
Aerofoil Stall Prediction in Incompressible Flow
Michel Vincent DePaul, 1972, 16 p, refs
Office National d'Etudes et de Recherches Aerospatiales, Paris (France)
ONERA-TP-1088

N72-19012
Some Recent Research on Airfoil Dynamic Stall with Application to Airfoil Design
Norman D. Ham, Sep. 1971, 30 p, refs
Massachusetts Inst. of Tech., Cambridge, Aeroelastic and Structures Research Lab.
AD-734699; ASRL-TR-165-1

N72-11904
Observations of Three-Dimensional Flow Patterns Obtained During Stall Development on Aerofoils, and on the Problem of Measuring Two-Dimensional Characteristics, Progress Report
N. Gregory, V.G. Quincey, C.L. OReilly and D.J.Hall, 1971, 31 p, refs
National Physical Lab., Teddington (England), Aerodynamic Div.
ARC-CP-1146; NPL-AERO-1309; ARC-31702

N72-11903
Two-Dimensional Low-Speed Tunnel Tests on the NACA 0012 Section Including Measurements Made During Pitching Oscillations at the Stall
G.F. Moss and P.M. Murdin, 1971, 43 p, refs
Royal Aircraft Establishment, Farnborough (England), Aerodynamics Dept.
ARC-CP-1145; RAE-TR-68104; ARC-30682

N72-11858
A Type of Stall with Leading Edge Transonic Flow and Rear Separation
J. Osborne and H.H. Pearcey
In: AGARD, Facilities and Tech. for Aerodyn. Testing at Transonic Speeds and High Reynolds Number, Aug. 1971, 11 p, refs
AGARD-CP-83-71

N71-29221
Unsteady Airfoil Stall and Stall Flutter
Lars E. Ericsson and J. Peter Reding, Jun. 1971, 135 p. refs
Lockheed Missiles and Space Co., Sunnyvale, Calif.
NASA-CR-111906; LMSC-A-6J-71-1

N71-20292
Utilization of a Fixed Base Simulator to Study the Stall and Spin Characteristics of Fighter Airplanes
Frederick L. Moore, Ernie L. Anglin, Mary S. Adams, Perry L. Deal and Lee H. Person, jr., Mar. 1971, 35 p, refs
National Aeronautics and Space Administration, Langley Research Center, Langley Station, Va.
NASA-TN-D-6117; L-7420

N71-20052
Aerodynamics of Mechanical High Lift Devices
D.M. McRae
In: AGARD, Assessment of Lift Augmentation Devices, Feb. 1971, 23 p, refs
AGARD-LS-43-71

N71-1[illegible]
An Experimental Study on the Unsteady Behavior of a Short Bubble on an Airfoil During Dynamic Stall with Special Reference to the Mechanism of the Stall Overshoot Effect
Koji Isogai, Jun. 1970, 27 p, refs
Massachusetts Inst. of Tech., Cambridge, Aeroelastic and Structures Research Lab.
AD-711540; ASRL-TR-130-2; AROD-4846-12

N70-34290
Leading Edge Separation on an Airfoil During Dynamic Stall
Stephen A. Patay, Oct. 1969, 56 p, refs
Massachusetts Inst. of Tech., Cambridge, Aeroelastic and Structures Research Lab.
AD-701771; ASRL-TR-156-1

N70-24268
Wind Tunnel Measurements of the Low Speed Stalling Characteristics of a Model of the Hawker-Siddeley Trident 1C
D. Isaacs, 1967, 61 p, refs
Royal Aircraft Establishment, Bedford (England), Aerodynamics Dept.
ARC-R/M-3608; RAE-TR-68108; ARC-30775

N70-23878
Reynolds Number and Mach Number Effects on the Maximum Lift and the Stalling Characteristics of Wings at Low Speeds
B. van den Berg, 21. Mar. 1969, 43 p, refs
Nationaal Lucht-en Ruimtevaartlaboratorium, Amsterdam (Netherlands)
NLR-TR-69025-U

N70-22877
Examples of Research on Airfoils in the Two-Dimensional Subsonic S-10 Wind Tunnel of CEAT, Toulouse (Exemples de Recherches sur les Profils dans la Soufflerie S-10 du CEAT, a Toulouse)
Emile Erlich, 1969, 16 p, refs
Office National d'Etudes et de Recherches Aerospatiales, Paris (France)
ONERA-TP-766

N70-21838
Problems of Aircraft Behaviour at High Angles of Attack
G.J. Hancock, Dec. 1969, 115 p, refs
Advisory Group for Aerospace Research and Development, Paris (France), Flight Mechanics Panel
AGARDograph-136

A74-36454
Calculation of the Static Stability of Aircraft at Large Angles of Attack (K raschetu staticheskoi ustoichivosti letatel'nykh apparatov na bol'shikh uglakh ataki)
G.V. Aleksandrov and G.E. Kuzmak
TsAGI, Uchenye Zapiski, vol. 3, no. 1, 1972, p 38-44

A74-27644
Some Aspects of Airfoil Stall in Low-Speed Flow
H.C. Rao
Journal of Aircraft, vol.11, Mar. 1974, p 177-180, refs

A74-18765
Nonlinear Aerodynamics of Aircraft in High-Angle-of-Attack Maneuvers
M. Tobak and L.B. Schiff
American Institute of Aeronautics and Astronautics, Aerospace Sciences Meeting, 12th, Washington, D.C., Jan. 30 - Feb. 1, 1974, 11 p, 12 refs
Paper 74-85

A74-13842
Reynolds Number Effects at Low Speeds on the Maximum Lift of Two-Dimensional Aerofoil Sections Equipped with Mechanical High Lift Devices
J.A. Thain
National Research Council, Canada, Division of Mechanical Engineering and National Aeronautical Establishment, Quarterly Bulletin, no. 3, 1973, p 1-24, 24 refs

A73-44692
On Problems of Flight over an Extended Angle-of-Attack Range
H.H.B.M. Thomas
Aeronautical Journal, vol. 77, Aug. 1973, p 412-423, 53 refs

A73-11015
On the Mechanism of Dynamic Stall
W. Johnson and N.D. Ham
American Helicopter Society, Journal, vol. 17, Oct. 1972, p 36-45, 13 refs

A72-44058
Application of a Time Dependent Boundary-Layer Analysis to the Problem of Dynamic Stall
S.J. Shamroth and H. McDonald
ASME, Transactions, Series E - Journal of Applied Mechanics, vol. 39, Sept. 1972, p 823-825, 6 refs

A72-37760
Prediction of the Stalling of a Wing Section in Incompressible Flow (Prévision du Décrochage d'un Profil d'Aile en Écoulement Incompressible)
M.V. DePaul
AGARD, Meeting on Fluid Dynamics of Aircraft Stalling, Lisbon, Portugal, Apr. 26-28, 1972, p 1-15, 15 refs
ONERA-TP-1088

A72-35577
A Stall Inhibitor System for the F-111
C.A. Anderson and J.E. Walker
In: NAECON '72; Proceedings of the National Aerospace Electronics Conference, Dayton, Ohio, May 15-17, 1972, Institute of Electrical and Electronics Engineers, Inc., 1972, p 222-226

A72-35374
A Series of Aerodynamic Experiments on Super-Stall (Una serie die esperienze aerodinamiche sul superstallo)
G. Rotondi
Ingegneria, May 1972, p 315-322

A72-32024
Some Recent MIT Research on Dynamic Stall
N.D. Ham
Journal of Aircraft, vol. 9, May 1972, p 378, 379, 5 refs

A72-16899
A Method for Analyzing Dynamic Stall
P. Crimi and B.L. Reeves
American Institute of Aeronautics and Astronautics, Aerospace Sciences Meeting, 10th, San Diego, Calif., Jan. 17-19, 1972, 13 p, 20 refs
Paper 72-37

A70-37392
Effect of Wing Leading Edge Geometry on Maneuvering Boundaries and Stall Departure
W.R. Burris and D.E. Hutchins
American Institute of Aeronautics and Astronautics, Aircraft Design and Operations Meeting, 2nd, Los Angeles, Calif., July 20-22, 1970, 8 p, 7 refs
Paper 70-9C4

A70-17258
Development of a Spread Fin as an Antisuperstall and Antispin Auxiliary Device (Entwicklung einer Spreizflosse als Antisuperstall- und Antitrudelhilfseinrichtung)
H. Neppert
DGLR-Fachbuchreihe, Volume 3, 1969, p 43-1 to 43-36, 6 refs
Deutsche Gesellschaft für Luft- und Raumfahrt, Braunschweig
Edited by Werner Schulz

A70-10046
The Aerodynamics of High-Lift Devices on Conventional Aircraft. I-General Description and Comments on C_{Lmax} and Stalling Behaviour
D.M. McRae
Aeronautical Journal, vol. 73, June 1969, p 535-541

Bibliography on Aircraft Buffeting

N74-26486
Comparison of Fokker F-28 Wind Tunnel and Flight Data. A Summary
J.T.M. VanDoorn, L.J. Erkelens, S.O.T.H. Han and Y.G. Kho, 5. Jan. 1973, 41 p, refs
National Aerospace Lab., Amsterdam (Netherlands), Flight Div.
NLR-TR-73007-U

N74-14725
Prediction of Buffet On-Set for Aircraft, Recent Progress in Wind Tunnel and Flight Test Data Correlation
P.C. Wherter
In: AGARD, Aerodyn. Drag, Oct. 1973, 8 p, refs
AGARD-CP-124

N74-14708
An Experimental Analysis and Buffet Investigation of the Shockless Lifting Airfoil No. 1
J.J. Kacprzynski, Aug. 1973, 52 p, refs
National Research Council of Canada, Ottawa (Ontario)
NRC-13673; LR-569

N74-14631
Transonic Single-Mode Flutter and Buffet of a Low Aspect Ratio Wing having a Subsonic Airfoil Shape
Larry L. Erickson, Jan. 1974, 24 p, refs
National Aeronautics and Space Administration, Ames Research Center, Moffett Field, Calif.
NASA-TN-D-7346; A-4966

N73-27905
Effects of Flaps on Buffet Characteristics and Wind-Rock Onset of an F-8C Airplane at Subsonic and Transonic Speeds
Richard C. Monaghan and Edward L. Friend, Aug. 1973, 27 p, refs
National Aeronautics and Space Administration, Flight Research Center, Edwards, Calif.
NASA-TM-X-2873; H-742

N73-25999
Maneuver and Buffet Characteristics of Fighter Aircraft
Edward J. Ray, Linwood W. McKinney and Julian G. Carmichael, Jul. 1973, 18 p, refs
National Aeronautics and Space Administration, Langley Research Center, Langley Station, Va.
NASA-TN-D-7131; L-8554

N73-16905
Evaluation of an Aeroelastic Model Technique for Predicting Airplane Buffet Loads
Perry W. Hanson, Feb. 1973, 62 p, refs
National Aeronautics and Space Administration, Langley Research Center, Langley Station, Va.
NASA-TN-D-7066; L-8460

N73-15020
Aerodynamic Design and Flight Test of US Navy Aircraft at High Angles of Attack
W.R. Burris and J.T. Lawrence
In: AGARD, Fluid Dyn. of Aircraft Stalling, Nov. 1972, 10 p, refs
AGARD-CP-102

N73-15019
Maneuver and Buffet Characteristics of Fighter Aircraft
Edward J. Ray, Linwood W. McKinney and Julian G. Carmichael
In: AGARD, Fluid Dyn. of Aircraft Stalling, Nov. 1972, 11 p, refs
AGARD-CP-102

N73-15018
The Dynamic Analysis of Buffeting and Related Phenomena
J.G. Jones
In: AGARD, Fluid Dyn. of Aircraft Stalling, Nov. 1972, 10 p, refs
AGARD-CP-102

N73-15017
On Airflow Separation and Buffet Onset During Fighter Aircraft Maneuvering
Peter J. Butkewicz
In: AGARD, Fluid Dyn. of Aircraft Stalling, Nov. 1972, 10 p, refs
AGARD-CP-102

N72-30004
Flight Measurements of Buffet Characteristics of the F-104 Airplane for Selected Wing-Flap Deflections
Edward L. Friend and Walter J. Sefic, Aug. 1972, 48 p, refs
National Aeronautics and Space Administration, Flight Research Center, Edwards, Calif.
NASA-TN-D-6943; H-666

N72-26349
Buffeting Measurements on a Wing-Body-Model with Strain Gauges at the Wings (Buffeting-Messungen an einem Flügel-Rumpf-Modell mit Dehnmeßstreifen am Flügel)
R. Vanino, Feb. 1972, p 153-178, refs
DLR-Mitt-72-06

N72-11886
Wind Tunnel Investigation of Buffet Loads on Four Airplane Models
R. Vanino and E. Wedemeyer
In: AGARD, Facilities and Tech. for Aerodyn. Testing at Transonic Speeds and High Reynolds Number, Aug. 1971, 15 p, refs
AGARD-CP-83-71

N72-11861
The Transonic Performance of Two Dimensional Jet Flapped Aerofoils at High Reynolds Numbers
D.J. Peake, H. Yoshihara, D. Zonars and W. Carter
In: AGARD, Facilities and Tech. for Aerodyn. Testing at Transonic Speeds and High Reynolds Number, Aug. 1971, 39 p, refs
AGARD-CP-83-71

N72-11857
A Method for Calculating the Transonic Buffet Boundary Including the Influence of Reynolds Number
F. Thomas and G. Redeker
In: AGARD, Facilities and Tech. for Aerodyn. Testing at Transonic Speeds and High Reynolds Number, Aug. 1971, 14 p, refs
AGARD-CP-83-71

N72-11044
A Hypothesis for the Prediction of Flight Penetration of Wing Buffeting from Dynamic Tests on Wind Tunnel Models
D.G. Mabey, 1971, 33 p, refs
Royal Aircraft Establishment, Bedford (England), Aerodynamics Dept.
ARC-CP-1171; RAE-TR-70189; ARC-32684

N71-24659
Thick High Aspect Ratio Wing, Part 2
Larry L. Erickson, Bruno J. Gambucci and Phillip R. Wilcox
In: NASA, Space Shuttle Technol. Conf., Vol. 3, Apr. 1971, p 201-229, refs
NASA-TM-X-2274

N71-19796
Buffet Load Measuring Technique, Final Report
A.M. Ellison, Feb. 1971, 109 p, refs
Lockheed Missiles and Space Co., Huntsville, Ala., Research and Engineering Center
NASA-CR-114287; HREC-5917-1; LMSC-HREC-D162888

N70-41732
Flow Over Airfoils in the Transonic Regime. Volume 1: Prediction of Buffet Onset, Final Technical Report, 15. Nov. 1968 - 12. Dec. 1969
Richard Magnus and Hideo Yoshihara, 1. Mar. 1970, 58 p, refs
General Dynamics/Convair, San Diego, Calif.
AD-709377; AFFDL-TR-70-16-Vol-1

N70-37755
Aeromechanics
B.H. Little, Jr.
In: AGARD, High Reynolds Number Subsonic Aerodynamics, Jun. 1970, 31 p, refs
AGARD-LS-37-78

N70-36608
Buffet and Aerodynamic Noise
Charles F. Coe
In: Space Transportation System Technol. Symp., Vol. 2, Jul. 1970, p 238-247
NASA-TM-X-52876-Vol-2

N70-33426
Determination of the Buffet Boundaries of Aircraft Wings in the Transonic Velocity Regime (Die Ermittlung der Schüttelgrenzen von Tragflügeln im transsonischen Geschwindigkeitsbereich)
Fred Thomas, 1970, 43 p, refs
National Research Council of Canada, Ottawa (Ontario)
NRC-TT-1408

N70-31890
Buffet and Static Aerodynamic Characteristics of a Systematic Series of Wings Determined from a Subsonic Wind-Tunnel Study
Edward J. Ray and Robert T. Taylor, Jun. 1970, 266 p, refs
National Aeronautics and Space Administration, Langley Research Station, Langley Station, Va.
NASA-TN-D-5805; L-7011

N70-29418
Wind Tunnel Techniques for the Study of Aeroelastic Effects on Aircraft Stability, Control and Loads
A. Gerald Rainey and Irving Abel
In: AGARD, Aeroelastic Effects from a Flight Mech. Standpoint, Mar. 1970, 16 p, refs
AGARD-CP-46

N70-15651
Buffeting Tests (Essais de Tremblement)
Francois Charpin, Jan. 1970, 13 p, refs
Transl. into English from French report
NASA-TT-F-12776; TP-664

N70-11570
F-105F Transonic Buffet Study and Effect of Maneuvering Flaps, Final Technical Report, 29. Mar. 1968 - 1. Apr. 1969
Milton Margolin and Jung G. Chung, 7. Jul. 1969, 241 p, refs
Fairchild Hiller Corp., Farmingdale, N.Y., Republic Aviation Div.
AD-693650; FHR-3649-1; AFFDL-TR-69-37

A74-35393
Wind Tunnel Instrumentation Considerations for Buffet Predictions
M.A. Bell
American Institute of Aeronautics and Astronautics, Aerodynamic Testing Conference, 8th, Bethesda, Md., July 8-10, 1974, 12 p, 5 refs
Paper 74-629

A74-26668
A Detailed Investigation of Flight Buffeting Response at Subsonic and Transonic Speeds
D.B. Benepe, A.M. Cunningham, Jr. and W.D. Dunmyer
AIAA, ASME and SAE, Structures, Structural Dynamics and Materials Conference, 15th, Las Vegas, Nev., Apr. 17-19, 1974, 11 p, 11 refs
AIAA Paper 74-358

A74-25310
Buffeting Tests with a Swept Wing in the Transonic Range (Essais de Buffeting d'une Aile en Flêche en Transsonique)
B. Monnerie and F. Charpin
Association Aéronautique et Astronautique de France, Colloque d'Aérodynamique Appliquée, 10th, Université de Lille I, Lille, France, Nov. 7-9, 1973, Paper, 30 p

A74-10985
The Calculation of the Buffeting Limits of Swept Wings (Die Berechnung der Schüttelgrenzen von Pfeilflügeln)
G. Redeker
Zeitschrift für Flugwissenschaften, vol. 21, Oct. 1973, p 345-359, 45 refs

A73-25542
Buffeting Pressures on a Swept Wing in Transonic Flight - Comparison of Model and Full Scale Measurements
C.E. Lemley and R.E. Mullans
American Institute of Aeronautics and Astronautics, Dynamics Specialists Conference, Williamsburg, Va., Mar. 19, 20, 1973, 6 p, 9 refs
Paper 73-311

A73-25539
Dynamic Effects of Shock-Induced Flow Separation
L.E. Ericsson
American Institute of Aeronautics and Astronautics, Dynamics Specialists Conference, Williamsburg, Va., Mar. 19, 20, 1973, 12 p, 37 refs
Paper 73-308

A73-34538
Beyond the Buffet Boundary
D.G. Mabey
Aeronautical Journal, vol. 77, Apr. 1973, p 201-215, 58 refs

A71-24863
Transonic Flight and Wind-Tunnel Buffet Onset Investigation of the F-8D Aircraft
E.K. Damstrom and J.F. Mayes
Journal of Aircraft, vol. 8, Apr. 1971, p 263-270, 8 refs

A71-20709
Effects of Vibration and Buffeting on Man
Henning E. von Gierke and Neville P. Clarke, 1971, p 198-223, 28 refs
In: Aerospace medicine (2nd edition)
Edited by H.W. Randel, Baltimore, Williams and Wilkins Co.

A71-12679
Transonic Buffet Characteristics of a 60-deg Swept Wing with Design Variations
J.F. Mayes, M.E. Lores and H.R. Barnard
Journal of Aircraft, vol. 7, Nov.-Dec. 1970, p 524-530, 13 refs

A70-25067
Calculation of the Low-Speed Buffeting of a Slender-Wing Aircraft
C.G.B. Mitchell
In: Symposium on Structural Dynamics, Loughborough University of Technology, Loughborough, Leics., England, March 23-25, 1970, Volume 2
Edited by D.J. Johns, Loughborough, Loughborough University of Technology, 1970, p D.4.1-D.4.24, 9 refs

A70-23020
Transonic Flight and Wind Tunnel Buffet Onset Investigation of the F-8D Aircraft-Analysis of Data and Test Techniques
E.K. Damstrom and J.F. Mayes
American Institute of Aeronautics and Astronautics, Fighter Aircraft Conference, St. Louis, Mo., Mar. 5-7, 1970, 12 p, 9 refs
Paper 70-341

Bibliography on Boundary Layer Separation

N74-21930
On Laminar Separation
V.V. Sychev, Jan. 1974, 31 p, refs
Transl. into English from Izv. Akad. Nauk SSSR, Mekh. Zhidk. Gaza (USSR), no. 3, 1972, p 47-59
NAL-TT-3

N74-20918
Prediction of the Turbulent Boundary Layer Separation, Ph.D. Thesis
F.-K. Chou, 1973, 113 p
Colorado State Univ., Fort Collins
Univ. Microfilms Order No. 74-5411

N74-19637
The Separating Turbulent Boundary Layer: An Experimental Study of an Airfoil Type Flow, Ph.D. Thesis
James Hassler Strickland, Jr., 1973, 237 p
Southern Methodist Univ., Dallas, Tex.
Univ. Microfilms Order No. 74-5178

N74-18939
The Separating Turbulent Boundary Layer: An Experimental Study of an Airfoil Type, Technical Report, 1. Oct. 1971 - 1. Jul. 1973
James H. Strickland and Roger L. Simpson, Aug. 1973, 241 p
Southern Methodist Univ., Dallas, Tex., Thermal and Fluid Sciences Center
AD-771170/8GA; WT-2; AROD-10092-2-E

N74-13009
Analytical Study of Subsonic Laminar Boundary Layer Separation and Reattachment Including Viscous-Inviscid Interaction
G.R. Inger and Birendra Dutt, May 1973, 54 p, refs
Virginia Polytechnic Inst. and State Univ., Blacksburg, Dept. of Aerospace Engineering
AD-767602; VPI-E-73-20; AFOSR-73-1686TR

N74-12995
Measurements in a Three Dimensional Incompressible Turbulent Boundary Layer in an Adverse Pressure Gradient under Infinite Swept Wing Conditions
B. van den Berg and A. Eisenaar, 15. Aug. 1973, 71 p, refs
National Aerospace Lab., Amsterdam (Netherlands)
NLR-TR-72092-U

N74-12990
The Separation Condition of Boundary Layers
K. Oswatitsch, Dec. 1973, 17 p, refs
Transl. into English of the "Die Ablesungsbedingung von Grenzschichten" (West. Ger.), 1958, p 357-367, Presented at the Boundary Layer Research Symp., Freiburg, 26.-29. Aug. 1957
NASA-TT-F-15200

N74-11132
Prediction of the Turbulent Boundary Layer Separation
Fang-Kuo Chou and Virgil A. Sandborn, Jul. 1973, 114 p, refs
Colorado State Univ., Fort Collins, Fluid Dynamics and Diffusion Lab.
AD-766845; CER73-74FKC-VAS3; THEMIS-CER-TR-22

N73-24319
The Kutta-Joukowsky Conditions in Three-Dimensional Flow
Robert Legendre, May 1973, 24 p, refs
Transl. into English from La Rech. Aerospatiale (French), no. 5, 1972, p 241-247
NASA-TT-F-14918

N73-23401
Evaluation of Separation Criteria and their Application to Separated Flow Analysis, Final Report, 24. Jan. 1972 - 24. Jan. 1973
Mansop Hahn, Paul E. Rubbert and Avtar S. Mahal, 24. Jan. 1973, 81 p, refs
Boeing Commercial Airplane Co., Renton, Wash.
AD-757531; D6-41070; AFFDL-TR-72-145

N73-15003
Parametric Studies of Separating Turbulent Boundary Layer Flows
Andrzej Wortman and W.J. Franks
In: AGARD, Fluid Dyn. of Aircraft Stalling, Nov. 1972, 9 p, refs
AGARD-CP-102

N72-15292
Scale Effects in Flows over Swept Wings
M.G. Hall, D. Kuechemann and Maskell, Mar. 1971, 55 p, refs
Royal Aircraft Establishment, Farnborough (England)
RAE-TR-71043

A74-33162
Solutions for Laminar Boundary Layers with Separation and Reattachment
J.E. Carter
American Institute of Aeronautics and Astronautics, Fluid and Plasma Dynamics Conference, 7th, Palo Alto, Calif., June 17-19, 1974, 12 p, 18 refs
Paper 74-583

A74-25321
Experimental and Theoretical Study of the Transonic Flow past a Half-Wing (Etude Expérimentale et Théorique de l'Écoulement Transsonique autour d'un Demi-Profil)
J. Delery, P. Laval and J.J. Chattot
Association Aéronautique et Astronautique de France, Colloque d'Aérodynamique Appliquée, 10th, Université de Lille I, Lille, France, Nov. 7-9, 1973, paper, 34 p, 25 refs

A74-25319
Example of Aerodynamic Instability under Supercritical Conditions about Profiles (Exemple d'Instabilite Aerodynamique en Regime Supercritique autour de Profils)
A. Dyment and P. Gryson
Association Aéronautique et Astronautique de France, Colloque d'Aérodynamique Appliquée, 10th, Université de Lille I, Lille, France, Nov. 7-9, 1973, Paper, 26 p, 7 refs

A74-20293
Attachment-Line Flow on an Infinite Swept Wing
T. Cebeci
AIAA Journal, vol. 12, Feb. 1974, p 242-245, 7 refs

A74-19779
Theoretical Suction and Pressure Distribution Bounds for Flow Separation in Retarded Flow
T. Cebeci and G.F. Witherspoon
Journal of Aircraft, vol. 11, Jun. 1974, p 61-64

A74-18814
On Laminar Boundary-Layer Separation
J.M. Klineberg and J.L. Steger
American Institute of Aeronautics and Astronautics, Aerospace Sciences Meeting, 12th, Washington, D.C., Jan. 30 - Feb. 1, 1974, 18 p, 45 refs
Paper 74-94

A74-16626
The Effect of Blowing on Laminar Separation
D.T. Tsahalis and D.P. Telionis
ASME, Transactions, Series E - Journal of Applied Mechanics, vol. 40, Dec. 1973, p 1133, 1134, 6 refs

A73-44831
Pressure Fluctuations Underlying Attached and Separated Supersonic Turbulent Boundary Layers and Shock Waves
C.F. Coe, W.J. Chyu and J.B. Dods, Jr.
American Institute of Aeronautics and Astronautics, Aero-Acoustics Conference, Seattle, Wash., Oct. 15-17, 1973, 15 p, 18 refs
Paper 73-996

A73-36262
Reynolds Number Effects on the Shock Wave - Turbulent Boundary Layer Interaction at Transonic Speeds
R.J. Vidal, C.E. Wittliff, P.A. Catlin and B.H. Sheen
American Institute of Aeronautics and Astronautics, Fluid and Plasma Dynamics Conference, 6th, Palm Springs, Calif., July 16-18, 1973, 15 p, 22 refs
Paper 73-661

A73-36217
Separation of a Supersonic Turbulent Boundary Layer at Moderate to High Reynolds Numbers
G.S. Settles and S.M. Bogdonoff
American Institute of Aeronautics and Astronautics, Fluid and Plasma Dynamics Conference, 6th, Palm Springs, Calif., July 16-18, 1973, 10 p, 18 refs
Paper 73-666

A73-36214
Prediction of Turbulent Separated Boundary Layers
G.D. Kuhn and J.N. Nielsen
American Institute of Aeronautics and Astronautics, Fluid and Plasma Dynamics Conference, 6th, Palm Springs, Calif., July 16-18, 1973, 12 p, 12 refs
Paper 73-663

A73-32814
Theoretical and Experimental Study of a Swept-Back Wing at Low Velocity over a Wide Range of Angles of Attack (Etude Théorique et Expérimentale d'une Aile en Fleche à Faible Vitesse et dans un Large Domaine d'Incidences)
M. Ledoux and B. Monnerie
Association Aéronautique et Astronautique de France, Colloque d'Aérodynamique Appliquée, 9th, Saint-Cyr-l'Ecole, Yvelines and Paris, France, Nov. 8-10, 1972, Paper, 25 p

A73-24815
On Kaplun's Method for Studying Separation
J. Buckmaster
In: Recent Research on Unsteady Boundary Layers; Symposium, Quebec, Canada, May 24-28, 1971, Proceedings, Volume 1, Quebec, Presses de l'Université Laval, 1972, p 462-475; Comments, p 476, 477; Author's Reply, p 477-480, 6 refs

A73-14379
Theoretical Investigation of Transition Phenomena in the Boundary Layer on an Infinite Swept Wing (Theoretische Untersuchung von Transitionsphänomenen in der Grenzschicht eines unendlich gestreckten gepfeilten Flügels)
E.H. Hirschel
Deutsche Gesellschaft für Luft- und Raumfahrt, Symposium über Tragflügel-Aerodynamik bei schallnahen Strömungen, Göttingen, West Germany, Oct. 26, 27, 1972, 24 p, 21 refs
Paper 72-124

A72-43331
Analysis and Correlation of Data on Pressure Fluctuations in Separated Flow
D.G. Mabey
Journal of Aircraft, vol. 9, Sept. 1972, p 642-645, 27 refs

A72-38812
Re-Developing Turbulent Boundary Layers behind Yawed Separation Bubbles
H.P. Horton
Aeronautical Quarterly, vol. 23, Aug. 1972, p 211-228, 25 refs

A72-32826
Three-Dimensional Flow Separations on Aircraft and Missiles
D.J. Peake, W.J. Rainbird and E.G. Atraghji
AIAA Journal, vol. 10, May 1972, p 567-580, 63 refs

A71-18641
Similar Solutions for a Family of Separated Turbulent Boundary Layers
Irwin E. Alber
American Institute of Aeronautics and Astronautics, Aerospace Sciences Meeting, 9th, New York, N.Y., Jan. 25-27, 1971, 16 p, 29 refs
Paper 71-203

A70-42206
Separation Criteria for Three-Dimensional Boundary Layers (O kriteriiakh otryva trekhmernogo pogranichnogo sloia)
G.M. Bam-Zelikovich
Akademiia Nauk SSSR, Izvestiia, Mekhanika Zhidkosti i Gaza, July-Aug. 1970, p 50-54

REPORT DOCUMENTATION PAGE

1. Recipient's Reference	2. Originator's Reference	3. Further Reference	4. Security Classification of Document
	AGARD-LS-74		UNCLASSIFIED

5. Originator Advisory Group for Aerospace Research and Development
North Atlantic Treaty Organization
7 rue Ancelle, 92200 Neuilly sur Seine, France

6. Title

Aircraft Stalling and Buffeting

7. Presented at

The von Kármán Institute, Brussels, and Ames Research Center, California.

8. Author(s)	9. Date
Various	February 1975
10. Author's Address	**11. Pages**
Various	172

12. Distribution Statement This document is distributed in accordance with AGARD policies and regulations, which are outlined on the Outside Back Covers of all AGARD publications.

13. Keywords/Descriptors		14. UDC
Buffeting	Transport aircraft	533.6.013.66:533.6.013.43
Stalling	Commercial aircraft	
Boundary layer separation		

15. Abstract

The material in this book has been assembled to support a Lecture Series presented by the authors at the von Kármán Institute, Brussels and at Ames Research Center (California) in March 1975.

After a review of the Fluid Mechanics of the Stall, the recent developments in Flow Separation Phenomena, Dynamic Response and Pre-stall Behaviour of Aircraft are presented. The Low Speed Stall Characteristics of the Boeing 747 and a Critical Review of Methods to Predict the Buffet Capability of Aircraft complete this publication.

This Lecture Series is sponsored by the Fluid Dynamics Panel, the von Kármán Institute, Brussels, and the Consultant and Exchange Programme of AGARD.